Swansea University
Prifysgol Abertawe

Development of a Novel Haemorheological Biomarker of Clot Lysis

Bethan Hannah Morgan
BSc (Hons)

A thesis submitted for the degree
of Doctor of Philosophy

September 2020

Abstract

Thrombosis is a leading contributor to death and disability, carrying high social and healthcare costs. Current treatment protocols in patients presenting with blood clots (such as those with ischemic stroke) recommend the administration of thrombolytic drugs; however, this option is associated with severe haemorrhagic side effects. Clinicians currently have access to a wide range of fibrinolytic biomarkers; however, these either rely on monitoring a single component of the fibrinolytic system or use arbitrary definitions of lysis, and thus have limited value.

This thesis presents the development and validation of a novel haemorheological biomarker, utilising advanced rheological techniques that measure fibrinolysis through the detection of a gel and de-gel point. This provides a global marker of coagulation and lysis based on the period of haemostatic functionality, *i.e.* the clots lifetime as a viscoelastic solid. This biomarker was evaluated in samples of blood and plasma, and the results demonstrate its potential use as a tool for the monitoring and development of thrombolytic therapies.

The work herein also investigates the influence of shear induced modification of clot structure on clot lysis through the use of controlled stress parallel superposition rheometry. Clots formed under increasing levels of shear stress were found to have increased resistance to lysis, a finding which has significance *in-vivo* when considering pathophysiologically relevant changes to flow, due to high blood pressure and narrowing of blood vessels. Finally, the effects of platelet mediated contraction were shown to have a negligible impact on the rheological measurements and the associated biomarker. This represents a significant advantage over current mechanical based techniques, such as thromboelastometry and thromboelastography.

DECLARATION

This work has not previously been accepted in substance for any degree and is not being concurrently submitted in candidature for any degree.

Signed .... [redacted] ..... (candidate)

Date .....12-Apr-2021.....

STATEMENT 1

This thesis is the result of my own investigations, except where otherwise stated. Where correction services have been used, the extent and nature of the correction is clearly marked in a footnote(s).

Other sources are acknowledged by footnotes giving explicit references. A bibliography is appended.

Signed .... [redacted] ..... (candidate)

Date .....12-Apr-2021.....

STATEMENT 2

I hereby give consent for my thesis, if accepted, to be available for photocopying and for inter-library loans after expiry of a bar on access approved by the Swansea University.

Signed .... [redacted] ..... (candidate)

Date .....12-Apr-2021.....

Acknowledgements

I gratefully acknowledge the funding received towards my PhD from both the Engineering and Physical Sciences Research Council (EPSRC) and Swansea University.

I would like to offer sincere thanks to Prof. Karl Hawkins, his patience and guidance have been integral to both this project and my personal/professional growth. I could not have asked for a better supervisor.

I would additionally like to extend thanks to all the members of the Biorheology and Complex Fluids research groups at Swansea University, in particular to Dr. Daniel Curtis, Dr. Bethan Thomas, Dr. Nafiseh Badiei, and Dr. Alex Holder for their time and expertise.

I also wish to acknowledge all of the volunteers who contributed samples for this research. This work could not have been done without individuals who were willing to put themselves in the chair, and I am eternally grateful for their contribution.

Thanks also go to my family for their continued support (and free childcare) over the course of this project, and to Dr. Benjamin Clifford and Dr. Dominic Fung who were always on hand to help with disasters.

Finally, I would like to recognise Red Bull GmbH, without whom this document would only be three pages long.

Dedication

Mae'r nhreuthawd ymchwil yn ymroddedig i cof annwyl am fy Nhadcu, fe ymrodd ei gefnogaeth i fy addysg. Rwy'n sicr basai fe'n falch.

This thesis is dedicated to the memory of my grandfather, who always supported my education. I know it would make him proud.

Contents

List of Figures **xvi**

List of Tables **xx**

List of Abbreviations **xxiii**

1 Introduction and Literature Review **1**

1.1 Thrombosis Pathology 2

1.2 Haemostasis 5

1.2.1 Vasoconstriction 6

1.2.2 Platelet Plug Formation 7

1.2.3 Coagulation 8

1.2.4 Fibrin Network Formation 13

1.2.5 Clot Contraction 15

1.2.6 Fibrinolysis 17

1.2.7 Current Fibrinolytic Biomarkers 22

1.3 Rheological Techniques for Monitoring Coagulation and Fibrinolysis 27

1.3.1 Thromboelastography and Thromboelastometry 28

1.3.2 Oscillatory Rheometry 31

1.3.3 Fibrinolysis 46

1.4 Relevant Rheological Developments 47

1.4.1 Rheological Detection of the Gel Point 47
1.4.2 Software Developments 52
1.5 Summary 54
1.6 Aims and Objectives 56
2 Theory and Methodology **58**
2.1 Rheological Properties of Materials 59
2.1.1 Viscosity 59
2.1.2 Elasticity 61
2.1.3 Viscoelasticity 62
2.2 Creep and Stress Relaxation 65
2.2.1 Creep and Creep Recovery 65
2.2.2 Stress Relaxation 67
2.3 Small Amplitude Oscillatory Shear 71
2.3.1 Ideal-Viscous Behaviour 73
2.3.2 Ideal-Elastic Behaviour 73
2.3.3 Viscoelastic Behaviour 74
2.4 Gelation 77
2.4.1 Transient Properties During Gelation 77
2.4.2 Chambon-Winter Gel Point Criterion 77
2.4.3 The Fractal Dimension 81
2.4.4 The De-Gel Point 83
2.5 Gel Point Detection 84
2.5.1 Discrete Sweeps 84
2.5.2 Fourier Transform Mechanical Spectroscopy 85

2.5.3 Optimally-Windowed Chirp 86

2.5.4 Practical Considerations 86

3 Optimisation and Validation of High Frequency Fourier Transform Mechanical Spectroscopy for Gel Point and de-Gel Point Detection 92

3.1 Methods 96

3.1.1 Sample Preparation 96

3.1.2 Data Collection 99

3.1.3 Data Analysis 108

3.1.4 Limitations 111

3.2 Results and Discussion 112

3.2.1 Gelatine Optimisation 112

3.2.2 Fibrin-Thrombin Validation 121

3.2.3 Establishing the Linear Viscoelastic Range of Pooled Platelet Free Plasma 125

3.2.4 Validation of the Optimised Procedure for Pooled Platelet Free Plasma and Whole Blood 128

3.2.5 Comparison of Gel Point Detection in Pooled Platelet Free Plasma using SMT and CMT Rheometers 131

3.3 Conclusions 134

4 Detection of Fibrinolysis Using High Frequency Fourier Transform Mechanical Spectroscopy 136

4.1 Methods 140

4.1.1 Sample Preparation 140

4.1.2 Data Collection 142

4.1.3 Data Analysis 143

4.1.4 Limitations 144
4.2 Results and Discussion 145
4.2.1 Impact of rtPA on Clot Formation and Lysis 145
4.2.2 Impact of Thrombin on Clot Formation and Lysis 156
4.2.3 Effect of Streptokinase on Clot Formation and Lysis 165
4.2.4 Relationships Between Rheological Parameters 175
4.2.5 Detection in Whole Blood 180
4.3 Conclusions 184
5 The Effects of Shear Induced Modification of Clot Microstructure on Coagulation and Lysis 186
5.1 Methods 189
5.1.1 Sample Preparation 189
5.1.2 Data Collection 190
5.1.3 Data Analysis 194
5.1.4 Limitations 196
5.2 Results and Discussion 197
5.2.1 Rheological Measurements of Clot Lysis 197
5.2.2 Confocal Microscopy 202
5.3 Conclusions 207
6 The Effect of Platelet Contraction on Coagulation and Lysis Measurements 208
6.1 Methods 211
6.1.1 Sample Preparation 211
6.1.2 Data Collection 212

6.1.3 Data Analysis 213
6.1.4 Limitations 214
6.2 Results and Discussion 215
6.2.1 Effect of Clot Contraction on Formation and Lysis 215
6.3 Conclusions 226
7 Thesis Conclusions **227**
Nomenclature **237**
Appendix A Participant Eligibility Guidelines **239**
Appendix B Gel Point Analysis Output **240**
Appendix C Amplitude Sweep of Silicone Oil **241**
Appendix D Assessment of i-Rheo for the Evaluation of Mature Blood Clots **242**
Appendix E Corn Trypsin Inhibitor **243**
Bibliography **259**

List of Figures

1.1 SEM Images of Fibrin Networks Illustrating Differences in Clot Microstructure 3

1.2 Virchow's Triad of Risk Factors Affecting Venous Thrombosis. . . 3

1.3 An Illustration Depicting Vascular Damage. 6

1.4 Illustrations Depicting an Unactivated and Activated Platelet. . . 7

1.5 A Representation of the Intrinsic Pathway of Coagulation. 10

1.6 A Representation of the Extrinsic Pathway of Coagulation. 11

1.7 A Representation of the Common Pathway of Coagulation. 12

1.8 A Schematic Representation Showing the Structure of a Fibrinogen Monomer. 13

1.9 A Schematic Representation of Fibrin Undergoing Polymerisation. 14

1.10 A Schematic Representation of Cross-linked Fibrin Polymers. . . . 14

1.11 A Series of Confocal Images Depicting the Mechanism of Platelet Action on Fibrin Fibres During Clot Contraction. 16

1.12 Illustration of a Proposed Method for Pathogenic Clot Formation Proposed by Peshkova *et al.* 17

1.13 A Representation of the Fibrinolytic Pathway. 18

1.14 A Schematic Representation of a D-Dimer Fibrin Degradation Product. 23

1.15 A Graph Illustrating a Typical Output from an Overall Haemostasis Potential Assay. 24

1.16 A Diagram Showing the Typical Set-up of a Thromboelastography/ Thromboelastometry Experiment. 28

1.17 Graphs Illustrating Typical Outputs from Thromboelastography/ Thromboelastometry Tests. 30

1.18 A Diagram Showing the Typical Set-up of a Viscoelastic Recorder. 34

1.19 A Graph Depicting the First Chambon-Winter Gel Point Reported for Whole Blood by Evans *et al.*. 37

1.20 Graphs Depicting the Comparison of the Fractal Dimension and Fibre Width of Whole Blood under Progressive Dilution with Saline. 39

1.21 A Graph Depicting the Evolution of Contractile Stress During Coagulation of Whole Blood With and Without the Contraction Inhibitor Blebbistatin. 43

1.22 A Graph Depicting the Evolution of Contractile Stress During Coagulation of Blood Plasma With and Without Red Blood Cells (RBCs). 43

1.23 Figure Depicting the Unconstrained Contraction and Constrained Contractile Stress of Blood Plasma Clots in the Presence and Absence of Red Blood Cells. 45

1.24 Graphs Depicting the Evolution of Contraction in Blood Plasma Clots With and Without Red Blood Cells (RBCs). 46

1.25 Graphs Depicting the Gel Point Parameters of Blood Samples from Stroke Patients Following Administration of Aspirin or Thrombolytic Therapy. 47

1.26 Graphs Depicting Example Gel Points Detected in 10 % Gelatine Solutions During Gelation Using Fourier Transform Mechanical Spectroscopy and Discrete Frequency Sweep Techniques. 48

1.27 Graphs Depicting Example Gel Points Detected in 10 % Gelatine Solutions During Gelation Using Fourier Transform Mechanical Spectroscopy and Simulated Discrete Frequency Sweep Techniques. 49

1.28 Graphs Depicting the Relationship Between the Fractal Dimension and Gel Time for 10 mg/ml Fibrin-Thrombin Gels having Thrombin Concentrations 0.01-0.15 NIH/ml. 50

1.29 Graphs Depicting the Operation of the Instrument Inertia Correction Written by Hudson *et al.* 53

2.1 The Parallel Plates Model: A Diagrammatic Representation of a Fluid Between Two Plates. 59

2.2 A Graph Illustrating the Relationship Between Shear Rate and Stress for Different Types of Materials. 60

2.3 A Schematic Representation of the Dashpot Model. 61

2.4 A Schematic Representation of the Spring Model. 62

2.5 A Schematic Representation of the Maxwell Model. 63

2.6 A Schematic Representation of the Kelvin-Voigt Model. 64

2.7 A Graph Depicting the Stress Applied to a Material as a Function of Time During a Creep Experiment. 65

2.8 A Graph Depicting the Strain Response as a Function of Time for an Ideal-Viscous Material Under Creep Testing. 66

2.9 A Graph Depicting the Strain Response as a Function of Time for an Ideal-Elastic Material Under Creep Testing. 66

2.10 A Graph Depicting the Strain Response as a Function of Time for Viscoelastic Materials Under Creep Testing. 67

2.11 A Graph Depicting the Strain Applied to a Material as a Function of Time During a Stress Relaxation Experiment. 68

2.12 A Graph Depicting the Stress Relaxation as a Function of Time for an Ideal-Viscous Material. 68

2.13 A Graph Depicting the Stress Relaxation as a Function of Time for an Ideal-Elastic Material. 69

2.14 A Graph Depicting the Stress Relaxation as a Function of Time for Viscoelastic Materials. 69

2.15 The Parallel Plates Model: A Diagrammatic Representation of a Fluid Between Two Plates. 71

2.16 A Graphic Representation of a Small Amplitude Oscillatory Shear Waveform and Corresponding Two Plates Model. 72

2.17 A Graphic Representation of Small Amplitude Oscillatory Shear Stress and Strain Waveforms. 72

2.18 A Graph Illustrating the Relationship between G', G'', and G^*. . . 75

2.19 Graphs Illustrating the Storage and Loss Moduli of Viscoelastic Materials as a Function of Frequency. 76

2.20 A Graph Illustrating the Theoretical Behaviour Predicted at the Gel Point. 78

2.21 A Graph Illustrating the Relationship Between the Stress Relaxation Modulus and Time in a Gelling System. 79

2.22 A Graph Illustrating the Relationship Between the Storage and Loss Moduli of a Critical Gel as a Function of Frequency. 79

2.23 A Graph Illustrating a Gel Point as Defined by Chambon and Winter. 80

2.24 A Diagram Showing a Percolation Cluster. 81

2.25 A Graph Illustrating a de-Gel Point Based on the Gel Point Criteria Defined by Chambon and Winter. 83

2.26 A Graph Illustrating a Discrete Frequency Sweep Waveform. . . . 84

2.27 A Graph Illustrating a Complex Waveform Generated from Two Discrete Frequencies. 85

2.28 A Graph Illustrating a Windowed Chirp Waveform. 86

2.29 A Graph Illustrating the Definition of the Linear Viscoelastic Region from an Amplitude Sweep Experiment. 87

2.30 An Illustration of Different Rheometer Geometries. 89

2.31 An Illustration of a Parallel Plate Geometry Showing Different Fills. 91

3.1 A Photograph Showing the Experimental Set-up of the AR-G2 Rheometer. 99

3.2 A Representative Diagram of an AR-G2 Rheometer. 100

3.3 A Photograph Showing the Experimental Set-up of the ARES-G2 Rheometer. 103

3.4 A Representative Diagram of an ARES-G2 Rheometer. 104

3.5 A Graph Illustrating the Definition of δ_{GP} and δ_f at the Apparent Gel Point. 108

3.6 Example Rheological Measurements of 2.5 % (w/v) Gelatine Undergoing Gelation as Detected Using Fourier Transform Mechanical Spectroscopy Over Different Frequency Ranges. 113

3.7 A Graph Showing the Relationship Between Fundamental Frequency and Sample Mutation Number for 2.5 % (w/v) Gelatine Obtained using Fourier Transform Mechanical Spectroscopy. 114

3.8 Graphs Showing the Relationship Between Fundamental Frequency on Gel Time and Phase Angle at the Apparent Gel Point in Samples of 2.5 % (w/v) Gelatine Obtained using Fourier Transform Mechanical Spectroscopy. 115

3.9 A Masterplot Showing the Relationship Between Testing Frequency and the Phase Angle Value at the Apparent Gel Point of 2.5 % (w/v) Gelatine. 116

3.10 A 3-D Plot Showing the Effect of Modulating the TRIOS Fluid Inertia Correction and Testing Frequency on the Phase Angle at the Apparent Gel Point of 2.5% (w/v) Gelatine Detected by Fourier Transform Mechanical Spectroscopy. 117

3.11 A Graph Showing the Effect of the TRIOS Fluid Inertia Correction on the Phase Angle of the Highest Frequency (at the Apparent Gel Point) at High Frequency During Fourier Transform Mechanical Spectroscopy Measurements of 2.5 % (w/v) Gelatine. 118

3.12 Graphs Showing the Gel Time and Phase Angle Measurements of 2.5 % (w/v) Gelatine Acquired Using Fourier Transform Mechanical Spectroscopy Utilising Three and Five Harmonics. 120

3.13 A Graph Showing the Effect of Thrombin Concentration on the Gel Time of 5 mg/ml Fibrin-Thrombin Gels Detected by High Frequency Fourier Transform Mechanical Spectroscopy. 121

3.14 A Graph Showing the Effect of Thrombin Concentration on the Fractal Dimension of the Gel Point of 5 mg/ml Fibrin-Thrombin Gels Detected by Low Frequency Discrete Sweep Rheometry and High Frequency Fourier Transform Mechanical Spectroscopy. . . . 122

3.15 SEM Images of Mature Fibrin-Thrombin and Pooled Platelet Free Plasma Clots. 123

3.16 A Graph Showing the Relationship between Thrombin Concentration and Fibre Thickness for Purified Fibrin-Thrombin Gels with Different Levels of Thrombin, and for Pooled Platelet Free Plasma. 124

3.17 A Graph Showing the Relative Uncertainty of Gel Point Values Obtained Using Low Frequency Discrete and High Frequency Fourier Transform Mechanical Spectroscopy Techniques of 5 mg/ml, 0.03-0.09 NIH/ml Fibrin-Thrombin Gels.-reload 125

3.18 A Graph Depicting the Linear Viscoelastic Region of Pooled Platelet Free Plasma as a Function of Strain. 126

3.19 A Graph Depicting the Linear Viscoelastic Region of Pooled Platelet Free Plasma as a Function of Stress. 127

3.20 Graphs Showing the Effect of Resultant Stress on Gel Point Parameters of Pooled Platelet Free Plasma. 128

3.21 Graphs Showing the Effect of Applied Strain on Gel Point Parameters of Pooled Platelet Free Plasma. 129

3.22 Graphs Showing the Effect of Increasing Stress on Gel Point Parameters of Whole Blood. 130

3.23 Graphs Showing the Effect of Increasing Strain on Gel Point Parameters of Whole Blood. 130

3.24 A Graph Depicting the Relationship between Fractal Dimension Obtained by Fourier Transform Mechanical Spectroscopy and Average Fibre Thickness from Scanning Electron Microscopy. 131

3.25 Example Rheological Profiles of Pooled Platelet Free Plasma Undergoing Coagulation. 132

4.1 Example Rheological Profile of Pooled Platelet Free Plasma Undergoing both Coagulation and Lysis. 145

4.2 A Graph Showing the Relationship Between Functional Clot Lifetime and Recombinant Tissue Plasminogen Activator Concentration in Pooled Platelet Free Plasma Detected by Fourier Transform Mechanical Spectroscopy. 148

4.3 A Graph Showing the Relationship Between Clotting Time and Recombinant Tissue Plasminogen Activator Concentration in Pooled Platelet Free Plasma Detected by Spectrophotometry. 150

4.4 A Graph Showing the Relationship Between Lysis Time and Recombinant Tissue Plasminogen Activator Concentration in Pooled Platelet Free Plasma Detected by Spectrophotometry. 151

4.5 A Graph Showing the Relationship Between Overall Fibrinolytic Potential and Recombinant Tissue Plasminogen Activator Concentration in Pooled Platelet Free Plasma Detected by Spectrophotometry. 152

4.6 A Graph Showing the Relationship Between Lysis Time and Recombinant Tissue Plasminogen Activator Concentration in Pooled Platelet Free Plasma Detected by Fourier Transform Mechanical Spectroscopy With and Without the Addition of 0.05 NIH/ml Thrombin and Spectrophotometry With the Addition of 0.1 NIH/ml Thrombin. 153

4.7 A Graph Showing the Relationship Between Gel Time and Thrombin Concentration in Pooled Platelet Free Plasma Detected by Fourier Transform Mechanical Spectroscopy. 158

4.8 A Graph Showing the Relationship Between Fractal Dimension During Coagulation and Thrombin Concentration in Pooled Platelet Free Plasma Detected by Fourier Transform Mechanical Spectroscopy. 159

4.9 A Graph Showing the Relationship Between Functional Clot Lifetime and Thrombin Concentration in Pooled Platelet Free Plasma Detected by Fourier Transform Mechanical Spectroscopy. 160

4.10 A Graph Showing the Relationship Between Lysis Time and Thrombin Concentration in Pooled Platelet Free Plasma Detected by Spectrophotometry. 163

4.11 A Graph Showing the Relationship Between Overall Fibrinolytic Potential and Thrombin Concentration in Pooled Platelet Free Plasma Detected by Spectrophotometry. 164

4.12 A Graph Showing the Relationship Between Gel Time and Streptokinase Concentration in Pooled Platelet Free Plasma Detected by Fourier Transform Mechanical Spectroscopy. 167

4.13 A Graph Showing the Relationship Between Fractal Dimension during Coagulation and Streptokinase Concentration in Pooled Platelet Free Plasma Detected by Fourier Transform Mechanical Spectroscopy. 168

4.14 Graph Showing the Relationship Between Functional Clot Lifetime and Streptokinase Concentration in Pooled Platelet Free Plasma Detected by Fourier Transform Mechanical Spectroscopy. 169

4.15 A Graph Showing the Relationship Between Fractal Dimension during Clot Lysis and Streptokinase Concentration in Pooled Platelet Free Plasma Detected by Fourier Transform Mechanical Spectroscopy.170

4.16 A Graph Showing the Relationship Between Lysis Time and Streptokinase Concentration in Pooled Platelet Free Plasma Detected by Spectrophotometry. 173

4.17 A Graph Showing the Relationship Between Overall Fibrinolytic Potential and Streptokinase Concentration in Pooled Platelet Free Plasma Detected by Spectrophotometry. 174

4.18 Graphs Showing the Relationships Between Rheological Parameters during Coagulation and Lysis in Pooled Platelet Free Plasma Detected by Fourier Transform Mechanical Spectroscopy. 177

4.19 Graphs Showing the Relationship Between Fractal Dimension during Lysis and Coagulation in Pooled Platelet Free Plasma as Detected by Fourier Transform Mechanical Spectroscopy. 179

4.20 Graph Showing the Relationship Between Functional Clot Lifetime and Streptokinase Concentration in Whole Blood Detected by Rheometry. 182

4.21 Graph Showing the Relationship Between the Fractal Dimension during Lysis and Coagulation of Whole Blood with Varying Streptokinase Concentration as Detected by Rheometry. 183

5.1 SEM Images Illustrating the Effect of Flow on Fibrin Network Structure 187

5.2 Illustration of the Net Strain Accumulated under Controlled Stress Parallel Superposition during the process of gelation or coagulation 191

5.3 A Photograph Showing the Experimental Set-up of the AR-G2 Rheometer Enabling Transfer of Samples to a Confocal Microscope. 193

5.4 A Figure Illustrating the Definition of the Moment of Free Movement from the Correlation of Consecutive Confocal Frames 195

5.5 A Graph Showing the Relationship Between $G'_{\max}$ and Unidirectional Shear Stress in Pooled Platelet Free Plasma Clots Detected by Rheometry. 199

5.6 Graphs Showing the Change in Storage Modulus Over Time for Pooled Platelet Free Plasma Clots Generated Under Different Levels of Unidirectional Shear Stress. 200

5.7 Graph Showing the Relationship Between Clot Lysis Time and Unidirectional Shear Stress in Pooled Platelet Free Plasma Clots Detected by Rheometry. 201

5.8 Confocal Images Showing the Mature Gel Structure of Pooled Platelet Free Plasma Clots Formed Under Controlled Stress Parallel Superposition. 202

5.9 Polar Graphs Showing the Percentage of Fibres Oriented at 10 ° Intervals for Mature Pooled Platelet Free Plasma Clots Formed Under Controlled Stress Parallel Superposition. 203

5.10 Graphs Showing the Relationship Between Fibre Length/Number and Unidirectional Shear Stress for Mature Pooled Platelet Free Plasma Clots Formed Under Controlled Stress Parallel Superposition.204

5.11 A Graph Showing the Relationship Between the Static Period and Unidirectional Shear Stress in Pooled Platelet Free Plasma Clots Detected by Confocal Microscopy. 205

5.12 Confocal Images Showing Gel Structures at the Moment of Free Movement for Pooled Platelet Free Plasma Clots Formed Under Controlled Stress Parallel Superposition. 206

6.1 A Graph Showing the Gel Time of Different Blood Fractions in Fixed Gap and Variable Gap Rheometrical Testing. 216

6.2 A Graph Showing the Fractal Dimension of Different Blood Fractions at the Gel Point in Fixed Gap and Variable Gap Rheometrical Testing.217

6.3 Graphs Showing the Relationship Between the Storage and Loss Moduli and Angular Frequency (ω) for Whole Blood Clots as Obtained by i-Rheo Software. 219

6.4 Graphs Showing the Relationship Between the Storage and Loss Moduli and Angular Frequency (ω) for Platelet Rich Plasma Clots as Obtained by i-Rheo Software. 220

6.5 Graphs Showing the Relationship Between the Storage and Loss Moduli and Angular Frequency (ω) for Platelet Free Plasma Clots as Obtained by i-Rheo Software. 221

6.6 Graphs Showing the Relationship Between the Storage and Loss Moduli and Angular Frequency (ω) for Platelet Rich Plasma + 10 μM tirofiban Clots as Obtained by i-Rheo Software. 222

6.7 A Graph Showing the Functional Clot Lifetime of Different Blood Fractions in Fixed Gap and Variable Gap Rheometrical Testing. . 223

6.8 A Graph Showing the Fractal Dimension during Lysis of Different Blood Fractions, in Fixed Gap and Variable Gap Rheometrical Testing. 224

A.1 Participant Eligibility Guidelines Presented to Each Volunteer Before Sample Collection 239

B.1 Graphs Showing the Results Output by Repeated Assessment of Error Prone Results Obtained for 2.5 % (w/v) Gelatine by Gel Point Analysis Software 240

C.1 Graphs Showing the Influence of Increasing Strain and Stress Amplitude on the Apparent Viscoelastic Behaviour of Silicone Oil . 241

D.1 Graphs Showing the Relationship Between the Storage and Loss Moduli and Angular Frequency (ω) for Mature Whole Blood Clots, Detected by Both the Conversion of Stress Relaxation Data by i-Rheo Software and Fourier Transform Mechanical Spectroscopy. 242

E.1 A Graph Showing the Influence of Corn Trypsin Inhibitor on the Gel Time of Platelet Poor Plasma Detected by Small Amplitude Oscillatory Shear 243

List of Tables

4.1 Ability of Current Markers to Predict Poor Clinical Outcomes Resulting from Thrombolytic Intervention in Acute Ischemic Stroke Patients 138

4.2 Probability values for Correlations between Coagulation and Lysis Parameters Detected by Fourier Transform Mechanical Spectroscopy of Pooled Platelet Free Plasma with Varying Recombinant Tissue Plasminogen Activator Concentration. 146

4.3 Rho values for Correlations between Coagulation and Lysis Parameters Detected by Fourier Transform Mechanical Spectroscopy of Pooled Platelet Free Plasma with Varying Recombinant Tissue Plasminogen Activator Concentration. 146

4.4 Average values of Coagulation and Lysis Parameters Detected by Fourier Transform Mechanical Spectroscopy of Pooled Platelet Free Plasma with Varying Recombinant Tissue Plasminogen Activator Concentration. 147

4.5 Probability values for Correlations between Coagulation and Lysis Parameters Detected by Spectrophotometric Overall Haemostatic Potential Assay of Pooled Platelet Free Plasma with Varying Recombinant Tissue Plasminogen Activator Concentration. 149

4.6 Rho values for Correlations between Coagulation and Lysis Parameters Detected by Spectrophotometric Overall Haemostatic Potential Assay of Pooled Platelet Free Plasma with Varying Recombinant Tissue Plasminogen Activator Concentration. 149

4.7 Probability values for Correlations between Coagulation and Lysis Parameters Detected by Fourier Transform Mechanical Spectroscopy of Pooled Platelet Free Plasma with Varying Thrombin Concentration.156

4.8 Rho values for Correlations between Coagulation and Lysis Parameters Detected by Fourier Transform Mechanical Spectroscopy of Pooled Platelet Free Plasma with Varying Thrombin Concentration. . . . 157

4.9 Average values of Coagulation and Lysis Parameters Detected by Fourier Transform Mechanical Spectroscopy of Pooled Platelet Free Plasma with Varying Thrombin Concentration. 157

4.10 Probability values for Correlations between Coagulation and Lysis Parameters Detected by Spectrophotometric Overall Haemostatic Potential Assay of Pooled Platelet Free Plasma with Varying Thrombin Concentration. 161

4.11 Rho values for Correlations between Coagulation and Lysis Parameters Detected by Spectrophotometric Overall Haemostatic Potential Assay of Pooled Platelet Free Plasma with Varying Thrombin Concentration. 161

4.12 Average values of Coagulation and Lysis Parameters Detected by Spectrophotometry of Pooled Platelet Free Plasma with Varying Thrombin Concentration. 162

4.13 Probability values for Correlations between Coagulation and Lysis Parameters Detected by Fourier Transform Mechanical Spectroscopy of Pooled Platelet Free Plasma with Varying Streptokinase Concentration. 165

4.14 Rho values for Correlations between Coagulation and Lysis Parameters Detected by Fourier Transform Mechanical Spectroscopy of Pooled Platelet Free Plasma with Varying Streptokinase Concentration. . 166

4.15 Average values of Coagulation and Lysis Parameters Detected by Fourier Transform Mechanical Spectroscopy of Pooled Platelet Free Plasma with Varying Streptokinase Concentration. 166

4.16 Probability values for Correlations between Coagulation and Lysis Parameters Detected by Spectrophotometric Overall Haemostatic Potential Assay of Pooled Platelet Free Plasma with Varying Streptokinase Concentration. 171

4.17 Rho values for Correlations between Coagulation and Lysis Parameters Detected by Spectrophotometric Overall Haemostatic Potential Assay of Pooled Platelet Free Plasma with Varying Streptokinase Concentration. 171

4.18 Average values of Coagulation and Lysis Parameters Detected by Spectrophotometry of Pooled Platelet Free Plasma with Varying Streptokinase Concentration. 172

4.19 Probability values for Correlations between Coagulation and Lysis Parameters Detected by Fourier Transform Mechanical Spectroscopy of Pooled Platelet Free Plasma. 175

4.20 Rho values for Correlations between Coagulation and Lysis Parameters Detected by Fourier Transform Mechanical Spectroscopy of Pooled Platelet Free Plasma. 175

4.21 Probability values for Correlations between Coagulation and Lysis Parameters Detected by Rheometry of Whole Blood with a Fixed Concentration of Recombinant Tissue Plasminogen Activator and Varying Streptokinase Concentration. 180

4.22 Rho values for Correlations between Coagulation and Lysis Parameters Detected by Rheometry of Whole Blood with a Fixed Concentration of Recombinant Tissue Plasminogen Activator and Varying Streptokinase Concentration. 181

4.23 Average values of Coagulation and Lysis Parameters Detected by Spectrophotometry of Pooled Platelet Free Plasma with Varying Streptokinase Concentration. 181

5.1 Probability Values for Correlations between Unidirectional Shear Stress and Coagulation and Lysis Parameters Detected by Rheometry of Pooled Platelet Free Plasma. 197

5.2 Rho Values for Correlations between Unidirectional Shear Stress and Coagulation and Lysis Parameters Detected by Rheometry of Pooled Platelet Free Plasma. 198

6.1 Probability Values for Two-tailed Paired t-Test for Fixed Gap and Variable Gap Experiments. 215

List of Abbreviations

CLT	Clot Lysis Time.
CT	Clotting Time.
$FCLT$	Functional Clot Lifetime.
GT	Gel Time.
LT	Lysis Time.
$MOFM$	Moment of Free Movement.
OCP	Overall Coagulation Potential.
OFP	Overall Fibrinolytic Potential.
OHP	Overall Haemostatic Potential.
SP	Static Period.
dGT	de-Gel Time.
CloFAL	Clot Formation and Lysis.
CMT	Combined Motor Transducer.
CSPS	Controlled Stress Parallel Superposition.
ECLT	Euglobulin Clot Lysis Time.
FEGSEM	Field Emission Gun Scanning Electron Microscope.
FII	Factor II, Thrombin.
FIX	Factor IX.
FOR	Free Oscillation Rheometry.

FTMS	Fourier Transform Mechanical Spectroscopy.
FV	Factor V.
FVII	Factor VII.
FVIII	Factor VIII.
FX	Factor X.
FXI	Factor XI.
FXII	Factor XII.
FXIII	Factor XIII.
FXIIIa	Factor 13.
GFC	Global Fibrinolytic Capacity.
HDMS	Hexamethyldisilazane.
HMWK	High Molecular Weight Kininogen.
HT	Haemorrhagic Transformation.
KLB1	Kallikrein.
LVR	Linear Viscoelastic Region.
n	Number of replicates.
NHA	Novel Haemostasis Assay.
OWCh	Optimally-Windowed Chirp.
P-PFP	Pooled Platelet Free Plasma.
PAI-1	Plasminogen Activator Inhibitor 1.
PAI-2	Plasminogen Activator Inhibitor 2.
PAP	Plasmin-α2-antiplasmin.
PFP	Platelet Free Plasma.
Pgn	Plasminogen.
PK	Prekallikrein.
Pn	Plasmin.

PPP	Platelet Poor Plasma.
PRP	Platelet Rich Plasma.
PRP+i	Platelet Rich Plasma + Inhibitor (Tirofiban 10 μM).
PS	Phosphatidylserine.
rt-PA	Recombinant Tissue Plasminogen Activator.
SAOS	Small Amplitude Oscillatory Shear.
SEM	Scanning Electron Microscopy.
SMT	Separate Motor Transducer.
STP	Simultaneous Thrombin/Plasmin.
t-PA	Tissue Plasminogen Activator.
TAFI	Thrombin Activatable Fibrinolysis Inhibitor.
TEG	Thromboelastography.
TEM	Thromboelastometry.
TF	Tissue Factor.
TFPI	Tissue Factor Pathway Inhibitor.
u-PA	Urokinase.
VTE	Venous Thromboembolism.
vWF	von Wildebrand Factor.

Chapter 1

Introduction and Literature Review

Thrombosis is defined as a pathological condition in which a blood clot restricts flow through blood vessels. These blood clots, or thrombi, can form in either arterial or venous blood vessels and may induce blockage either at the site of formation, or through a process of fracture and embolisation resulting in the blockage of narrower vessels such as those within organs.[1] Thrombosis is recognised as a leading contributor to death and disability, encompassing several prominent conditions including stroke, pulmonary embolism, myocardial infarction, and deep vein thrombosis. These conditions carry high social and healthcare costs and are collectively responsible for the deaths of 1 in 4 people worldwide.[1,2] Advances in the analysis of clot formation and behaviour have significantly improved the detection of thrombosis in at risk patients and have driven our understanding of thrombosis pathology forwards. However, areas of our understanding, including the role of platelet driven clot contraction, require further investigation and treatment options remain associated with high risks highlighting the need for advancements in fibrinolytic assessment.[1]

1.1 Thrombosis Pathology

The first description of thrombosis was provided by a franciscan monk, Guillaume de Saint-Pathus, who reported the case of a Norman cobbler named Raoul under the care of Henri de Perche in 1271. The manuscript discloses Raoul's symptoms, which included oedema and pain in the calf spreading to the thigh, now recognised as characteristic of deep vein thrombosis. At the time, Henri de Perche was unable to reach a diagnosis and Raoul is reported to have visited the tomb of King Saint Louis, where he was miraculously healed after applying dust from the tomb directly to his leg.[3] Since this time, significant advances in medical science have enabled modern clinicians to quickly reach a diagnosis of thrombosis, and has provided more reliable treatment options for patients.

Haemostatic mechanisms allow the flow of blood to be limited following injury and result in the formation of clots at the site of damage. Disruption of these mechanisms can lead to thrombosis, wherein the blood clot formed causes blockage of blood vessels, resulting in reduced blood flow to the downstream vasculature.[4,5]

The clinical conditions associated with thrombosis are generally defined by the site of occlusion; where this occurs (i) in the legs it is known as deep vein thrombosis, (ii) in the heart as myocardial infarction, (iii) occlusion within the lungs is referred to as pulmonary embolism, and (iv) where vessel occlusion occurs in the brain it is known as stroke. Despite the differences in presentation and clinical outcomes amongst these conditions, the underlying pathophysiology is similar and relates to the same set of risk factors.

The risk of thrombosis is now understood to be largely related to the structure of the fibrin network formed during coagulation, since dense compact clots formed from thin fibrin fibres with multiple branch points are more difficult to dissolve by the process of fibrinolysis, and pre-dispose an individual to thrombotic events. The density of clot structure can be thought of as a spectrum, with very loose open structures composed of thick fibrin fibres at one end, and very dense tight clots formed from a fine mesh of thin fibrin fibres at the other, as illustrated in Figure 1.1. Clots tending towards the denser end of the spectrum, and associated with thrombosis, are less susceptible to lytic breakdown. This is due to the fact that the individual fibres have fewer binding sites for lytic agents, in addition to the structure being less permeable.[6–9]

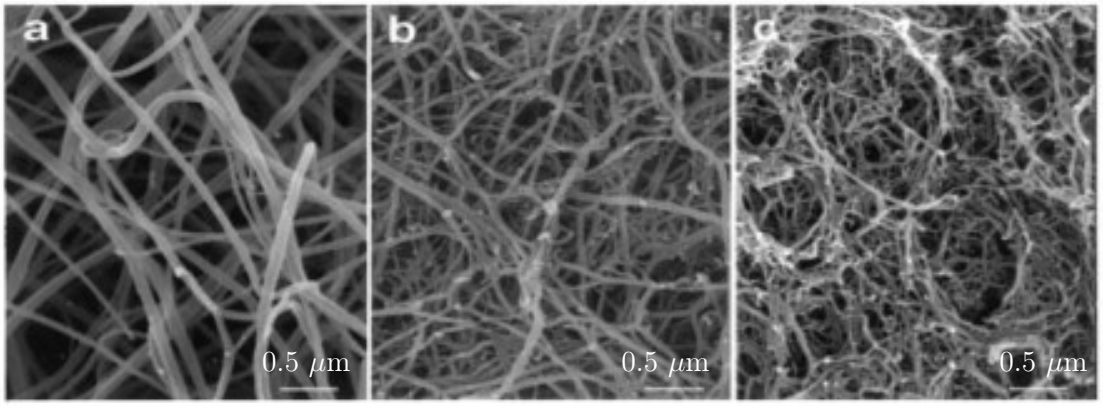

Figure 1.1: SEM Images of Fibrin Networks Illustrating Differences in Clot Microstructure[i].

(a) Open structure composed of thick fibres $\Longrightarrow$ (c) tight structure composed of thin fibres.

The origin of modern thrombosis theory can be traced back to 1856 when German pathologist Rudolph Virchow characterised the key factors that contribute to thrombosis risk, which are presented in Virchow's triad depicted in Figure 1.2. His work remains widely accepted and the triad, which was developed from his original descriptions following his death, is still considered the basis for thrombotic pathology in modern medicine.[1,10,11]

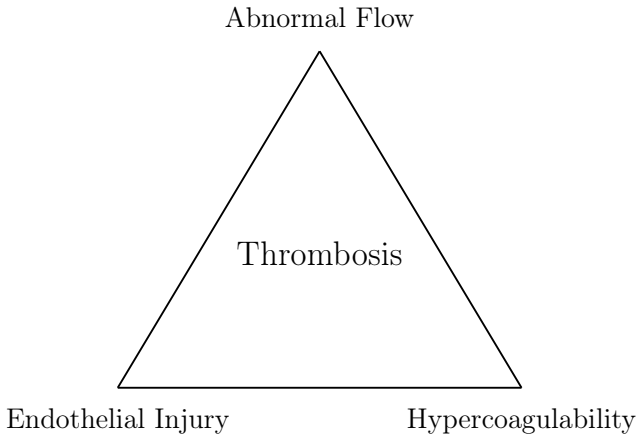

Figure 1.2: Virchow's Triad of Risk Factors Affecting Venous Thrombosis.

[i]Reprinted from Biophysical Journal, 77/5, Ryan EA, Mockros LF, Weisel JW and Lorand L, Structural Origins of Fibrin Clot Rheology, p2813-2826, Copyright (1999), with permission from Elsevier.

Endothelial Injury

Endothelial cell injury is a key trigger for coagulation, with irritation of the vessel lining leading to activation of the coagulation cascade and clot formation. Additionally, damage to these cells and the associated inflammatory stimulation results in downregulation of the production of coagulation inhibitors, reducing control over the clot formation process. The conversion of this typically anti-coagulant surface to a pro-coagulant site is considered to contribute to thrombosis risk, as any failures in the regulation of this process have the potential to contribute to pathogenic clot formation.[10,12,13]

Abnormal Flow

Turbulent flow is often caused by atherosclerotic plaques, leading to stenotic vessels, as well as branching of the blood vessels. Turbulence has been associated with many pathological conditions that result in increased blood flow or the hardening/narrowing of vessel walls, which inhibit laminar flow. Healthy laminar flow of blood obeys the Fåhræus–Lindqvist effect, which describes the way large blood components, such as cells, are concentrated in the centre of the lumen at the point of highest flow rate. When this flow becomes disturbed, platelets and other cellular components may contact the vessel wall leading to endothelial cell damage and localised pockets of stagnation can occur.[14–16]

In contrast, static or slow blood flow is often caused by long periods of inactivity, injury, and heart failure. This results in collection of blood around the valves and is of particular significance in deep vein thrombosis, where thrombus formation starts in the valve pockets of veins in the calf.[17] This stagnation also disrupts laminar flow, resulting in the deposition of blood components at the vessel wall. The low flow rate prevents the clearance/dilution of blood components including activated coagulation factors at the endothelial wall, promoting clot formation at inappropriate sites leading to an increased risk of embolisation.[15,16]

Hypercoagulability

Many coagulopathies have been shown to lead to an increased risk of thrombosis, either by reducing the influence of negative feedback mechanisms, or by enhancing the process of coagulation. The resultant changes during coagulation lead to rapidly generated clots which have a denser network structure, as associated with thrombosis further discussed in Section 1.2.[18]

1.2 Haemostasis

Human blood is a non-Newtonian fluid composed of ≈ 46 % solid material including cellular components, such as erythrocytes, leukocytes, and platelets. The cellular components of blood are suspended in the fluid phase known as the blood plasma which contains proteins, including those required for coagulation and fibrinolysis, ions, fats, and hormones as well as dissolved gases.[19]

Blood circulates freely around the body through a network of blood vessels supplying oxygen and critical molecules to organs and tissues. Accidents and injuries can lead to damage to blood vessels, and depending on the extent of the damage this can result in significant bleeding. Haemostasis is the process by which blood loss following injury is limited. This process is essential to maintaining healthy blood flow; however, inappropriate triggering of the haemostatic pathways can lead to extreme disease states such as thrombosis and disseminated intravascular coagulation.[4,5]

Damage to blood vessels involves the disruption of endothelial cells resulting in the exposure of collagen which is found below the endothelial layer, shown in Figure 1.3. Intact endothelial cells produce anticoagulant molecules such as thrombomodulin, as well as platelet aggregation inhibitors including nitric oxide and prostacyclin in order to prevent inappropriate coagulation. When endothelial cells become damaged they stop producing these inhibitory molecules and instead begin secreting von Wildebrand factor (vWF) which triggers haemostatic mechanisms. The exposed collagen acts as a binding site for platelets and stimulates the intrinsic pathway of coagulation discussed later in this chapter. Damage to the vessel wall can also lead to the exposure of smooth muscle cells which express tissue factor (TF) that is responsible for the activation of the extrinsic pathway of coagulation which is also discussed later in the present chapter.[4,12]

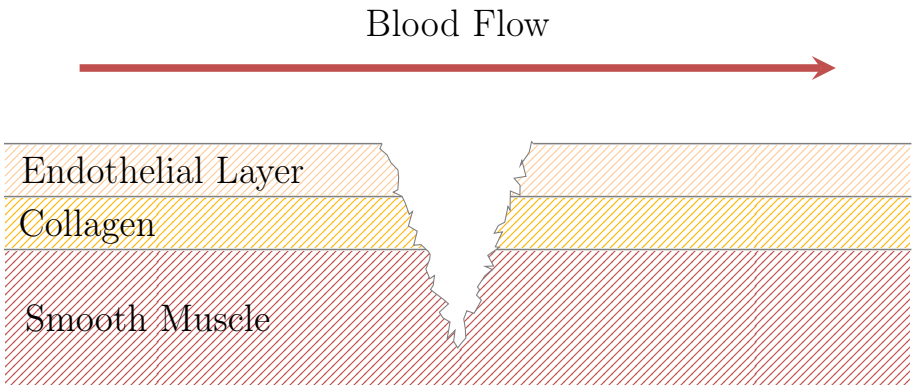

Figure 1.3: An Illustration Depicting Vascular Damage.

Haemostasis is considered to occur in three essential stages:

1. Vasoconstriction - Constriction of the blood vessels limits blood flow in the damaged region,
2. Platelet Plug Formation - Activated platelets immediately form a weak plug over the site preventing blood loss, and
3. Coagulation - The blood gels to form a clot composed of fibrin fibres which stabilises the plug and seals the wound until the damage is repaired.

This results in a stable clot forming over the wound site. During formation the clot undergoes contraction, where activated platelets pull on fibrin strands. The damaged tissue can then be repaired and finally, the clot is broken down through the process of fibrinolysis.[4]

1.2.1 Vasoconstriction

Vasoconstriction is the body's immediate response to damage where the vessel wall contracts to reduce blood flow at the site of injury. Vasoconstriction is initially triggered by local sympathetic pain receptors. As the process of haemostasis continues, thromboxane A2 as well as serotonin and ADP are released from α-granules secreted by activated platelets, maintaining vasoconstriction until bradykinin release during coagulation initiates vasodilation.[20]

Following the initial constriction of the blood vessels, platelets bind to the exposed collagen layer to form a plug over the wound site.[20,21]

1.2.2 Platelet Plug Formation

Platelets are cell like structures which lack nuclei and are derived from the cytoplasm of megakaryocytes. They have two primary states; activated and unactivated. Unactivated platelets are 2-3 μm biconvex disks which circulate freely in the blood, as shown in Figure 1.4 (a). Following adhesion to exposed collagen at the site of damage, platelets activate and undergo a conformational change which includes the localisation of organelles at the centre of the platelet. Cytoskeletal rearrangement during activation results in a structural transformation from biconvex disks to small spheres which have many surface protrusions (filopodia), shown in Figure 1.4 (b). This activation is inhibited by both prostacyclin and nitric oxide which are generated by healthy endothelial cells, while activation is enhanced by exposure to vWF released by damaged endothelial cells.[21,22]

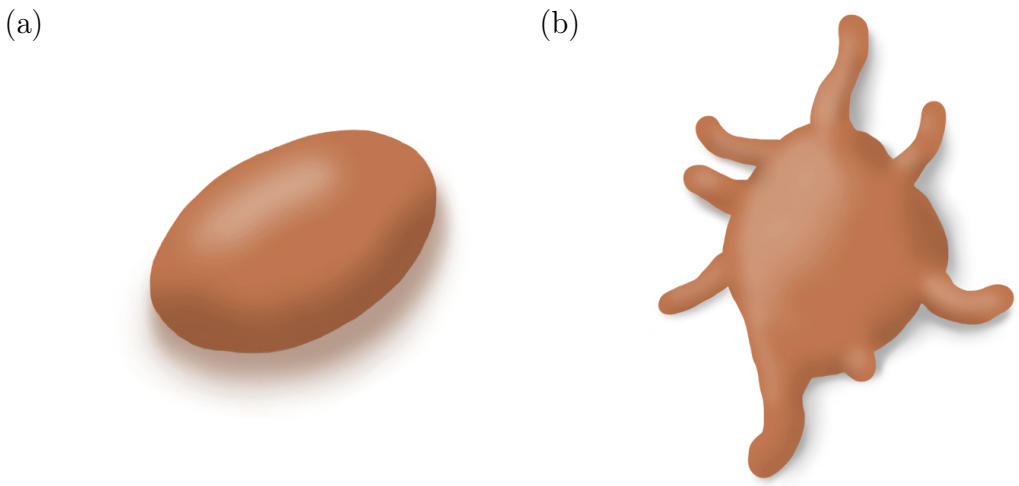

Figure 1.4: Illustrations Depicting an Unactivated and Activated Platelet.

(a) Unactivated platelet and (b) activated platelet.

During activation phosphatidylserine (PS), which is usually present on the cytoplasmic face of the platelet membrane, becomes exposed on the platelet surface where it enhances coagulation by interacting with several coagulation factors. Platelets additionally release α-granules during activation which contain a range of pro-coagulant factors. Both PS and α-granules enhance the aggregation of platelets to form a platelet plug which covers the wound and limits blood flow out of the vessel.[23]

The platelet plug is then stabilised by a fibrin network which is formed as a result of coagulation.[4]

1.2.3 Coagulation

Coagulation is the process by which blood gels to form a network of fibrin fibres which strengthen and seal the platelet plug formed over a wound. This occurs through the systematic activation of zymogens which ultimately leads to the formation of fibrin polymers.[4]

The coagulation cascade, also known as the waterfall model, originated from the work of Davie and Ratnoff in 1964[24] and is still the most widely accepted description of coagulation. However, several journal articles have shown the model to be insufficient in describing *in-vivo* events. Since the model was proposed from *in-vitro* experiments it remains an accurate descriptor for many experimental and diagnostic systems despite lacking the consideration of physiological factors. As such, support for a newer cell-based model is growing to explain the process of coagulation *in-vivo*.[24–28]

The Coagulation Cascade

The coagulation cascade is typically described as occurring through three distinct pathways:

- The Intrinsic or Contact Activated Pathway,
- The Extrinsic or Tissue Factor Pathway, and
- The Common Pathway.

However, these pathways are not independent and act in unison as a single system, perpetuating and feeding back into each other.[25,27]

The Intrinsic Pathway

The intrinsic pathway, otherwise known as the contact activation pathway, is triggered when blood components come into contact with the exposed collagen layer that is revealed by damage to the endothelial layer. This pathway can also be activated by contact with foreign surfaces and is particularly influenced by negatively charged particles, for example glass. This pathway is also the mechanism by which coagulation is induced by low temperatures and is a factor that must be considered in the storage and handling of blood plasma.[29,30]

The intrinsic pathway, depicted in Figure 1.5 occurs as follows. Factor XII (FXII) adheres to collagen and undergoes auto activation (FXIIa) - the mechanism by which this occurs is complex and not fully understood.[31] The presence of FXIIa leads to a prekallikrein (PK) - high molecular weight kininogen (HMWK) - factor XI (FXI) complex. HMWK is thought to be the main surface contact point for this complex and other factors and co-factors are brought into proximity by surface bound HMWK.[32–36]

Within this complex, PK is activated to form plasma kallikrein (KLB1) by FXIIa. KLB1 is released from the complex and triggers the reciprocal activation of further FXII. Free KLB1 in combination with FXIIa induces bradykinin liberation through the cleavage and activation of HMWK, which initiates vasodilation and increases vascular permeability.[37,38] KLB1 also cleaves α-FXIIa to form β-FXIIa which activates the complement system of the innate immune response leading to inflammation of the wound.[39]

Following this, interaction between FXIIa and HMWK activates factor XI (FXI - FXIa) which then combines with Ca^{2+} ions present in the blood, as well as PS on the surface of activated platelets, to activate factor IX (FIX - FIXa) which feeds into the common pathway at a low rate. Following the initial slow activation of the common pathway, a feedback loop is triggered catalysing the activation of factor VIII (FVIII - FVIIIa) which then forms a complex with FIXa referred to as 'factor X activating factor' or 'tenase'. This activated complex stimulates the common pathway at a much higher rate than FIXa alone.[40]

This pathway is inhibited by antithrombin which degrades FXIIa, FXIa and FIXa as well as factor X (FXa) and factor II (FIIa, thrombin) of the common pathway. Antithrombin has a constant activity; however, its action is enhanced by the presence of heparins which are known to act as anti-coagulants.[41]

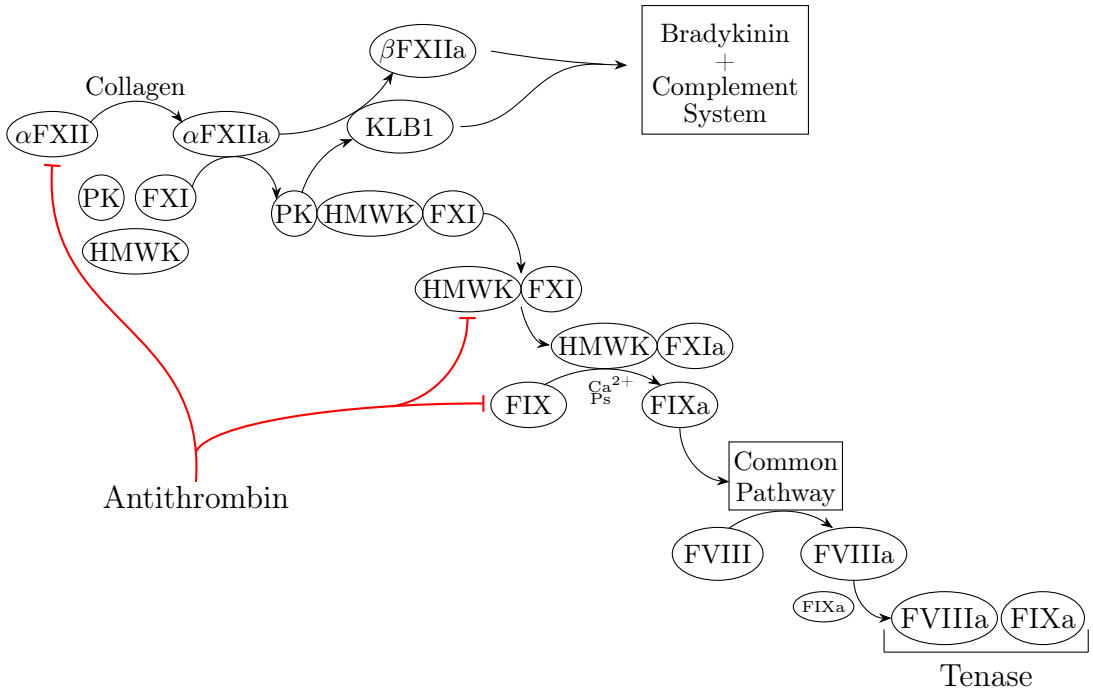

Figure 1.5: A Representation of the Intrinsic Pathway of Coagulation.

The Extrinsic Pathway

The extrinsic pathway, or the tissue factor pathway, is initiated by cellular damage and leads to more rapid clot formation than the intrinsic pathway. The extrinsic pathway which generates a 'thrombin burst' to quickly initiate clot formation is thought to be the main contributor to *in-vivo* coagulation.[42]

This pathway, illustrated in Figure 1.6 is initiated by tissue factor (TF), a transmembrane glycoprotein expressed by the smooth muscle cells found just below the vascular endothelium. Damage to the endothelial layer leads to the exposure of these cells to the vessel lumen and allows contact between TF and its circulating ligand, factor VII (FVII), which upon binding becomes activated (FVIIa) forming a complex on the cell surfaces. This complex activates FIX (of the intrinsic pathway) and directly stimulates the common pathway. Factors from the common pathway feedback to enhance FVII activation.[43]

Although coagulation and inflammation are often considered as separate systems, the pathways are highly integrated and bi-directional. During inflammation and sepsis, TF presentation by endothelial cells and circulating monocytes and macrophages is induced by inflammatory cytokines released upon exposure to endotoxin. This triggers the extrinsic pathway of coagulation during infection and inflammatory stimulation, and in the case of sepsis can lead to disseminated intravascular coagulation.[44,45] The reciprocal interaction also oc-

curs, during extrinsic coagulation the TF-FVIIa complex additionally triggers the release of inflammatory cytokines and chemokines, promoting inflammation under pro-coagulatory conditions.[46] The vascular endothelium is also activated by vasoconstrictive agents involved in the immune response, leading to the release of coagulation enhancers including vWF which also interacts with leukocytes to stimulate local inflammatory responses.[44,45]

The extrinsic pathway is regulated by the tissue factor pathway inhibitor (TFPI) which is produced by both unactivated platelets and healthy endothelial cells, suppressing thrombin generation by inhibiting FX of the common pathway as well as the TF-FVIIa complex.[47]

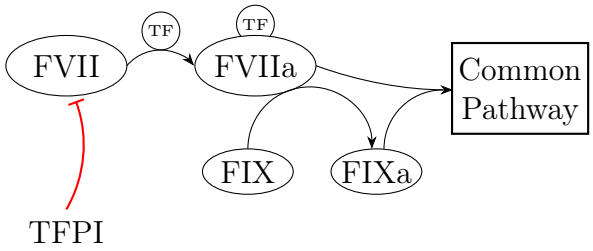

Figure 1.6: A Representation of the Extrinsic Pathway of Coagulation.

The Common Pathway

Both FIXa and tenase from the intrinsic pathway and the TF-FVIIa complex formed as a result of the extrinsic pathway activate FX - FXa, which is the first step in the common pathway depicted in Figure 1.7. FXa is localised on the negatively-charged surface of activated platelets and converts prothrombin (FII) to thrombin (FIIa), requiring PS, Ca^{2+}, and factor V (FV). FIIa has four key functions; it cleaves fibrinogen molecules into fibrinopeptides which polymerise to form fibrin strands, it activates factor XIII (FXIII) which is responsible for cross linking the fibrin strands to generate a stable network, it contributes to continued platelet activation, and activates protein C.[48]

Protein C is an inhibitor of coagulation which is activated by FIIa when bound to the endothelial cell surface protein thrombomodulin. Protein C in combination with protein S and PS degrades FV of the common pathway, as well as FVIIIa of the intrinsic pathway, halting coagulation.[49]

The common pathway also interacts with inflammatory pathways, with thrombin able to induce interleukin production by endothelial cells through protease-activated receptors 1,3, and 4. The coagulation inhibitor protein C also has an anti-inflamatory action, reducing tumour necrosis factor-α production.[44]

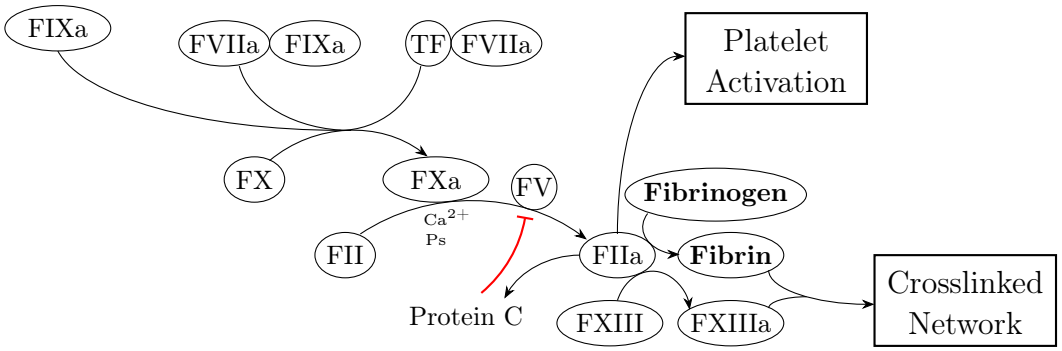

Figure 1.7: A Representation of the Common Pathway of Coagulation.

Cell Based Coagulation

The cell based model of coagulation differs from the coagulation cascade model in that it proposes that coagulation is primarily governed not by circulating coagulation factors, but rather by exposure to cell surfaces; although, it also defines coagulation as happening in three phases:

- Initiation, occurring on a tissue factor bearing cell,
- Amplification, where coagulation factors and platelets are activated, and
- Propagation, where thrombin generation occurs on platelet surfaces.[50]

Initiation

In the cell based model coagulation is initiated on smooth muscle cells which expose blood to TF. If a strong enough stimulus is present then enough FXa, FIXa and FIIa are activated to *initiate* coagulation.[50]

Amplification

In the amplification phase of coagulation platelets adhere to the site of damage and are activated. This leads to the accumulation of activated coagulation factors at the platelet surface and the *amplification* of coagulation occurs.[50]

Propagation

During the propagation phase of coagulation active proteases accumulate on the platelet surface which *propagate* a thrombin burst and the polymerisation of fibrin.[50]

1.2.4 Fibrin Network Formation

The fibrin network is formed primarily through the action of thrombin (FIIa) and Factor XIIIa on fibrinogen. Fibrinogen is cleaved by thrombin to form the active monomer fibrin following activation of the coagulation cascade discussed in Section 1.2.3. These fibrin monomers then polymerise to form protofibrils. FXIIIa acts upon these protofibrils to allow the formation and branching of the fibrin fibres into a stable network.[51]

Fibrinogen is a hexameric glycoprotein which circulates within the blood typically at a concentration of 2.8 ($\pm$0.6) mg/ml. It is composed of two of each of the three subunit types (α, β and γ) which are assembled within the endoplasmic reticulum. The subunits are arranged as shown in Figure 1.8 as a thin flexible fibre having three nodes. The D domains make up the two external nodes and are composed of one each of the C-terminal domains of β and γ subunits as well as containing a portion of the α subunit, with the αC domain protruding from the structure. The central E node is comprised of the N-terminal domains of all six subunits connected to the D nodes by a flexible linker.[52–54]

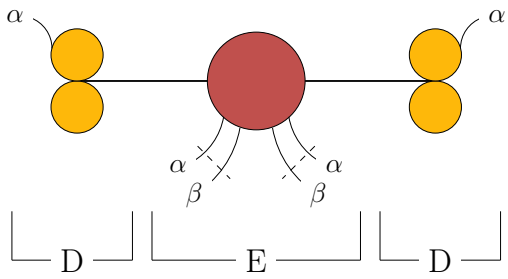

Figure 1.8: A Schematic Representation Showing the Structure of a Fibrinogen Monomer.

Binding domains from the α and β subunits protrude from the E domain. Thrombin is able to cleave these exposed N-termini sites which allows association with and binding to the D domain of neighbouring fibrin molecules as depicted in Figure 1.9.[52,54]

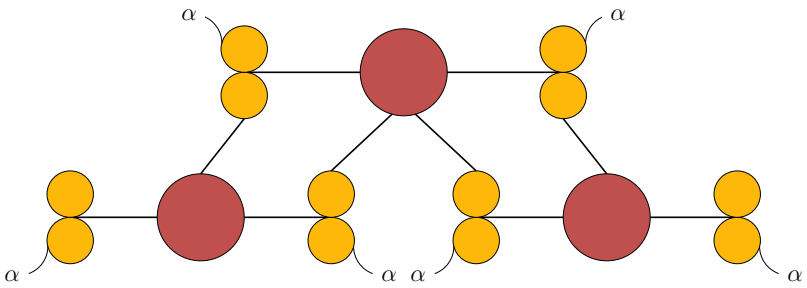

Figure 1.9: A Schematic Representation of Fibrin Undergoing Polymerisation.

The structure is then stabilised by FXIIIa which enables the cross linking of fibrin protofibrils through the formation of γ-glutamyl-ϵ-lysyl amide cross links between the exposed αC domains as well as the γC domains. This effectively joins the two D domains of neighbouring fibrin units end to end stabilised through the E domain of an adjacent molecule as shown in Figure 1.10.[55]

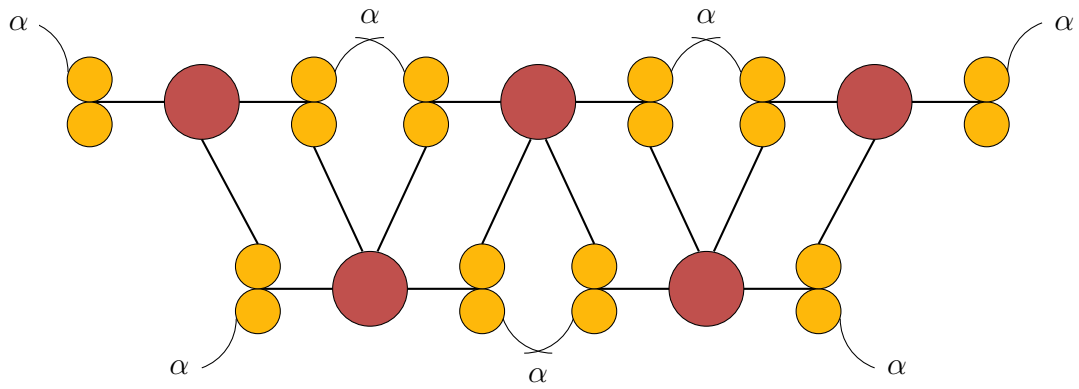

Figure 1.10: A Schematic Representation of Cross-linked Fibrin Polymers.

The branching of fibrin fibres is necessary for the formation of a functional 3-D network which has the appropriate biophysical characteristics to perform haemostasis. However, thin fibres with many branch points are associated with thrombosis pathology. The majority of branch points within fibrin networks appear as an intersect of three fibrin fibres of consistent diameter and are believed to result from the divergence of protofibrils during fibre formation.[56]

Both genetic and environmental factors can influence the structure of the clot, although most mechanisms ultimately influence the concentration of fibrinogen, the interactions of the fibrin fibres, or the rate of thrombin generation. Some key factors include age, diabetes, the use of non-steroidal anti-inflammatory drugs and heritable coagulopathies. The local concentration of thrombin greatly influences the structure of the formed clot. Lower thrombin concentrations typically

lead to the formation of a loose network formed from fewer thick fibrin fibres with few branch points shown previously in Figure 1.1 (a),[57] while higher concentrations of thrombin lead to denser clots formed from many thin fibrin fibres with several branch points shown in Figure 1.1 (c).[51,57]

1.2.5 Clot Contraction

During the formation of a fibrin clot, activated platelets within the network begin applying tension to individual fibrin fibres drawing them towards the platelet. This results in the formation of platelet-fibrin bundles and the alignment of fibrin fibres along the axis of applied tension. The action of platelets on the fibres causes a decrease in the bulk surface area of the clot which is referred to as clot contraction.[58]

Clot contraction has been shown to occur in three distinct phases. Phase one of contraction is an initial exponential relationship which is dependent on the ratio of fibrin to platelet concentration. Phase two is identified by a linear rate of contraction and is substantially altered by the presence of erythrocytes, which reduce the contractile forces generated during this phase. Phase three is a final exponential phase, induced when the contractile forces overcome the resistance inferred by erythrocytes, and is dependent on the action of FXIIIa during crosslinking.[59]

During platelet mediated contraction the filopodia, which extend from the body of activated platelets, stretch along a fibrin fibre before the filopodia tip adheres to the fibre. The tip of the filopodia relies on the transmembrane integrin αIIbβ3 (glycoprotein IIb/IIIa) to provide a link between extracellular fibrin and the intracellular contractile cytoskeleton.[60,61] The internal contractile ability of platelets is provided by actin and myosin structures within the platelet interior, the action of which are analogous to smooth muscle contraction.[62] The action of this contractile system results in retraction of the filopodia which pulls the fibrin fibre towards the platelet body. As the fibre is drawn towards the platelet from the tip of the filopodia a kink forms in the fibre, this series of events is depicted in Figure 1.11. The fibre then remains attached to the platelet body as further filopodia extend and retract drawing a bundle of fibrin in a hand over fist mechanism towards the platelet body.[61]

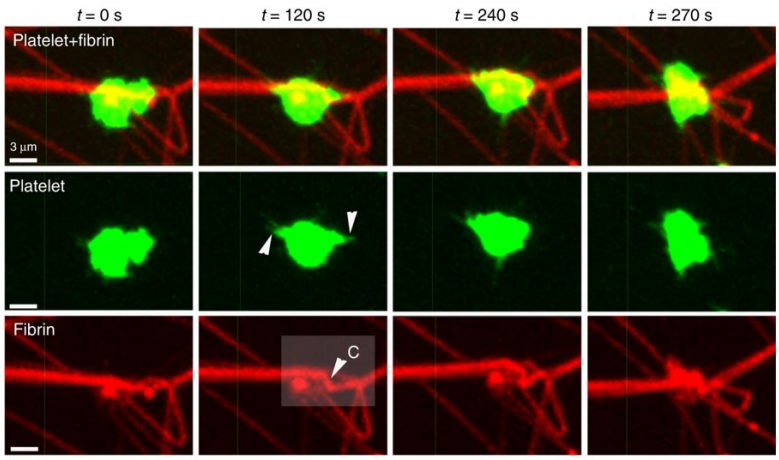

Figure 1.11: A Series of Confocal Images Depicting the Mechanism of Platelet Action on Fibrin Fibres Clot Contraction[ii].

Arrows identify the extension of platelet filopodia, while c identifies the formed fibre kink.

In 2018 Peshkova *et al.* investigated the extent of clot contraction in patients following venous thromboembolism (VTE). The research involved taking scanning electron micrograph (SEM) images of clots extracted from patients by thrombectomy, as well as the optical tracking of blood clots and measurement of standard laboratory markers for coagulation and platelet activation. The research found that the clots underwent intravital contraction *in-vivo* as shown by SEM images of the extracted clots. The study reported a significant reduction in the extent of clot contraction in VTE patients as compared to healthy controls. This reduction was attributed to platelet exhaustion, owing to the observed reduction in induced platelet activation for this group. When the subtypes of VTE were examined the research showed a significantly reduced level of clot contraction in patients who had experienced pulmonary embolism compared with those who had experienced deep vein thrombosis, indicating a potential role for clot contraction in the predisposition to fracture and embolisation. As a result Peshkova *et al.* proposed a potential mechanism for the formation of pathogenic clots which is depicted in Figure 1.12.[63] Clot contraction has also been shown to increase the rate of clot lysis, suggesting that it may play a role in the resistance to lysis observed in thrombosis patients.[64]

[ii]Reprinted from Nature Communications, 8/1274, Kim OV, Litinov RI, Alber MS and Weisel JW, Quantitative structural mechanobiology of platelet-driven blood clot contraction, Copyright (2017) Springer Nature.

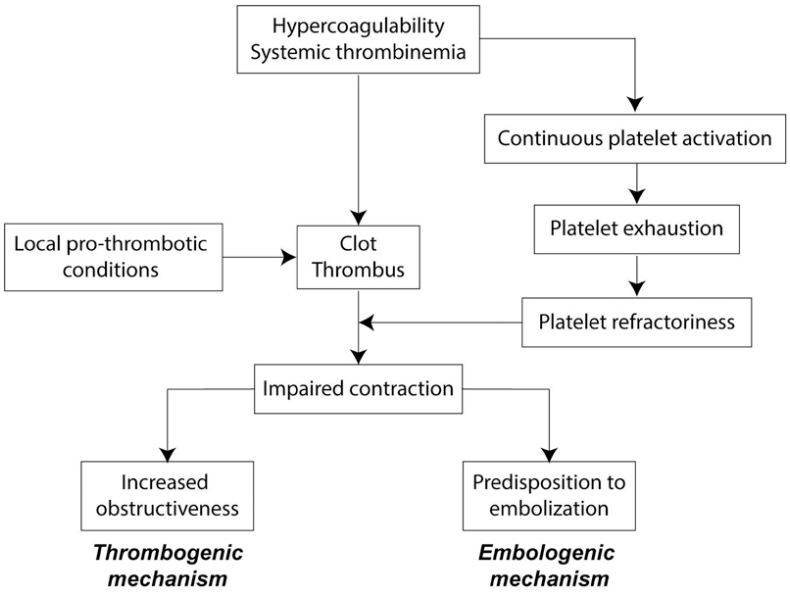

Figure 1.12: The Method for Pathogenic Clot Formation Proposed by Peshkova *et al.*[iii].

1.2.6 Fibrinolysis

Fibrinolysis is the process by which a blood clot is broken down when it is no longer required. There are two types of fibrinolysis; primary, which represents the normal physiological process of clot dissolution that happens within healthy vessels, and secondary, which represents the pathological or therapeutic breakdown of blood clots.[65]

The pathway for fibrinolysis is shown in Figure 1.13 and involves the plasmin (Pn) mediated breakdown of the fibrin network. The inactive precursor to Pn, plasminogen (Pgn), is found circulating freely in the plasma and, due to its high affinity for fibrin, binds to fibres during coagulation becoming incorporated into the clot.[66]

[iii]Reprinted from TH Open, 02/01, Peshkova AD, Malyasyov DV, Bredikhin RA, Minh GL, Andrianova IA, Tutwiler V, Nagaswami C, Weisek JW and Litvinov RI, Reduced Contraction of Blood Clots in Venous Thromboembolism Is a Potential Thrombogenic and Embologenic Mechanism, e104-115, Copyright (2020) Georg Thieme Verlag KG.

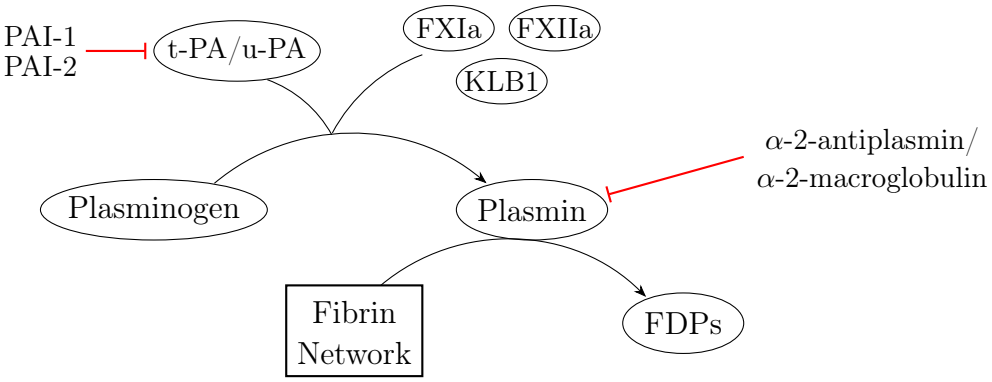

Figure 1.13: A Representation of the Fibrinolytic Pathway.

In primary fibrinolysis, Pgn is converted into the active Pn primarily by tissue plasminogen activator (t-PA) although it is also influenced by FXIa, FXIIa and KLB1 of the coagulation cascade. Pgn is also activated by urokinase (u-PA) which is produced by monocytes, macrophages and the urinary epithelium. The primary source of t-PA is intact endothelial cells, from which it is slowly released into the blood vessels. This limits clot growth, and over the course of several days leads to breakdown of the clot. The activation of Pgn by t-PA forms a feedback loop wherein activated Pn acts upon t-PA increasing its affinity for fibrin/Pgn as well as its catalytic efficiency.[66]

t-PA is inhibited by plasminogen activator inhibitor 1 (PAI-1) and plasminogen activator inhibitor 2 (PAI-2) which irreversibly inhibit the action of t-PA and promote its clearance by the liver, while active Pn is inhibited by α2-antiplasmin and α2-macroglobulin. α2-macroglobulin is only associated with Pn inhibition in pathological conditions and α2-antiplasmin is considered to be the main *in-vivo* inhibitor.[66,67] α2-antiplasmin is released by platelets and acts on circulating Pn; however, the fibrin network surrounding the clots surface protects clot bound Pn from its action.[66] The cleavage of fibrin strands by Pn is inhibited by thrombin activatable fibrinolysis inhibitor (TAFI) which removes a portion of the C-terminus of fibrin associated with Pgn activation.[66]

Secondary fibrinolysis, which represents clinical conditions associated with inappropriate fibrinolysis as well as therapeutically enhanced fibrinolysis, occurs following the same pathway as primary fibrinolysis, where therapeutic intervention may contribute to enhancement of any stage of the pathway dependent on the agent selected for use. Secondary fibrinolysis is associated with two opposing conditions, which relate to the over stimulation of fibrinolysis in hyperfibrinolysis, and failure of the system to effectively break down fibrin networks known as fibrinolysis shutdown.[68,69]

Hyperfibrinolysis

Hyperfibrinolysis is associated with the over activity of the fibrinolytic system resulting in the premature breakdown of fibrin clots. This condition usually presents clinically as diffuse bleeding that is resistant to intervention. Studies have found that trauma patients displaying hyperfibrinolysis have an increased mortality rate of 44-82 %, with the majority of deaths resulting from exsanguination.[69–71] In thrombosis patients receiving fibrinolytic therapy this is a risk associated with overdose, and is of particular concern for stroke patients where fibrinolytic therapy is associated with a high risk of cerebral haemorrhage.[72–74]

Fibrinolysis Shutdown

In contrast to hyperfibrinolysis, fibrinolysis shutdown is the failure of the fibrinolytic system to effectively limit coagulation and clear fibrin within an appropriate period. Fibrinolysis shutdown is associated with multi-organ failure, believed to be caused by inappropriate fibrin deposition, and intravascular coagulation.[69] This extreme state is not known to be a side effect of therapy; rather, in thrombosis patients, failure of the stimulated fibrinolytic system to clear the occluding clot may lead to further and potentially irreversible damage as a result of prolonged ischemia.

The process of fibrinolysis is thought to be substantially influenced by the aggregation of platelets, as well as contraction of the clot. This is partially due to the production of PAI-1 by platelets, and the local thrombin concentration around platelet aggregates leading to a local increase in fibre thickness. Contraction of the clot also reduces the fluid phase within the clot, and as a result reduces the available concentration of Pgn, as well as limiting permeation.[64,75] The rate of fibrinolysis is also dependent on the fibrin network microstructure; although thin fibrin fibres can be cleaved more rapidly than thicker fibres, thinner fibrin fibres have been shown to have fewer exposed binding sites available for both t-PA and Pgn. Additionally, in clots containing thicker fibres with the same concentration of fibrinogen there are fewer fibres per unit volume. This means that despite thicker fibres taking longer to break down individually, the overall dissolution of the clot occurs faster, as determined by research conducted by Wolberg *et al.* using purified fibrin-thrombin systems.[51,76]

While it is generally accepted that clot structure profoundly influences the risk of thrombosis and rate of rt-PA induced fibrinolysis, where higher density clots are more resistant to lysis than their porous counterparts in model systems, this is not always true in a physiological context. A recent study of clot structure and lytic efficiency in systemic lupus erythematosus has revealed an unexpected relationship. The 2019 study by Litvinov *et al.* has shown that despite a substantial increase in thrombosis risk, systemic lupus erythematosus patients display more porous clots composed of thicker fibres than healthy counterparts. However, these open networks were found to be more structurally rigid than healthy clots which is consistent with an increased propensity to embolise. This was reported to be a result of an increased level of cross-linking, generating fibres which were individually stiffer than their thinner counterparts. The work proposes a further four additional mechanisms which may be involved in the behaviour of these fibres: elevated fibrinogen concentration, elevated phosphorylation of the fibres, a reduction in thrombin activity, and the adherence of plasma proteins such as albumin to the fibres providing structural support. As expected, these open clots were more susceptible to rt-PA induced lysis than the healthy controls. In patients in remission, clot microstructure was found to revert to a healthy-like state; however, these clots still displayed a substantially increased susceptibility to lysis.[77]

Although it is known that network architecture does play a significant role in resistance to lysis, the work by Litvinov *et al.* suggests that FXIIIa cross-linking may play a larger role in the pathological behaviour of clots than previously thought.[56,77] This may be due to the fact that exposure of αC regions of fibrin provides access to further t-PA binding sites. Furthermore, lysis has been shown to be impeded in fibres which are not under mechanical strain because access to plasmin binding sites is limited when fibres are lax.[78] Therefore the increased stiffness of the individual fibres observed during systemic lupus erythematosus recovery may result from individual fibres maintaining their structure during the initial stages of breakdown, leaving the additional plasmin binding sites exposed.

In addition to the structural element, thrombosis patients have been shown to have higher concentrations of PAI-1 and display resultant longer lysis times. It is worth noting that in this context, the rate of fibrinolysis was also found to correlate with both stiffness and clot architecture.[79]

In imaging studies, the movement of t-PA through the clot is often seen as a lysis front dissolving the clot from the edges inwards, this is a result of external t-PA being applied to a fully formed clot where permeation through the structure is necessary. In a physiological context constantly circulating t-PA is considered to be present within the network and breakdown of the fibrin network appears to occur in two distinct phases; the network is initially broken down into large 3-D fragments of fibres, which then slowly dissolve. The clusters of fibrin surrounding platelets as a result of clot contraction are particularly resistant to lysis, and are often seen to be a product of intermediary clot lysis.[56]

It has been previously shown that platelet contraction inhibitors increase the rate of fibrinolysis, thought to be caused by increased permeability of uncontracted networks allowing greater access for rt-PA to platelet dense regions of the clot.[56] Where pre-formed contracted and uncontracted clots were subjected to perfusion with rt-PA by Sutton *et al.*, it was again found that the contracted clots were less susceptible to lysis by rt-PA.[80] However, the most recent experimental work, performed by Tutwiler *et al.* in 2019, indicates that when structurally dense whole blood clots are generated through the addition of thrombin the clots remain susceptible to external lysis after contraction, and impairing contraction through the addition of inhibitors results in longer lysis times. While for internal lysis, platelet mediated contraction was found to increase the proximity of fibres, which increases the local rt-PA to fibrin ratio, and as a result increases the rate of lysis.[64]

The abnormal clot structure associated with thrombosis is generally more resistant to lysis than that of healthy clots.[51,76] However, the complex nature of this relationship coupled with variation in network architecture between patients suggests that the selection of an optimum dosage of thrombolytic therapy, based on the assessment of individual clot characteristics, could be beneficial, since disruption of the fibrinolytic pathway can lead to further pathophysiological conditions. The current gold standards for monitoring the interplay between coagulation and fibrinolysis are thromboelastometry and thromboelastography; however, these techniques have come under significant criticism, discussed further in Section 1.3.1. It is one of the aims of this research to build evidence for a new biomarker which, in the future, may be capable of predicting this optimum dose in a step towards personalised medicine.

1.2.7 Current Fibrinolytic Biomarkers

Clinicians currently have access to a wide range of fibrinolytic biomarkers, most of which are standard laboratory assays and rely on monitoring a single component of the fibrinolytic system, and so the clinical benefits of these tests are limited. A more appropriate approach than determining the concentrations or activities of individual lytic factors is needed and there is a drive to develop and improve global fibrinolytic biomarkers.[81] *In-vivo*, the components of the lytic system are continuously generated and lysis is prevented by the presence of an excess of inhibitors which become depleted, or are prevented from action around a thrombus allowing breakdown to occur. This mechanism complicates the development of fibrinolytic biomarkers, as these inhibitors are present in *in-vitro* blood samples, and so direct evidence of lysis in whole blood or plasma cannot be achieved without sample modification.[82,83]

The ideal fibrinolytic assay is able to detect both hypofibrinolytic conditions and hyperfibrinolytic conditions. In order to satisfy both of these targets, the biomarker must be sensitive enough to detect hypofibrinolytic conditions while avoiding the addition of high concentrations of exogenous activators such as rt-PA, or activation of the intrinsic pathway of coagulation, so that hyperfibrinolytic conditions are not masked. Additionally, a robust test that is able to monitor the interplay between coagulation and fibrinolysis would be desirable.[81,82]

Plasmin-antiplasmin Complex Assay

α2-antiplasmin is the primary inhibitor of Pn *in-vivo* and has a strong affinity for unbound Pn. *In-vitro*, the presence of α2-antiplasmin prevents the direct detection of plasmin action; however, the presence of the plasmin-α2-antiplasmin (PAP) complex is evidence that the activation of Pgn to Pn has occurred, and that lysis is taking place *in-vivo*. This test is typically an immunoassay and several commercial kits are available.[84] There are few clinical applications for this assay outside congenital deficiencies, as the PAP complex is not considered to be a rate limiting factor in fibrinolysis, typically circulating at high concentrations.[81]

D-dimer Assays

D-dimer is a fibrin degradation product generated during clot lysis, consisting of two D domains and one E domain of fibrin originating from two fibrin monomers which have been cross linked and broken down, as shown in Figure 1.14. Since D-dimer cannot be formed from intact fibrinogen, the presence of D-dimers in the blood is a strong indication that both clot formation and lysis have taken place, with D-dimer concentration being directly detected by immunoassay.[85]

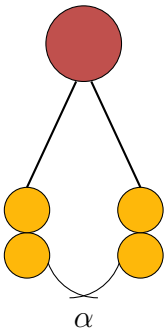

Figure 1.14: A Schematic Representation of a D-Dimer Fibrin Degradation Product.

The detection of D-dimer in patient samples is often used as an early clinical test to rule out thromboembolism as the absence of D-dimer in the blood suggests that the patient has no thrombi. Whilst D-dimer can be used to rule out thromboembolism and other related pathologies, its presence is not sufficient evidence of a pathogenic state and further diagnostic tests are required to establish pathology.[85]

A complementary D-dimer assay is also available involving the exposure of a patient's plasma to a plasminogen-free fibrin clot with the addition of rt-PA. In this assay, known as the global fibrinolytic capacity (GFC) assay, fibrinolysis is halted after a period of incubation through the addition of aprotinin, the D-dimer concentration is then measured and compared to the initial D-dimer concentration of the plasma. This provides insight into the patient's fibrinolytic efficiency.[86,87]

Alternatively, the GFC assay may be performed in whole blood through the addition of excess thrombin, which causes the blood to clot rapidly stabilising the fibrinolytic pathways. A control test is run on a sample containing aprotinin and the difference in D-dimer concentration is used to provide evidence of fibrinolytic efficiency.[88]

Turbidity and Fluorometric Assays

Several assays are available which utilise spectrophotometric turbidity and fluorometric measurements including the overall haemostasis potential (OHP) assay, the clot formation and lysis assay (CloFAL), and the simultaneous thrombin/plasmin (STP) assay and novel haemostasis (NHA) assays.

The OHP assay is one of the most commonly used coagulation and fibrinolysis assays. For the test, two turbidity measurements are performed on citrated blood plasma treated with either thrombin or TF with and without the addition of rt-PA. The absorbance curve for the sample is measured at 405 nm and allows a number of values to be calculated including the clotting time, the time to 1/2 absorbance during clotting, and clot lysis time, defined as the time from 1/2 absorbance during clotting to 1/2 absorbance during break down as shown in Figure 1.15. Additionally, the area under the curve detected with the addition of rt-PA indicates the overall haemostatic potential (OHP), while the area under the curve of samples without rt-PA represents the overall coagulation potential (OCP). The difference between these values indicates the overall fibrinolytic potential (OFP).[81,89]

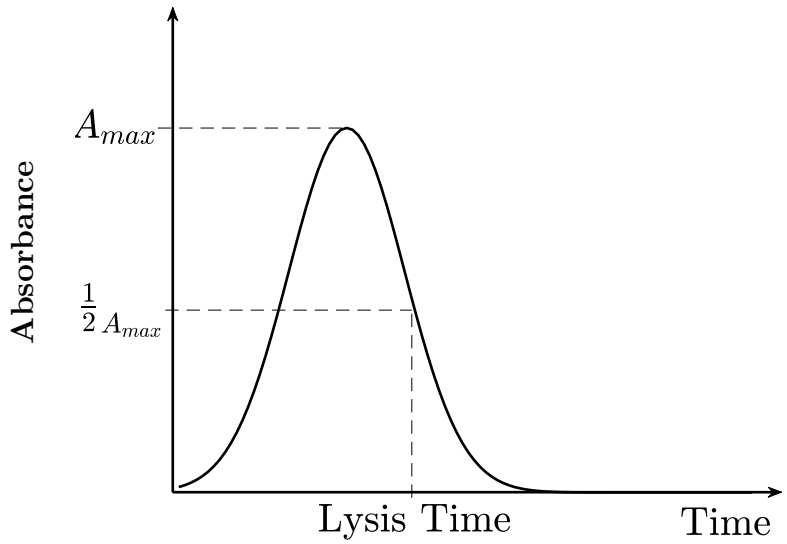

Figure 1.15: A Graph Illustrating a Typical Output from an Overall Haemostasis Potential Assay.

The CloFAL assay is also a spectrophotometric assay whereby lipidated TF, trace $CaCl_2$ and rt-PA are added to citrated blood plasma in order to trigger the formation and lysis of clots. The absorbance curve is plotted and the clot lysis time can be defined in several ways; however, as with other spectrophotometric tests clot lysis times are arbitrarily defined.[90]

Both the STP and NHA assays rely on fluorometric techniques where platelet poor plasma is mixed with fluorometric substrates for both thrombin and plasmin. In STP, the substrates are added into separate wells of a microplate, while in NHA the substrates are added in the same well but utilise separate excitation and emission wavelengths. These tests provide thrombin and plasmin generation curves from which both coagulation and fibrinolytic potentials can be determined.[91,92]

Euglobulin Assays

Euglobulin is a fraction of blood plasma which is isolated through acidification and precipitation of patient blood samples. Globulins, including coagulation and fibrinolytic proteins, have a low solubility in weak ionic conditions, and so form a precipitate at low pHs. This means that when platelet free plasma is treated to pH 5.9 the euglobulin fraction precipitates while soluble proteins including PAI-1 remain in solution and can be washed away to give a fibrinolytically active fraction, with a reduced concentration of fibrinolytic inhibitors.[93]

The euglobulin clot lysis time (ECLT) assay was developed in the 1950s. In the original ECLT assay the euglobulin fraction of plasma was re-calcified to form a clot and the time to lysis was monitored visually over 4-6 hours. This process was then accelerated through the addition of kaolin or exposure to glass, reducing the lysis time to 2-10 minutes. Since this activates the intrinsic pathway of coagulation it drives fibrinolysis through the FXIIa and kallikrein pathway rendering lysis independent of Pgn activators.[94] The ECLT assay was updated in 2003 to a turbidity based assay wherein clot lysis time is defined as the time at which the absorbance ($\lambda = 405$ nm) of a re-calcified euglobulin sample drops to < 0.05 Au.[95]

An alternative to the ECLT assay is the fibrin lawn test which involves the formation of a purified fibrin clot in a Petri dish. The euglobulin fraction of plasma is added to the Petri dish leading to lysis of the pre-formed fibrin clot. After 17 hours the zone of lysis is measured and compared to a control plate in which the euglobulin has been rendered inactive by heating to 80 °C.[96] The procedure is also compatible with absorbance measurements which allow for the more rapid determination of lysis.[82]

Thromboelastography and Thromboelastometry

Thromboelastography (TEG) and thromboelastometry (TEM) are common mechanical assays used to detect the structural changes in blood clots during coagulation and fibrinolysis. The techniques involve measuring the movement of a pin within a cup filled with a blood sample to study the changing mechanical properties of the clot. Owing to their speed and the detailed information they are able to provide, these tests are considered the "gold standard" in detecting coagulopathies and fibrinolysis in tandem. Both TEG and TEM techniques are further discussed in the following section.[97]

1.3 Rheological Techniques for Monitoring Coagulation and Fibrinolysis

The rheological properties of materials have been used to study and explain the behaviour of fluids for a variety of applications ranging from the characterisation of the motion of water through a syringe, to determining whether paint will drip when applied to a wall.[98,99] More recently, with the development of more advanced rheometers and complex mathematical algorithms, rheological techniques including small amplitude oscillatory shear (SAOS) have undergone significant advancement allowing the dynamic properties of complex materials to be studied. Whereas conventional rheology was concerned with whether a material would be classified as Newtonian or not, techniques such as SAOS allow the real-time characterisation of materials that display both viscous and elastic components, such as gels. Not only can this kind of rheological test quantify the viscous and elastic nature of a material, but they can also be used to look at dynamic systems where these behaviours change with time or environment.

As discussed in Section 1.2.4, during clot formation fibrinogen within the blood is cleaved by thrombin to generate fibrin monomers. These monomers undergo polymerisation forming a gel like network of fibres extending in all directions. As the clot forms, the blood transitions from a sol state to a gel and therefore exhibits significant changes in viscoelastic behaviour.[100,101]

Several research groups have previously studied the viscoelastic changes in blood, paying particular attention to incipient clot formation, associated with coagulopathies such as thrombosis, myocardial infarction (MI), peripheral vascular disease, cancer, and diabetes. Over time, this research has stimulated the in depth study of the rheological properties of blood clot formation and breakdown, the area on which this thesis builds.[102–104] The viscoelastic properties of blood clots are a key marker for several pathologies which involve the partial occlusion of a blood vessel by a blood clot, as these behaviours determine whether a clot will deform, rupture or embolise under different flow conditions.[105]

Established rheological techniques for studying coagulation and fibrinolysis have an advantage over standard laboratory tests, offering faster results and providing substantial information regarding a patient's global coagulatory and fibrinolytic behaviour.[97] However, these standard rheological tests do not offer the same level of detail regarding clot microstructure as imaging techniques such as confocal microscopy and SEM. Advances utilising SAOS rheology are now able to combine rapid viscoelastic testing with detailed information regarding the clot microstructure comparable to advanced imaging techniques.[106–108]

1.3.1 Thromboelastography and Thromboelastometry

TEG and TEM are currently the "gold standard" techniques for the combined monitoring of coagulation and fibrinolysis, due to their advantages over standard laboratory assays. TEG and TEM both rely on the same principles, but involve different experimental set ups.[97]

TEG involves monitoring the movement of a pin suspended within a cup filled with whole blood that has been spiked with kaolin shown in Figure 1.16. The cup containing the blood sample is then rotated. As the blood clots the elasticity of the sample changes generating resistance and causing lateral motion of the pin. This motion can be plotted graphically and used to examine the mechanical properties of the clot. In the case of hyperfibrinolysis, the clot breaks down spontaneously causing a detectable dampening in the movement of the pin.[109]

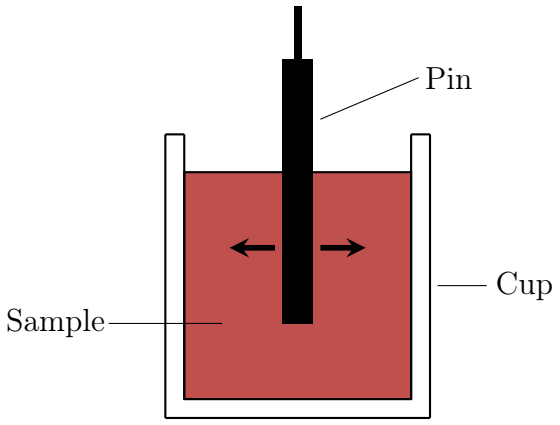

Figure 1.16: A Diagram Showing the Typical Set-up of a Thromboelastography/ Thromboelastometry Experiment.

TEM also involves studying the movement of a pin within a cup; however, in the case of TEM the cup is stationary and the pin rotates within the sample and the motion of the pin is detected optically. As the blood clots the movement of the pin becomes restricted, this dampening of the pin's motion is recorded and interpreted in a similar fashion to TEG, with increasing freedom of movement following clotting indicating a hyperfibrinolytic state. There are a series of TEM tests which are often performed, including INTEM which activates the intrinsic pathway of coagulation through the addition of phospholipids and ellagic acid, and EXTEM which activates the extrinsic pathway of coagulation through the addition of TF. In order to confirm hyperfibrinolysis an APTEM test is run alongside either the INTEM or EXTEM test, in which the sample is spiked with aprotinin. The aprotinin inhibits fibrinolysis and acts as a control, allowing the distinction between normal clot contraction and fibrinolysis.[83]

TEM techniques are considered to be superior to TEG in the detection of fibrinolysis; however, both are only capable of detecting hyperfibrinolytic states.[109] Both TEG and TEM results can also be compared with a second test of the same technique in the presence of platelet inhibitors (abciximab and cytochalasin D) in order to reveal the independent contribution of platelet activation to coagulation and fibrinolysis.[110]

TEG and TEM output similar results as seen in Figure 1.17, in which R is the reaction time, or the time until the initial formation of a clot, α is an index value which describes a patient's coagulable state, and MA is the maximum amplitude which can be thought of as the clot strength. The presence of a reduction in amplitude during the second phase is indicative of hyperfibrinolysis.

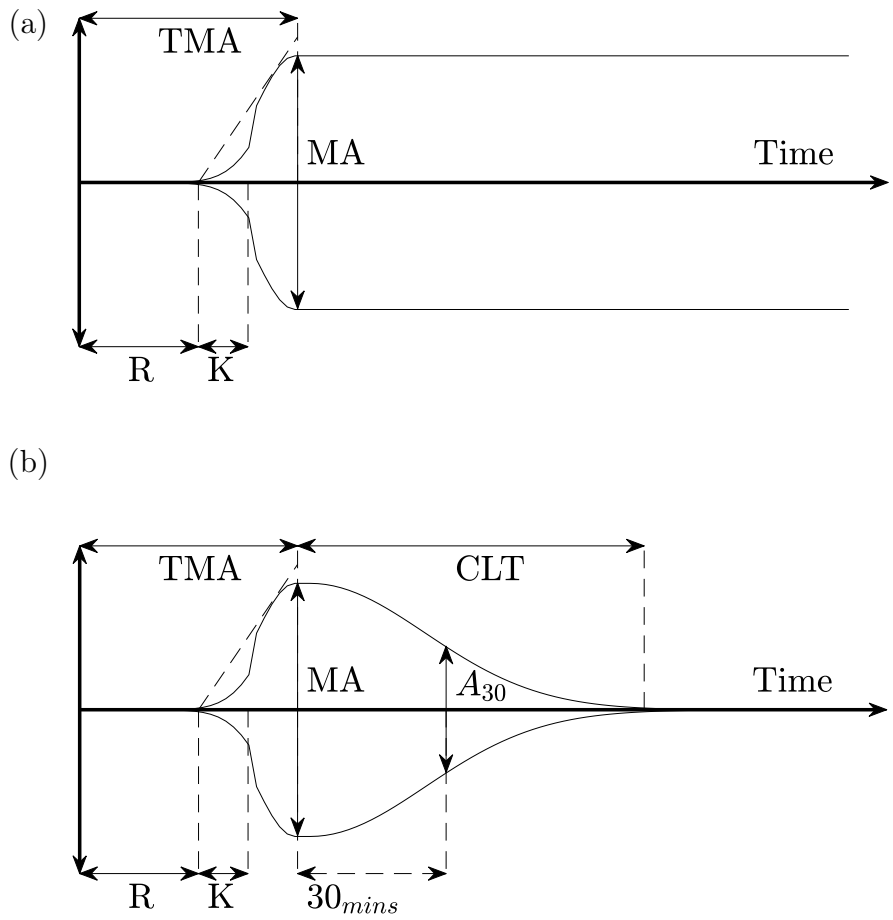

Figure 1.17: Graphs Illustrating Typical Outputs from Thromboelastography/ Thromboelastometry Tests.

(a) Healthy output and (b) hyperfibrinolytic output.
Where R: reaction time, K: kinetics, MA: maximum amplitude, TMA: time to maximum amplitude, A_{30}: amplitude at 30 minutes, and CLT: clot lysis time.[111]

TEM is currently used in clinical settings to guide decisions regarding transfusions, in particular during and after cardiac surgery; however, the techniques have come under heavy criticism.[112–114] In a review of a number of rheology based techniques for blood coagulation studies, Evans *et al.* report that TEG and TEM measurements are an assessment of clot 'rigidity' and as such are not sufficiently sensitive to fibrin network formation. This is due to the fact that high viscosity Newtonian fluids would produce a substantially 'rigid' response to these measurements despite having no elastic component. Additionally, the review notes that values derived from TEG measurements have not been sufficiently linked to viscoelastic parameters, and that the strain rates generated during TEG testing are in the range of 8-16 % which puts the testing parameters outside the linear viscoelastic region (LVR) of the material.[114,115] These ideas are supported by original statements made by McIntire *et al.* in 1977, who concluded that

the measurements associated with the clot are empirical and as such are not rheologically relevant values and so no direct comparisons between TEG/TEM data and any other rheological theories or determinations on clot viscoelasticity are possible.[116]

1.3.2 Oscillatory Rheometry

Advanced SAOS techniques, described in Chapter 2, are able to monitor the sol-gel transition of blood undergoing coagulation with a higher degree of accuracy, and through more rheologically relevant parameters than TEG/TEM.[114,116]

Free Oscillation Rheometry

Free oscillation rheometry (FOR) techniques involve a cup containing a sample connected to a torsion wire. The cup is rotated to a set position and released, the dampening amplitude of the resulting oscillations are measured optically along with the frequency of the oscillations before the step is repeated. During coagulation, changes in the viscoelastic behaviour of the sample lead to changes in both the amplitude and frequency of the oscillation.[114,117]

In 2003, Ranby *et al.* examined the use of FOR techniques in a study of blood clotting using a 10 Hz FOR rheometer. The purpose of the work was to validate the use of FOR techniques in detecting coagulation in whole blood as well as blood plasma. The detected rheological parameters were compared to the results of visual inspections of the blood clots upon sample tilting. For the purposes of the visual examination, clotting time was defined as either an increase in the adhesion of the samples to the cup walls, the loss of mobility of small air bubbles on the sample surface, or the appearance of a wrinkly skin on the sample surface. The firm clot time was noted as either the loss of sample surface orientation with tilting, or the ability to invert the cup without loss of sample.[117]

The G^* trace obtained from FOR correlated with that detected by conventional oscillatory techniques in blood plasma. The work found that the greatest correlation between the visual clotting results and the FOR results was through ΔG^*. The coagulation time was defined as the moment at which ΔG^* >0.01 Pa. They found that this coagulation time correlated strongly with the visual clotting time in both whole blood and blood plasma. The authors claim superior detection by the FOR technique which showed a lower standard deviation in G^* traces than the standard oscillatory results.[117]

In 2002, Ramström *et al.* investigated the impact of platelets on the coagulation of blood, again using a 10 Hz FOR rheometer, in which the coagulation time was defined by a pre-established value of dampening and frequency, and a complete coagulation time was defined by a plateau in the data. The work found that the addition of two platelet activators; thrombin receptor activating peptide and collagen to whole blood and platelet rich plasma (PRP) samples led to a reduction in the clotting time as detected by FOR.[118]

The study also noted that clot contraction resulted in detachment of the clot from the cup walls and as a result an increase in the damping and frequency of the cup during FOR measurements. Further to this, testing was performed on whole blood with the addition of abciximab, an inhibitor of platelet contraction. This resulted in an increase in the clotting time as detected by FOR, which was attributed to an associated decrease in thrombin concentration.[118]

Tynngård *et al.* conducted a study in 2008 which looked at the ability of FOR to detect coagulation during pregnancy, where coagulation is known to be enhanced, and in thrombocytopenia, a haematological condition associated with an increased risk of bleeding that is diminished with platelet infusion.[119] This work used the definition of clotting time provided by Ranby *et al.* but further included the calculation of G' from the rheological data and evaluation of $G'_{\max}$ as a measure of the elasticity of the mature clot. In order to prevent the clot contraction observed by Ranby *et al.* the FOR cup was coated with gold.[117,119] The study found that FOR was able to detect significant differences in clotting time, G', and $G'_{\max}$ between pregnant and non-pregnant women, with pregnant women showing a shorter clotting time. This finding supports the ability of the technique to detect hyper-coagulable states. In addition to this, the study found there was a significant difference in the detected values of $G'_{\max}$ at each trimester, with $G'_{\max}$ appearing to increase over the course of pregnancy.[119]

Tynngård *et al.* also showed that in thrombocytopenic patients the clotting time was substantially similar to healthy donors both before and after the administration of platelets. The value of $G'_{\max}$ was found to be significantly lower in thrombocytopenia patients when compared to healthy donors, as well as showing sensitivity to platelet transfusion. This work suggested that FOR is able to monitor both platelet functionality and plasma coagulability, and is capable of detecting both enhanced and impaired coagulation through the measurement of $G'_{\max}$.[119]

More recently in 2015, Thomas *et al.* conducted a comparison of TEM and FOR viscometers in the detection of low molecular weight heparins, which impede coagulation, in blood sampled from venous catheters of patients having undergone oesophageal resection. In this instance the cup of the FOR rheometer was again coated with gold and in addition to detecting coagulation a decrease in the value of G' was used to detect clot lysis. In contrast to the previous literature discussed, they found that while prolonged clot formation as a result of low molecular weight heparin could be detected by both techniques, neither technique was able to detect changes in clot stability in terms of MA or $G'_{\max}$. However, the work did show a weak correlation between the dose of heparins and lysis detected by both techniques.[120]

Small Amplitude Oscillatory Shear

Between 1969-1973, Kaibara and Fukada investigated the use of a viscoelastic recorder in the detection of purified fibrin-thrombin gels as well as bovine and human blood plasma. The viscoelastic recorder utilises a concentric cylinder geometry depicted in Figure 1.18 where the outer cup is oscillated vertically in order to apply a strain to the sample, and the motion of the rod contained within the sample is detected. They acknowledged the dependence of the rheological moduli on both the frequency and amplitude of the displacement which during the studies were 10 Hz and 56 μm respectively.[116,121,122]

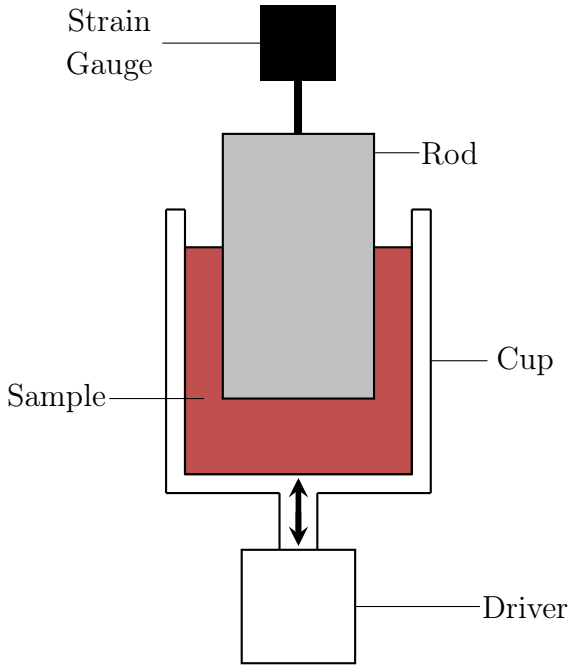

Figure 1.18: A Diagram Showing the Typical Set-up of a Viscoelastic Recorder.

In 1969, Kaibara and Fukada investigated the influence of coagulation on G' and G'' in both whole blood and plasma. They determined the viscosity of both blood and plasma before the onset of coagulation through a shear rate ($\dot{\gamma}$) ramp. They found that whole blood displays a non-Newtonian behaviour, while blood plasma displayed an almost Newtonian behaviour.[122]

Kaibara and Fukada then assessed the influence of plasma dilution on the values for G' and G'' finding that the values of both moduli decreased as the plasma was diluted. This indicated that the values of the moduli were influenced by the concentration of cross-linking monomer units. The work found that the presence of erythrocytes in whole blood led to a reduction in both G' and G'' during coagulation, but ultimately gave higher values of both moduli in the mature clots.[122]

In 1970, Kaibara and Fukada furthered this work to study the influence of wave frequency and amplitude on the viscoelastic behavior of both whole blood and blood plasma. The study noted a frequency and amplitude dependence of G' and tracked the linear to non-linear progression of Lissajous plots from whole blood and plasma during coagulation. The work concluded that the structure of fibrin networks equilibrates with the amplitude of oscillation until a threshold is reached, at which the network structure is disturbed and a decrease in G' is observed.[123]

In 1973, Kaibara further investigated the increasing G' and G'' in order to determine a rate constant for the coagulation process, which was compared in purified fibrin-thrombin gels of differing concentration as well as bovine and human plasma. The work was able to attribute the observed increases in G' and G'' to stages of the fibrin network formation and crosslinking.[121]

In 1974, Glover *et al.* investigated the use of a Weissenberg rheogoniometer in detecting coagulation, which applies a sinusoidal shear stress to a sample placed between two plates in order to determine the G', and G'' of a material under shear stresses equivalent to 0-200 Pa. The testing was performed using both parallel plate and cone and plate geometries. The results indicated a negative relationship between shear stress and ${G'}_{\max}$.[124] It is worth acknowledging that the control samples tested at 0 shear had much higher platelet counts than the samples subjected to shear stresses.

Further to this work, in 1975 Glover *et al.* investigated the effect of platelet count using the same technique with no additional shear stress. They found that ${G'}_{\max}$ increased with increasing platelet concentration. They additionally tested the technique using plasma samples collected from thrombocytopenia patients which showed significantly higher ${G'}_{\max}$ values than healthy samples of the same platelet concentration.[125]

These techniques were further tested by Isogai *et al.*, who examined the ability of the viscoelastic recorder utilised by Kaibara and Fukada to detect disease states. The work examined viscoelastic curves from healthy donors and patients having a range of conditions including diabetes, myeloid leukemia and infection. The results found a correlation between ${G'}_{\max}$ and fibrinogen concentration, as well as higher ${G'}_{\max}$ values in patients with connective tissue disease, neoplasm and infectious diseases. The work went on to investigate the influence of platelets on ${G'}_{\max}$ and found no clear relationship; however, the authors noted that when looking at individual curves, the times taken to initiate clotting, the rate of coagulation and ${G'}_{\max}$ and ${G''}_{\max}$, were highest in platelet rich plasma followed by whole blood and lowest was platelet poor plasma.[102] In their review Evans *et al.* acknowledge that both the viscoelastic recorder and Weissenberg rheogoniometer techniques operate at a single frequency of measurement. Therefore the values of G' and G'' are dependent on the frequency at which the test is performed, meaning that results are not necessarily directly comparable and detection of a Chambon-Winter gel point is not possible using these devices.[114]

In 2005, Williams *et al.* performed a study of the coagulation of whole blood using Fourier transform mechanical spectroscopy (FTMS), probing the coagulating material using an ARES rheometer (TA instruments). The experimental set up included the use of a concentric cylinder geometry with a 1mm gap as well as a cone and plate geometry. The FTMS waveforms applied equated to complex waves having a maximum amplitude of 20 %, with harmonic frequencies in the range of 0.1-10 Hz. The waveforms were processed by Fourier transform and the resultant evolution of $G'(\omega)$ and $G''(\omega)$ was used to model the process of coagulation. In the models, the frequency dependence of $tan(\delta)$ revealed that at lower values of α, low frequency modes dominate the relaxation spectra, whilst the high frequency modes are dominant at higher values of α. This indicates a shift from long relaxation times to shorter relaxation times with increasing α. This finding was attributed to an increasing number of fibre nodes giving rise to an increase in the value of α. This was determined to be consistent with models wherein molecular clusters of fibrin fibres are present within the samples prior to the gel point.[126]

Gel Point Measurements

SAOS techniques that probe materials at multiple frequencies can be used to detect the gel point of a material. The first description of the detection of a Chambon-Winter gel point during the coagulation of blood was published in 2008 by Evans *et al.*, the results of which are shown in Figure 1.19.[127]

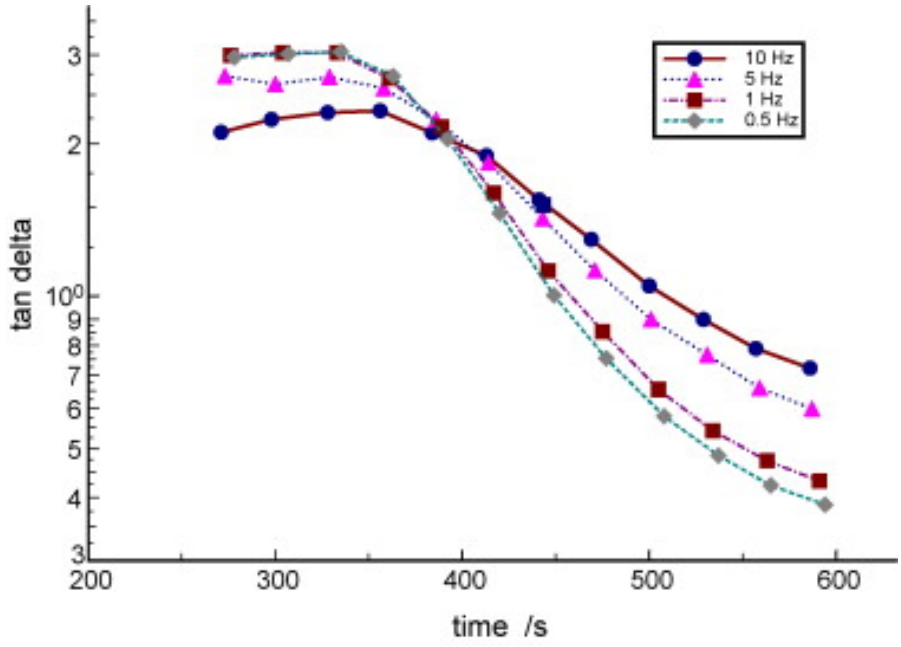

Figure 1.19: A Graph Depicting the First Chambon-Winter Gel Point Reported for Whole Blood by Evans *et al.*[iv].

The paper describes the use of controlled strain FTMS in the investigation of whole blood samples from healthy patients. The SAOS measurements were conducted on an ARES rheometer (TA instruments) using a concentric cylinder geometry with a 1mm gap. The applied waveforms were complex waves with a frequency range spanning 0.5-10 Hz and a maximum amplitude reported to be within the LVR. This technique was run in parallel with TEG measurements and showed a clear qualitative relationship between the techniques. However, the results indicated that TEG measurements were less sensitive than FTMS techniques, with R occurring 6 minutes after the gel point. Therefore, the TEG measurements were shown to be incapable of detecting the establishment of a viscoelastic solid response and thus the onset of haemostatic functionality. The authors propose that the TEG measurements may also be subject to errors in MA time, since the value did not correspond to the time of maximal stress established by FTMS. Additionally, the research determined a healthy value of incipient clot microstructure for whole blood through the calculation of the fractal dimension

[iv]Reprinted from Journal of Non-Newtonian Fluid Mechanics, 148/1-3, Evans PA, Hawkins K, Williams PR and Williams RL, Rheometrical detection of incipient blood clot formation by Fourier transform mechanical spectroscopy, p122-126, Copyright (2007), with permission from Elsevier.

(d_f) of d_f=1.74 ($\pm$0.07) from the viscoelastic properties at the gel point. This healthy value was found to be in agreement with the value predicted by percolation theory (Section 2.4.3).[127]

Evans *et al.* went on to compare FTMS gel point measurements of coagulating whole blood with TEG and FOR techniques. The FTMS technique used an ARES rheometer (TA instruments) equipped with a parallel plate geometry. The applied FTMS waveforms consisted of harmonic frequencies between 0.2-3.2 Hz and were maintained at an amplitude within the LVR of the material. The study found that the time to incipient clot formation detected at the gel point was significantly shorter (3.28 minutes) than either TEG (8.70 minutes) or FOR (19.71 minutes) techniques. Evans *et al.* propose that the non-linear strain applied during TEG and FOR testing may be responsible for the prolongation of clotting time. In addition to this, the paper notes that FOR procedures do not appear to allow for attenuation of wave amplitude in the sol phase, which led the authors to conclude that both TEG and FOR were inappropriate tests for detecting incipient clot formation, while the gel point measurements were found to be able to provide a global coagulation profile.[128]

Continuing from the work above, in 2010, Evans *et al.* reported the further use of gel point measurements in studying the effect of heparin on healthy blood samples. Gel points were detected using an ARES rheometer (TA instruments) fitted with an acrylic concentric cylinder geometry. The work was conducted using both FTMS measurements in which the waveforms contained frequencies between 0.2-3.2 Hz and had a maximum amplitude within the LVR, and discrete sweep measurements within the LVR. The work found that as well as displaying prolonged clotting times, samples treated with heparin displayed a significant decrease in d_f. This finding was consistent with previous research into the effect of heparin on clot structure and indicated the effectiveness of gel point measurements as a marker for clotting time and clot microstructure. Comparison of the results with existing techniques including TEG led the authors to conclude that the more accurate measurements available using FTMS could supplant techniques such as TEG in the future. At the time of this work, detection of clot lysis by TEG was possible, and as well as correlating the administration of heparin to the values of d_f, the authors found a relationship between d_f and the clot lysis index ($LY30 = \frac{A_{30}}{MA} \cdot 100$) detected by TEG at low concentrations of heparin. This was reported to relate to the ability of macromolecules such as t-PA to permeate more open clot structures.[129,130] Although the methods in the paper describe the use of both FTMS and discrete sweep techniques to assess the gel point, no comparison of the two techniques or conclusions regarding them are given.

In 2014 Lawrence *et al.* published a study on a new structural biomarker (d_f) able to detect the dilution of whole blood through the detection of Chambon-Winter gel points for coagulating blood. The study looked at the parameters obtained from the gel point measurements with the progressive dilution of blood with saline. The rheological tests were performed on an AR-G2 rheometer (TA instruments) using four discrete frequencies in the range of 0.2-2 Hz, with each having a peak stress amplitude of 0.03 Pa, from which a gel time and d_f were calculated. The samples were also imaged using helium ion microscopy which is conceptually similar to SEM. The results showed that above 20 % dilution the value of d_f was sensitive to the dilution, and coincided with a decrease in fibre width, shown in Figure 1.20.[131]

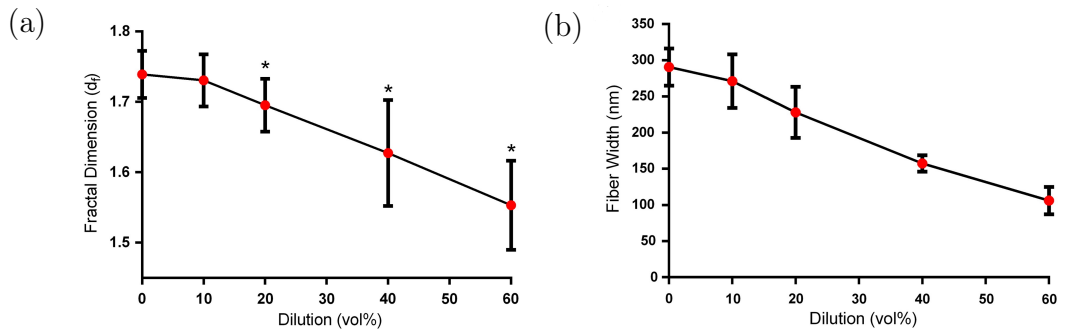

Figure 1.20: Graphs Depicting the Comparison of the Fractal Dimension and Fibre Width of Whole Blood under Progressive Dilution with Saline[v].

(a) Fractal dimension detected by rheometry and (b) fibre width detected by helium ion microscopy.

Lawrence *et al.* published a further study in 2014 examining clot microstructure values associated with rheological tests on whole blood from patients receiving warfarin treatment. The research was conducted using a similar set up to that described in the previous paper; however, in this research a concentric cylinder geometry was fitted to the AR-G2 rheometer. The patients were divided into two groups, those receiving warfarin for the treatment of venous thromboembolism (VTE) and those receiving warfarin for a range of other clinical reasons. The research showed no detectable difference between the two groups using standard laboratory markers; however, VTE patients exhibited

[v]Reprinted from Thrombosis Research, 134/2, Lawrence, MJ, Kumar SK, Hawkins K, Boden S, Rutt H, Mills G, Sabra A, Morris RHK, Davidson SJ, Badiei N, Brown MR, Williams PR and Evans P, A new structural biomarker that quantifies and predicts changes in clot strength and quality in a model of progressive haemodilution, p488-494, Copyright (2014), with permission from Elsevier.

significantly higher d_f values detected by the rheological tests than their non-VTE counterparts, despite showing no significant difference in gel time. The researchers propose that this is due to sub-optimum warfarin treatment inadequately controlling coagulation in patients having increased thrombotic potential which had been undetectable by standard techniques, highlighting the value of d_f as an additional coagulation biomarker.[132]

Research conducted in 2015 by Davies *et al.* compared values for d_f obtained from whole blood during coagulation with SEM images of mature clots in lung cancer patients (who were divided into early and advanced groups) and healthy controls. The rheometrical detection was conducted using an AR-G2 rheometer fitted with a double-gap concentric cylinder, it is unclear whether the research utilised FTMS or discrete sweep analysis. The work found no significant differences in time based biomarkers, including gel time, between healthy or lung cancer patients. Standard laboratory assays found differences in platelets and fibrinogen concentrations between healthy patients and cancer patients, although the results from both groups fell within the laboratory normal ranges. Other standard assays for coagulation and lysis indicated differences between healthy and cancer patients, but were not able to distinguish between early and advanced stages of lung cancer progression. However, a strong correlation between the values obtained for d_f and the severity of lung cancer were detected and confirmed through SEM imaging of mature clot microstructure. This demonstrates a relationship between d_f values and mature clot microstructure, in addition to providing further evidence of the enhanced sensitivity of rheological analysis of coagulation.[133]

In 2015, Lawrence *et al.* compared the values for d_f obtained at the gel point with SEM images of whole blood from patients undergoing treatment for myocardial infarction. The study found that as well as corresponding with SEM images of mature clot structure, the d_f biomarker was able to detect percutaneous coronary intervention. The authors report an observed decrease in d_f from 1.751 to 1.634 immediately following the administration of anti-platelet and thrombin inhibitors, which recovered 24 hours after treatment. The study noted that 8 of the 38 patients tested were low responders to the treatment, and that the mean d_f of this group was 1.761 in comparison to the rest of the group who showed a mean d_f value of 1.735. Lawrence *et al.* acknowledged that this was not sufficient evidence for the biomarker in itself, but that the results warranted a larger study to assess the link between ineffective antiplatelet therapy and the d_f.[134]

In 2016, Lawrence *et al.* examined the relationship between temperature and the measured gel point of whole blood using an AR-G2 rheometer (TA instruments) fitted with a double gap concentric cylinder geometry. Gel points were detected using four discrete frequencies between 0.2-2 Hz. Whole blood from healthy volunteers was measured at temperatures ranging from 27-43 °C. The study found that increasing temperatures between 27 °C and 43 °C resulted in a decrease in the time to gel point as well as a corresponding increase in d_f. The research also found significant decreases in d_f and the time to gel point when the temperature was reduced below 37 °C; however, there were no significant effects when samples were tested above 37 °C.[135]

Work published in 2016 by Davies *et al.* showed that the d_f of whole blood collected from healthy volunteers was significantly altered by exercise and correlated with SEM images of mature clots. Rheological analysis of whole blood from healthy volunteers before and after exercise was performed using a DHR-2 rheometer (TA instruments) using discrete frequency sweeps. The d_f obtained during coagulation was shown to increase from the healthy value of 1.72 to 1.79 following maximal exercise and then decreasing to 1.71 in the 1 hour period following the exertion.[136] This was confirmed by work conducted in 2018 by Lawrence *et al.* who found a significant increase in detected values of d_f following moderate intensity leg exercise as well as in response to tyramine infusion leading to noradrenaline release in the leg.[137]

Later in 2016 Davies *et al.* investigated the influence of sepsis and the associated inflammatory response on the gel point of whole blood samples. Mature clots were also imaged by SEM. The research showed that the d_f values detected were sensitive to sepsis with increases in d_f associated with increasing severity of sepsis and a significantly lower value of d_f obtained for patients experiencing septic shock. These results correlated well with SEM imaging and the authors showed that the value of d_f was a significant predictor of mortality.[138]

A study published in 2017 by Knowles *et al.* studied the influence of platelet activity on the parameters associated with the gel point. In this study the effects of aspirin, prasugrel, and ticagrelor on platelet function and the d_f values obtained from SAOS measurements were compared and validated using SEM imaging techniques. The rheology methods included the use of a Discovery HR-2 rheometer (TA instruments) fitted with a double gap concentric cylinder geometry. Healthy volunteers received either aspirin alone, prasugrel alone, combination asprin and prasugrel, or combination aspirin and tricagrelor. The results of the study showed a strong correlation between d_f and both the fibrinogen concentration

and platelet activity. No significant changes in d_f were observed in the group that received aspirin monotherapy; however, significant reductions in detected values of d_f were observed in all other treatment groups. These d_f values were found to be predictors of mature clot structure detected by SEM imaging and the study concluded that the rheological detection of d_f has potential as a tool in quantifying thrombotic risk.[139]

It is acknowledged that platelet mediated clot contraction influences the pathological nature of blood clots. In 2015, Tutwiler *et al.* investigated the impact of several parameters on the contraction of fibrin-thrombin networks including the evaluation of rheometric data under low oscillatory shear strain. The rheometrical procedure involved the detection of G' and G'' in coagulating samples of reconstituted whole blood with the addition of thrombin and $CaCl_2$. The procedure was carried out using an AR-G2 rheometer (TA instruments) fitted with a parallel plate having a gap of 400 μm where an oscillatory strain of 3 % was applied to the samples at a frequency of 0.8 Hz. Optical assays of clot contraction showed that the concentration of platelets greatly influenced the extent of clot contraction, with increasing platelet concentration leading to an increase in the degree of contraction observed. The rheometrical studies on various platelet concentrations indicated a shift towards the viscous properties of the clot at higher platelet levels.[59]

In addition to the detection of G' and G'' the contractile force was detected and reported as the axial force applied to the rheometer geometry by the contracting clot. The study found that the treatment of blood plasma with blebbistatin to inhibit myosin-driven platelet contraction resulted in an eightfold reduction in the detected contractile forces shown in Figure 1.21, highlighting the role of myosin-driven contraction in the process.[59]

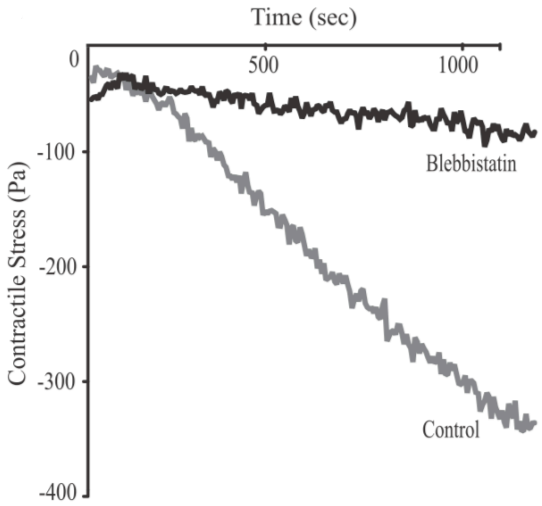

Figure 1.21: A Graph Depicting the Evolution of Contractile Stress During Coagulation of Whole Blood With and Without the Contraction Inhibitor Blebbistatin[vi].

The study additionally noted that in platelet controlled samples the presence of red blood cells increased the contractile forces generated by the clot despite a reduction in the overall contraction detected through optical techniques shown in Figure 1.22.[59]

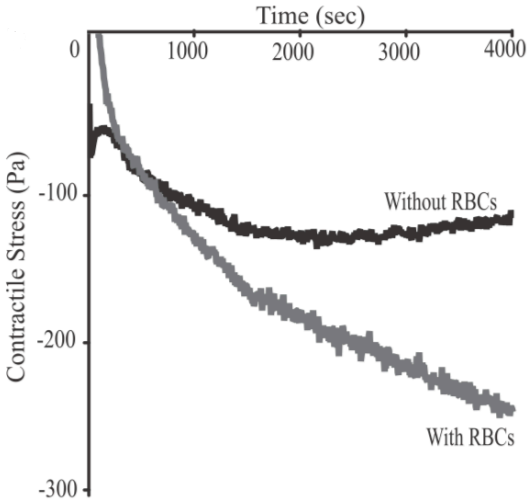

Figure 1.22: A Graph Depicting the Evolution of Contractile Stress During Coagulation of Blood Plasma With and Without Red Blood Cells (RBCs)[vi].

[vi]Reprinted from Blood, 127/1, Tutwiler V, Litvinov RI, Lozhkin AP, Peshkova AD, Lebedeva T, Ataullakhanov FI, Spiller KL, Cines DB, and Weisel JW, Kinetics and mechanics of clot contraction are governed by the molecular and cellular composition of the blood, p149-159, Copyright (2015), with permission from American Society of Hematology

In 2017, Kim *et al.* examined the influence of clot contraction on fibrin network arrangement in PRP samples collected from healthy volunteers. This study used an AR-G2 rheometer (TA instruments) fitted with a parallel plate geometry. The testing utilised an oscillatory wave at a torque that resulted in a 1 % strain response, which was applied at a frequency of 1 Hz over the testing period. The study reported that initial increases in the detected axial force, associated with the structural changes during coagulation, became asymptotic when contraction ended. Additionally, they noted that platelet contraction and network rearrangement appeared to occur in three closely related phases; pre-contraction, active contraction and final contraction. Inhibition of the platelets contractile ability by blebbistatin and abciximab significantly decreased the axial force generated by the clot during coagulation, highlighting again the dependence of this process on the myosin-driven contractile system.[61] In this work, Kim *et al.* also showed that the material properties of the clot are influenced by platelet contraction. Treatment of samples with the platelet contractile inhibitors blebbistatin and abciximab significantly decreased the detected values for G' and G''.[61]

In 2017, Tutwiler *et al.* performed further work measuring the contraction of blood through both the detection of the axial force and an optical tracking system. In this work it is suggested that the optical system was able to measure unconstrained clot retraction, while the rheometrical evaluation was able to monitor constrained retraction by confining the samples to a fixed gap. The measurements were conducted using an AR-G2 rheometer fitted with a parallel plate geometry set at a 400 μm gap. Plasma samples were studied to determine the relationship between platelet contractility and the elasticity of both the fibrin network and erythrocytes by testing samples with and without erythrocytes.[140]

Tutwiler *et al.* claim that in the unconstrained samples the presence of blood cells reduced the degree of clot contraction, while in the constrained samples the presence of blood cells increased the contractile force depicted in Figure 1.23.[140] However, the figure appears to show a reduction in the relative clot size which would indicate an increased level of clot contraction.

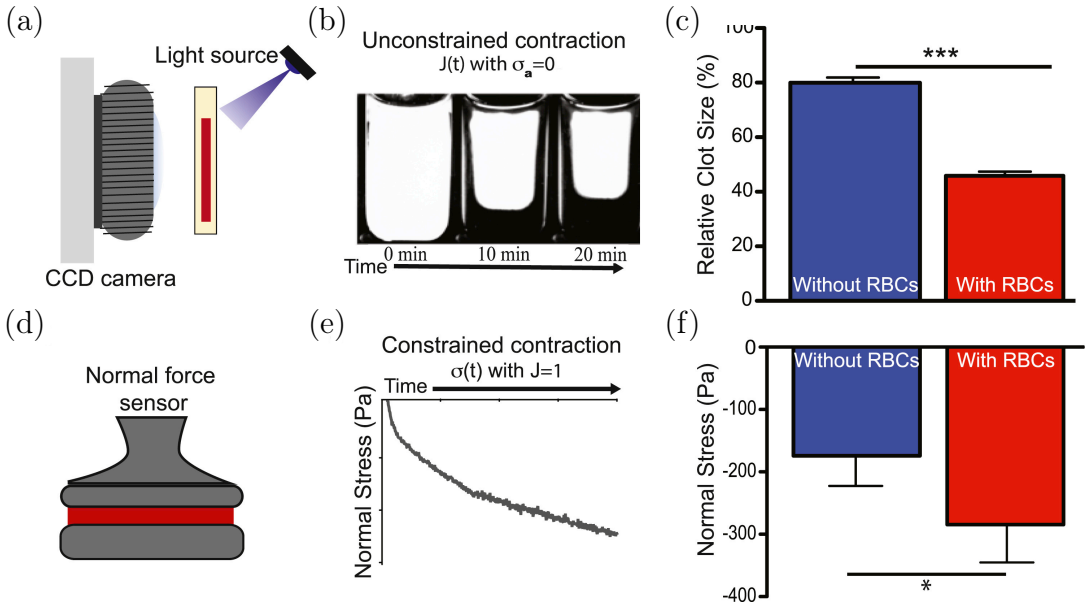

Figure 1.23: Figure Depicting the Unconstrained Contraction and Constrained Contractile Stress of Blood Plasma Clots in the Presence and Absence of Red Blood Cells[vii].

(a) Experimental set up for unconstrained clot contraction, (b) evolution of clot contraction, (c) relative clot size, (d) experimental set up for constrained clot contraction, (e) evolution of contractile stress, and (f) contractile stress generated.

Figure 1.24 shows the changes in contraction and axial force over time, indicating that the presence of erythrocytes leads to a reduction in clot contraction. The study concludes that with the addition of a cellular component there is an increase in the contractile force generated by the platelet-fibrin network, but a reduction in the overall degree of clot contraction.[140]

[vii]Reprinted from Biophysical Journal, 112/4, Tutwiler V, Wang H, Litvinov RI, Weisel JW and Shenoy VB, Interplay of Platelet Contractility and Elasticity of Fibrin/Erythrocytes in Blood Clot Retraction, p714-723, Copyright (2017), with permission from Biophysical Society.

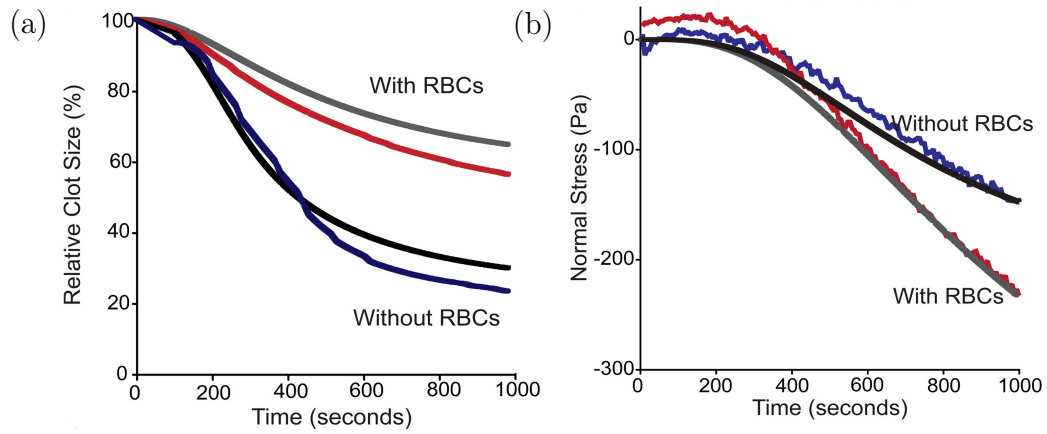

Figure 1.24: Graphs Depicting the Evolution of Contraction in Blood Plasma Clots With and Without Red Blood Cells (RBCs)[viii].

(a) Relative clot size and (b) contractile stress.
Grey and black lines show theoretical model.

1.3.3 Fibrinolysis

A 2015 study by Stanford *et al.* examined whether changes in the clot microstructure of stroke patients could be related to therapeutic intervention. The study was conducted on stroke patients with a comparable healthy control group, whole blood was analysed using an AR-G2 rheometer (TA instruments) fitted with a double gap concentric cylinder. Patient samples were tested immediately upon admission, and at 2 and 24 hours following treatment. The study found significantly higher values for d_f and fibrinogen concentration in the stroke cohort compared to a healthy control group. A portion of the patients went on to receive thrombolytic treatment whereas the remainder received aspirin. There was no observed difference in gel time in either group at any time point, despite the patients who had received thrombolytic treatments showing an increased clotting time detected by standard coagulation assays at 2 hours. However, a significant decrease in d_f value was observed in both treatment groups at 2 hours following treatment. In patients who had received thrombolytic therapy there was a decrease in d_f from 1.71 to 1.66 following treatment, shown in Figure 1.25, which was consistent with the changes in fibre width seen in SEM images where the clot appeared more porous with fewer branching points.[141]

[viii]Reprinted from Biophysical Journal, 112/4, Tutwiler V, Wang H, Litvinov RI, Weisel JW and Shenoy VB, Interplay of Platelet Contractility and Elasticity of Fibrin/Erythrocytes in Blood Clot Retraction, p714-723, Copyright (2017), with permission from Biophysical Society.

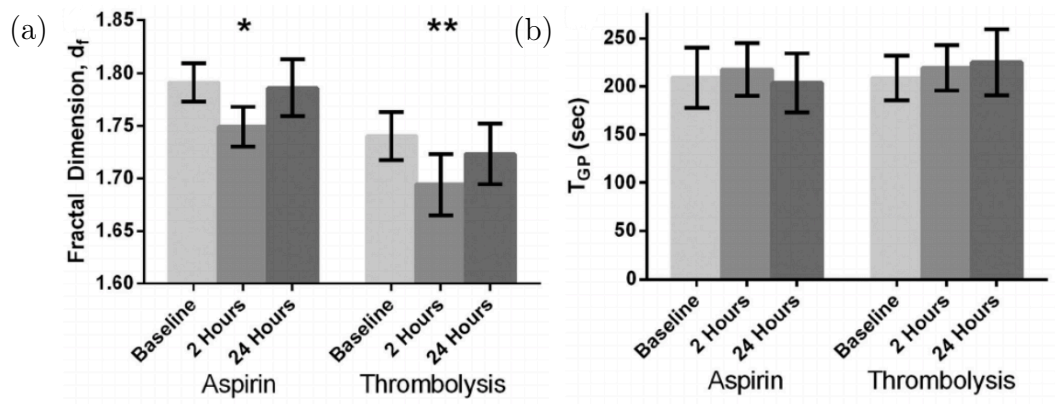

Figure 1.25: Graphs Depicting the Gel Point Parameters of Blood Samples from Stroke Patients Following Administration of Aspirin or Thrombolytic Therapy[ix].

(a) Fractal dimension and (b) gel time.
Error bars indicate the 95 % confidence interval.

1.4 Relevant Rheological Developments

There have been recent advances in the rheological characterisation of materials which provide the initial underpinning of the work presented in this thesis. These are outlined in this section.

1.4.1 Rheological Detection of the Gel Point

Previous work measuring the evolution of rheological properties during coagulation of blood and blood plasma has included the use of both Fourier transform mechanical spectroscopy and discrete frequency sweeps. In 2008, Hawkins *et al.* investigated the possibility that anomalous values detected during rheological characterisation of the gel point may be due to inappropriate rheological techniques. Hawkins *et al.* compared the values detected at the gel point of 5-10 % gelatine gels using both oscillatory frequency sweeps and FTMS techniques. One set of FTMS experiments were conducted using an ARES rheometer (TA instruments)

[ix]Reprinted from BMC Neurology, 15/35 Stanford SN, Sabra A, D'Silva L, Lawrence M, Morris RHK, Storton S, Brown MR, Evans V, Hawkins K, Williams PR, Davidson SJ, Wani M, Potter JF and Evans PA, The changes in clot microstructure in patients with ischaemic stroke and the effects of therapeutic intervention: a prospective observational study, Copyright (2020) BioMed Central

fitted with a couette measuring system applying complex waveforms of between 0.2-3.2 Hz having a maximum amplitude within the linear viscoelastic region of the material. A comparable set of FTMS experiments was run on an AR-G2 rheometer (TA instruments) fitted with a cone and plate geometry. The work found that the stress relaxation exponent (α) was independent of the concentration of gelatine and the temperature at which the test was run with a value of 0.69 $\pm$0.01 which was in agreement with an earlier study.

The value of α was also determined by stress relaxation experiments and confirmed at 0.7 ($\pm$0.01) which equates to a δ value of 63 °. The study reports that FTMS techniques are less prone to errors resulting from sample mutation than discrete frequency sweeps. When the FTMS results were compared to those conducted using discrete frequency sweeps the authors observed that the results from the discrete frequency sweeps did not agree with the results from FTMS, and corresponded to decreased values for α and increased values for gel time. These errors became exacerbated with more rapid gelation, the lowest recorded value being $\alpha = 0.26$ an example of which is shown in Figure 1.26.[142]

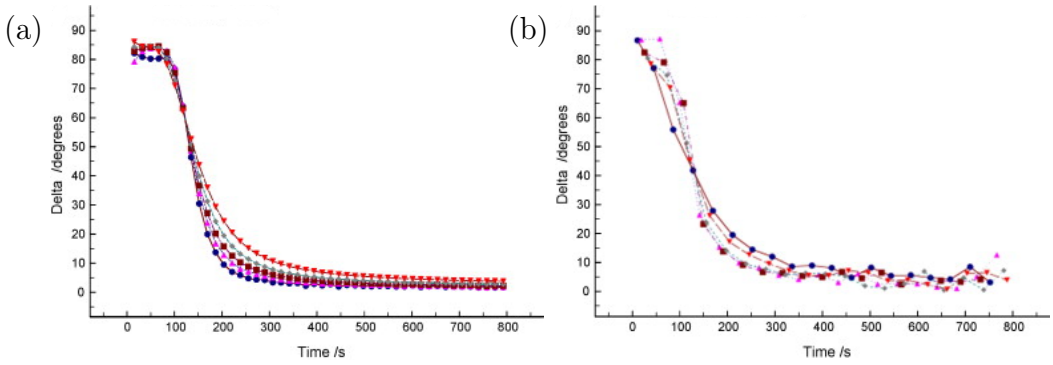

Figure 1.26: Graphs Depicting Example Gel Points Detected in 10 % Gelatine Solutions During Gelation Using Fourier Transform Mechanical Spectroscopy and Discrete Frequency Sweep Techniques[x].

(a) Fourier transform mechanical spectroscopy and (b) discrete frequency sweep.

When the testing temperature was lowered below 23.5 °C the FTMS tests also became influenced by sample mutation, which was corrected by increasing the lowest frequencies applied during testing, effectively shortening the sampling time.

[x]Reprinted from Journal of Non-Newtonian Fluid Mechanics, 148/1-3, Hawkins K, Lawrence M, Williams PR and Williams RL, A study of gelatin gelation by Fourier transform mechanical spectroscopy, p127-133, Copyright (2008), with permission from Elsevier.

The authors concluded that discrete frequency sweeps are more prone to errors resulting from sample mutation and that FTMS was a superior technique in this regard provided that the fundamental frequency of the waveform is sufficiently high enough to exclude mutational errors.[142]

Conversely, in 2010 Hawkins *et al.* again compared FTMS and discrete sweep techniques in the study of gelatine gelation before investigating the coagulation of fibrin-thrombin gels. The study was conducted using an AR-G2 rheometer (TA instruments) fitted with a cone and plate geometry. The work collected gel point data from 10 % gelatine using FTMS waveforms of 0.2-3.2 Hz at a torque which led to a resultant maximum strain amplitude <20 %. Discrete sweep tests were simulated from this data by excluding data points from the results in such a way that for each FTMS waveform a single frequency result was analysed. This showed strong agreement between the FTMS and simulated discrete sweep results shown in Figure 1.27.[143] It is of note that the simulation of discrete frequency sweeps in this way would exclude errors in the measurement as a result of both sample mutation and any inertial interference generated during the frequency transition of a real world test.

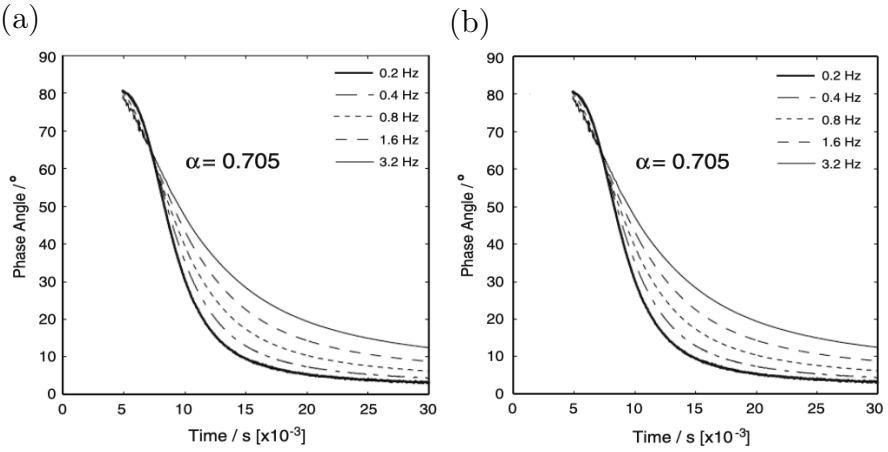

Figure 1.27: Graphs Depicting Example Gel Points Detected in 10 % Gelatine Solutions During Gelation Using Fourier Transform Mechanical Spectroscopy and Simulated Discrete Frequency Sweep Techniques[xi].

(a) Fourier transform mechanical spectroscopy and (b) simulated discrete frequency sweep.

[xi]Reprinted by permission from Springer-Verlag: Springer Nature Rheologica Acta The development of rheometry for strain-sensitive gelling systems and its application in a study of fibrin–thrombin gel formation, Hawkins K, Evans PA and Lawrence M, copyright Springer-Verlag (2010).

Fibrin-thrombin gels were not investigated using FTMS, as the linear strain amplitudes were reported to be below the detection threshold of the rheometer, and so the gel points were detected using discrete frequency sweeps. Fibrin-thrombin gels comprised of 8 mg/ml fibrinogen and varied thrombin concentrations between 0.05-0.15 NIH/ml were investigated and a negative relationship between thrombin concentration and gel time, and a positive relationship between thrombin concentration and d_f was found.[143]

In 2011, Curtis *et al.* furthered this by exploring the correlation between the measured gel time and values of d_f in fibrin-thrombin gels. The work involved the use of an AR-G2 rheometer (TA instruments) fitted with a cone and plate geometry and tested at frequencies between 0.2-2 Hz. They noted that previous work conducted by Hawkins *et al.* led to d_f values that were consistent with diffusion limited cluster-cluster aggregation and reaction limited cluster-cluster aggregation, where the value of d_f decreased with increasing gel time. Curtis *et al.* performed gel point measurements using purified fibrin-thrombin gels of 10 mg/ml fibrinogen and thrombin concentrations in the range of 0.01-0.15 NIH/ml which confirmed the relationship between d_f and gel time shown in Figure 1.28, before modelling the generation of fibrin-thrombin gels using a molecular dynamics simulation.[144]

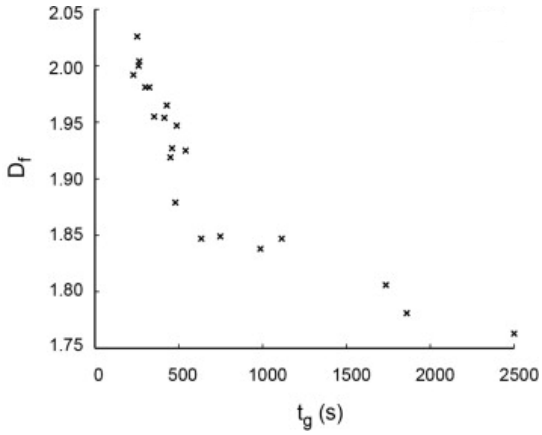

Figure 1.28: Graphs Depicting the Relationship Between the Fractal Dimension and Gel Time for 10 mg/ml Fibrin-Thrombin Gels having Thrombin Concentrations 0.01-0.15 NIH/ml[xii].

[xii]Reprinted from Journal of Non-Newtonian Fluid Mechanics, 166/16, Curtis DJ, Brown MR, Hawkins K, Evans PA, Lawrence MJ, Rees P and Williams PR, Rheometrical and molecular dynamics simulation studies of incipient clot formation in fibrin-thrombin gels: An activation limited aggregation approach, p932-938, Copyright (2011), with permission from Elsevier.

Further to this work, Brown *et al.* investigated the relationship between the d_f and thrombin concentration using the data collected by Curtis *et al.* in 2011, and found that the Pearson correlation between d_f and thrombin concentration was R=0.26. From this, Brown *et al.* concluded that d_f was not able to characterise mature network structures and generated a mathematical model for coagulation, which confirmed that the value for d_f was not enough in itself to characterise the mature clot structure owing to the significant spread in mature structures resulting from d_f values within the healthy range. Brown *et al.* defined a value of d_s, the spectral dimension, and performed a numerical experiment which found that the value of d_s was able to discriminate between mature clot structures associated with a single d_f value and giving a Spearman's correlation coefficient of Rho=-0.99.[144,145]

In 2013, Curtis *et al.* investigated the relationship between d_f and d_s further using fibrin-thrombin gels having a fibrinogen concentration of 10 mg/ml and thrombin concentrations in the range of 0.01-0.19 NIH/ml. The gels were studied using an AR-G2 rheometer (TA instruments) fitted with a double gap concentric cylinder geometry, where the data was collected either by discrete frequency sweeps or FTMS. The gel formation was also measured using confocal microscopy. The study revealed that with thrombin concentrations in the range of 0.01-0.13 NIH/ml the increases in thrombin concentration decreased the gel time and increased the value of d_f, while for thrombin concentrations in the range of 0.13-0.19 NIH/ml increases in thrombin concentration did not substantially alter the gel time or d_f. The authors then estimated values of d_s for the gels and found that for thrombin concentrations in the range of 0.01-0.13 NIH/ml there was a significant negative correlation between thrombin concentration and d_s while no further progression in the value of d_s was found at thrombin concentrations above 0.13 NIH/ml. The authors found a significant correlation of R=-0.926 between the values of d_f and d_s, and concluded that the values of d_f are predictive of mature gel microstructure.[146]

In 2015, Badiei *et al.* investigated the effect of shear stress on the gel point characteristics of blood through controlled stress parallel superposition (CSPS) rheology on both purified fibrin-thrombin gels and whole blood. The study was performed on an AR-G2 rheometer (TA instruments) using discrete frequency sweeps between 0.2-2 Hz, the work utilised CSPS techniques in which a unidirectional shear is superimposed on top of SAOS oscillations to simulate a flow component during measurement. The work used shear stresses in the range of 0-0.35 Pa and showed that when an increased rotational stress was applied alongside SAOS gel point measurements, the d_f values obtained at the gel point

increased, which was reported to be consistent with flow enhanced thrombin generation. Evaluation of confocal and SEM images of the clots formed under shear showed an increase in fibre diameter, as well as enhanced fibre bundling associated with the higher rates of shear. Additionally, a threshold shear value of 0.235 Pa for whole blood was identified, which indicated the maximum amount of shear stress the forming structure was able to withstand without significantly disturbing incipient clot formation. The authors stated that the low unidirectional stresses imposed have physiological relevance in that they simulate the wall shear stresses associated with blood flow within venous structures, and postulate that clots formed under higher rates of shear stress may have enhanced resistance to clot lysis.[147]

1.4.2 Software Developments

In 2010 Evans *et al.* reported the development of a new software for automating gel point detection using rheometrical data obtained from healthy and heparinised whole blood samples.[130,148]

Rheometrical data collected from SAOS measurements of a gelling system at a minimum of 3 frequencies is exported from the rheometer control software as an Excel file containing oscillatory data including time, frequency, δ, G', G'', $\tan(\delta)$, third harmonic ratio, and the raw value of δ. The requirements for the validity of the output include resolution of the measurement and an absence of wall slip.

The software isolates the values of δ and time for each frequency and generates an overlaid graphical plot of δ against time for each frequency. The user is then required to select a search region over which a polynomial least squares function will be applied to each frequency series. This region should include a portion of the plateau on both sides of the drop in δ indicative of gelation. The software is then able to detect the intercepts of the least squares fits and uses the values of both time and δ to determine the α, d_{f} and gel time of the mean intercept point. The software additionally presents the raw phase, mutation number and third harmonic ratio at the gel point so that users are able to assess the validity of the gel point and the potential error contributions from inertia, sample mutation and non-linearity (discussed in Section 2.5.4). In addition, the software provides a value for the deviation from the intercept point, from which the confidence in the determination can be assessed. In this way the software is able to detect gel points in data which contains noise without the influence of user bias.[148]

In 2017, it was noticed by Hudson *et al.* that the inertia correction that is routinely applied to raw data by the software that controls most combined motor transducer (CMT) rheometers can contain errors in the inertia constant (I_c), while separate motor transducer (SMT) rheometers are more reliable. Hudson *et al.* showed that variations in the error associated with this calculation are random between different CMT rheometers and even differ between individual CMT rheometers of the same make and model. It was noted that these errors manifest as high levels of deviation in gel point measurements illustrated in Figure 1.29 (a).[149]

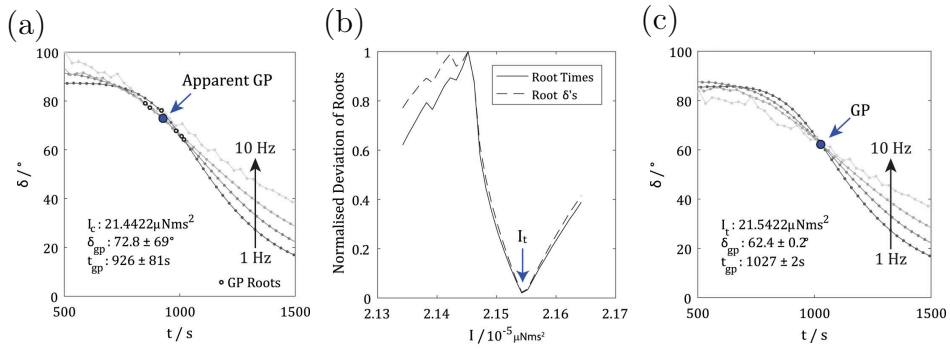

Figure 1.29: Graphs Depicting the Operation of the Instrument Inertia Correction Written by Hudson *et al.*[xiii]

(a) Example gel point before correction, (b) root of a gel point detected by iterative correction, and (c) corrected gel point.

Building on the automatic gel point detection software presented by Evans *et al.*, Hudson *et al.* developed a post-processing correction that introduces incremental adjustments to I_c and monitors the standard deviation of the resultant gel point. The script is then able to identify the root of the normalised deviation of both δ and time at the apparent gel point shown in Figure 1.29 (b). Since this gel point and associated value for I_c presents the most accurate gel point in terms of exhibiting a frequency independent phase angle, this can be considered the true gel point. This method is prevented from generating false gel point results by the frequency dependent nature of I_c. The paper reports that gel point measurements collected on CMT rheometers were brought back in line with results collected using an SMT rheometer through processing by the software.[149]

[xiii]Reprinted from Hudson RE, Holder AJ, Hawkins KM, Williams PR and Curtis DJ(2017) An enhanced rheometer inertia correction procedure (ERIC) for the study of gelling systems using combined motor-transducer rheometers, Physics of Fluids 29/121602, with the permission of AIP Publishing.

In 2016, Tassieri *et al.* developed a piece of software called i-Rheo which is able to perform Fourier transforms of raw data collected from stress relaxation experiments. Since errors caused by inertia (discussed in Section 2.5.4) dominate at higher frequencies, SAOS is only able to provide characterisation for a limited frequency range. By using the i-Rheo processing software, this limitation can be overcome in order to characterise viscoelastic materials over a frequency range that would be impossible to test using standard techniques. Additionally, the test requires only a single step strain making it much faster to perform than conventional frequency sweeps. Tassieri *et al.* tested this procedure on several materials including gelatine gels and the frequency resolved stress relaxation data was compared to values from conventional tests. The results showed a strong correlation between the frequency resolved stress relaxation procedure and standard testing indicating that this technique could be useful in characterising materials over an extended frequency range in a short period of time. The software requires an input stress relaxation experiment comprised of time, stress, and strain data and is valid for measurements subject to the practical considerations discussed in Section 2.5.4.[150]

1.5 Summary

Blood obtained from thrombotic patients displays abnormal clot microstructures which are less permeable and contain more thinner fibres than their healthy counterparts, associated with thrombosis. Until recently it was thought that this microstructure was responsible for the longer clot lysis times observed in thrombosis patients. However, the dense structure that has been thought to predispose individuals to thrombotic events is not a strict rule, and clots having an open structure composed of stiffer fibres have also been found to correspond with an increased propensity to embolise. Furthermore, denser structures composed of stiff fibres have been observed to correspond with shorter lysis times than less stiff equivalents. Therefore, in the case of thrombosis it appears that two material properties influence lysis time, where structurally dense clots display longer lysis times, but stiffer fibres result in shorter lysis times.

The rate and efficiency of fibrinolysis is a key determinant of how patients are likely to respond to treatment with rt-PA. Currently the most common assays used to monitor fibrinolysis are spectrophotometric assays, in which fibrin generation leads to an increase in sample turbidity and lysis results in a corresponding decrease. However, the definitions involved in these assays are arbitrary, and the detected times often relate to either a pre-determined absorbance value or a pre-determined percentage increase/decrease in absorbance. Although not widely used, TEG and TEM are considered to be the gold standard for the tandem detection of both coagulopathies and fibrinolytic potentials. However, these mechanical tests do not measure viscoelastic properties and cannot easily be related to the dynamic rheological properties of the clot. An evolving body of work on the rheological detection of coagulation parameters using SAOS has led to evidence that the detection of a Chambon-Winter gel point in coagulating blood may be a useful tool in detecting pathological risks, including thrombosis. While FTMS is considered a superior detection technique for gel point measurements, as it is less prone to sample mutation error, its use in studies of coagulation has been limited due to concerns regarding the linearity of measurements.

This thesis intends to build upon these areas by first developing an FTMS procedure using an SMT rheometer for testing blood samples, which adheres to the LVR. This procedure should surpass TEG and TEM in the same way that existing gel point procedures have, while additionally avoiding error contributions from both instrument inertia and sample mutation. This thesis will then go on to investigate the detection of fibrinolysis in human samples through measurement of a de-gel point. Novel definitions of clot lysis times will be based on the period of true haemostatic functionality of the clot. The influence of a range of biochemical factors on lysis will be investigated and compared to the commonly used spectrophotometric assays. The biochemical manipulations are expected to modulate clot structure, as well as highlighting differences between the actions of different thrombolytic agents, and will examine the impact of thrombin induced structural density on clot lysis parameters in healthy blood plasma. The final sections of the thesis will study the influence of shear fields and fibre stretching on the bulk properties of the material during the formation and breakdown of blood clots, which are known to play a significant role in clot architecture and has relevance to *in-vivo* clot formation. This section will also investigate the potential application for i-Rheo software in characterising mature clot structure and evaluating mature clot properties.

1.6 Aims and Objectives

The scope of this research is to develop and validate a novel rheological biomarker for fibrinolysis, and to investigate the potential applications of the technique with consideration given to the influence of both biochemical and biomechanical modifications of clot structure. The specific aims of this research are:

1. Development of strain controlled Fourier transform mechanical spectroscopy for the detection of coagulation in pooled platelet free plasma.
    - Establish an optimised Fourier transform mechanical spectroscopy procedure using a model gelling system.
    - Validate the optimised Fourier transform mechanical spectroscopy procedure using purified fibrin-thrombin systems with comparison against conventional techniques.
    - Confirm that the Fourier transform mechanical spectroscopy test waveforms produce linear viscoelastic data in plasma and whole blood.
    - Compare the reliability of the optimised Fourier transform mechanical spectroscopy procedure with conventional rheometrical techniques.
2. Investigation of Fourier transform mechanical spectroscopy as a tool to predict patient response to thrombolytic therapy.
    - Determine the effect of fibrinolytic agents on rheometrical clot formation and lysis parameters.
    - Investigate the effect of simulated pathological clot structure on clot lysis through biochemical manipulation.
    - Compare the rheometrical data with standard absorbance based assays.
    - Identify potential relationships between coagulation and clot lysis parameters.
    - Apply the rheometrical technique to a physiologically relevant whole blood system.

3. Examination of the influence of clot structure on lysis without the addition of exogenous coagulation enhancers through biomechanical manipulation.
    - Simulate the influence of shear stresses exerted on a thrombus during formation and examine the effect on mature clot characteristics and lysis.
    - Investigate the underlying mechanisms involved in the mechanics of lysis in clots formed under shear through the comparison of rheometrical results with advanced imaging techniques.
4. Further investigate the influence of force on fibres by examining the impact of platelet contraction on clot formation and lysis.
    - Determine whether tension applied to fibres impacts rheometrical detection.
    - Determine whether the detection of lysis characteristics is influenced by clot contraction.
    - Investigate the rheological behaviour of different blood fractions during coagulation and lysis.

Chapter 2

Theory and Methodology

Rheology is the science of deformation and flow. The measurement of rheology is known as rheometry, which encompasses many techniques used to investigate the behaviour of materials. Small amplitude oscillatory shear (SAOS) techniques involve the application of an oscillatory stress or strain to a material and evaluation of the corresponding response to provide measurements of viscoelasticity. This section will provide an introduction to rheology including the theory of linear viscoelasticity and an overview of the Chambon-Winter gel point criterion.

2.1 Rheological Properties of Materials

2.1.1 Viscosity

The parallel plates model is frequently used to describe the behaviour of materials under stress. The model pictured in Figure 2.1 can be thought of as a series of layers stacked on top of each other representing the layers of a fluid placed between two moving plates with a height (h).[151]

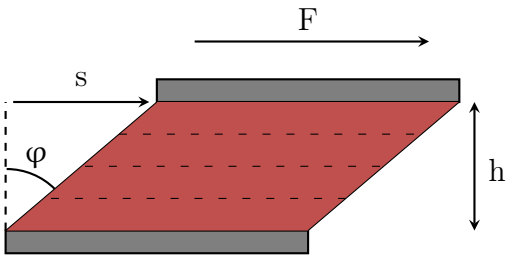

Figure 2.1: The Parallel Plates Model: A Diagrammatic Representation of a Fluid Between Two Plates.

When a motion with a force (F) is applied through the top plate, the layers below will move, each with a lesser displacement than the layer above giving a deflection angle (φ). This is caused by internal friction between the layers, the viscosity (η).[151]

The shear stress (σ) is the component of stress applied to a material which occurs along the plane of the layers, defined as:

$$\sigma = \frac{F}{A} \qquad \text{(Eq. 2.1)}$$

where A is the area upon which the force acts.[151]

The Shear strain (γ) is the measure of the degree of displacement of the material resulting from the applied stress, defined by:

$$\gamma = \frac{s}{h} \qquad \text{(Eq. 2.2)}$$

$$\gamma = \tan \varphi \qquad \text{(Eq. 2.3)}$$

The shear rate ($\dot{\gamma}$) is an expression of the relative velocity of each layer under stress and can be calculated as:

$$\dot{\gamma} = \frac{\Delta\gamma}{\Delta t} \qquad \text{(Eq. 2.4)}$$

$\dot{\gamma}$ may then be used to calculate η using Newton's law for ideal-viscous behaviour:[151]

$$\eta = \frac{\sigma}{\dot{\gamma}} \qquad \text{(Eq. 2.5)}$$

Newtonian and Non-Newtonian Fluids

For Newtonian fluids the relationship between $\dot{\gamma}$ and σ is constant and the material has an inherent η when measured at a fixed temperature as depicted in Figure 2.2 (a), where Newton's law is obeyed. In contrast, non-Newtonian fluids do not obey this relationship and in response to increasing stress the material may display shear thinning behaviour where η decreases with increasing σ as shown in Figure 2.2 (b), shear thickening where η increases with increasing σ as shown in Figure 2.2 (c), or Bingham plastic behaviour, where the material flows with an inherent η only after a threshold σ is reached shown in Figure 2.2 (d).[151]

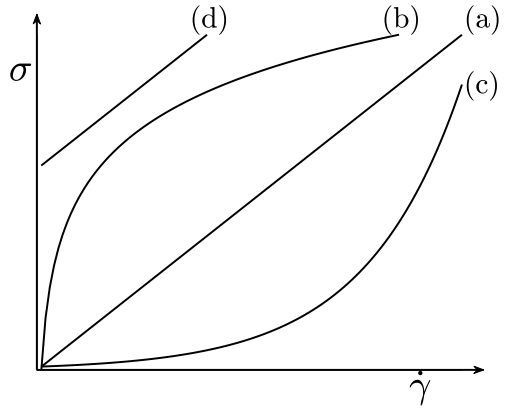

Figure 2.2: A Graph Illustrating the Relationship Between Shear Rate and Stress for Different Types of Materials.

(a) Newtonian fluids, (b) shear thinning materials, (c) shear thickening materials, and (d) Bingham plastics.

The ideal-viscous behaviour of Newtonian fluids is often characterised by the dashpot model illustrated in Figure 2.3. As the piston is pushed into the sample, material flows through the gap between the piston and the cylinder wall, and the speed at which the piston moves through the material is directly proportional to the force applied. When the force is removed from the piston, movement of the piston immediately stops and the system remains static.[151]

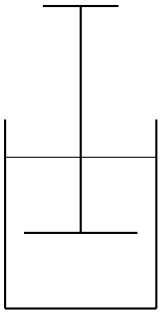

Figure 2.3: A Schematic Representation of the Dashpot Model.

2.1.2 Elasticity

The two plates model, previously illustrated in Figure 2.1, can also be used to describe the elastic behaviour of materials provided the following conditions are met; the material is being tested in the linear viscoelastic region (LVR), further discussed in Section 2.5.4, and the material is securely attached to the top and bottom plate (*i.e.* there is no wall slip) as described in Section 2.5.4. In this instance the relationship between σ and γ can be defined as a constant, the shear modulus (G):[151]

$$G = \frac{\sigma}{\gamma} \qquad \text{(Eq. 2.6)}$$

to resolve this with time:

$$\dot{\sigma} = \frac{\Delta\sigma}{\Delta t} \qquad \text{(Eq. 2.7)}$$

$$\dot{\gamma} = \frac{\dot{\sigma}}{G} \qquad \text{(Eq. 2.8)}$$

This is the definition of Hooke's law for ideal-elastic behaviour which states, for ideal-elastic materials, the level of deformation the material undergoes is proportional to the force applied, providing the measurement remains within the LVR.[151]

The behaviour of ideal-elastic materials can be characterised by a spring model, as depicted in Figure 2.4. In this model, as the spring is either compressed or extended it immediately shows a corresponding deformation and the extent to which the spring is stretched or compressed is proportional to the force acting upon it. Additionally, there is a constant associated with the stiffness of the spring which defines the amount of deformation that will occur as a result of the applied force. When the force is removed the spring recoils immediately and completely.[151]

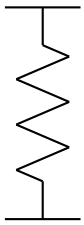

Figure 2.4: A Schematic Representation of the Spring Model.

2.1.3 Viscoelasticity

Viscoelastic materials display neither ideal-viscous (*i.e.* Newtonian) nor ideal-elastic (*i.e.* Hookean) behaviour, instead they display elements of both. However, one of these behaviours often dominates.[151]

Viscoelastic liquids typically include polymer solutions and polymer melts, from which a significant amount of the behaviour is influenced by the solvent phase. Viscoelastic solids include cross-linked materials, gels, and concentrated solutions, in which the majority of the observed behaviour is driven by the insoluble phase.

The two most common models which serve to describe these responses are the Maxwell model which describes viscoelastic liquids, and the Kelvin-Voigt model which describes viscoelastic solids. These models can be described through either a series or parallel combination of the dashpot and spring representations.[151]

The Maxwell Model

The Maxwell model illustrated in Figure 2.5 describes viscoelastic liquid behaviour, and is depicted by a spring coupled in series with a dashpot. When a force is applied to the system the spring immediately deforms under the stress such that the deformation is proportional to the force applied. While the force is maintained the piston in the dashpot slowly moves and continues to move until the force is removed. When the force is removed from the system the spring immediately recoils while the dashpot remains stationary; since the motion of the dashpot is not recoverable the system will not return to its original position.[151]

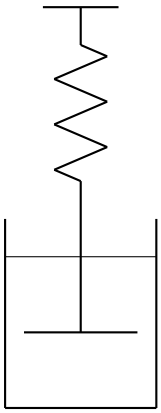

Figure 2.5: A Schematic Representation of the Maxwell Model.

This model relies on the assumption that the total strain is the sum of both the elastic (γ_e) and viscous(γ_v) strains:

$$\gamma = \gamma_e + \gamma_v \qquad \text{(Eq. 2.9)}$$

and that the total shear rate is the sum of the shear rates of both components of the system:

$$\dot{\gamma} = \dot{\gamma}_e + \dot{\gamma}_v \qquad \text{(Eq. 2.10)}$$

Since the material obeys both Newton's law (Equation 2.5) and Hooke's law (Equation 2.8):[151]

$$\dot{\gamma} = \frac{\sigma}{\eta} + \frac{\dot{\sigma}}{G} \qquad \text{(Eq. 2.11)}$$

The Kelvin-Voigt Model

The Kelvin-Voigt model shown in Figure 2.6, depicts an instance where a dashpot and spring are connected in parallel. As a force is applied to the system the two components deform in unison. Therefore the spring does not undergo immediate deformation, rather both the dashpot and spring move with time while the force is applied. When the force is removed the recoil of the spring is dampened as the spring must also draw the dashpot back to its original position. This results in the slow return of both the spring and the dashpot to their original undeformed state.[151]

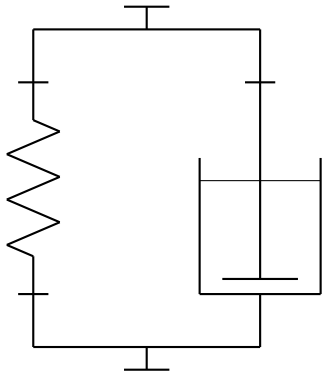

Figure 2.6: A Schematic Representation of the Kelvin-Voigt Model.

Both the displacement under stress and return to the undisplaced state occur as an exponential function of time. This model relies on the assumption that the stress is equally applied to both components of the system.

It also relies on the assumption that both of the components of the system are displaced by the same amount and the stress is the sum of both the elastic and viscous components:

$$\gamma = \gamma_v = \gamma_e \qquad \text{(Eq. 2.12)}$$

$$\sigma = \sigma_v + \sigma_e \qquad \text{(Eq. 2.13)}$$

Since the material also obeys both Newton's law (Equation 2.5) and Hooke's law (Equation 2.8):[151]

$$\sigma = \eta \cdot \dot{\gamma} + G \cdot \gamma \qquad \text{(Eq. 2.14)}$$

2.2 Creep and Stress Relaxation

Creep and stress relaxation tests can be used to characterise the viscoelastic behaviour of materials. Creep tests involve the application and removal of a step stress where the strain response is monitored. Stress relaxation techniques involve the application of a fixed displacement (step strain) and the stress response is monitored.[151]

2.2.1 Creep and Creep Recovery

Creep and creep recovery tests involve the application and removal of stress as shown in Figure 2.7 to examine behaviours such as those discussed above. The material is under no stress (σ_0) before the test. At time t_0 a stress of σ_{max} is applied to the material, this stress is maintained until time t_1 (creep) where the stress is reduced to zero (σ_0). No stress is applied and the strain response is monitored until time t_2 (creep recovery).[151]

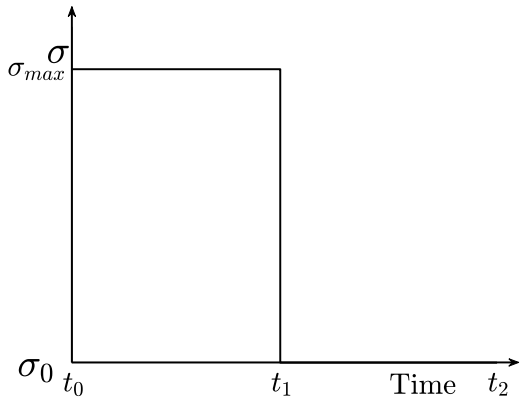

Figure 2.7: A Graph Depicting the Stress Applied to a Material as a Function of Time During a Creep Experiment.

Where stress is initially applied at t_0 and removed at t_1.

As described previously for ideal-viscous materials the strain will increase between t_0 and t_1 in a linear fashion relative to the applied stress. Between t_1 and t_2 when the stress is removed the strain remains constant as no further deformation or recoil occurs. This is depicted in Figure 2.8.[151]

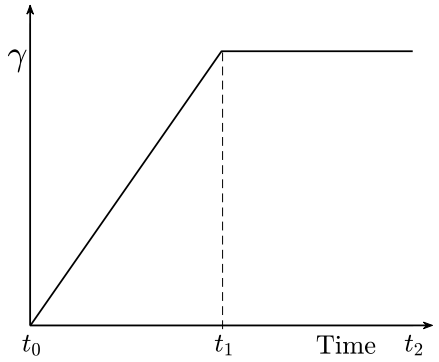

Figure 2.8: A Graph Depicting the Strain Response as a Function of Time for an Ideal-Viscous Material Under Creep Testing.

Where stress is initially applied at t_0 and removed at t_1.

For ideal-elastic materials the strain will increase instantaneously to γ_{max} at t_0 with the application of stress where it will remain constant until t_1. With the removal of stress at t_1 the strain will instantaneously decrease to γ_0 as the material returns to its undeformed state where it will remain constant as long as no further stress is applied as shown in Figure 2.9.[151]

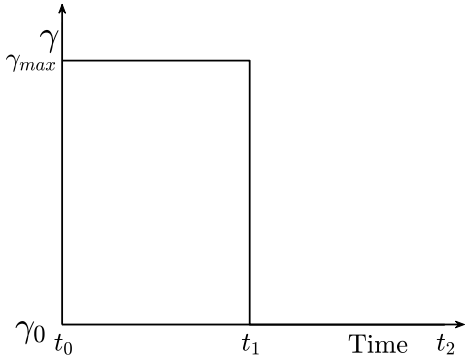

Figure 2.9: A Graph Depicting the Strain Response as a Function of Time for an Ideal-Elastic Material Under Creep Testing.

Where stress is initially applied at t_0 and removed at t_1.

Viscoelastic materials will show an increase in strain with the applied stress between t_0 and t_1. However, the creep recovery $(t_1 - t_2)$ response is different for viscoelastic liquids and solids. Viscoelastic liquids, shown in Figure 2.10 (a), will reform slowly and show a level of permanent deformation which will not recover owing to the dominant viscous behaviour described by the Maxwell model. Viscoelastic solids, shown in Figure 2.10 (b), will reform completely owing to the elastic characteristics of the material described by the Kelvin-Voigt model.[151]

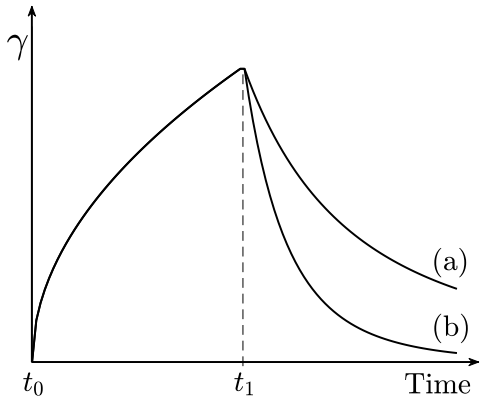

Figure 2.10: A Graph Depicting the Strain Response as a Function of Time for Viscoelastic Materials Under Creep Testing.

(a) Viscoelastic liquids and (b) viscoelastic solids.
Where stress is initially applied at t_0 and removed at t_1.

From a creep test $(t_0 - t_1)$ the materials creep compliance modulus $J(t)$ can be determined as:[151]

$$J(t) = \frac{\gamma(t)}{\sigma} \qquad \text{(Eq. 2.15)}$$

2.2.2 Stress Relaxation

Stress relaxation experiments are performed by the application of a step strain as shown in Figure 2.11. Between time t_0 and time t_1 the material is subjected to a small constant strain (γ_1) in order to reduce the influence of any stress the sample may have been subjected to during set-up. At t_1 the maximum strain (γ_{max}) is applied. This level of strain is then maintained until time t_2, and the stress response is monitored.[151]

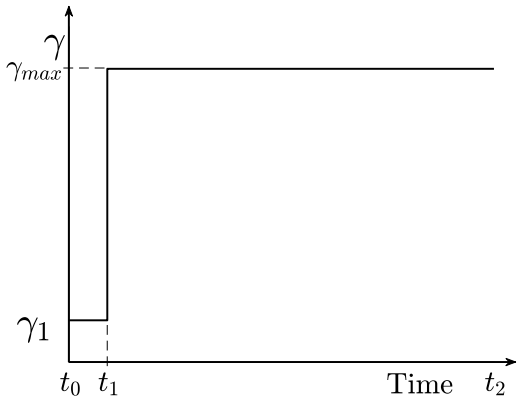

Figure 2.11: A Graph Depicting the Strain Applied to a Material as a Function of Time During a Stress Relaxation Experiment.

Where strain is substantially applied between t_1 and t_2.

For an ideal-viscous material, when a strain displacement (σ_{max}) is imposed upon the material an instantaneous increase in stress is detected. The material is then permanently deformed and an almost immediate relaxation to σ_0 can be observed, as shown in Figure 2.12.[151]

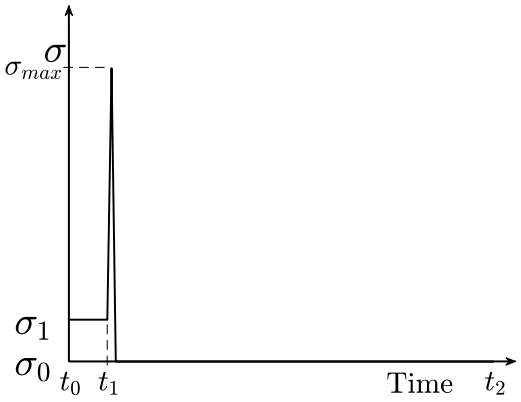

Figure 2.12: A Graph Depicting the Stress Relaxation as a Function of Time for an Ideal-Viscous Material.

Where strain is substantially applied between t_1 and t_2.

In contrast, ideal-elastic materials immediately deform under stress to give a strain proportional to the stress, *i.e.* the increase in strain at t_1 results in an increase in stress to σ_{max}. σ_{max} must be maintained between t_1 and t_2 in order to hold the strain constant as shown in Figure 2.13; release of the stress would cause the material to recoil and γ would return to 0. No relaxation occurs for ideal-elastic materials.[151]

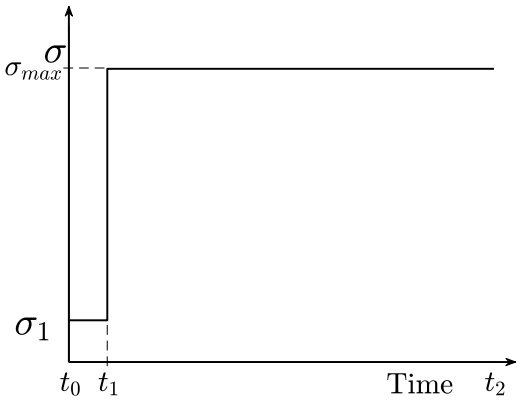

Figure 2.13: A Graph Depicting the Stress Relaxation as a Function of Time for an Ideal-Elastic Material.

Where strain is substantially applied between t_1 and t_2.

All viscoelastic materials display an increase in stress to σ_{max} at t_1 as a result of the imposed strain. This is followed by a gradual stress relaxation response between $t_1 and t_2$. For viscoelastic liquids, depicted in Figure 2.14 (a), a delayed but complete relaxation can be observed, as the material requires a lower and lower stress to maintain the displacement; this occurs as the viscous properties of the material cause it to permanently deform and eventually reach σ_0. Viscoelastic solids, shown in Figure 2.14 (b), gradually relax between $t_1 - t_2$, however they do not reach σ_0. Instead, the stress required to maintain the displacement reaches an equilibrium, at which point the elastic nature of the material would still cause the system to recoil if the stress were removed.[151]

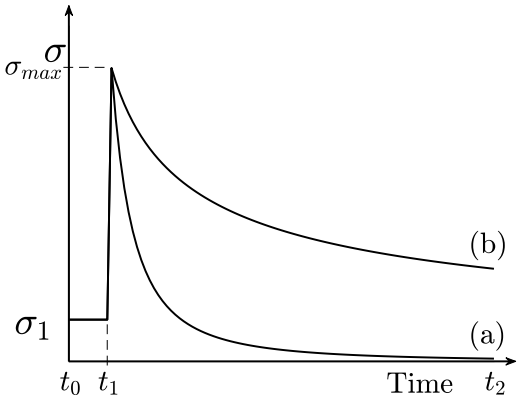

Figure 2.14: A Graph Depicting the Stress Relaxation as a Function of Time for Viscoelastic Materials.

(a) Viscoelastic liquids and (b) viscoelastic solids.
Where strain is substantially applied between t_1 and t_2.

From the results of a stress relaxation test a material's stress relaxation modulus ($G(t)$) can be determined as:[151]

$$G(t) = \frac{\sigma(t)}{\gamma} \qquad \text{(Eq. 2.16)}$$

Viscoelasticity and Stress Relaxation

If a viscoelastic spring and dashpot model is considered under a stress relaxation test, initially at t_1 only the spring is displaced and σ=σ_{max}. The spring then acts to recoil and transfers the strain to the dashpot which undergoes a permanent displacement. The energy being applied to the system is initially taken by the spring and subsequently dissipated through the dashpot. This will cause a gradual relaxation of σ until either σ_0 is reached for a viscoelastic liquid, when all of the displacement experienced by the spring has been transferred to the dashpot and no further stress is required to maintain γ, or an equilibrium is reached in a viscoelastic solid, where the spring and dashpot have equilibrated and the transfer of energy stops.

This can be described through the Maxwell model, which describes the monotonic relaxation of stress in response to an imposed strain, as:

$$\sigma(t) = \sigma_0 e^{\frac{-Gt}{\eta}} \qquad \text{(Eq. 2.17)}$$

Since the relaxation time (τ_r) is defined as the time at which the stress has relaxed to $\frac{1}{e}$ and can be considered a ratio of viscosity to elasticity:[151]

$$\tau_r = \frac{\eta}{G} \qquad \text{(Eq. 2.18)}$$

then:

$$\sigma(t) = G \cdot \gamma \cdot e^{(\frac{-t}{\tau_r})} \qquad \text{(Eq. 2.19)}$$

2.3 Small Amplitude Oscillatory Shear

The principal of motion in SAOS can be described using the previous two plates model pictured in Figure 2.15. Where, as in Figure 2.1, F is the force acting on the material, s is the displacement of the material, h is the height of the material and φ is the angle of deflection. However, in this case these variables may either be positive or negative depending on the direction of motion at a given time.[151,152]

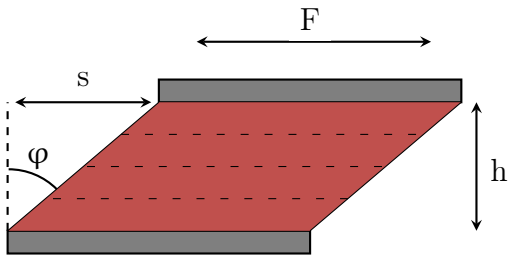

Figure 2.15: The Parallel Plates Model: A Diagrammatic Representation of a Fluid Between Two Plates.

SAOS can be performed through either stress or strain controlled experiments. Here we consider stress controlled SAOS, but the theory is equally applicable to strain controlled systems. In SAOS a stress is applied to a material as a sine wave having a frequency f and an amplitude σ_0:

$$\sigma = \sigma_0 \cos \omega t \qquad \text{(Eq. 2.20)}$$

where:

$$\omega = 2\pi f \qquad \text{(Eq. 2.21)}$$

This relates to the displacement during oscillation in such a way that, as illustrated in Figure 2.16, A_{max} is equivalent to s_{max}, A_0 is equivalent to the originating position and A_{min} is equivalent to s_{min}.[151,152]

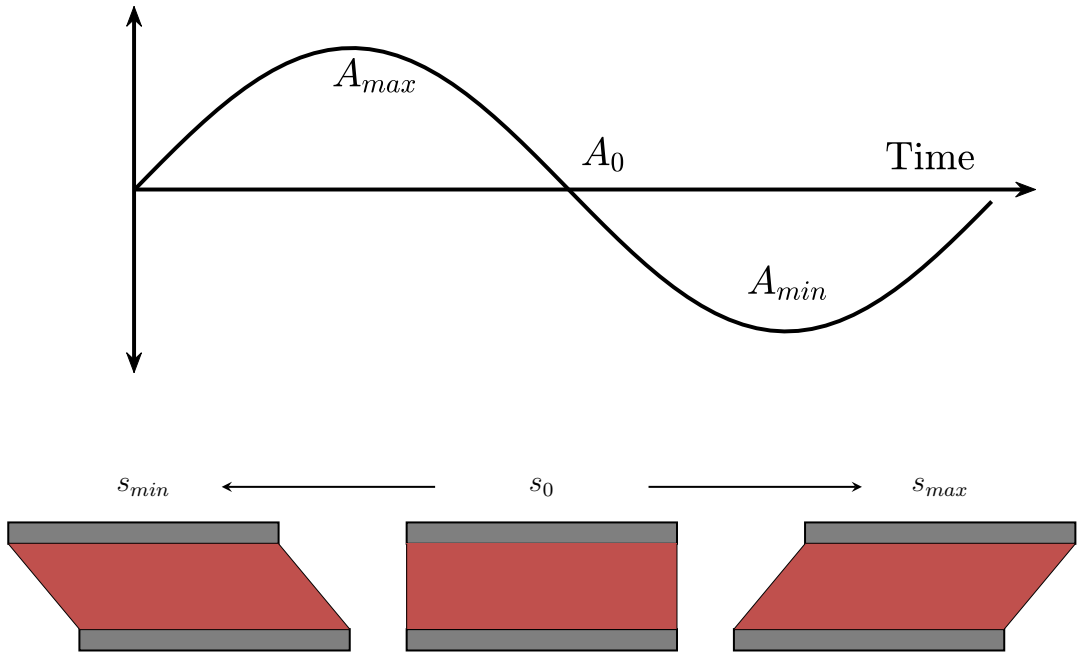

Figure 2.16: A Graphic Representation of a Small Amplitude Oscillatory Shear Waveform and Corresponding Two Plates Model.

The phase angle (δ) corresponds to the lag between the applied stress and resultant strain as shown in Figure 2.17.[151,152]

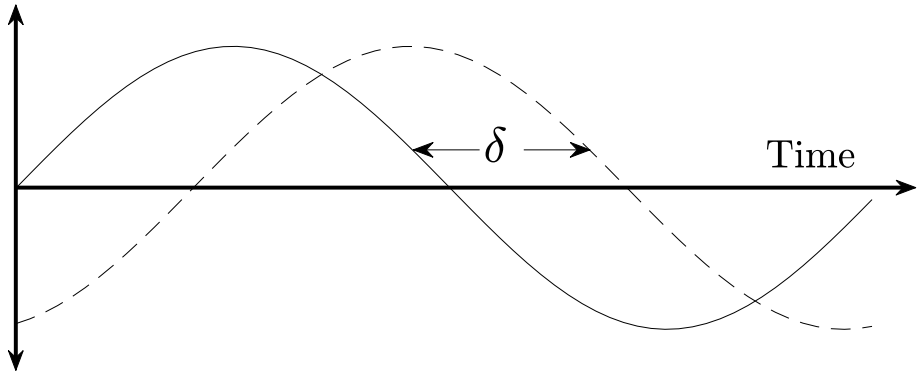

Figure 2.17: A Graphic Representation of Small Amplitude Oscillatory Shear Stress and Strain Waveforms.

Where δ is the lag between the applied stress (solid) and resultant strain (dashed).

2.3.1 Ideal-Viscous Behaviour

For ideal-viscous materials, as described previously, the displacement of the sample occurs slowly in a time dependent manner with the application of stress. Ideal-viscous materials undergoing SAOS obey a complex adaptation of Newton's law (Equation 2.5) in which η^* is the complex viscosity of the material which is related to the time element of the wave.

$$\eta^* = \frac{\sigma(t)}{\dot{\gamma}(t)} \qquad \text{(Eq. 2.22)}$$

The relationship between η^* and $\dot{\gamma}$ is constant, and as such, the material behaves in a way that the stress applied is directly in phase with the strain rate. As a result, the strain is always out of phase with the stress and δ=90 °.[151,152]

$$\gamma = \gamma_0 \sin \omega t \qquad \text{(Eq. 2.23)}$$

2.3.2 Ideal-Elastic Behaviour

For ideal-elastic materials, the displacement of the sample occurs instantaneously with the application of stress. In SAOS the material obeys a complex adaptation of Hooke's law (Equation 2.8) in which G^* is the complex shear modulus of the material, related to the stress relaxation modulus.

$$G^* = \frac{\sigma(t)}{\gamma(t)} \qquad \text{(Eq. 2.24)}$$

As G^* is directly proportional to γ the material behaves in a way that the strain response of the material is always in phase with the applied stress. As such, for ideal-elastic materials δ=0 °.[151,152]

$$\gamma = \gamma_0 \cos \omega t \qquad \text{(Eq. 2.25)}$$

2.3.3 Viscoelastic Behaviour

Since viscoelastic materials display elements of both viscous and elastic behaviour $0\ ^\circ < \delta < 90\ ^\circ$:

$$\gamma = \gamma_0 \cos(\omega t - \delta) \qquad \text{(Eq. 2.26)}$$

by trigonometry this then yields:

$$\gamma = \gamma_0 \cos\delta \cos\omega t + \gamma_0 \sin\delta \sin\omega t \qquad \text{(Eq. 2.27)}$$

The shear stress and strain may then be expressed as:

$$\sigma^* = \sigma_0 e^{i(\omega t)} \qquad \text{(Eq. 2.28)}$$

$$\gamma^* = \gamma_0 e^{i(\omega t - \delta)} \qquad \text{(Eq. 2.29)}$$

and G^* can be defined as:

$$G^* = \frac{\sigma^*}{\gamma^*} = (\frac{\sigma_0}{\gamma_0}) e^{i\delta} \qquad \text{(Eq. 2.30)}$$

and split into its real and imaginary components; the storage modulus (G') and the loss modulus (G''):[151,152]

$$G^* = G' + iG'' \qquad \text{(Eq. 2.31)}$$

where G' is the real component of the complex modulus and represents the elastic behaviour of the material which immediately deforms under stress storing the applied energy. G'' is the imaginary component of the complex modulus representing the viscous properties of a material which deforms slowly with the application of stress and where the energy applied is lost through permanent displacement. These relationships can be expressed as a vector as shown in Figure 2.18.[151,152]

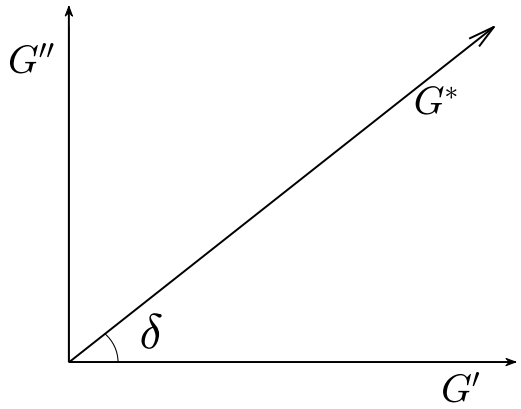

Figure 2.18: A Graph Illustrating the Relationship between G', G'', and G^*.

Through application of *Pythagorean theorem* it is possible to determine the individual components G' and G'' from G^*:

$$G^* = \sqrt{(G')^2 + (G'')^2} \qquad \text{(Eq. 2.32)}$$

G' and G'' may also be considered as:

$$G' = (\frac{\sigma_0}{\gamma_0}) \cos \delta \qquad \text{(Eq. 2.33)}$$

$$G'' = (\frac{\sigma_0}{\gamma_0}) \sin \delta \qquad \text{(Eq. 2.34)}$$

which leads to the definition of the loss tangent ($\tan \delta$) as:

$$\tan(\delta) = \frac{G''}{G'} \qquad \text{(Eq. 2.35)}$$

G' and G'' may also be considered in terms of the material's stress relaxation response from the Maxwell model as:[152]

$$G'(\omega) = \frac{G \cdot \omega^2 \cdot {\tau_r}^2}{1 + \omega^2 \cdot {\tau_r}^2} \qquad \text{(Eq. 2.36)}$$

$$G''(\omega) = \frac{G \cdot \omega \cdot \tau_r}{1 + \omega^2 \cdot {\tau_r}^2} \qquad \text{(Eq. 2.37)}$$

Frequency and Viscoelasticity

If a viscoelastic liquid is observed under increasing applied frequency both G' and G'' will increase; however, the increase in G' is larger than that of G'' as shown in Figure 2.19 (a). This means that for viscoelastic liquids, overall the relative elastic nature of the material increases with increasing frequency which corresponds to a decrease in δ. However, for viscoelastic solids G' is almost independent of the frequency of the test while G'' increases as shown in Figure 2.19 (b) which leads to an increase in δ with increasing frequency.[151,152]

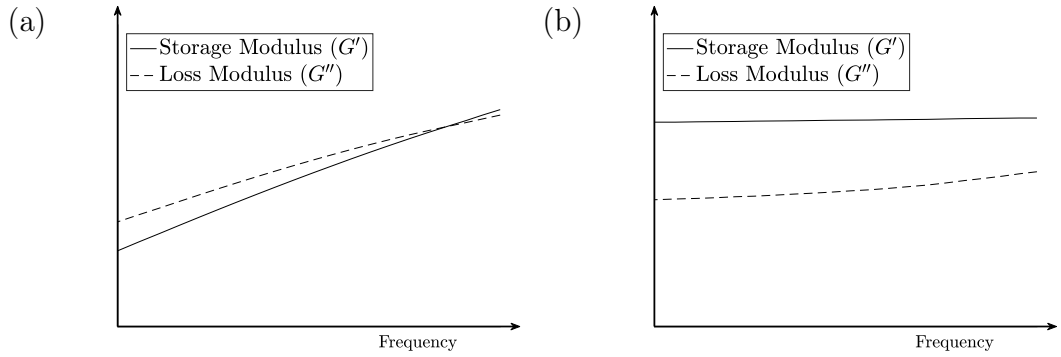

Figure 2.19: Graphs Illustrating the Storage and Loss Moduli of Viscoelastic Materials as a Function of Frequency.

(a) Viscoelastic liquids and (b) viscoelastic solids.

2.4 Gelation

The process of gelation can be considered as a transition from viscoelastic liquid to a viscoelastic solid behaviour. During this transition, the material passes through the gel point, which represents the precise moment at which this change occurs.[153]

2.4.1 Transient Properties During Gelation

In a gelling system, there is a transition from a behaviour dominated by the viscous component (G'') to a behaviour dominated by the elastic component (G'). In the case of fibrin network formation as the soluble fibrinogen is converted to insoluble fibrin and polymerises, resulting in gelation and a dominance in elasticity.

Initially the material can be thought of as a solution of large molecules which display viscoelastic liquid stress relaxation characteristics (the sol phase), where stress relaxation is quick and complete. This holds true even as the network begins to form, as the initial fragments of network behave as larger molecules within a dispersion, and the material remains able to flow and relax. At the moment that a self-similar fibrin network spans the entire sample the material is known as a 'critical gel'. Following this, the network grows and the sample behaves as a viscoelastic solid with slow and incomplete stress relaxation characteristics (the gel phase). The material is no longer fully able to flow and the presence of a distinct elastic component now impedes relaxation.

The precise moment at which the network first becomes sample spanning is the critical gel (also known as the gel point), which obeys the Chambon-Winter Gel Point criterion associated with percolation theory described below.[153]

2.4.2 Chambon-Winter Gel Point Criterion

The gel point, considered as the moment of transition from viscoelastic liquid to viscoelastic solid, can be theoretically defined as the moment at which the zero shear viscosity (η_0) of a sample extends to infinity while the equilibrium shear rigidity modulus (G_∞) becomes non-zero, depicted in Figure 2.20. This state is known as the critical gel.[153]

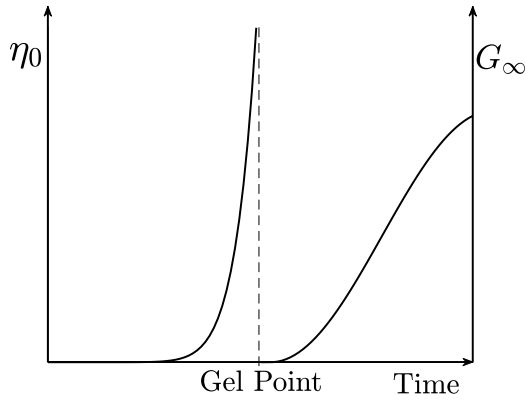

Figure 2.20: A Graph Illustrating the Theoretical Behaviour Predicted at the Gel Point.

Where η_0 extends to infinity and G_∞ becomes non-zero.

Since the direct detection of this phenomena is not possible, Chambon and Winter further developed this definition and showed a unique stress relaxation behaviour of the critical gel. In the moments before the critical gel, while the system is in the sol state, the stress relaxation of the system is complete and the material fully relaxes as shown by $G(t)$ in Figure 2.21 (a). This relaxation time increases as further crosslinking occurs until the material reaches a critical gel shown by Figure 2.21 (b). The increase in relaxation time follows an inverse power law:

$$G(t) = S \cdot t^{-\alpha} \qquad \text{(Eq. 2.38)}$$

where S is the strength of the gel and α is the stress relaxation exponent. In the moments after the critical gel, relaxation is incomplete and the material can be characterised as a viscoelastic solid shown by Figure 2.21 (c).[153,154]

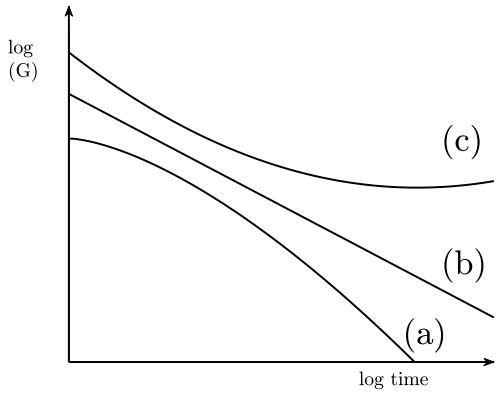

Figure 2.21: A Graph Illustrating the Relationship Between the Stress Relaxation Modulus and Time in a Gelling System.

(a) Viscoelastic liquid, (b) critical gel, and (c) viscoelastic solid.

In addition to this, Chambon and Winter proposed that, for a stoichiometrically balanced chemical reaction, the gel point must be entirely material dependent, and as such independent of the frequency at which the test is performed:

$$G'(\omega) = G''(\omega) = A\omega^{\alpha} \qquad \text{(Eq. 2.39)}$$

where A is a constant of the material under test. In relation to Figure 2.19 which depicts G' and G'' as a function of frequency for viscoelastic solids and liquids, the critical gel appears as shown in Figure 2.22, where the storage and loss moduli scale with each other resulting in δ being independent of frequency.

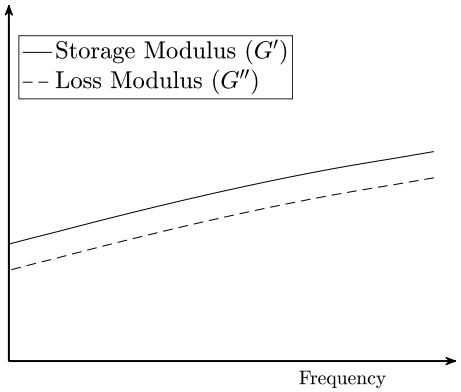

Figure 2.22: A Graph Illustrating the Relationship Between the Storage and Loss Moduli of a Critical Gel as a Function of Frequency.

In combination with Equation 2.35 this leads the gel point to be practically defined under SAOS as the moment at which δ is independent of ω as seen in Figure 2.23.[153,154]

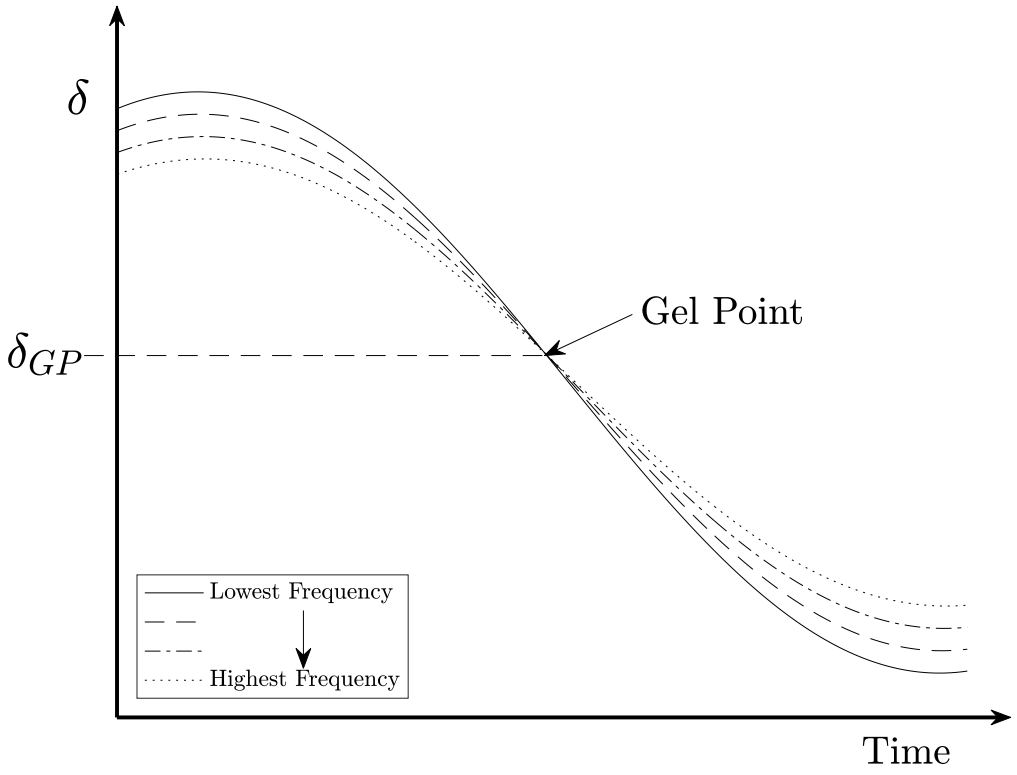

Figure 2.23: A Graph Illustrating a Gel Point as Defined by Chambon and Winter.

Where the gel point is defined as the moment at which δ is independent of frequency during the sol-gel transition.

Therefore, at the gel point:

$$tan(\delta) = \frac{G''}{G'} = tan(\frac{\alpha\pi}{2}) \qquad \text{(Eq. 2.40)}$$

and so the value of α can be derived from the value of δ at the instant of frequency independence as:[153,154]

$$\alpha = \frac{2 \cdot \delta_{GP}}{\pi} \qquad \text{(Eq. 2.41)}$$

2.4.3 The Fractal Dimension

Classic percolation theory describes the formation of clusters within a lattice where the probability (p) of a box being occupied is equal for each box and independent of the occupation of neighbouring boxes. Each box also has a corresponding probability $1 - p$ of being empty as seen in Figure 2.24, where the probability of box A being occupied is not dependent on the status of boxes B, C, or D.

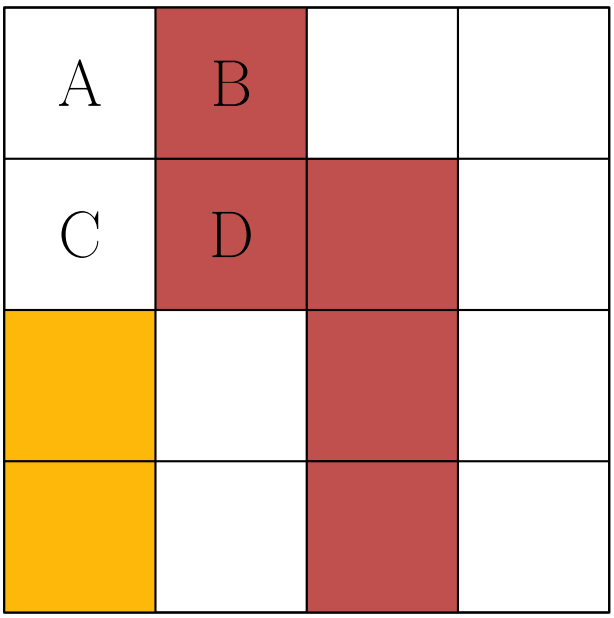

Figure 2.24: A Diagram Showing a Percolation Cluster.

Where two or more neighbouring boxes are both occupied, the aggregate is known as a cluster, shown by the shaded boxes in Figure 2.24. Percolation theory defines a critical occupation probability (p_c) at which an infinite cluster exists, spanning the distance between two opposite sides of an infinite lattice, as represented by the red cluster in Figure 2.24.

A fractal object is an extension of this, where a self-similar pattern can be seen as independent of the size of the boxes it is mapped through. The fractal dimension (d_f) is an expression of the complexity with which an object, in this case a cluster, fills the space that it occupies, with higher values of d_f indicating greater levels of structural complexity.[155]

The polymerisation of macromolecules can be modelled using a version of kinetic percolation theory where the probability (p) associated with the structure relates to the probability of a monomer diffusing to the branch point of a proto-polymer over a distance. This model is similar to that of diffusion limited aggregation, but differs in that sites having a low p value become blocked for further binding. In this instance p=p_c is reached when the range of molecular weights spans to infinity, *i.e.* the range of molecular weights spans from that of the smallest unreacted monomer to the infinitely large cluster associated with the critical gel. Considering this structure as a spherical lattice the d_f can then be considered:

$$R \approx m^{(\frac{1}{d_f})} \qquad \text{(Eq. 2.42)}$$

where R is the radius of gyration and m is the molecular mass of the material.[156]

Since the gel point is defined as the moment at which there is a sample spanning structure which is self-similar, this can be related to percolation theory and a fractal dimension for the molecular cluster can be obtained. Muthumakunar *et al.* defined the relationship between α at the gel point and the d_f as:

$$d_f = \frac{(D-2\alpha)(D+2)}{2(D-\alpha)} \qquad \text{(Eq. 2.43)}$$

where D is the Euclidean dimension, and in this instance D=3 for a three dimensional space.[157]

2.4.4 The De-Gel Point

The de-gel point can be associated with de-gelation, shown in Figure 2.25, at which a transition from viscoelastic solid behaviour, through a critical state, to viscoelastic liquid behaviour takes place. The d_f value which can be obtained at the de-gel point can be assumed to relate to the last sample spanning structure present.[158]

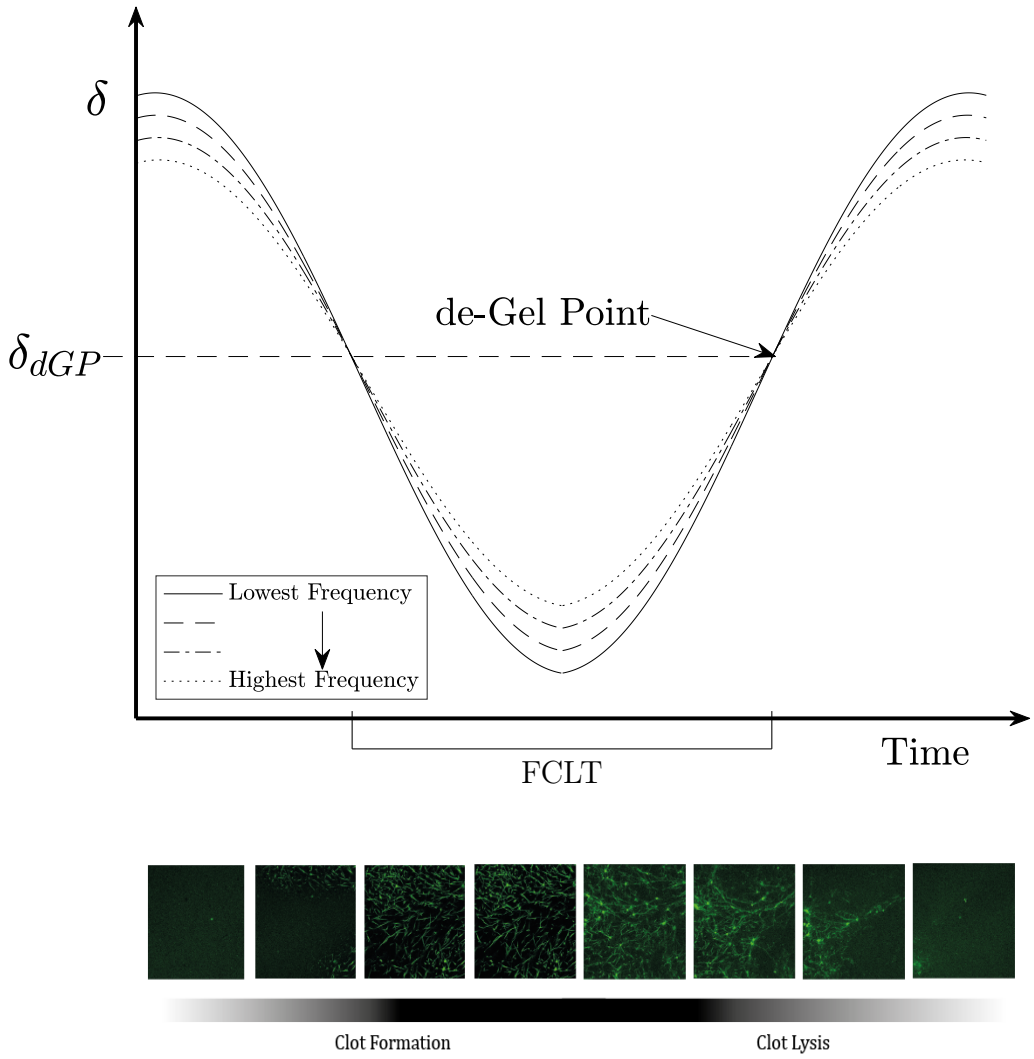

Figure 2.25: A Graph Illustrating a de-Gel Point Based on the Gel Point Criteria Defined by Chambon and Winter.

Where the de-gel point is defined as the moment at which δ is independent of frequency during the gel-sol transition.

Confocal images collected by Dr N. Badiei (College of Engineering, Swansea University) illustrate changes in network architecture over the time period.

In the case of blood clotting and fibrin network formation the time between the gel point and de-gel point of blood can be defined as the functional clot lifetime ($FCLT$). The $FCLT$ unequivocally represents the period during which the fibrin network can support a stress, and thus marks the period of haemostatic functionality of the clot.

2.5 Gel Point Detection

Since the gel point is defined as the moment that δ is independent of frequency, the detection procedure requires the monitoring of a sample undergoing gelation at several different frequencies. Rheometrically, this can typically be performed in three different ways.

2.5.1 Discrete Sweeps

The detection of gel points using discrete frequency sweeps involves the application of oscillatory waves as a repeating series of frequencies. These waveforms change frequency at set intervals as shown in Figure 2.26 in order to build a plot of changing parameters over time.

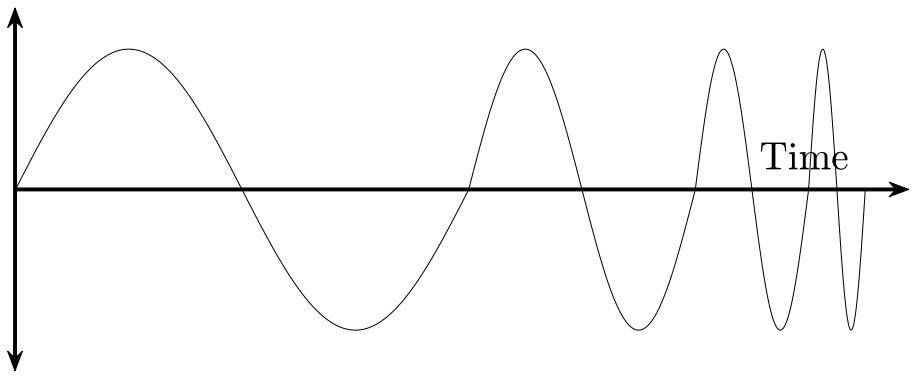

Figure 2.26: A Graph Illustrating a Discrete Frequency Sweep Waveform.

The key advantage of this technique is the ability to accurately control the amplitude of the oscillation and ensure that the material remains within the LVR described in Section 2.5.4. However, as each frequency is probed at large time intervals, errors can arise from sample mutation which is detailed in Section 2.5.4.[142,143]

2.5.2 Fourier Transform Mechanical Spectroscopy

Fourier transform mechanical spectroscopy (FTMS) allows the application of multiple frequencies as a single complex waveform where multiple waveforms, typically built from the harmonics of a user defined fundemental frequency, are added together as shown in Figure 2.27.

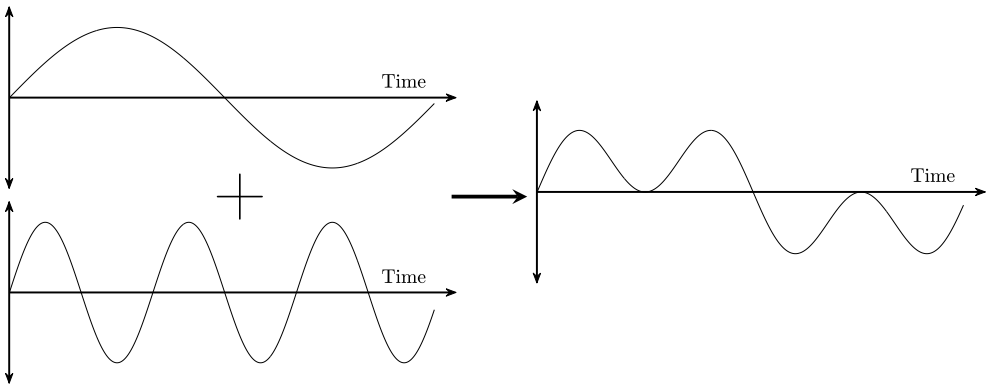

Figure 2.27: A Graph Illustrating a Complex Waveform Generated from Two Discrete Frequencies.

During FTMS the applied stress takes the form:

$$\sigma = \sum_{i=1}^{m} \sigma(\omega_i) = \sum_{i=1}^{m} \sigma_i \sin \omega_i t \qquad \text{(Eq. 2.44)}$$

where m is the number of frequency components and σ_i and ω_i relate to the i^{th} component.[159]

The application of this complex wave to a sample results in a corresponding complex wave, from which the contributions at each frequency can be derived in terms of both amplitude and phase using Fourier transform.

This technique has the advantage of limiting errors from sample mutation, since each frequency is monitored continuously. However, the maximum amplitude of these complex waveforms is higher than that of the fundamental frequency alone, due to the superposition of the waveforms. Since the magnitude of the response at each frequency is a property of the material the total amplitude cannot easily be predicted. As a result this technique requires additional care to be taken to remain within the LVR of the material.[142,143]

2.5.3 Optimally-Windowed Chirp

Optimally-Windowed Chirp (OWCh) waveforms are a recent development in SAOS and involve the use of a chirp waveform in which the frequency of the waveform increases over the course of the wave as shown in Figure 2.28. As with FTMS, the corresponding waveform can be interpreted by applying a Fourier transform. This technique enables the testing of a wider range of frequencies than FTMS over a shorter time period than discrete frequency sweeps. A window is applied to the amplitude of the waveform in order to reduce spectral leakage during Fourier analysis.[160]

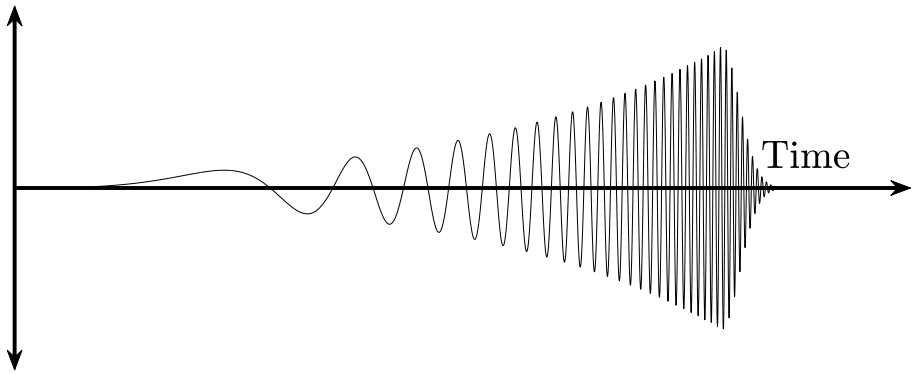

Figure 2.28: A Graph Illustrating a Windowed Chirp Waveform.

2.5.4 Practical Considerations

The Linear Viscoelastic Region

The linear viscoelastic region (LVR) is the range of stresses or strains in which the behaviour of a material is not substantially influenced by the rheological testing, and apparent values of G' and G'' are independent of the stress applied.

The LVR can be determined by performing an amplitude sweep and observing the values of G' and G''; a sharp decrease in the values of the moduli at a certain stress or strain value is indicative of the end of the LVR as shown in Figure 2.29.[151]

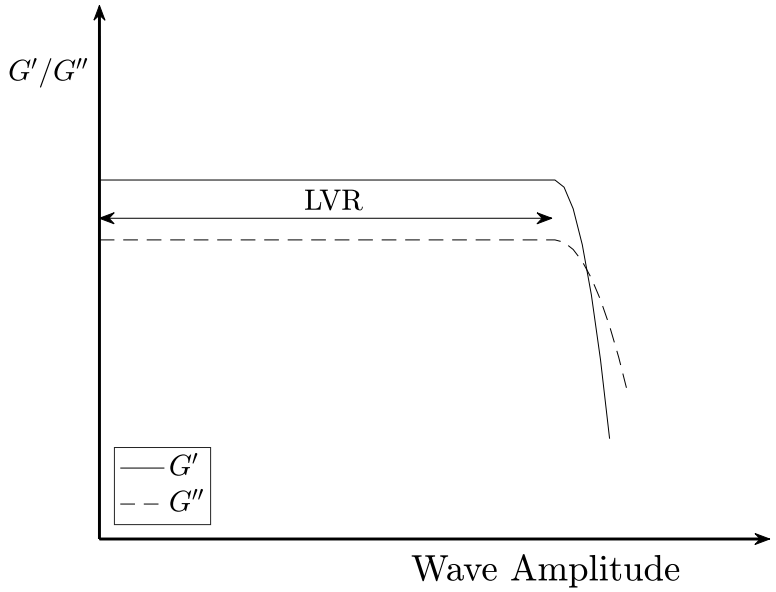

Figure 2.29: A Graph Illustrating the Definition of the Linear Viscoelastic Region from an Amplitude Sweep Experiment.

G' (solid) and G'' (dashed).

Wall Slip

In materials such as suspensions and emulsions which are subjected to large velocity gradients or inhomogeneous stress fields, the suspended particles can tend away from the geometry surface. This results in a thin layer of low viscosity solvent immediately adjacent to the plate or wall of the geometry giving rise to an apparent 'slip'.[161,162]

The slip velocity (μ_s) is the difference between the velocity of the wall and of the fluid at the wall surface, where μ_s is related to both the fluidity of the slip layer (ϕ) and σ, and can be calculated as:

$$\mu_s = \sigma \cdot \phi \qquad \text{(Eq. 2.45)}$$

Rheological measurements and the subsequent calculation of material properties often rely on the assumption that μ_s=0, which is not true where wall slip occurs. μ_s can be determined by measuring viscosity of a material at different gap sizes. Since the slip layer forms an additional component in the parallel plate model given in Figure 2.1.1, the system containing slip will follow the equation:

$$F = \mu_s + h\frac{\delta\gamma}{\delta t} + \mu_s \qquad \text{(Eq. 2.46)}$$

When measurements are collected at varying gap sizes, the discrepancy in the measured viscosity can be related back to this equation to determine the properties of the slip layer. This characterisation can be used to retroactively correct for the error; however, in the case of gelling systems this approach is impractical due to the evolving nature of the material.

In SAOS measurements the wall slip phenomena can be visualised in the waveforms as a 'flat topped' sinusoidal wave which is non-linear. This effect can produce large errors in steady shear measurements and lead to a significant reduction in the apparent viscosity of the material being tested.[161]

Wall slip can be detected for rheological procedures either by observing the material behaviour at a range of gap sizes or utilising different geometries in order to confirm that the moduli are independent of the test set-up; alternatively waveforms can be monitored for signs of slip during oscillatory procedures. Where wall slip is present this can be reduced to a negligible effect by roughening the surfaces of both the upper and lower geometry.[161]

Inertia

Both fluid and instrument inertia may dominate SAOS measurements of low viscosity fluids or weak gels. Instrument inertia arises from the acceleration of the moving parts of a rheometer, while fluid inertia is a result of the acceleration of a sample. Most rheometer control software includes a correction which recalculates the values of the moduli using values from an inertial calibration. However, in instances where inertia dominates the detected response, significant errors can still occur. This can be detected by examining the raw δ values obtained from experiments; inertia is considered to dominate where $\delta > 150$ °.[163] In SAOS procedures the level of inertia is highly dependent on the frequency at which the waves are produced, with lower frequencies being less prone to inertial artefacts; this is often the limiting factor in selecting a frequency range within which to test.[149]

Geometry Selection and Gap Size

Several different types of geometry may be utilised during SAOS procedures, including bob and cup, depicted in Figure 2.30 (a), concentric cylinders, depicted in Figure 2.30 (b), cone and plates, depicted in Figure 2.30 (c), and parallel plates which are depicted in Figure 2.30 (d).

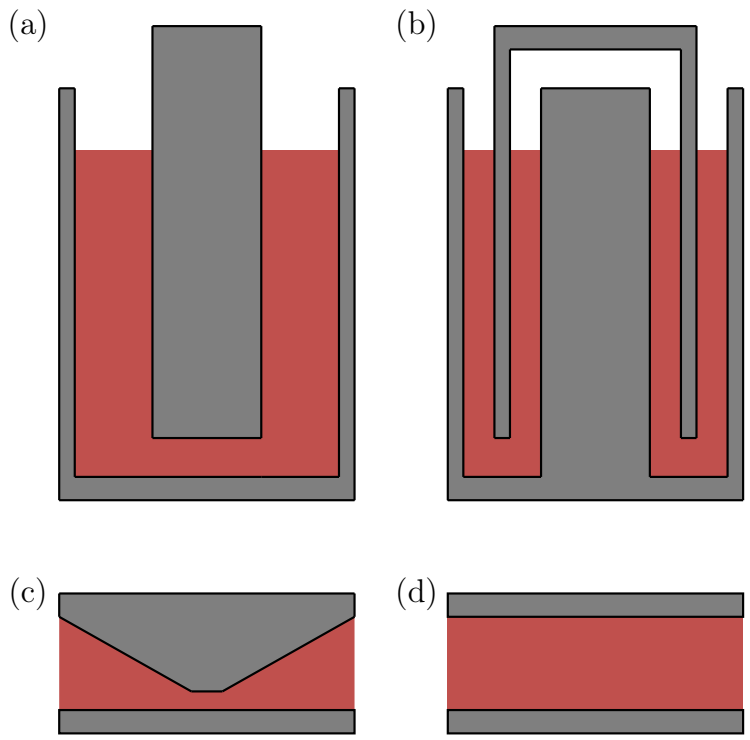

Figure 2.30: An Illustration of Different Rheometer Geometries.

(a) Bob and cup, (b) concentric cylinder, (c) cone and plate, and (d) parallel plate.

The bob and cup geometry consists of a base having an upwardly projecting cylinder to form a cup within which a sample is placed. The upper geometry comprises a second cylinder (the bob), which is lowered into the cup containing the sample. This geometry is particularly well adapted to measuring low viscosity fluids due to the large surface area in contact with the sample. However, it is not compatible with axial force adjustments and requires a large sample volume for testing.

The double concentric cylinder geometry is similar to a bob and cup, consisting of a base having two upwardly projecting cylinders between which a sample is placed, the upper geometry comprises a third cylinder which is lowered into the gap containing the sample. This geometry is also well adapted to measuring low viscosity fluids, and is less prone to errors resulting from surface tension and fill as the sample surface area is very small. However, the concentric cylinder is not compatible with axial force adjustments as the upper cylinder must be used at a fixed position; in addition, the double concentric cylinder also requires a large sample volume for testing.

The cone and plate geometry requires a much smaller sample volume than the concentric cylinder, and has a distinct advantage over parallel plate geometries as the shape of the geometry allows for the application of a uniform shear rate across the gap. However, it is also not compatible with an axial force maintained measurement, where the gap is varied to control a fixed axial force, as the cone must be used at a fixed truncation gap.

The parallel plate geometry also requires a much smaller sample volume than the concentric cylinder geometry and is compatible with axial force adjustments as the gap size can be independently set. However, a non-uniform shear rate is applied across the sample gap. When using a parallel plate the gap size is a user defined variable and should be selected according to the testing parameters. Gap sizes which are very small are usually avoided, as at very low values any errors in gap calibration are apparent. However, smaller gap sizes are best suited to low viscosity fluids as the surface area to volume ratio is increased.[151]

The gap size can also be selected in order to minimise the impact of fluid inertia on the sample by remaining within the gap loading limit, within which the propagating wave is reflected back from the stationary surface such that every point within the gap is in motion and in phase with the motor surface. In order to maintain the error in δ below 1 ° the gap size should not exceed $1/40^{\text{th}}$ of the wavelenth (λ) which can be calculated using:[164]

$$\lambda = 2\pi/\ cos\frac{\delta}{2} \cdot \sqrt{\frac{\omega \cdot \rho}{\eta^*}} \qquad \text{(Eq. 2.47)}$$

However, in large particle suspensions the minimum gap size is limited by the size of the particles. Since larger particles have a tendency to be pushed towards the outer edges of the sample when placed under shear, the gap size must be maintained at a size ten times greater than that of the largest particle in order to minimise the influence of this phenomenon.[163]

Surface Tension

Errors in rheological measurements can be introduced through the influence of surface tension at the material-air or material-oil interface around the perimeter of the geometry. Asymmetry within this contact line can lead to the detection of an additional torque signal during measurement, resulting in significant errors in the apparent viscosity and other moduli.

In order to minimise errors generated in this way it is necessary to ensure that the rheometer is correctly filled, as depicted in Figure 2.31. In best practice solvent traps or low viscosity silicone oil are used to prevent evaporation, which could lead to surface tension induced errors, during long tests.

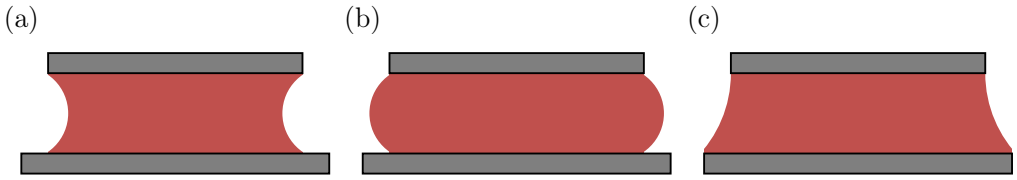

Figure 2.31: An Illustration of a Parallel Plate Geometry Showing Different Fills. (a) Underfill, (b) correct fill, and (c) overfill.

In addition to surface tension being present at the surface-air / surface-oil interface, errors may be introduced by the presence of bubbles within the sample and great care must be taken to ensure that no bubbles are introduced during sample loading.[165]

Sample Mutation

Errors from sample mutation commonly occur in rapidly gelling systems where the properties of the material significantly change over the sampling period. The mutation number (N_{mu}) can be defined as:

$$N_{mu} = \frac{2\pi}{\omega G'} \cdot \frac{\Delta G'}{\Delta t} \qquad \text{(Eq. 2.48)}$$

where the measurements are considered dominated by the error if n_{mu} >0.15.[142]

The effects of sample mutation can be negated by reducing the sampling time of the procedure either by sampling at a higher frequency, or reducing the number of waveforms sampled. However, this may be limited, as inertial influence is more apparent with increasing frequency, and the impact of measurement instability may be more apparent when sampling a reduced number of waveforms.[142,166]

Chapter 3

Optimisation and Validation of High Frequency Fourier Transform Mechanical Spectroscopy for Gel Point and de-Gel Point Detection

The study of blood clotting and associated pathologies is of high value to the medical community, with conditions relating to thrombosis considered leading contributors to global morbidity and mortality. The structure of fibrin fibre networks formed during the process of coagulation is known to be denser in patients with diseases associated with thrombosis, and therefore, it's measurement can provide a biomarker of such disease. The structure of the fibrin network influences the mechanical properties of the clot, and results in differences in the viscoelastic behaviour.[18,105,131,141]

The viscoelastic properties associated with thrombosis can be measured using rheometry, and recent studies have shown that small amplitude oscillatory shear techniques have the potential to identify abnormalities in coagulation. This is achieved by characterisation of the incipient clot structures associated with these events, through detection of the Chambon-Winter gel point.[127–130,132–134,136,137,139]

Current rheometrical methods for the characterisation of incipient clots rely on the measurement of whole blood samples during the course of coagulation. However, this has several drawbacks when considering the investigation and development of therapies: (i) the rate of sample degradation and the inability to pool blood means that each sample of blood must be collected on an individual basis for each test, (ii) the high degree of biological variation requires many participants to be involved in a single study. This leads to resource intensive and time-consuming research, which limits the number of parameters that can be studied. These obstacles can be overcome through the use of purified fibrin-thrombin model systems which have provided valuable insights into the relationships between rheological parameters.[143,146] However, these model systems lack the complexity of the physiological system and have limited application in investigating the impact of factors associated with the coagulation cascade.

Platelet free plasma (PFP), obtained from centrifugation of individual blood samples can be pooled into a batch, which avoids the pitfalls associated with the use of both whole blood and model systems to provide a standard test material. This standard test material has been utilised since the 1950's and allows the coagulation cascade in all of its complexity to be manipulated experimentally, as well as permitting the material to be stored (by freezing at -80 °C) for use at a later date.[167] PFP does have the disadvantage of lacking cellular components, and therefore cannot account for the influence of platelets, erythrocytes, or leukocytes. PFP has been used extensively in other areas of research, but its use in the rheological characterisation of the incipient clot is particularly challenging, due to rheometrical constraints. The nature of PFP makes gel point detection difficult as the material has a narrow and transient linear viscoelastic region (LVR) that is bound by the limits of the instrument and a transient critical stress and strain. PFP also gels relatively rapidly leading to mutational artefacts caused by significant changes to the material's rheological properties over a testing cycle. In addition, PFP has a relatively low initial viscosity compared to whole blood, making measurements prone to artefacts from both instrument and fluid inertia.

Previous studies of coagulation have relied on the application of discrete frequency sweeps at relatively low frequencies (<3 Hz) using combined motor transducer (CMT) rheometers.[143] The rapidity of plasma gelation leads to difficulties resulting from sample mutation, which is exacerbated by the low frequencies employed. Of particular concern is the potential for this to lead to self-biasing data, where tests that show rapid clot formation are more likely to be subject to mutational artefacts, and therefore more likely to be excluded from analysis. This difficulty could theoretically be overcome by utilising Fourier transform mechanical spectroscopy (FTMS) at higher frequencies, where the simultaneous collection of data in a comparatively short time frame would reduce the effects of sample mutation.[142] However, the use of high frequency FTMS measurements requires the consideration of both the linearity of measurements, as the total wave amplitude in FTMS is significantly greater than that of a single frequency wave, and sample and instrument inertia which become more apparent with increasing frequency.[143]

There are advantages and disadvantages associated with the absence of blood cells and platelets in PFP. The lack of cells in the material leads to a decrease in the initial viscosity, further exacerbating the effect of inertia. However, the removal of the largest components (such as red and white blood cells) also allows for measurements to be conducted at lower gap sizes whilst satisfying the criterion that the gap must be ten times the largest particle size. In principle, it is possible to adhere to the gap loading limit at higher frequencies, thereby negating the effect of inertia.[163,164]

The use of a separate motor transducer (SMT) rheometer, in which instrument inertia can be considered negligible, coupled with the ability to test at low gap sizes may allow for the detection of gel points at high frequencies without artefacts resulting from either sample mutation or inertia. Additionally, the use of higher frequencies requires a lower strain to be applied to the material in order to generate a well defined and resolvable stress response.[149] However, the linearity of measurements is of particular concern, and so must be investigated in order to develop a gel point detection procedure. The multiwave nature of FTMS does not allow the use of the third harmonic to monitor linearity during gelation, therefore alternative methods must be utilised to assess the linearity of measurements. Thus, in line with the aforementioned considerations, the work in this section aims to develop an appropriate FTMS procedure that is capable of detecting the gel point in PFP samples.

In order to develop this procedure the work begins with the investigation of gelatine, which is a well characterised model for gelling systems, for initial optimisations of the rheometrical procedure. The model fibrin-thrombin system will then be used to validate the procedure for coagulation, as manipulation of the ratio of fibrinogen:thrombin provides a means of varying the incipient and mature clot structure in a controlled manner. The gel point measurements will be further validated by comparison of the fractal dimension (d_{f}) values with measurements from imaging studies in order to confirm the relationship between rheometrical measurements of incipient structures and mature clot architecture. Following optimisation and validation of the new procedure using model systems, the linearity of measurements for PFP and whole blood will be confirmed and the results will be compared to conventional CMT tests.

3.1 Methods

3.1.1 Sample Preparation

Gelatine

A solution of 2.5 % (w/v) gelatine was made up by the addition of granular gelatine (Fisher Scientific, UK: 10774751) to distilled water which had been heated to 60 °C. The solution was held at 60 °C in a waterbath and frequently mixed by gentle agitation for 45 minutes. The solution was then aliquoted and stored for up to four weeks at 4 °C until use. Immediately prior to testing the solution was heated to 35 °C in a waterbath in order to melt the samples before being loaded onto the rheometer for testing.

Fibrin Thrombin

A 44.45 mg/ml stock of purified plasminogen depleted human fibrinogen (Enzyme Research Laboratories, UK: FIB1) was reconstituted using tris buffered saline (Sigma Aldrich, UK: T5912) which was diluted to 1 x solution using distilled water (TBS). The reconstituted solution was allowed to fully dissolve in a waterbath at 37 °C before being aliquoted and stored at -80 °C until use. Before use the fibrinogen was allowed to thaw at room temperature and stored at room temperature for a maximum of 8 hours.

Thrombin (Enzyme Research Laboratories, UK: HT 1002a) was reconstituted to a concentration of 500 NIH/ml using distilled water at room temperature before being aliquoted and stored at -80 °C until use. The thrombin was allowed to thaw at room temperature before being diluted to a final stock concentration of 5 NIH/ml in distilled water which was stored at 4 °C for a maximum of 2 hours before use.

Tween 20 (J. T. Baker, USA: 7374.1000) was added to TBS to make up a 1 % wt. stock solution of TBS-Tween 20, which was stored at 4 °C until use.

Immediately before testing, the fibrinogen, thrombin, and TBS-Tween 20, in addition to $CaCl_2$ (Sigma Aldrich, UK: 21115-100ML), were combined in TBS to make up solutions of 5 mg/ml Fibrinogen, 0.1 % wt Tween 20, 0.005 M $CaCl_2$, and either 0.03, 0.06 or 0.09 NIH/ml thrombin. These solutions were mixed gently by aspirating the sample into the pipette tip and slowly releasing several times.

Blood and Plasma

Blood samples were collected from the median cubital vein of healthy volunteers using a 21-gauge butterfly line (Greiner Bio-One, UK: 450085) by a trained phlebotomist under ethical approval (SUMS RESC: 2018-0063). All volunteers declared themselves healthy and free from the influence of agents that may interfere with coagulation testing (see Appendix A). The first 3 ml of blood was collected in an additive free vacuette® tube (Greiner Bio-One, UK: 454241) and discarded to minimise tissue factor present as a result of the venipuncture. The desired volume of blood was then collected in 9 ml citrated (3.8 %) vacuette® tubes (Greiner Bio-One, UK: 455322). The citrated samples were inverted 6-8 times to ensure adequate mixing of the sample and additive. The sodium citrate present within the samples acts as a reversible anti-coagulant by chelating free Ca^{2+} ions which are required for coagulation. This can be reversed by the addition of $CaCl_2$ at a 1:1 concentration with the sodium citrate, which results in the original concentration of Ca^{2+} ions being restored.

Pooled Platelet Free Plasma

36 ml of citrated blood was collected into 9 ml Vacuette® tubes from each volunteer as described above. Owing to the time taken to collect and prepare samples, blood draws were performed on separate occasions to generate multiple batches containing plasma from several donors each, giving a total of 20 individual donors.

The Vacuette® tubes were placed into a swinging rotor centrifuge (Eppendorf, UK: 5810R) at 25 °C and centrifuged at 2500 xg for 15 minutes in order to separate the cellular components and platelets from the plasma. The platelet poor plasma (PPP) was then siphoned from the top of the tube using a pipette into 50 ml plastic centrifuge tube (Greiner Bio-One, UK: 210270) leaving approximately 1 ml undisturbed to prevent contamination from the buffy layer. At this stage plasma from multiple donors was combined in each container.

These containers were then subjected to a second centrifugation step at 2500 xg, for 15 minutes at 25 °C in order to remove residual platelets and generate platelet free plasma (PFP). The PFP was then siphoned from the top of the tubes using a pipette into a cell culture flask (Greiner Bio-One, UK: 658190) which was gently inverted several times to ensure appropriate mixing of samples. Approximately 1 ml of the PPP was left in the centrifuge tube to ensure there was no contamination from disturbance of the pellet. The pooled PFP was then aliquoted and stored at -80 °C until use.

Before use, samples from each of the batches were thawed at 37 °C for 5 minutes in a waterbath and inverted gently to ensure any precipitate was re-suspended. The samples were then combined proportionally to produce pooled PFP (P-PFP) containing equal volumes from 20 donors. The plasma samples were re-calcified with 18 mM (final concentration) $CaCl_2$ to induce coagulation and mixed gently by aspirating the sample into the pipette tip and slowly releasing it several times.

Whole Blood

Citrated blood was collected as described above from individual donors, the samples were held at room temperature for a maximum of two hours. Coagulation was initiated through the addition of 18mM $CaCl_2$ (final concentration) and mixed gently by aspirating the sample into the pipette tip and slowly releasing it several times.

Scanning Electron Microscopy Sample Preparation

Fibrin-thrombin gels and P-PFP clots were formed in a 24 well cell culture plate (Costar: 3524) as described above and allowed to mature. Following clot maturation the samples were washed using cocodalyte buffer (SPI Supplies, US: 02619-RA) before being treated with 2 % gluteraldehyde solution (Sigma Aldrich, UK: G5882-100ML) overnight. The samples were again washed using cocodalyte buffer and subjected to incrementally increasing concentrations of ethanol (Fisher, UK: E/0650DF/17) from 30-100 %. The samples were then treated with a 50 % (v/v) solution of ethanol and hexamethyldisilazane (HDMS) (Sigma Aldrich, UK: 440191-100ML). The samples were washed with 100 % HDMS several times before final suspension in 100 % HDMS which was allowed to evaporate. The samples were fixed to SEM pin stubs (Agar Scientific, UK: G301F) using carbon tape and sputter coated (Quorum, UK: Q150T ES) with a 15 nm gold coating.

3.1.2 Data Collection

Small amplitude oscillatory shear as described in Section 2.3 was conducted using either a stress controlled or strain controlled rheometer. In this thesis the commercially available stress controlled rheometer AR-G2 (TA instruments, UK) was used along with the strain controlled rheometer ARES-G2 (TA instruments, UK). Complementary scanning electron microscopy (SEM) (Hitachi, JP) provided images which allow for the visual assessment of mature clot micro-structure.

AR-G2

The AR-G2 rheometer, shown in Figure 3.1, is a dual mode rheometer capable of conducting both stress controlled and strain controlled measurements. However, its native mode is stress controlled and its strain control functions utilise feedback loops making it less desirable as a strain controlled instrument.

Figure 3.1: A Photograph Showing the Experimental Set-up of the AR-G2 Rheometer.

The AR-G2 set up consists of a Peltier plate base upon which a sample is loaded, and the rheometer head which contains a combined motor and transducer system. The Peltier plate is connected to a waterbath and is able to maintain constant temperatures between -40 and 200 °C.[168] The components of the AR-G2 head are shown in Figure 3.2 which include a geometry attached to a central shaft, a thrust plate surrounded by bearing actuators which make up the magnetic bearing, an induction drag cup motor and an angular position sensor. The angular displacement and angular velocity of the shaft is detected by an optical encoder.[168]

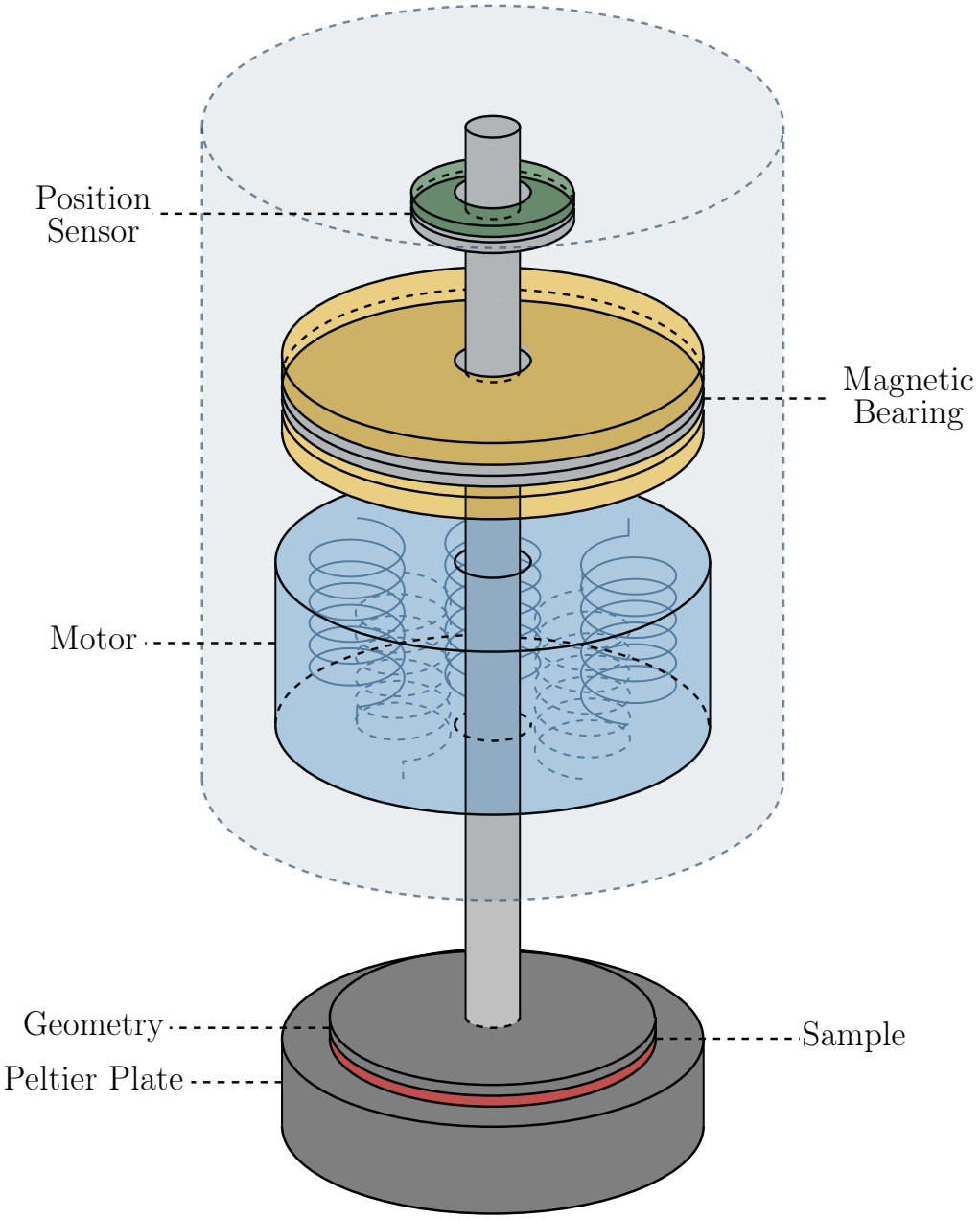

Figure 3.2: A Representative Diagram of an AR-G2 Rheometer.

One of the main considerations in rheometer design is the influence of friction between the stationary and moving parts. While many rheometer designs use an air bearing to reduce the friction, the AR-G2 operates using a magnetic bearing which allows for a much wider gap between the components, further reducing internal friction. This magnetic bearing uses an iron thrust plate which is held by electromagnetic actuators positioned both above and below the plate. The position of the rheometer shaft is detected by a magnetic position sensor which feeds back to the actuators to maintain the fixed axial position of the shaft. The AR-G2 uses a normal force transducer in place of a standard normal force sensor, which is isolated from the motor and bearing. This allows for the accurate detection of normal forces by minimising movement of the head in the vertical direction.

The motor used by the AR-G2 is a drag cup motor which, due to its unique rotor and stator design, lends itself to low friction applications transferring motion to the shaft and geometry. Porous carbon radial air bearings maintain a stiff support in the radial direction ensuring that the geometry is held stable in place over the sample.

The low-inertia optical encoder is used to detect the angular displacement and angular velocity of the shaft. It utilises a photocell to detect differences in the light patterns between a rotating and static transparent disk positioned between the photocell and a light source.

Both the magnetic thrust bearing and drag cup motor allow the AR-G2 to function accurately at low torques giving the AR-G2 an operating range of 0.003 μN.m - 200 mN.m. However, with this rheometer design instrument inertia remains an obstacle to high resolution measurements at low torques, with a typical motor inertia of 18 μN.m.s.[168]

In order to compensate for the inertia generated by both the instrument and the sample the TRIOS software, which is used to control the AR-G2 rheometer, includes the following inertia corrections:

$$G' = G'_{raw} - I_c\omega^2 k_g \qquad \text{(Eq. 3.1)}$$

where I_c is a calibrated inertia constant and k_g is a geometry inertia factor.

AR-G2 Rheometer Procedures

The AR-G2 rheometer calibration was validated using silicone viscosity standard (Brookfield Engineering, USA: 1000) prior to testing. Before initiating each test the temperature of the Peltier plate was set and instrument calibration was performed. The geometry was then attached to the rheometer shaft via the spindle and calibrated. Zero gaping was then performed, during which the geometry was lowered until an axial force was detected when contact with the Peltier plate was made. The head was then raised and precision mapping with three iterations performed. The samples were loaded onto the rheometer and the head brought down to the truncation gap for the geometry. Upon contact of the geometry with the sample the geometry was gently rotated in order to ensure that the sample was fully homogenised and spread evenly throughout the gap.

The fill was then inspected and adjusted when necessary to ensure no under or over fill was present. Samples were sealed with silicone oil (Brookfield Engineering, USA: 10) to prevent evaporation during the test and the measurement procedure *i.e.* gel point detection, was initiated. Upon completion of the measurements the head was raised and both the Peltier plate and geometry were washed using a dilute soap solution and rinsed with distilled water. The components were then sterilised using a 70 % ethanol solution before being rinsed again with distilled water.

The gel point detection procedure performed on fibrin-thrombin gels has been previously reported in the literature and involved the application of discrete frequency sweeps at 2, 1.6, 0.7 and 0.3 Hz using a 1 ° cone and plate geometry with a diameter of 60 mm.[143] The stress applied was 0.09 Pa and testing was conducted at 24 °C on gels containing 5 mg/ml fibrinogen and a thrombin concentration ranging from 0.03-0.09 NIH/ml (number of replicates (n)=5). The linearity of measurements was confirmed through monitoring the third harmonic in the waveform of the strain response in the vicinity of the gel point.

Gel points were measured herein for P-PFP using a 60 mm parallel plate geometry at a gap of 175 μm. A stress of 0.09 Pa was applied and the linearity of measurements was confirmed through the absence of third harmonic signals in the vicinity of the gel point. The tests were conducted at 37 °C using frequencies of 0.4, 0.7, 1.3 and 1.7 Hz (n=5).

ARES-G2

In contrast to the AR-G2 rheometer, the ARES-G2's native mode is strain controlled. Its control software also includes an auto-strain adjust function which allows users to specify a strain and torque range within which the measurement must remain. Thus, in principle, despite being a controlled strain instrument, it can operate in a fixed stress-range mode. The ARES G2 rheometer set up is shown in Figure 3.3

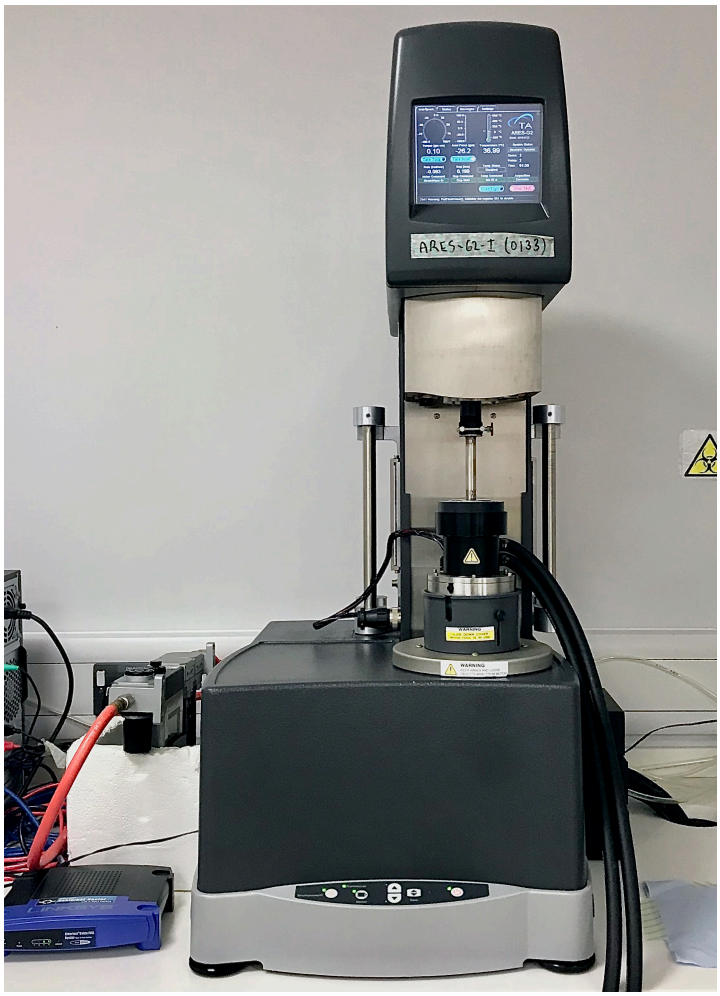

Figure 3.3: A Photograph Showing the Experimental Set-up of the ARES-G2 Rheometer.

The ARES-G2 is a separate motor transducer rheometer in which the motor is positioned below the sample and moves the Peltier plate attachment while torque transducers are positioned in the head of the instrument as illustrated in Figure 3.4. The isolation of these two functions negates the impact of instrument friction and inertia and allows for high accuracy torque measurements to be made.[163,169]

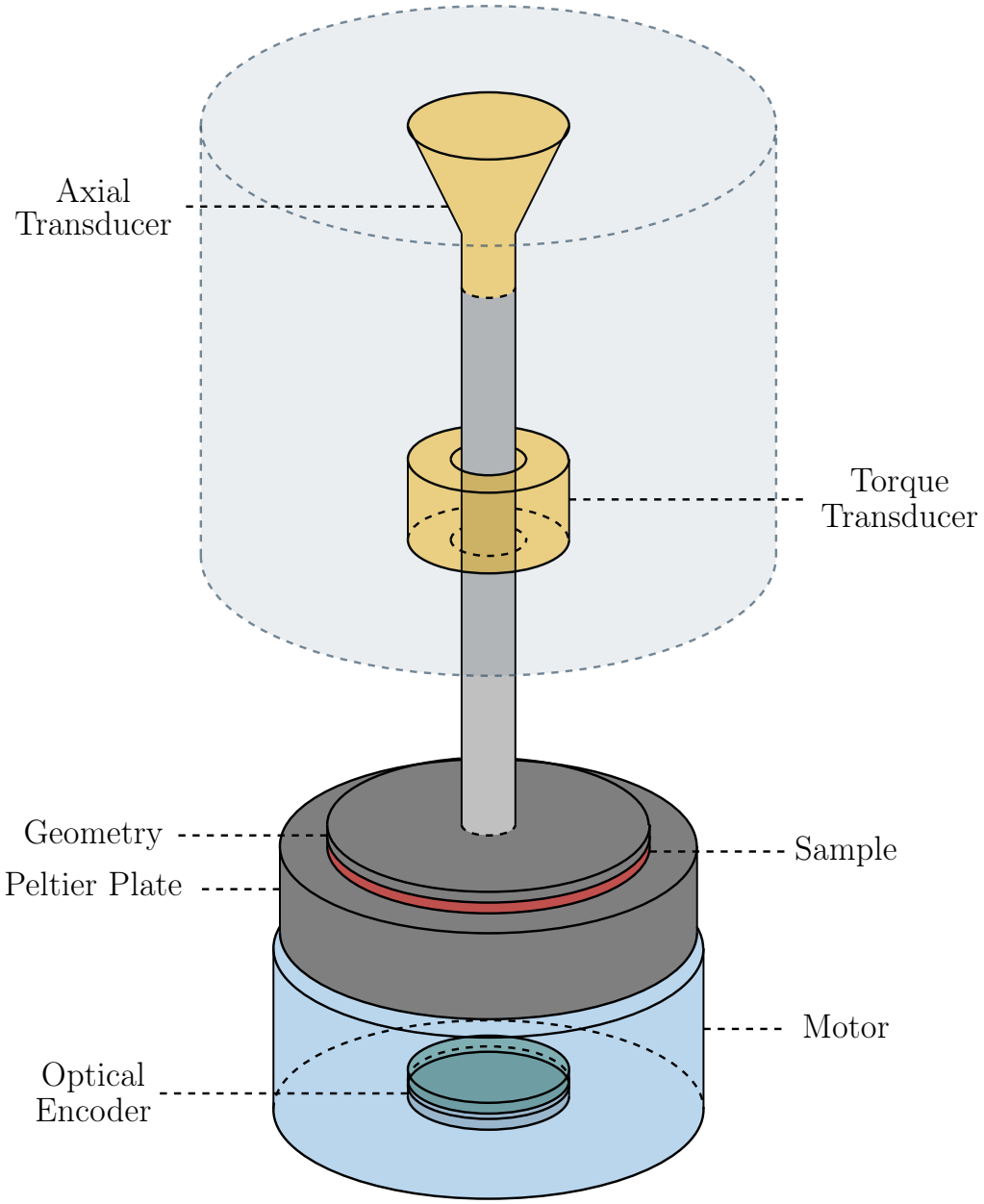

Figure 3.4: A Representative Diagram of an ARES-G2 Rheometer.

The ARES-G2 uses a direct drive motor to apply a strain to the sample. The motor includes a rigid air bearing system and friction-free motor combined with non-contact temperature sensing and an optical encoder which is able to detect the displacement of the motor with a high level of accuracy. In these experiments a Peltier plate attachment was connected to a waterbath capable of maintaining a temperature in the range -40 to 180 °C.[169]

The detection system within the ARES-G2 includes a torque rebalance transducer as well as a force rebalance transducer which allows for independent detection of the shear stress and axial force. The torque rebalance transducer used in the ARES-G2 rheometer monitors the current required to maintain the shaft at a fixed position during the application of shear strain, and includes an air bearing in addition to a capacitive angle sensor. Since the torque transducer is effectively static and independent of the shaft there is no requirement for instrument friction and inertia corrections. The force rebalance transducer, which uses an axial servo constraint system, is able to maintain the shaft in a fixed position with a high degree of accuracy or can be set to dynamically adjust the gap in order to compensate for changes in axial forces.[169]

Although the ARES-G2 design eliminates instrument inertia, measurements may still be subject to sample inertia. The TRIOS software, which is used to control the ARES-G2 rheometer, includes an in built correction, which via iterative methods, can be used to compensate for sample inertia:

$$\delta = \delta_{raw} - \Theta \qquad \text{(Eq. 3.2)}$$

where Θ is the phase shift due to fluid inertia, calculated from the values of G^* and fluid density (ρ) for the material.

ARES-G2 Rheometer Procedures

The ARES-G2 rheometer motor calibration was checked and the normal force transducer, torque transducer, and geometry mass were calibrated before validating using both a silicone viscosity standard (Brookfield Engineering, USA: 1000) and PDMS (TA instruments, UK: 711.00026) prior to testing. Before each run the temperature of the Peltier plate was set and the geometry was attached to the rheometer shaft. The zero gap position was then measured, during which the geometry was lowered until an axial force was detected when contact with the Peltier plate was made. The head was then raised and the samples were loaded onto the rheometer.

The procedure was then initiated; during the first step of the procedure the head was brought down to the specified gap while the motor rotated the Peltier plate at 0.5 rad/s in order to ensure that the sample was fully homogenised and spread evenly throughout the gap. The fill was inspected and adjusted when necessary to ensure no over or under fill was present. Samples were sealed with

silicone oil (Brookfield Engineering, USA: 10) to prevent evaporation during the test and the measurement was initiated. Upon completion of testing the head was raised and both the Peltier plate and geometry were washed using a dilute soap solution and rinsed with distilled water, the components were then sterilised using a 70 % ethanol solution before being rinsed again with distilled water.

The auto-strain adjust function was used in all gel point detection procedures, which effectively allowed unconstrained strain adjustments (0.1-300 %) while limiting the torque applied to within 0.02 μN.m of the value specified for each test. This function was utilised in order to obtain measurements which both produced a resolvable torque response, and which adapted to the transient linear range of gelling systems.

The Fourier transform mechanical spectroscopy (FTMS) procedures were initially optimised using 2.5 % (w/v) gelatine gels using a parallel plate geometry at a gap size of 200 μm. Gelation was initiated by applying a rapid temperature ramp from 35 °C, at which the samples were loaded, to 15 °C, the final temperature being reached before gelation occurred. The temperature was selected to initiate gelation at a similar rate to that of blood, in terms of the time taken to reach a gel point. The fundamental frequency of multiplex waveforms was varied from 0.5-5 Hz with each waveform including the second, fourth, eighth and tenth harmonics (n=3), in order to conduct FTMS measurements over a wide range of frequencies. The auto-strain adjust function was implemented which limited the stress of the fundamental frequency to 0.085 Pa, previously established as being within the LVR of the material (n=3).[170] In order to reduce the maximum amplitude of the waveform, gel point measurements were also performed with the addition of only the second and fourth harmonics to the waveform. This was done to confirm that reliable gel points were detectable using a reduced number of frequency components. This was performed at a fundamental frequency of 2.5 Hz, a gap size of 200 μm, and with the stress of the fundamental frequency limited to 0.085 Pa (n=3).

The gel point detection of fibrin-thrombin gels was then performed on samples containing 5 mg/ml fibrinogen and a thrombin concentration ranging from 0.03-0.09 NIH/ml at 24 °C using FTMS at a fundamental frequency of 2.5 Hz including the second and fourth harmonics. To ensure the measurements remained linear the system was operated with an auto-strain adjust function which maintained the stress of the fundamental frequency to 0.04 Pa. The work was conducted using a parallel plate geometry with a gap size of 200 μm and compared to results obtained from the AR-G2 rheometer (n=5).

The linear viscoelastic region (LVR) of P-PFP was established by performing amplitude sweeps at 37 °C using an FTMS procedure at a fundamental frequency of 2.5 Hz. This was conducted during the sol phase by testing P-PFP without the addition of $CaCl_2$, and both in the vicinity of the gel point and during the mature gel phase by initiating the coagulation of P-PFP using $CaCl_2$ and delaying the start of the test by 200 and 1000 s respectively. This allowed capture of the LVR during different stages of gelation. The amplitude sweep was performed by utilising the strain-adjust feature in TRIOS over an oscillation time procedure, where the procedure was initiated with a fundamental strain of 0.1 % set to double with each measurement until a torque of 50 μN.m was reached.

Determination of an LVR at the precise moment of gelation is not possible, due to the transient nature of the material. In order to confirm that the FTMS measurements of P-PFP were within the LVR of the material at the gel point, gel point measurements were performed at different fundamental stress levels of 0.02, 0.04 and 0.06 Pa. In order to test the suitability of these testing parameters in whole blood the same procedures were used to detect the gel points of citrated whole blood, where five blood samples were collected from individuals and tested at stresses of 0.02, 0.04 and 0.06 Pa within 2 hours of collection (n=5).

Scanning Electron Microscopy

Scanning electron microscopy (SEM) imaging was performed using a Hitachi S-4800 field emission gun scanning electron microscope (FEGSEM) which applies a focused beam of electrons to the sample. The electrons are then deflected from the sample surface with a scatter pattern that relates to the sample topology, which is then used to generate an image of the sample surface. Samples were prepared as described in Section 3.1.1 (n=3) and the button was loaded onto an SEM stub which was passed below a height tool to confirm that the stub height was appropriate for the equipment. The sample stubs were then loaded into the equipment and placed under vacuum. The samples were imaged at x10k x50k and x100k magnification using secondary electron detection mode and applying an acceleration voltage of 10 kV at a working distance of 13000 μm.

3.1.3 Data Analysis

Gelatine gel points were initially analysed using the in-house 'gel point analysis' software described in Section 1.4.2 in order to determine the mutation number (N_{mu}). Tests were considered to be subject to mutational artefacts where N_{mu}>0.15. However, deviations apparent in the gel point data, resulting from the artefacts under investigation, made assessment of the gel point parameters using this software inconsistent, see Appendix B. As a result, the phase angle (δ_{GP}), gel time (GT), and the phase angle of each frequency (δ_f) at the apparent gel point were determined by eye from plots of δ vs time at each frequency. The apparent gel point was defined from the frequency independent value of δ considering the lowest frequencies tested, as these were less vulnerable to the influence of inertia, as shown in Figure 3.5. The values of δ_{GP} and GT at each frequency were subjected to statistical analysis by ANOVA and used to calculate the value of GT and δ_{GP} for 2.5 % (w/v) gelatine with a 99 % confidence interval. Results found to be influenced by sample mutation were discarded as invalid measurements at this stage. The values of δ_f (see Figure 3.5) were then assessed for each individual frequency and considered to deviate from δ_{GP} where all the values collected at that frequency fell outside of the established 99 % confidence interval.

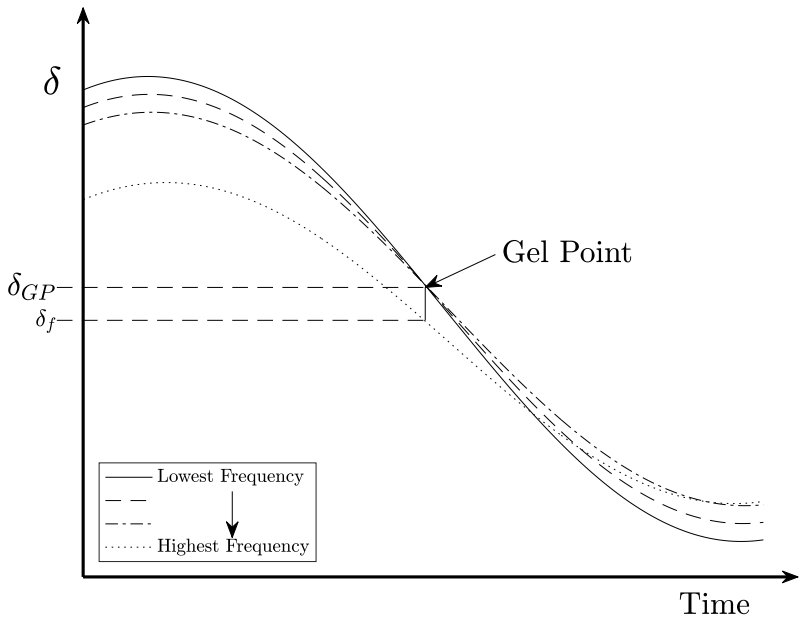

Figure 3.5: A Graph Illustrating the Definition of δ_{GP} and δ_f at the Apparent Gel Point.

In order to investigate the fluid inertia correction provided in the TRIOS software, the correction applied was manipulated by varying the density value input to the software at each frequency. Since the samples had a density of 1.025 g/ml, the correction was assessed by inputting density values between 0-2 g/ml resulting in the application of corrections ranging from no correction (0 g/ml), to approximately twice the appropriate correction (2 g/ml). The δ_{GP}, GT and δ_f were determined as above at each frequency and density tested. Pearson linear correlation analysis was then performed to determine whether the value of δ_{GP} was influenced by the value of the input density. Further correlation analysis was performed at each density value to determine whether the correction applied led to a relationship between δ_{GP} and the frequency of the test procedure.

The $deviation(\%)$ of δ_f was determined at each density value by:

$$deviation(\%) = \frac{(\delta_{GP} - \delta_f)}{\delta_{GP}} \cdot 100 \qquad \text{(Eq. 3.3)}$$

and δ_f was considered to have deviated from δ_{GP} where $deviation(\%)$ was >5 %.

Fibrin-thrombin, plasma, and blood data subjected to correlation analysis were evaluated by Spearman's ranked correlation test. This test type was selected both to maintain consistency, as non-linear trends were anticipated for many relationships, and to answer the primary research question on whether the rheometrical results were influenced by experimental factors.

Gel points for fibrin-thrombin gels detected using both the AR-G2 and ARES-G2 were analysed using 'gel point analysis' software described in Section 1.4.2. This produced a GT and d_{f} value as well as a confidence interval, which was used to calculate the degree of uncertainty in the measurement:

$$Uncertainty = \frac{ConfidenceInterval}{d_f} \qquad \text{(Eq. 3.4)}$$

The statistical analysis performed included Spearman's ranked correlation analysis to determine the correlation coefficient for both GT and d_{f} with the concentration of thrombin for values obtained by FTMS. Additionally, t-tests and f-tests were performed between the two techniques at each thrombin concentration for both GT and d_{f}. The uncertainty in the gel point determinations was compared for the two techniques by t-test which included results from all three thrombin concentrations.

The fibre thickness was measured for ten fibres in each sample from SEM images taken at x50k magnification using the length measuring tool in imageJ software (NIH, USA). These measurements were then subjected to Spearman's ranked correlation analysis to determine the correlation coefficient relating the fibre diameter to the thrombin concentration as well as comparing the average fibre diameter at each thrombin concentration to d_{f} values obtained using the ARES-G2.

In order to identify the LVR of P-PFP, amplitude sweep data was evaluated to establish the stress or strain at which G' and G'' became dependent on the amplitude of the oscillation. Due to the transient nature of the gelling system, during the measurement taken in the vicinity of the gel point the end of the LVR was considered to be indicated by the deviation of G' and G'' from the expected increase due to the growth of viscoelasticity.

Gel points obtained for both P-PFP and whole blood under varying fundamental stresses were analysed using 'gel point analysis' software described in Section 1.4.2.

The parameters at the gel point including GT, d_{f} and G' of the highest frequency at the gel point (G'_{GP}) were compared by Spearman's rank correlation analysis to determine whether any dependence of the gel point parameters on the stress or strain of the measurements was present. Dependence was determined to be negligible where the probability of a relationship was greater than 0.1 ($p>0.1$).

Gel points obtained by FTMS using the ARES-G2 and discrete sweeps collected using the AR-G2 were analysed using 'gel point analysis' software described in Section 1.4.2. This produced a raw phase, n_{mu}, GT and mean d_{f} values for each dataset. The d_{f} values obtained by FTMS measurements were compared to fibre thickness values measured from SEM images while the raw phase and n_{mu} values from each technique were used to assess the validity of the measurements.

3.1.4 Limitations

The study of different frequency ranges using gelatine resulted in unclear gel points that could not be detected by the 'Gel Point Analysis' software. Therefore, these gel points were determined by eye as the intersect of δ at the lowest frequencies tested, which were less prone to the inertial errors introduced.

The Gel point detection procedure can monitor for the presence of a third harmonic component in order to confirm linearity of measurements. However, this approach is not possible using FTMS due to software limitations and the multiwave nature of such tests. Attempts were made to monitor the third harmonic by inputting a negligible strain at the third harmonic in order to collect the data; however, this proved to be an unreliable method for detecting the linearity of the procedures.

Fibrin-thrombin gel points detected using conventional techniques on the AR-G2 rheometer resulted in several invalid or undetectable gel points. In order to directly compare the reliability of the two techniques five repeats were run on each rheometer and gel points detected using the AR-G2 were forced through analysis software for the comparison despite several runs being invalid. For the investigation of P-PFP multiple repeats were performed in order to collect five valid data sets for comparison.

3.2 Results and Discussion

3.2.1 Gelatine Optimisation

Frequency Range

Figure 3.6 shows the phase angle as a function of time for 2.5 % (w/v) gelatine using Fourier transform mechanical spectroscopy (FTMS) over different frequency ranges. Figure 3.6 (a) shows data collected at 0.5-5 Hz where sample mutation has dominated the measurement leading to uncertainty in the gel point. Figure 3.6 (b) shows data collected in the median frequency range tested (1-10 Hz) where a clear gel point can be determined. Figure 3.6 (c) shows data collected at 3.5-35 Hz where the data at the higher frequencies tested deviated from the expected frequency independent values at the gel point. Additionally, a large amount of noise can be observed in measurements at the highest frequencies.

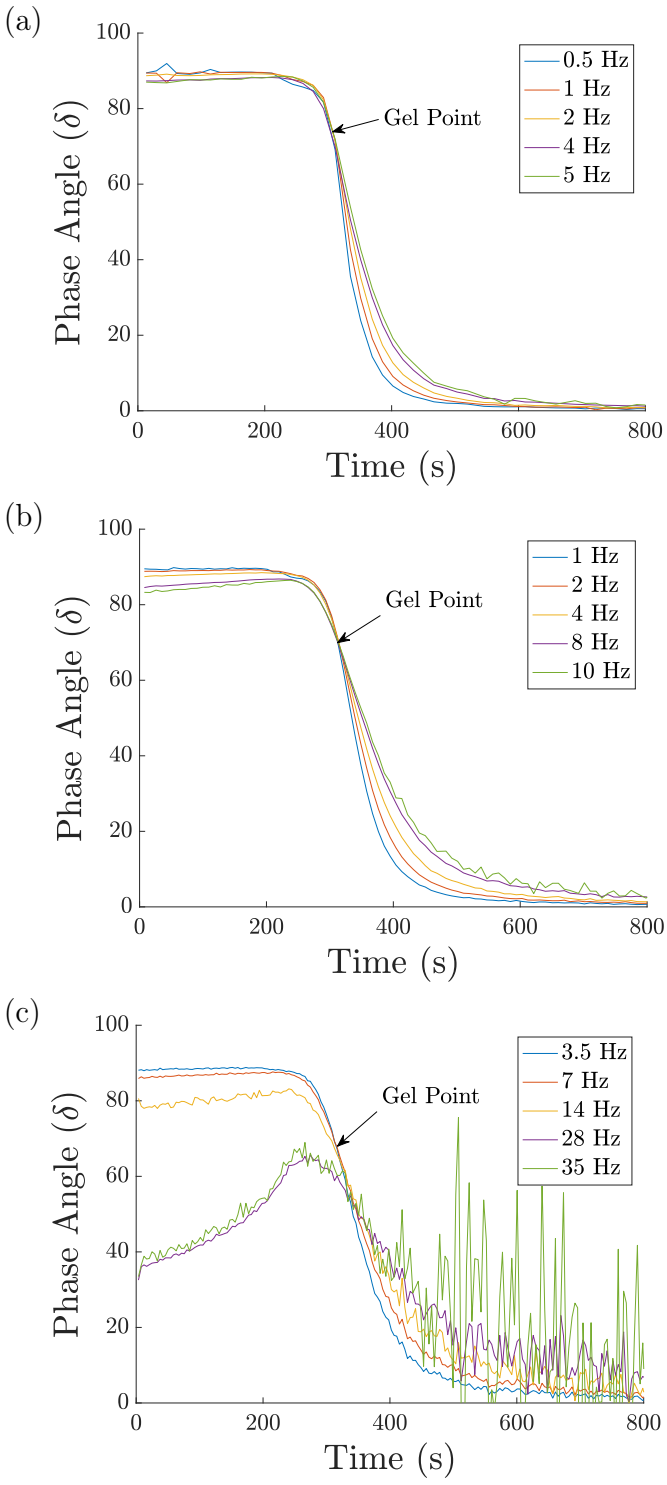

Figure 3.6: Example Rheological Measurements of 2.5 % (w/v) Gelatine Undergoing Gelation as Detected Using Fourier Transform Mechanical Spectroscopy Over Different Frequency Ranges.

(a) 0.5-5 Hz, (b) 1-10 Hz, and (c) 3.5-35 Hz.

Examination of the relationship between sample mutation number (N_{mu}) and the fundamental testing frequency revealed that gel point data obtained from waveforms with a fundamental frequency of less than 2 Hz were subject to errors resulting from sample mutation artefacts. These artefacts are considered to be present where N_{mu} >0.15 as illustrated in Figure 3.7.

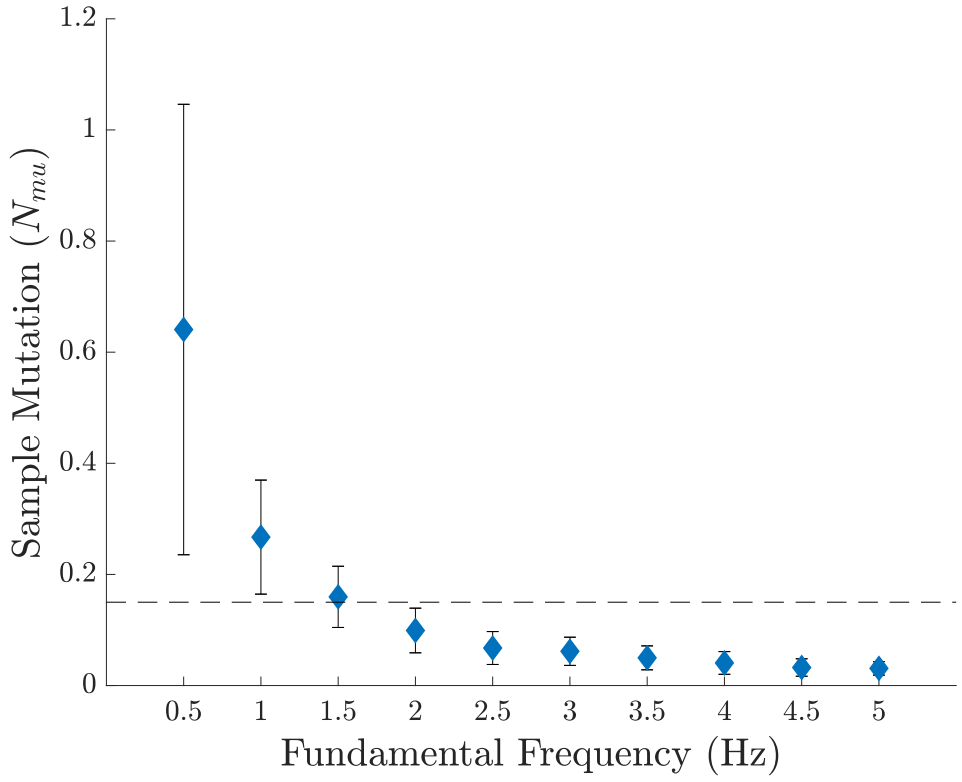

Figure 3.7: A Graph Showing the Relationship Between Fundamental Frequency and Sample Mutation Number for 2.5 % (w/v) Gelatine Obtained using Fourier Transform Mechanical Spectroscopy.

Error bars indicate standard deviation (n=3).
N_{mu} =0.15 threshold (dashed line).

Analysis of gel point parameters by ANOVA revealed statistically significant differences in GT (p<0.01); however, no true outliers were identified by post-hoc tests. These results were used to calculate a mean GT which was found to be equal to 312 (±5) s at each frequency as shown in Figure 3.8 (a). When considering δ_{GP} as assessed by ANOVA, the values were found to be anomalous from all others at 0.5 Hz (p<0.001) as shown in Figure 3.8 (b). A mean value for δ_{GP} value of 68.7 (±0.5) ° was obtained by excluding values subject to sample mutation.

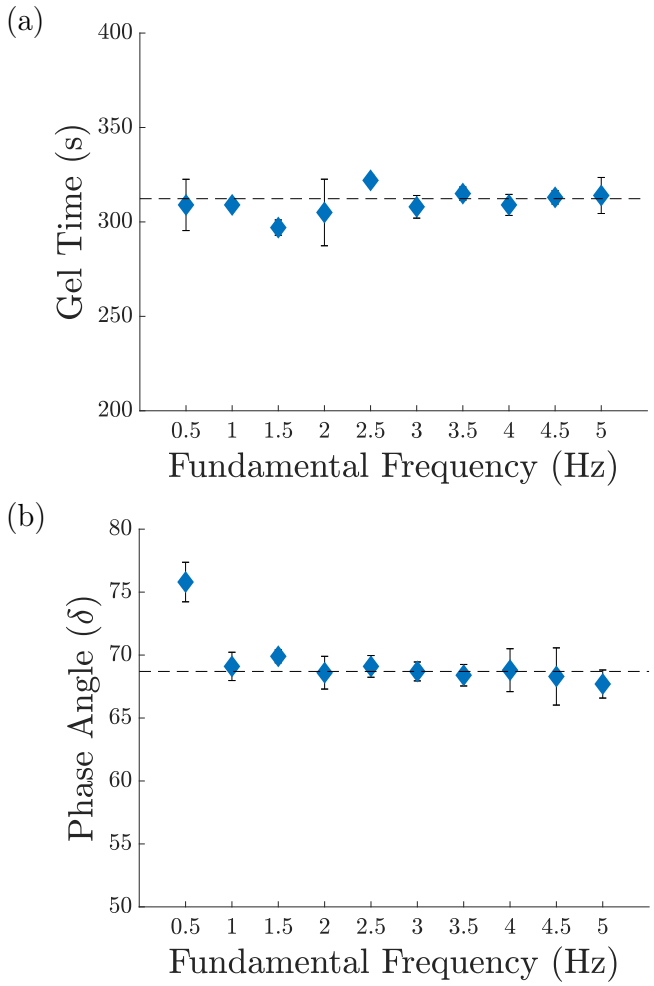

Figure 3.8: Graphs Showing the Relationship Between Fundamental Frequency on Gel Time and Phase Angle at the Apparent Gel Point in Samples of 2.5 % (w/v) Gelatine Obtained using Fourier Transform Mechanical Spectroscopy.

(a) Gel time and (b) phase angle at the apparent gel point.
Error bars indicate standard deviation (n=3).
Mean values, excluding N_{mu} >0.15 (dashed line).

The value of δ_f was determined at the apparent gel point for each frequency detected. This was done by locating the apparent gel point of the lowest frequencies and reading a value for δ for each frequency at the apparent GT. At frequencies above 20 Hz the value of δ_f can be seen to deviate from the expected value for a frequency independent gel point as shown in Figure 3.9.

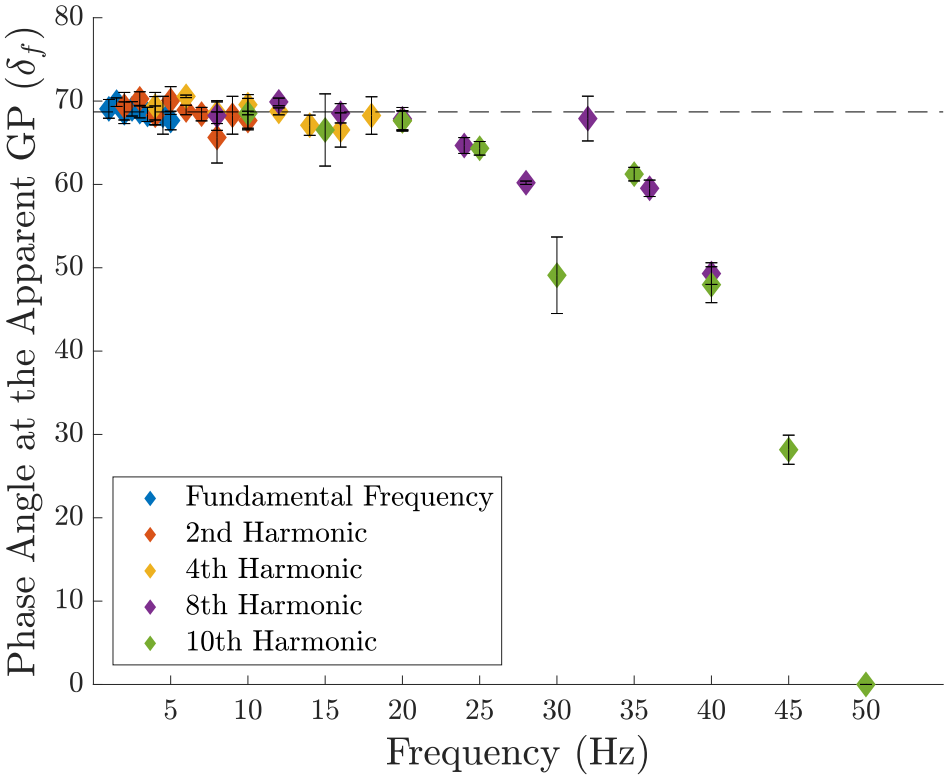

Figure 3.9: A Masterplot Showing the Relationship Between Testing Frequency and the Phase Angle Value at the Apparent Gel Point of 2.5 % (w/v) Gelatine.

The Apparent Gel Points were Detected Using Fourier Transform Mechanical Spectroscopy with Different Frequency Ranges, in a Series of Measurements. Error bars indicate standard deviation (n=3). δ_{GP} (dashed line).

Examination of gel points collected from 2.5 % (w/v) gelatine revealed the potential artefacts due to sample mutation at low frequencies (<2 Hz), as well as deviations from the expected gel point at high frequencies (>20 Hz). Since the SMT rheometer is not subject to instrument inertia, these artefacts can be attributed to fluid inertia and possibly transducer compliance. Relatively large standard deviations were observed at moderately high frequencies (15-20 Hz). Based on these findings, in order to minimise errors due to sample mutation and inertia/resonance, a frequency range of 2.5-10 Hz within the range was used for experiments on pooled platelet free plasma (P-PFP).

Fluid Inertia Correction

The TRIOS rheometer control and analysis software includes several data processing functions including a correction for fluid inertia. In order to confirm that the correction was suitable, and that the appropriate frequency ranges were selected, the inertia correction was manipulated by changing the sample density parameter. The value of the inertia correction significantly influenced the value of δ ($p<0.001$, rho=0.94) and GT ($p<0.001$, rho=-0.77). At 0 and 0.5 g/ml, δ_{GP} was found to be dependent on the test frequency ($p=0.003$ and $p=0.002$), indicating that the application of an inadequate correction gives rise to false apparent gel points at which the phase angle is not frequency independent when tested at different frequency ranges despite being discernible from each measurement. However, with corrections at and above the appropriate level, modulating the level of correction gave rise to frequency independent gel points having higher values of δ_{GP} as shown in Figure 3.10.

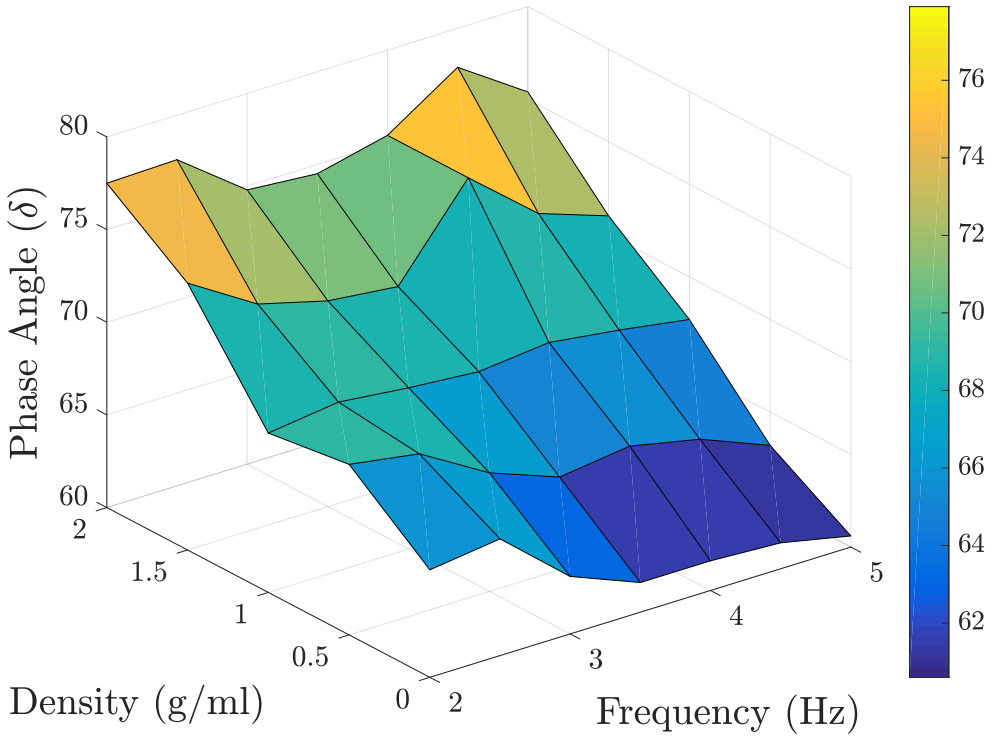

Figure 3.10: A 3-D Plot Showing the Effect of Modulating the TRIOS Fluid Inertia Correction and Testing Frequency on the Phase Angle at the Apparent Gel Point of 2.5% (w/v) Gelatine Detected by Fourier Transform Mechanical Spectroscopy.

Further examination of the *deviation*(%) of δ_f at the highest frequencies tested, taking different levels of inertia correction into account, led to the determination of the same maximum frequency as above (20 Hz). Above this frequency δ_f deviated from the respective δ_{GP} independently of the fluid inertia correction as shown in Figure 3.11.

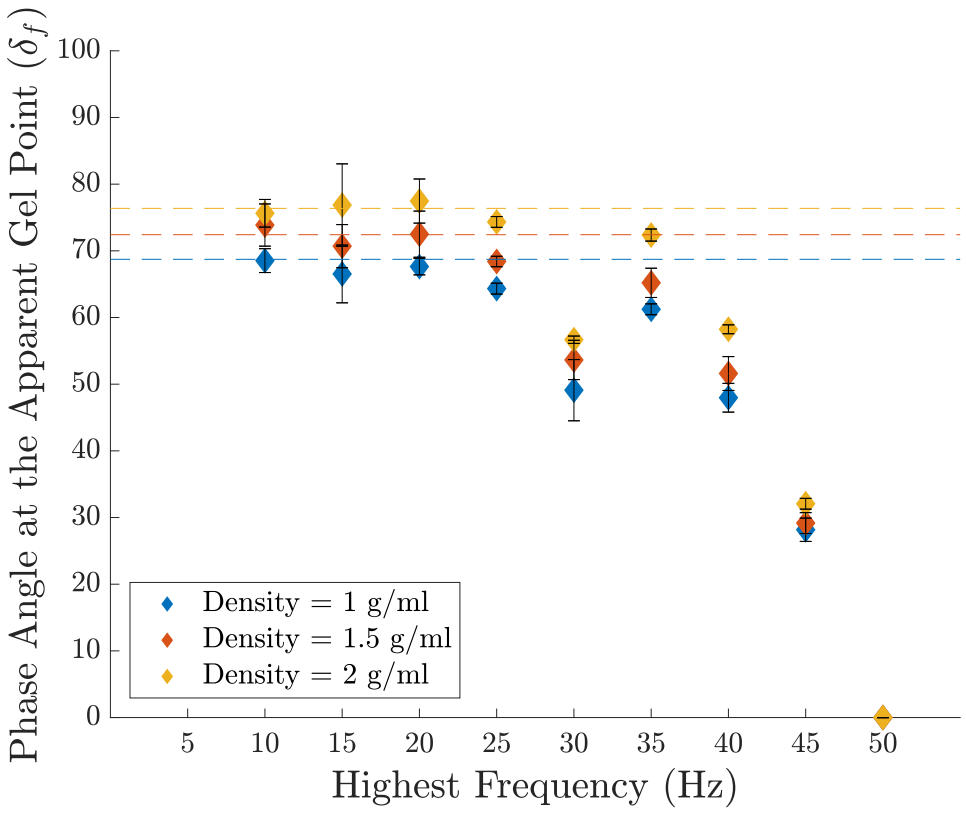

Figure 3.11: A Graph Showing the Effect of the TRIOS Fluid Inertia Correction on the Phase Angle of the Highest Frequency (at the Apparent Gel Point) at High Frequency During Fourier Transform Mechanical Spectroscopy Measurements of 2.5 % (w/v) Gelatine.

Error bars indicate standard deviation (n=3).
Average δ_{GP} (dashed lines).

Changes in the fluid inertia correction (by modulating the sample density) were found to significantly influence the values for δ and GT at the gel point. Since a reliable correction was not possible through TRIOS it was determined necessary to negate the influence of fluid inertia during future testing. This can be achieved by working at gap sizes well within the gap loading limit. For fibrin-thrombin gels and P-PFP a gap size of 200 μm was determined to be appropriate at the given frequency range, by applying Equation 2.47 to preliminary data in order to calculate the wavelength of the propagating shear wave, λ.

Number of Harmonics Utilised

The narrow and transient linear viscoelastic region (LVR) of P-PFP gives rise to significant experimental challenges which require particular consideration. Since each frequency applied in an FTMS wave increases the total amplitude of the waveform, using a reduced number of harmonics might allow for more resolvable waveforms whilst remaining within the LVR. However, reducing the number of harmonics may also reduce certainty in the gel point measurement. In order to confirm that reliable gel points can be detected when testing using a reduced number of harmonics the gel points of 2.5 % (w/v) gelatine were measured at 2.5 Hz using FTMS waves made up of three and five harmonics. Analysis by t-test revealed no significant differences in the values of δ or GT when gel points were detected using 3 or 5 harmonics (p=0.21, p=0.71) as shown in Figures 3.12(a) and 3.12(b) respectively. No statistically significant difference in the variance was detected in either δ (p=0.07) or GT (p=0.96) leading to the conclusion that testing with three harmonics allows for accurate detection of the gel point.

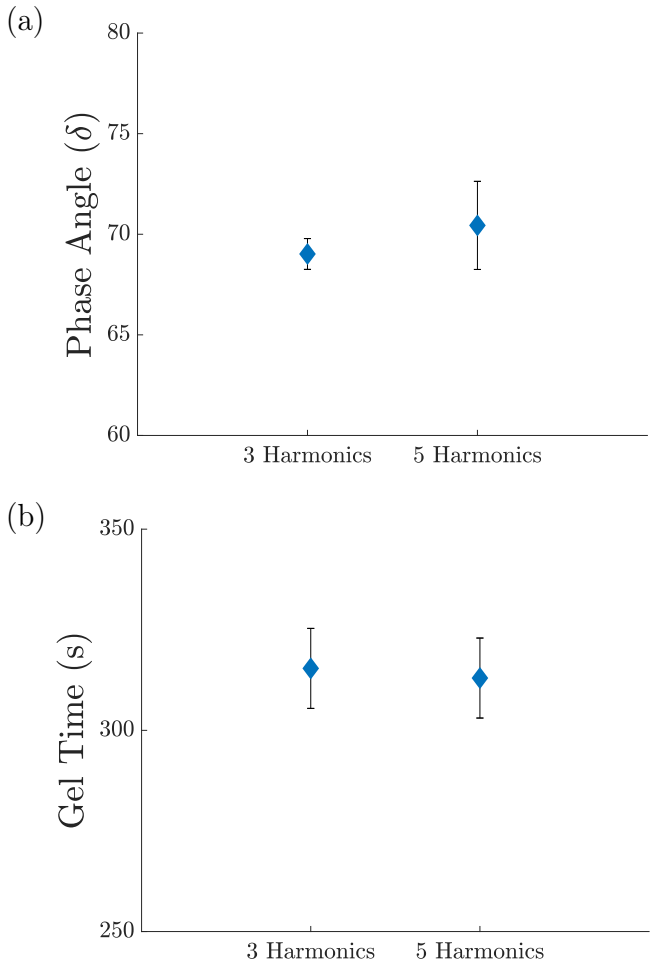

Figure 3.12: Graphs Showing the Gel Time and Phase Angle Measurements of 2.5 % (w/v) Gelatine Acquired Using Fourier Transform Mechanical Spectroscopy Utilising Three and Five Harmonics.

Error bars indicate standard deviation (n=3).

The above process of optimisation led to the development of a gel point detection procedure involving the use of FTMS techniques using three frequencies between 2.5-10 Hz at the selected gap size of 200 μm.

3.2.2 Fibrin-Thrombin Validation

In order to validate the optimised FTMS procedure above, fibrin-thrombin gels were used as a model system that undergoes clotting. Additionally, these results were used to confirm the relationship between the incipient clot structure and the mature clot structure assessed by scanning electron microscopy (SEM). The rheological properties, including GT and fractal dimension (d_f), and clot architecture are known to be influenced by the concentration of thrombin.[57,146] As shown in Figure 3.13 the optimised FTMS technique showed a dependence of gel time on the thrombin concentration ($p<0.001$, and rho=-9.2), which is consistent with previous findings.[57,146]

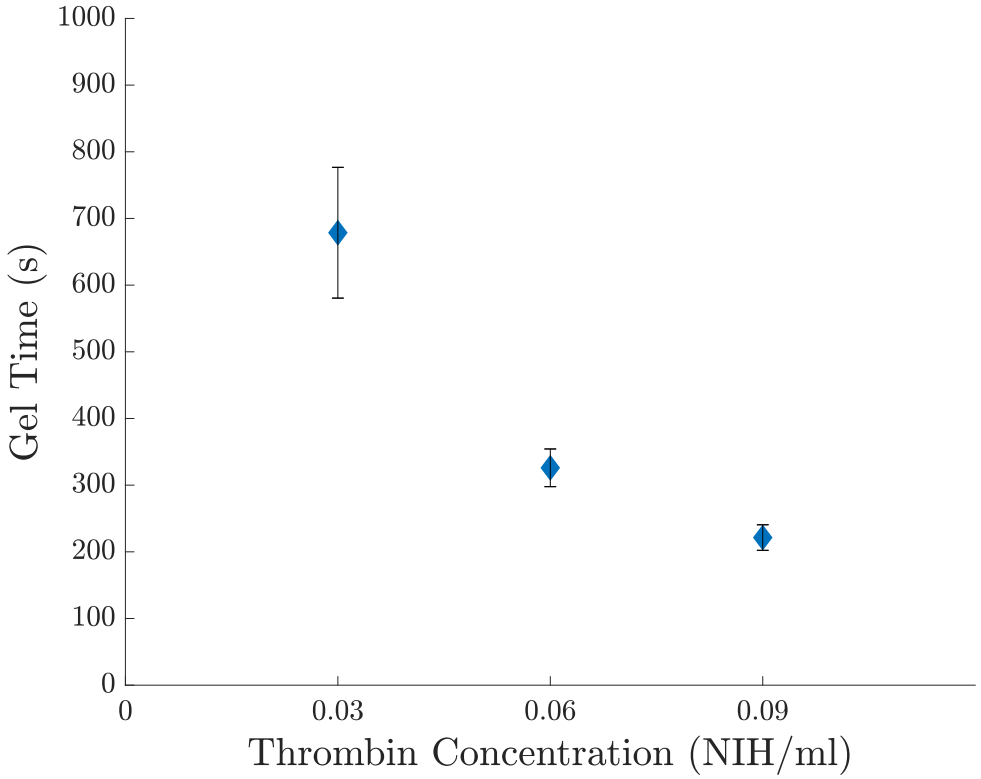

Figure 3.13: A Graph Showing the Effect of Thrombin Concentration on the Gel Time of 5 mg/ml Fibrin-Thrombin Gels Detected by High Frequency Fourier Transform Mechanical Spectroscopy.

Error bars indicate standard deviation (n=5).

The d_f values obtained using FTMS showed a strong correlation (p=0.007, rho=0.66) between the obtained d_f and thrombin concentration as shown in Figure 3.14 which is also consistent with trends found in previous work.[57,146]

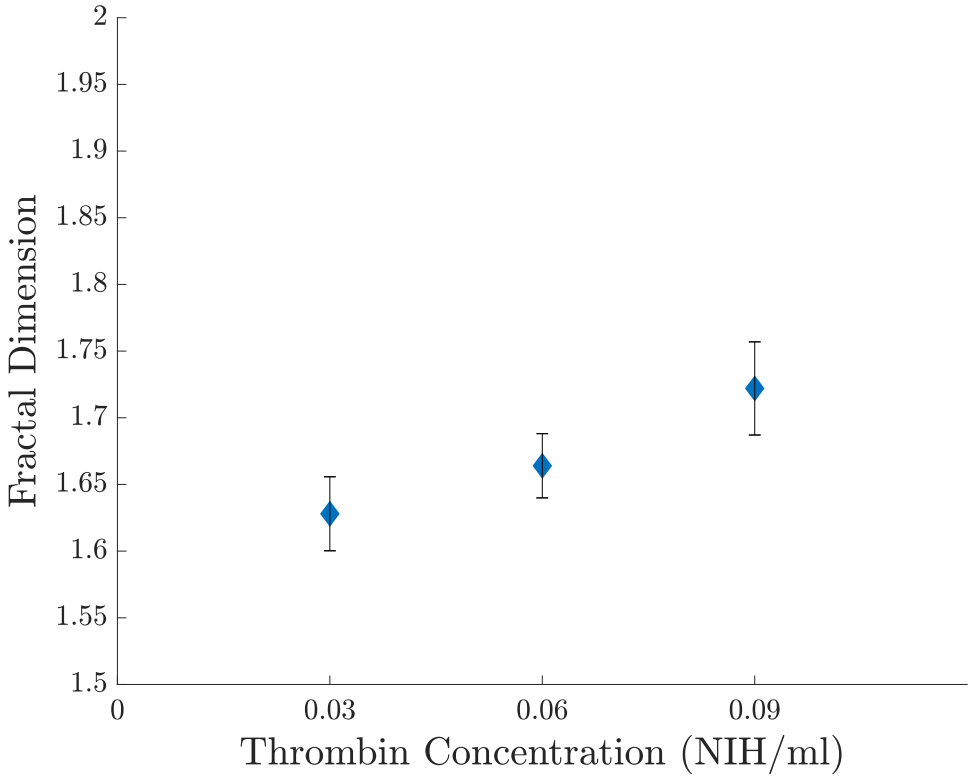

Figure 3.14: A Graph Showing the Effect of Thrombin Concentration on the Fractal Dimension of the Gel Point of 5 mg/ml Fibrin-Thrombin Gels Detected by Low Frequency Discrete Sweep Rheometry and High Frequency Fourier Transform Mechanical Spectroscopy.

Error bars indicate standard deviation (n=5).

SEM images (examples shown in Figure 3.15) of fibrin-thrombin gels were analysed to determine the fibre thickness of clots formed at different thrombin concentrations.

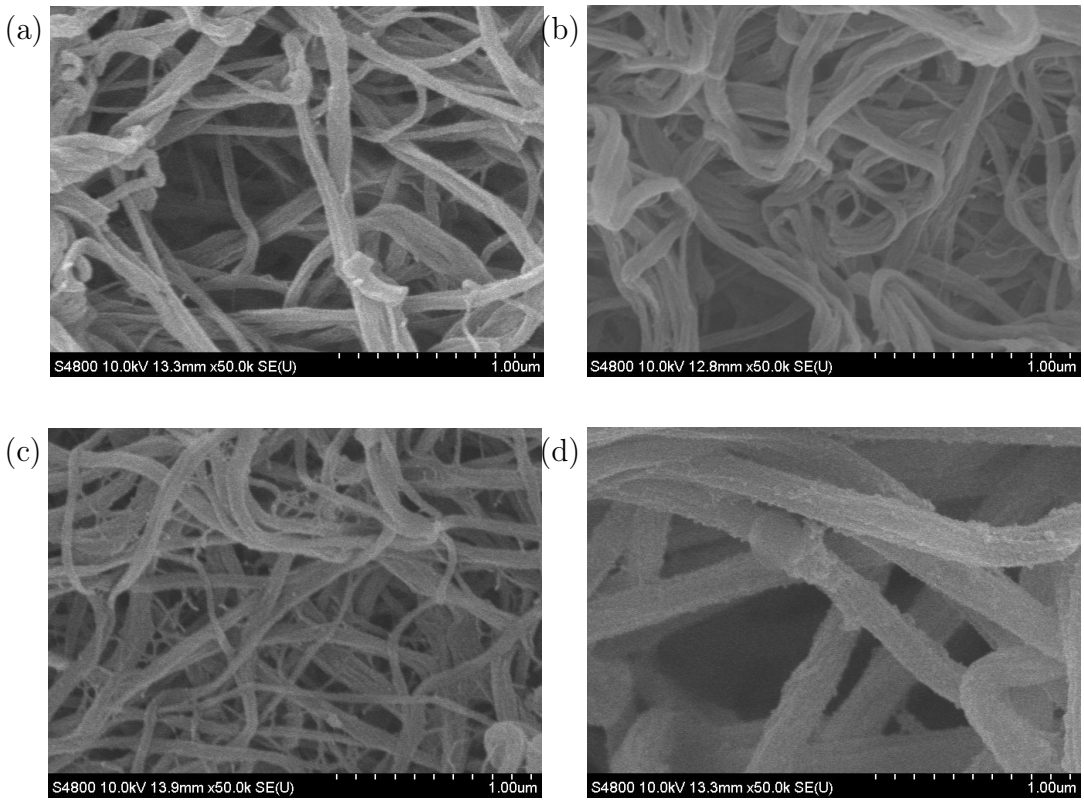

Figure 3.15: SEM Images of Mature Fibrin-Thrombin and Pooled Platelet Free Plasma Clots.

SEM images depicting the mature clot structure of 5 mg/ml fibrin and (a) 0.03 NIH/ml thrombin, (b) 0.06 NIH/ml thrombin, (c) 0.09 NIH/ml thrombin, and (d) pooled platelet free plasma.
Distance between scale-bar graduations: 0.1 μm.

A statistically significant relationship was found between the measured fibre thickness and thrombin concentration ($p<0.001$, rho=-0.51) as shown in Figure 3.16. Further statistical analysis showed a correlation between the average fibre thickness and the d_f detected by FTMS ($p<0.001$, rho=-0.86). This provides clear evidence for the validity of the FTMS testing procedures, as the increasing thrombin concentration led to denser clot structures composed of thinner fibres consistent with the literature,[57,146] and these differences in microstructure were identifiable through the d_f values obtained by FTMS and confirmed by SEM imaging.

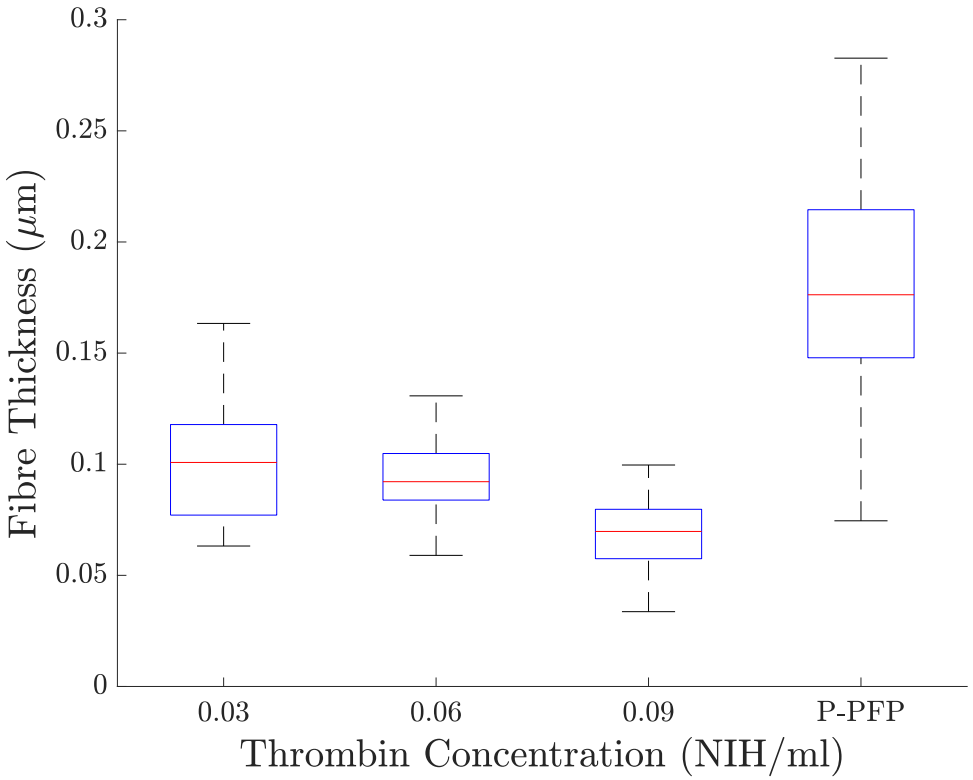

Figure 3.16: A Graph Showing the Relationship between Thrombin Concentration and Fibre Thickness for Purified Fibrin-Thrombin Gels with Different Levels of Thrombin, and for Pooled Platelet Free Plasma.

Linear extrapolation of the relationship between d_f values determined using FTMS and fibre thickness led to a prediction that for P-PFP which had an average fibre thickness of 0.180 ($\pm$0.04) μm determined by SEM, a d_f value in the region of 1.4 is expected.

Comparison of the relative uncertainty of gel point measurements of fibrin-thrombin gels tested using both low frequency discrete sweep techniques and FTMS is shown in Figure 3.17. Statistical analysis revealed a significant difference between the uncertainties, with the FTMS techniques resulting in gel points with uncertainties an order of magnitude lower than discrete sweep measurements ($p<0.001$).

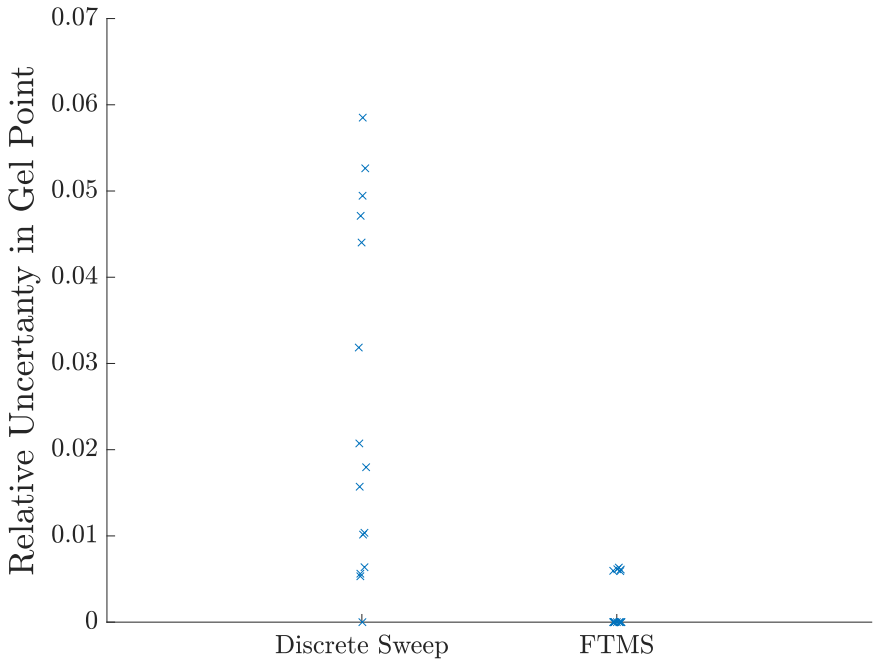

Figure 3.17: A Graph Showing the Relative Uncertainty of Gel Point Values Obtained Using Low Frequency Discrete and High Frequency Fourier Transform Mechanical Spectroscopy Techniques of 5 mg/ml, 0.03-0.09 NIH/ml Fibrin-Thrombin Gels.

3.2.3 Establishing the Linear Viscoelastic Range of Pooled Platelet Free Plasma

The LVR of P-PFP was determined to establish a target range of stress/strain within which the measurement must remain in order to be linear. Figure 3.18 shows that during the sol phase, measurements below 200 % are poorly resolved. An LVR could not be determined from this data with confidence. However, in the vicinity of the gel point the LVR is in the range of 0.8-20 % strain and at the mature gel phase the LVR decreases further to 0.1-2.5 % strain. The lack of an overlap in these regions of linearity and resolution makes it impractical to implement a constant strain FTMS procedure which would be adequately resolved while remaining within the LVR of the material.

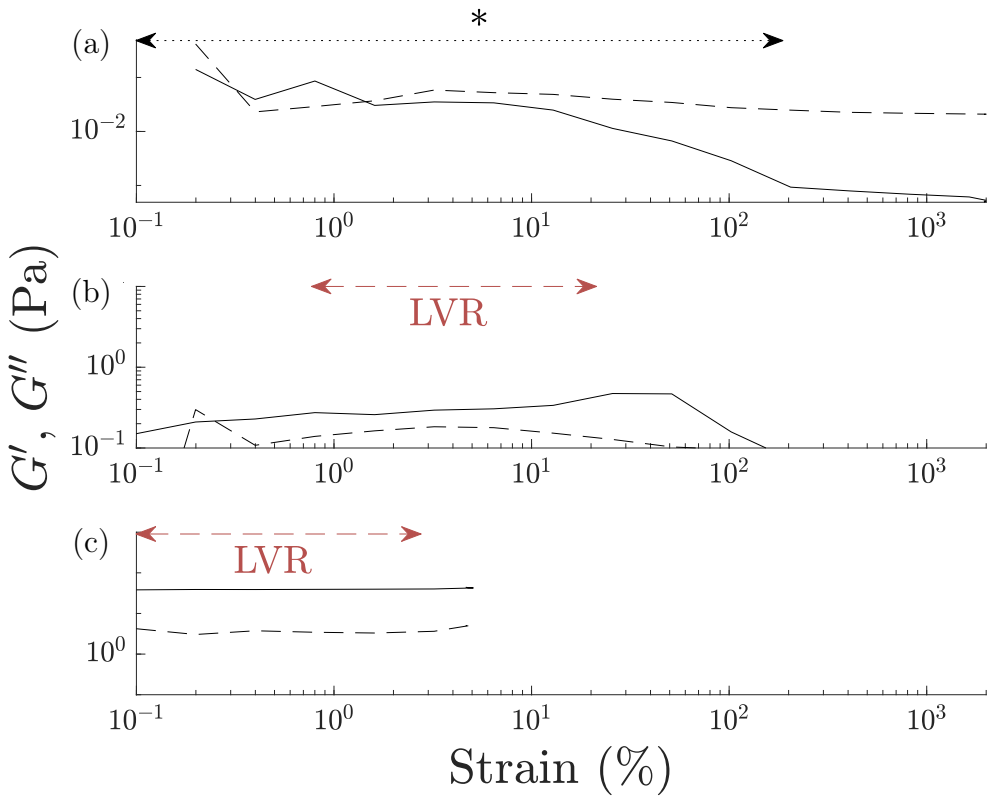

Figure 3.18: A Graph Depicting the Linear Viscoelastic Region of Pooled Platelet Free Plasma as a Function of Strain.

(a) Sol phase[i], (b) in the vicinity of the gel point, and (c) the mature gel phase. G' (solid) and G'' (dashed).

Where the same amplitude sweep is plotted as a function of stress as shown in Figure 3.19, the sol phase can be seen to be poorly resolved below 0.04 Pa. In the vicinity of the gel point the LVR can be observed as 0.001-0.06 Pa and in the mature gel phase the LVR can be seen to be 0.001-1 Pa. This leads to the conclusion that stresses applied in the region 0.04-0.06 Pa would adhere to the LVR throughout the coagulation process while remaining well resolved.

[i]The region 0.1-200 % denoted with an asterisk appears to show a region of linearity, further investigation revealed this to be an artefact of the test, see Appendix C.

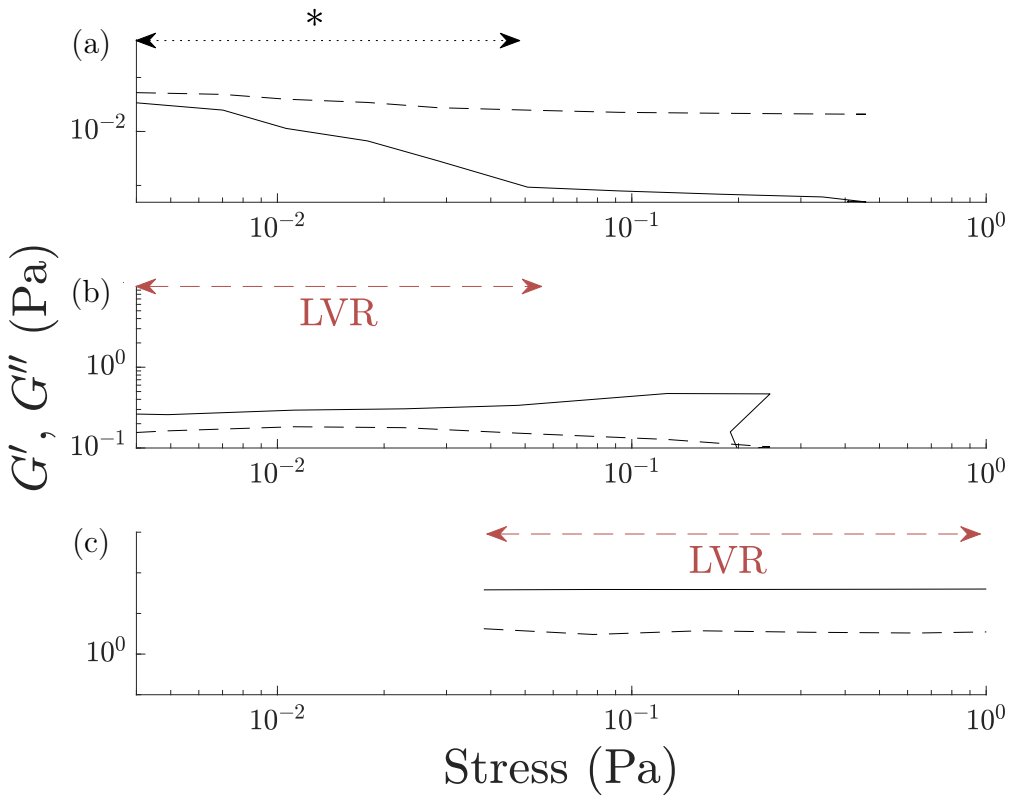

Figure 3.19: A Graph Depicting the Linear Viscoelastic Region of Pooled Platelet Free Plasma as a Function of Stress.

(a) Sol phase[ii], (b) in the vicinity of the gel point, and (c) the mature gel phase. G' (solid) and G'' (dashed).

Based on the results obtained above, a stress of 0.04 Pa was initially selected for investigation, and an FTMS procedure was performed on P-PFP at a frequency range of 2.5-10 Hz.

[ii]The region 0.001-0.04 Pa denoted with an asterisk appears to show a region of linearity, further investigation revealed this to be an artefact of the test, see Appendix C.

3.2.4 Validation of the Optimised Procedure for Pooled Platelet Free Plasma and Whole Blood

Detection of an LVR in the vicinity of the gel point of plasma allowed for the determination of a range of stresses at which measurements would likely be both linear and well resolved. Detection of an LVR at the precise moment of gelation is not possible, and therefore the linearity of these measurements was confirmed by detecting gel points using FTMS procedures at different applied levels of stress. Spearman's rank correlation analysis confirmed that gel point measurements within the range 0.02-0.06 Pa were independent of the measurement as shown in Figure 3.20 which shows no relationship between the GT (p=0.16), d_f (p=1) or G'_{GP} (p=0.39) and the stress applied.

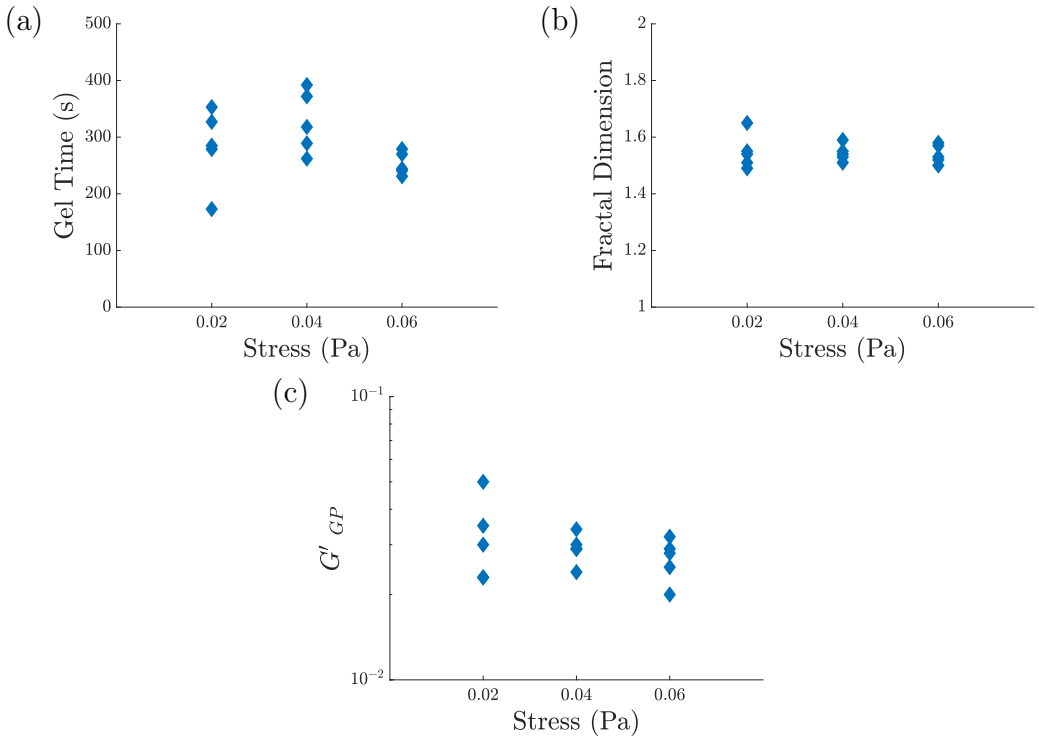

Figure 3.20: Graphs Showing the Effect of Resultant Stress on Gel Point Parameters of Pooled Platelet Free Plasma.

(a) Gel time, (b) fractal dimension, and (c) G' at the gel point.

This was further confirmed by evaluation of the gel point parameters and the strain at the gel point which was also found to be independent as shown in Figure 3.21. No relationship between the GT (p=0.13), d_f (p=0.66) or G'_{GP} (p=0.13) and the strain applied was identified.

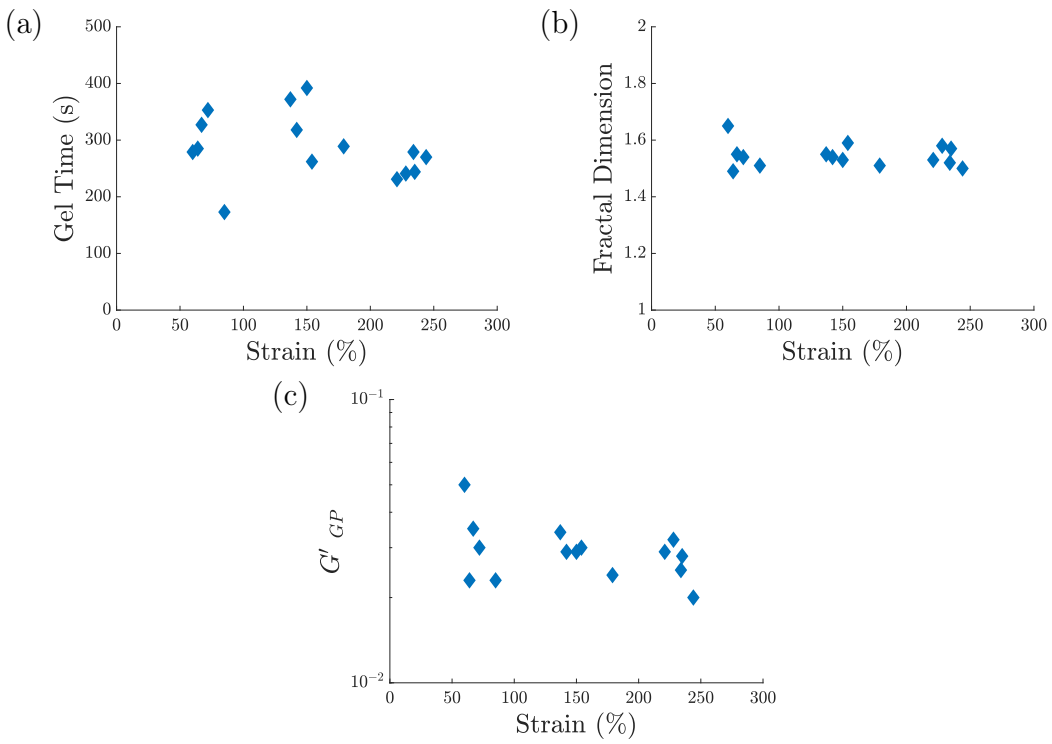

Figure 3.21: Graphs Showing the Effect of Applied Strain on Gel Point Parameters of Pooled Platelet Free Plasma.

(a) Gel time, (b) fractal dimension, and (c) G' at the gel point.

No evidence of inertia in the form of deviations from the gel points of plasma was observed. Additionally, N_{mu} was found to be <0.15. Since the gel point measurements were not found to be dependent on the input strain and measured stress, it was concluded that these procedures satisfy the conditions of linearity at the gel point, and are free from known sources of error.

The linearity of measurements using the optimised procedure was also confirmed using whole blood samples. No relationship between the GT (p=0.25), d_{f} (p=0.87) or G'_{GP} (p=0.48) and the stress applied were found, as shown in Figure 3.22. Additionally, no relationship was identified between the GT (p=0.52), d_{f} (p=0.3) or G'_{GP} (p=0.86) and the strain applied, as shown in Figure 3.23. Figures 3.22c and 3.23c show a wide spread of G' values obtained in whole blood samples. Since samples were collected from individual donors these differences could be explained by biological variation between the samples, associated with differences in cell fraction which can range from 36-53 % in healthy populations and would contribute to the elasticity of the sample.[171] These differences were not as pronounced in either the gel time or fractal dimension, which are measures of the fibrin network formation and subject to a smaller degree of individual variation in healthy samples.

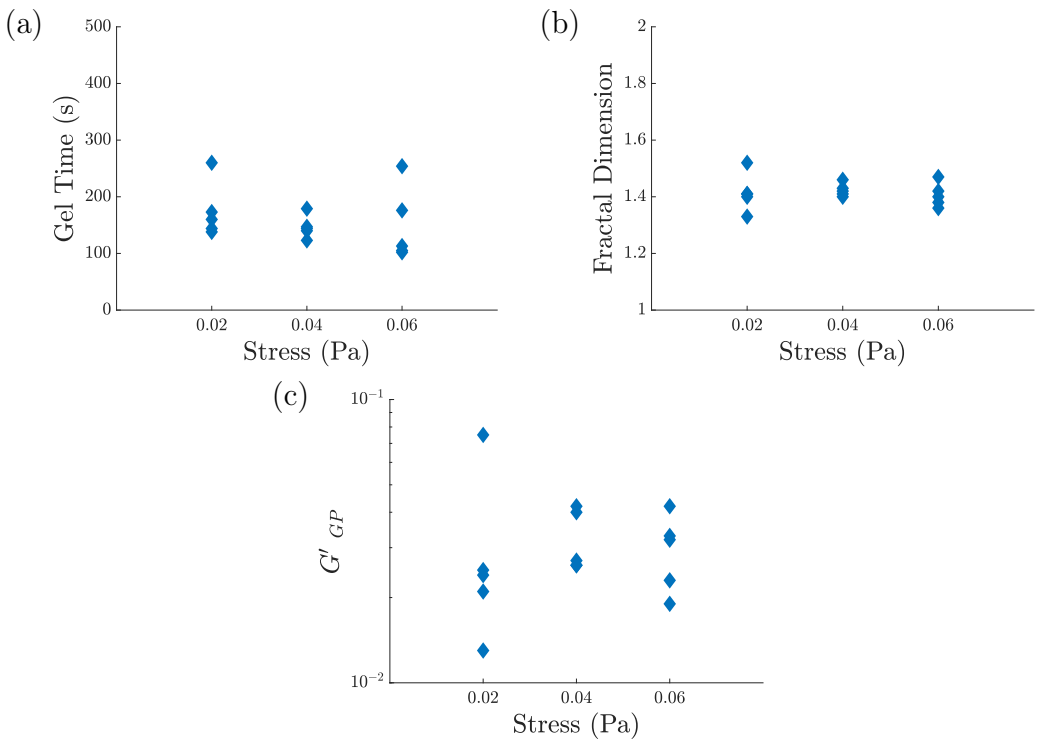

Figure 3.22: Graphs Showing the Effect of Increasing Stress on Gel Point Parameters of Whole Blood.

(a) Gel time, (b) fractal dimension, and (c) G' at the gel point.

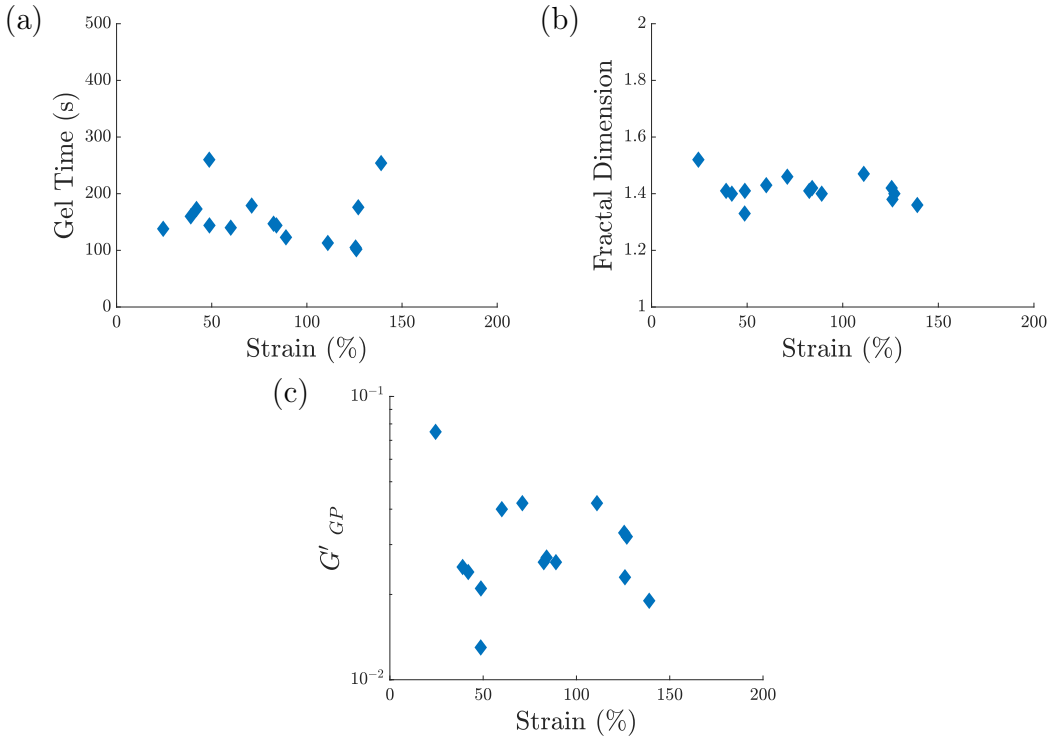

Figure 3.23: Graphs Showing the Effect of Increasing Strain on Gel Point Parameters of Whole Blood.

(a) Gel time, (b) fractal dimension, and (c) G' at the gel point.

3.2.5 Comparison of Gel Point Detection in Pooled Platelet Free Plasma using SMT and CMT Rheometers

Following optimisation and validation of the FTMS procedure, gel point measurements of P-PFP were performed on the SMT rheometer using FTMS and compared to results obtained using conventional discrete sweep techniques on a CMT rheometer. When gel points were detected using comparable conventional techniques a total of eleven attempts at measuring the gel point of P-PFP were required to obtain five gel point measurements where a clear change in the dependence of phase angle on frequency was detected, *i.e.* a 45.5 % success rate. Comparatively, the FTMS technique produced acceptable data each time the procedure was run, *i.e.* five runs - a 100 % success rate. The d_f values obtained by FTMS were found to be in agreement with the predicted value from SEM fibre thickness results, which can be seen in Figure 3.24.

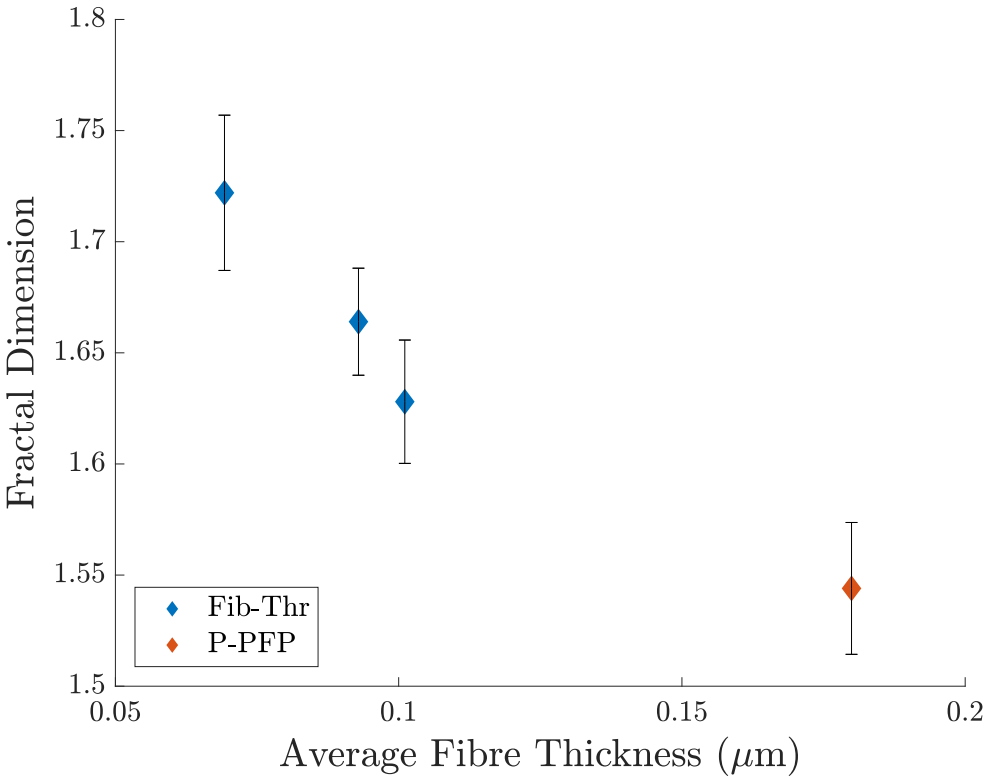

Figure 3.24: A Graph Depicting the Relationship between Fractal Dimension Obtained by Fourier Transform Mechanical Spectroscopy and Average Fibre Thickness from Scanning Electron Microscopy.

Error bars indicate standard deviation (n=5).

A qualitative comparison of the gel point measurements detected by FTMS and discrete frequency sweeps can be seen in Figure 3.25. Upon analysis it was noted that two of the measurements conducted using conventional techniques were found to be subject to mutation errors with N_{mu} >0.15, whereas no mutational errors were identified in the FTMS data.

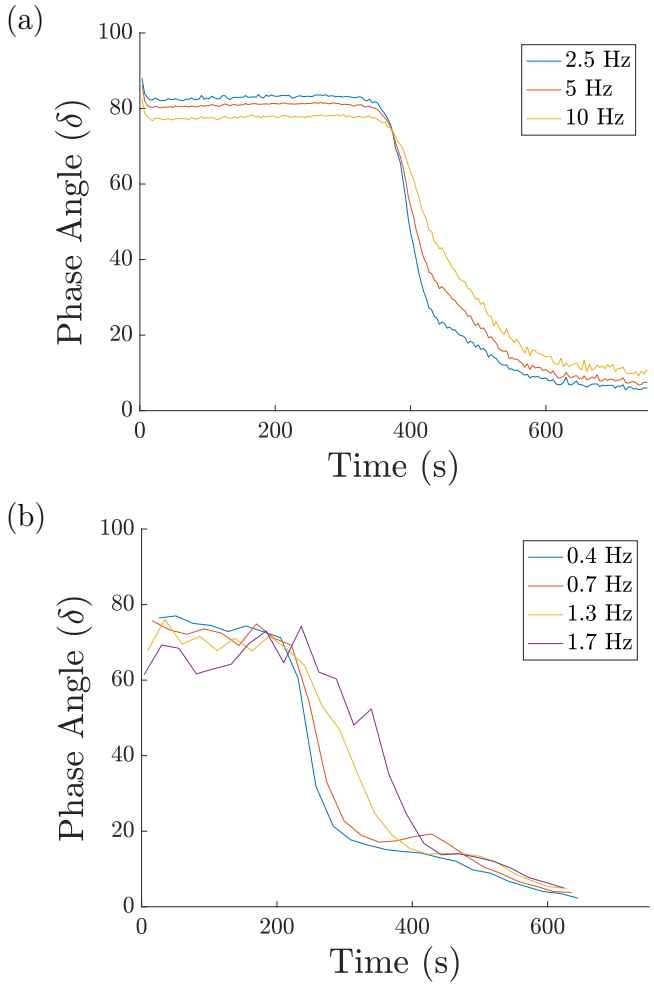

Figure 3.25: Example Rheological Profiles of Pooled Platelet Free Plasma Undergoing Coagulation.

(a) Fourier transform mechanical spectroscopy and (b) discrete frequency sweeps.

The raw phase angle associated with the measurements taken using a CMT rheometer was found to be 175-178 ° at the gel point. This is substantially higher than the 150 ° limit suggested by the rheometer manufacturer.[163] During the FTMS procedures using an SMT rheometer the raw phase angle was 60-65 ° with no inertial correction required. This comparison revealed that gel points of P-PFP detected by conventional discrete sweep techniques are unreliable, highlighted by the detection of high sample mutation numbers and the low acquisition of acceptable gel points. The high raw phase angle detected while using the CMT rheometer also indicated artefacts associated with inertia in the measurements, which are known to dominate measurements where the raw phase is >150 °.

3.3 Conclusions

The fractal dimension afforded by rheological detection of the gel point of blood has been previously investigated as a biomarker for thrombotic disease and therapeutic intervention. However, the use of blood as a standardised material brings about issues arising from donor variability and storage. Plasma, derived from centrifugation of whole blood, can be pooled in large volumes and used as a standardised material for the preclinical assessment and development of therapies for blood clots. However, the rheological characterisation of plasma, in particular measurement of the gel point, is challenging due to the narrow and transient linear viscoelastic region, the rapidity of gelation which leads to sample mutation artefacts, and the influence of both instrument and fluid inertia limiting the appropriate frequency ranges for testing.

The ability of Fourier transform mechanical spectroscopy (FTMS) to overcome issues encountered due to sample mutation was investigated, along with the use of a SMT instrument which can, in principle, be used to obtain reliable data at high frequencies. During this study, the influence of frequency on gel point measurements of a model gelling system - gelatine at a concentration of 2.5 % (w/v) was studied, showing that at frequencies above 2 Hz sample mutation was negligible.

The results also revealed previously unquantified artefacts at frequencies over 20 Hz which can be attributed to fluid inertia and/or transducer compliance. As a result of this work, an optimum frequency range of 2-20 Hz was established within which measurements are free from artefacts caused by sample mutation and inertia.

Use of the fluid inertia correction provided by TRIOS control software was investigated. However, corrected gel point parameters were found to be unreliable and identification of the appropriate correction was not possible from results. Therefore, it was concluded that measurements should be performed below both the maximum frequency identified (20 Hz) and the gap loading limit (200 μm) to negate any influence from fluid inertia.

The technique was validated using model fibrin thrombin gels which confirmed that the new detection protocol is sensitive to agents known to effect the gel point, and that the incipient clot structures detected are predictors of the mature clot structure observed by scanning electron microscopy.

Gel point measurements using pooled platelet free plasma (P-PFP) were then obtained via FTMS at three frequencies within the identified range on a separate motor transducer instrument, and the linearity of the measurements was confirmed for both P-PFP and whole blood.

Comparison of the new procedures to conventional discrete sweep techniques showed that the novel high frequency FTMS procedure is able to detect gel points in P-PFP with improved reliability, less variation, better reproducibility, and showing a reduced contribution from known sources of error.

Chapter 4

Detection of Fibrinolysis Using High Frequency Fourier Transform Mechanical Spectroscopy

Thrombolysis is a key treatment option for venous thrombosis patients, which involves breaking down the clot by the action of a therapy. However, its use remains associated with a high risk of severe side effects. Within this group stroke patients are the most at risk, with many thrombolytic agents contraindicated by the condition due to the risk of cerebral haemorrhage. The acknowledged efficacy of the therapy has generated interest in new tools for assessing patient suitability for thrombolytic therapy in order to reduce these risks while maintaining the availability of treatment options. Fourier transform mechanical spectroscopy (FTMS) procedures, the optimisation and validation of which were presented in Chapter 3, can be used to detect the gel point of pooled platelet free plasma (P-PFP) systems. In principle, rheometry can also be used to detect the de-gel point of these systems. Thus offering biomarkers for monitoring lysis and efficacy of thrombolytic treatment.

Currently rt-PA is the only thrombolytic therapy approved for the treatment of acute ischemic stroke; however, its use is associated with increased risk of haemorrhagic transformation (HT). At the present time eligibility for treatment is somewhat arbitrarily determined by factors including age, co-morbidities, and current medications. It is known to be effective in improving outcomes at three months for patients outside current eligibility criteria when administered successfully.[172–174] As such there is a predicted benefit to determining likely responses to intervention in addition to assessing the probability of poor outcomes for each individual, in order to reduce the risk of harm and to open treatment to those who, under the current clinical guidelines, may not receive it.

The cause of increased HT risk has been investigated in many studies and generally accepted mechanisms in acute stroke treated with rt-PA involve high blood pressure, platelet concentration, vascular weakness/stiffness, and increased blood brain barrier permeability.[172,175–177]

An alternative thrombolytic, streptokinase, is contraindicated in stroke patients due to the increased risk of HT well above that for rt-PA, with clinical trials of streptokinase in acute stroke patients being suspended due to the high mortality rates observed.[178,179] The mechanism for the increased rates of HT in streptokinase therapy have been reported as a result of the inefficient breakdown of occluding thrombi, which go on to embolise and cause further damage to the cerebral vasculature.[180] In this case rheometry may prove to be capable of detecting and predicting the risk of these events through monitoring of mechanical properties and structure during clot breakdown.

In addition to the risk of HT, many potential markers for clinical outcomes in acute stroke have been investigated, and to date several key factors in predicting poor outcomes in intravenous rt-PA administration have been identified. These are summarised in Table 4.1.

Table 4.1: Ability of Current Markers to Predict Poor Clinical Outcomes Resulting from Thrombolytic Intervention in Acute Ischemic Stroke Patients

Marker	**At Admission**	**Within 24hrs**	**Within 6 Months**	**Ref.**
Clot Permeability	✓	✓	x	[181]
Coagulation Time	x	x	✓	[181]
Clot Lysis Time	✓	✓	x	[181]
D-dimer Generation	✓	✓	x	[181]
Thrombin Generation	✓	x	x	[181]
PAI-1 Concentration	✓	x	x	[181]
FVIII Activity	x	✓	-	[182]

✓: $p<0.05$, x : $p>0.05$, - : not tested

Mechanical based biomarkers have not found widespread use in predicting clinical outcomes, with thromboelastography having been shown to be independent of rt-PA treatment outcomes for stroke patients when tested upon admission and 10 minutes after treatment with rt-PA.[183] However, gel point detection has shown that the fractal dimension and fibrinogen concentration, along with standard coagulation assays (PT and APTT) are capable of detecting rt-PA therapy.[141]

In 2017 Bannish *et al.* showed that at low doses of rt-PA, coarse clots are lysed more rapidly than finer counterparts, while at high rt-PA doses they are lysed more slowly. This was reported to be a result of rt-PA release by kinetic unbinding during fibre degradation, as the fibre it is coupled to is lysed.[184] This provides key evidence suggesting that the fractal dimension may be a useful tool in predicting responses to rt-PA therapy, suggesting a link between clot structure and lysis.

Despite thromboelastography and thromboelastometry being acknowledged as the "gold standard" for the tandem detection of these systems, spectrophotometric assays, such as the overall haemostasis potential assay, are more commonly utilised in clinical settings.[81,89,97]

Rheological measurement of both coagulation and lysis may prove useful in predicting poor outcomes for patients, since it can be linked directly to several factors identified in Table 4.1 including permeability (which is determined by clot structure), coagulation time, and clot lysis time. In addition to this, the potential biomarker acts as a global marker and may capture many factors including those known to be associated with clinical outcomes.

The aim of this chapter is to utilise the FTMS technique in order to detect fibrinolysis in P-PFP, develop new biomarkers of clot lysis, and explore their response to rt-PA and streptokinase. The work will also investigate the influence of abnormal clot structures associated with thrombotic conditions, such as stroke, on fibrinolysis through modulation of the thrombin concentration. The rheometrical detection techniques will be compared to the overall haemostasis potential assay. From the study of the model P-PFP system the relationships between rheological parameters will be investigated. The work will conclude with the evaluation of a physiologically relevant system, through the detection of the coagulation and lysis of whole blood using rheometry, in the presence of a fixed concentration of rt-PA and increasing concentrations of the thrombolytic drug streptokinase.

4.1 Methods

4.1.1 Sample Preparation

Pooled Platelet Free Plasma

Pooled platelet free plasma (P-PFP) was collected as described in Section 3.1.1. Recombinant tissue plasminogen activator (rt-PA) (Hyphen BioMed, FR: RP007C) was reconstituted to a stock concentration of 1 mg/ml with distilled water at room temperature before being aliquoted and stored at -20 °C until use. Streptokinase (Sigma Aldrich, UK: S3134-50KU) was reconstituted to a stock concentration of 3,500 U/ml with distilled water at room temperature before being aliquoted and stored at -20 °C until use.

The rt-PA was thawed at room temperature and diluted with distilled water to give final stock concentrations of 0.873, 1.31, 1.75 and 2.20 μM. A fixed volume of the stock rt-PA was then added to P-PFP along with 18 mM final concentration of $CaCl_2$ (Sigma Aldrich, UK: 21115-100ML) to give final rt-PA concentrations of 5, 10, 15 and 20 nM. Samples were then mixed gently by drawing the sample into the pipette tip and slowly releasing it several times and were loaded on to rheometer for testing as outlined in Section 4.1.2.

Thrombin (Enzyme Research Laboratories, UK: HT 1002a) was prepared as described in Section 3.1.1 and added to P-PFP to give final concentrations of 0, 0.02 0.06 and 0.1 NIH/ml along with 10 nM rt-PA as described above and 18 mM $CaCl_2$. The samples were mixed by gently drawing material into the pipette tip and slowly releasing it several times before being loaded for testing.

Streptokinase was thawed at room temperature and further diluted to give final stock concentrations of 800, 1,600, 2,400, and 3,200 U/ml. A fixed volume of streptokinase was then added to P-PFP along with 18 mM final concentration of $CaCl_2$ to give final streptokinase concentrations of 20, 40, 60, and 80 U/ml. Samples were mixed gently by drawing the fluid into the pipette tip and slowly releasing it several times before being loaded on to the rheometer for testing.

For spectrophotometric analysis, samples were prepared as described above with the addition of thrombin at a final concentration of 0.05 NIH/ml. 1 ml of sample was then transferred to a cuvette before testing was initiated. Where additional thrombin concentrations were tested this resulted in final thrombin concentrations of 0.05, 0.07, 0.11 and 0.15 NIH/ml.

Whole Blood

Whole blood was collected from the median cubital vein of healthy volunteers using a 21-gauge butterfly line (Greiner Bio-One, UK: 450085) by a trained phlebotomist under ethical approval (SUMS RESC: 2018-0063). All volunteers declared themselves healthy and free from the influence of agents that may interfere with coagulation testing (see Appendix A). The first 3 ml of blood was collected in an additive free vacuette® tube (Greiner Bio-One, UK: 454241) and discarded to minimise factors present as a result of the venipuncture. A further 3 ml of blood was collected in an additive free vacuette® tube for testing. Immediately following venipuncture, rt-PA and streptokinase were added as described above to give a final rt-PA concentration of 5 nM and final streptokinase concentrations of 0, 10, 20, 30, 40, 50, and 60 U/ml. Samples were immediately loaded onto the rheometer plates for testing.

4.1.2 Data Collection

Rheometry

The gel point detection procedure optimised in Chapter 3 was conducted on P-PFP using the ARES-G2 rheometer (TA instruments, UK) described in Section 3.1.2. The auto-strain adjust function was used in all gel point detection procedures, which effectively allowed unconstrained strain adjustments (0.1-300 %) while limiting the torque applied to within 0.02 μN.m of the value specified to give a fundamental stress of 0.04 Pa. P-PFP samples were prepared as described above and loaded onto the ARES-G2 rheometer. The Fourier transform mechanical spectroscopy (FTMS) procedure optimised in Chapter 3 was used to monitor both the coagulation and lysis of P-PFP with the addition of rt-PA, thrombin, and streptokinase (n=5).

The gel point detection procedure discussed in Section 3.1 was conducted on whole blood samples using the AR-G2 rheometer (TA instruments, UK) described in Section 3.1.2. Whole blood samples were tested on the AR-G2 rheometer using discrete frequency sweeps at a frequency range of 0.4-2 Hz. The test applied a stress of 0.09 Pa and 0.14 Pa over the period of coagulation and clot lysis respectively, at a gap of 380 μm. The linearity of measurements was confirmed through monitoring for the presence of third harmonic response at the gel point (n=5).

Spectrophotometry

Samples of P-PFP were prepared as described above and Parafilm was placed over the top of the cuvette in order to limit evaporation during the test. The cuvette was positioned within the cell holder of a Novaspec Plus® visible spectrophotometer (Amersham BioSciences, UK). A blank reading of the sample was taken at the beginning of the test and the absorbance (A) of light at 405 nm was monitored over time. Base tests were performed on P-PFP with the addition of 0.05 NIH/ml thrombin in the absence of any lytic agents (n=5).

4.1.3 Data Analysis

Both the gel points and de-gel points obtained for P-PFP were determined using 'gel point analysis' software described in Section 1.4.2. This produced gel time (GT) and fractal dimension at the gel point ($d_{\mathrm{f}\ GP}$) values as well as a de-gel time (dGT) and value of the fractal dimension at the de-gel point ($d_{\mathrm{f}\ dGP}$). The functional clot lifetime ($FCLT$) was calculated as the period between GT and dGT. The GT, $FCLT$, $d_{\mathrm{f}\ GP}$ and $d_{\mathrm{f}\ dGP}$ detected during each test were assessed by Spearman's ranked correlation analysis for each agent.

All of the rheometrical data collected for P-PFP was combined and Spearman's ranked correlation analysis was used to test for any relationships between the rheological parameters GT, $FCLT$, $d_{\mathrm{f}\ GP}$ and $d_{\mathrm{f}\ dGP}$. Furthermore, stepwise regression analysis was performed between gel point parameters and both the $FCLT$ and $d_{\mathrm{f}\ dGP}$ values in order to identify any predictive value of gel point measurements for lysis results.

Data collected from whole blood samples was analysed in the same way as data for P-PFP using 'gel point analysis' software and compared by Spearman's ranked correlation analysis.

Absorbance readings were analysed to give both a clotting time (CT), defined as the time to 1/2 A_{max} during coagulation, and a lysis time (LT) defined as the time between 1/2 A_{max} during coagulation and 1/2 A_{max} during lysis. The overall haemostatic potential (OHP) was calculated from the area under the graph. The area under base readings was analysed to give an average overall coagulation potential which was used to calculate the overall fibrinolytic potential (OFP) for each test (n=5). These parameters were compared by Spearman's ranked correlation analysis.

4.1.4 Limitations

The spectrophotometric detection of coagulation and lysis of plasma resulted in many of the experiments exceeding the maximum absorbance limit of the equipment. Since it is known that the dilution of plasma leads to changes in the clot microstructure under investigation, samples were not diluted in order to compensate for this. As a result the maximum absorbance was not recorded or analysed and data regarding times in many cases was effectively defined as the time to 1/2 the maximum absorbance detectable by the equipment. This would also impact the area under the curve calculated from the data. Results are still expected to follow the trends associated with the measurement but are not directly comparable to literature values. In addition, the spectrophotometer used did not have temperature control capability and so results were expected to differ slightly from the rheometrical results owing to the temperature difference in the experimental set up (room temperature vs 37 °C).

In the study of streptokinase concentration on the rheometrical detection of P-PFP coagulation and lysis, several results at 80 U/ml did not display either a gel point or de-gel point as the high concentration of lytic agent impeded coagulation. As a result of this, of the five repeats run only two data sets were available at this concentration. This data is displayed in the relevant figures but was excluded from statistical analysis. Additionally, a suspected outlier was identified in data collected at a streptokinase concentration of 60 U/ml, this was confirmed by Grubbs' test and excluded from statistical analysis but is indicated in the corresponding figures.

4.2 Results and Discussion

4.2.1 Impact of rtPA on Clot Formation and Lysis

Rheology

The detection of the de-gel point in pooled platelet free plasma (P-PFP) under the optimised FTMS procedure was confirmed, and an example gel point and de-gel point can be seen in Figure 4.1. This represents a significant advancement as it is the first reported fibrinolytic de-gel point in plasma detected using FTMS.

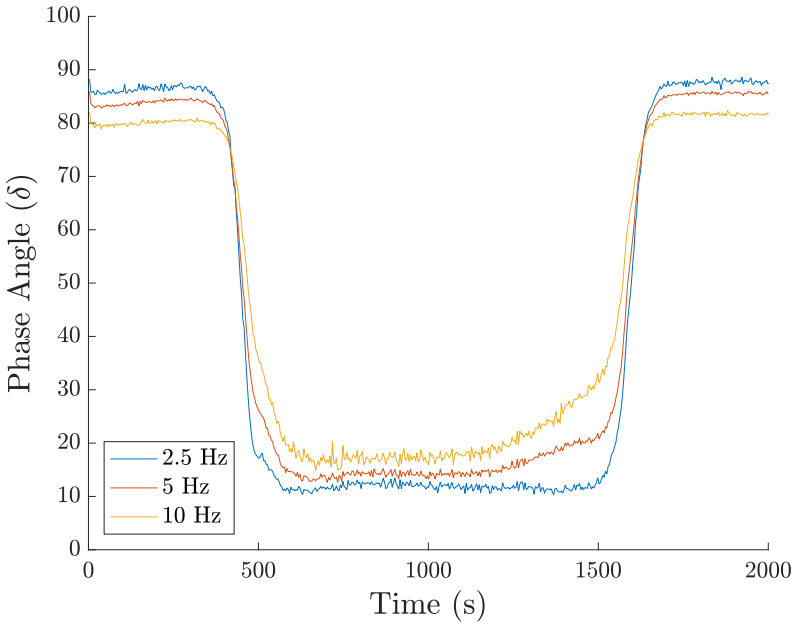

Figure 4.1: Example Rheological Profile of Pooled Platelet Free Plasma Undergoing both Coagulation and Lysis.

The generation of this measurement represents the initial demonstration of the novel biomarker for thrombosis patients, which has a potential future application in assessing the suitability of patients for therapeutic intervention.

Following the detection of the de-gel point, rheological data was collected at a range of rt-PA concentrations. Statistical analysis shown in Tables 4.2 and 4.3 revealed that rt-PA concentration has a statistically significant effect on functional clot lifetime ($FCLT$). Table 4.4 indicates the average values for results which were not found to be dependent on rt-PA concentration.

Table 4.2: Probability values for Correlations between Coagulation and Lysis Parameters Detected by Fourier Transform Mechanical Spectroscopy of Pooled Platelet Free Plasma with Varying Recombinant Tissue Plasminogen Activator Concentration.

	$[rtPA]$	*Gel Time*	$d_{\mathbf{f}\ GP}$	$FCLT$	$d_{\mathbf{f}\ dGP}$
$[rtPA]$	-	0.36	0.83	**0.02**	0.15
Gel Time	0.36	-	0.84	0.83	0.17
$d_{\mathbf{f}\ GP}$	0.83	0.84	-	0.93	0.14
$FCLT$	**0.02**	0.83	0.93	-	0.18
$d_{\mathbf{f}\ dGP}$	0.15	0.17	0.14	0.18	-

$[rtPA]$: recombinant tissue plasminogen activator concentration, $d_{\mathrm{f}\ GP}$: fractal dimension during coagulation, $d_{\mathrm{f}\ dGP}$: fractal dimension during lysis.

Table 4.3: Rho values for Correlations between Coagulation and Lysis Parameters Detected by Fourier Transform Mechanical Spectroscopy of Pooled Platelet Free Plasma with Varying Recombinant Tissue Plasminogen Activator Concentration.

	$[rtPA]$	*Gel Time*	$d_{\mathbf{f}\ GP}$	$FCLT$	$d_{\mathbf{f}\ dGP}$
$[rtPA]$	-	0.22	-0.05	**-0.50***	0.33
Gel Time	0.22	-	0.05	-0.05	-0.32
$d_{\mathbf{f}\ GP}$	-0.05	0.05	-	-0.02	0.34
$FCLT$	**-0.50***	-0.05	-0.02	-	-0.31
$d_{\mathbf{f}\ dGP}$	0.33	-0.32	0.34	-0.31	-

$[rtPA]$: recombinant tissue plasminogen activator concentration, $d_{\mathrm{f}\ GP}$: fractal dimension during coagulation, $d_{\mathrm{f}\ dGP}$: fractal dimension during lysis.
* $p<0.05$, ** $p<0.01$, *** $p<0.001$

Table 4.4: Average values of Coagulation and Lysis Parameters Detected by Fourier Transform Mechanical Spectroscopy of Pooled Platelet Free Plasma with Varying Recombinant Tissue Plasminogen Activator Concentration.

Gel Time (s)	$d_{\mathbf{f}\ GP}$	$FCLT\ (s)$	$d_{\mathbf{f}\ dGP}$
345 ±85	1.51 ±0.03	-	1.47 ±0.05

$d_{\mathrm{f}\ GP}$: fractal dimension during gelation, $d_{\mathrm{f}\ dGP}$: fractal dimension during lysis. Values which were found to be dependent on recombinant tissue plasminogen activator concentration are not presented.

The relationship between rt-PA concentration and $FCLT$ suggests that between 0-10 nM rt-PA (where $FCLT$ at 0 nM is theoretically infinite) increasing concentrations of rt-PA lead to a decrease in $FCLT$, shown in Figure 4.2. However, at concentrations above 10 nM the system appears to reach saturation and the influence of additional rt-PA has a minimal effect, with lysis occurring in the region of 1500 s. This indicates that the measurement would be sensitive to the presence of rt-PA at clinical doses, but unable to distinguish between dose intervals.[185]

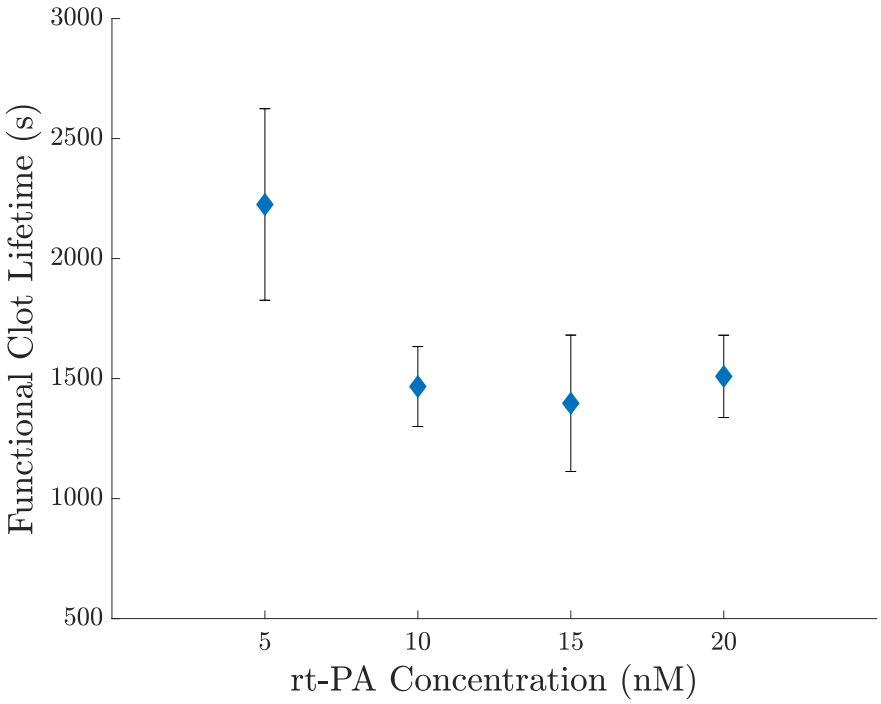

Figure 4.2: A Graph Showing the Relationship Between Functional Clot Lifetime and Recombinant Tissue Plasminogen Activator Concentration in Pooled Platelet Free Plasma Detected by Fourier Transform Mechanical Spectroscopy.

Error bars indicate standard deviation (n=5).

Spectrophotometry

Statistical evaluation of the influence of rt-PA concentration on spectrophotometric parameters, shown in Tables 4.5 and 4.6, revealed a significant relationship between rt-PA concentration and both the clotting time (CT) and lysis time (LT), as well as the overall fibrinolytic potential (OFP).

Table 4.5: Probability values for Correlations between Coagulation and Lysis Parameters Detected by Spectrophotometric Overall Haemostatic Potential Assay of Pooled Platelet Free Plasma with Varying Recombinant Tissue Plasminogen Activator Concentration.

	$[rtPA]$	*Clotting Time*	*Lysis Time*	OFP
$[rtPA]$	-	**<0.01**	**<0.001**	**<0.001**
Clotting Time	**<0.01**	-	**<0.01**	**<0.01**
Lysis Time	**<0.001**	**<0.01**	-	**<0.001**
OFP	**<0.001**	**<0.01**	**<0.001**	-

$[rtPA]$: recombinant tissue plasminogen activator concentration, OFP: overall fibrinolytic potential.

Table 4.6: Rho values for Correlations between Coagulation and Lysis Parameters Detected by Spectrophotometric Overall Haemostatic Potential Assay of Pooled Platelet Free Plasma with Varying Recombinant Tissue Plasminogen Activator Concentration.

	$[rtPA]$	*Clotting Time*	*Lysis Time*	OFP
$[rtPA]$	-	**0.63****	**-0.97*****	**0.93*****
Clotting Time	**0.63****	-	**-0.58****	**0.66****
Lysis Time	**-0.97*****	**-0.58****	-	**-0.93*****
OFP	**0.93*****	**0.66****	**-0.93*****	-

$[rtPA]$: recombinant tissue plasminogen activator concentration, OFP: overall fibrinolytic potential.

* p<0.05, ** p<0.01, *** p<0.001

Figure 4.3 shows a relationship between rt-PA concentration and CT which was not detected during rheometrical procedures, where rt-PA concentrations of 15 nM and 20 nM appear to show increased CT. This may be more pronounced in the spectrophotometric system due to the addition of 0.05 NIH/ml thrombin at the beginning of the test. Further evaluation in this section will examine whether this is a result of the spectrophotometric detection system being more sensitive, or whether FTMS is also capable of detecting the relationship when a fixed concentration of exogenous thrombin is added to the system.

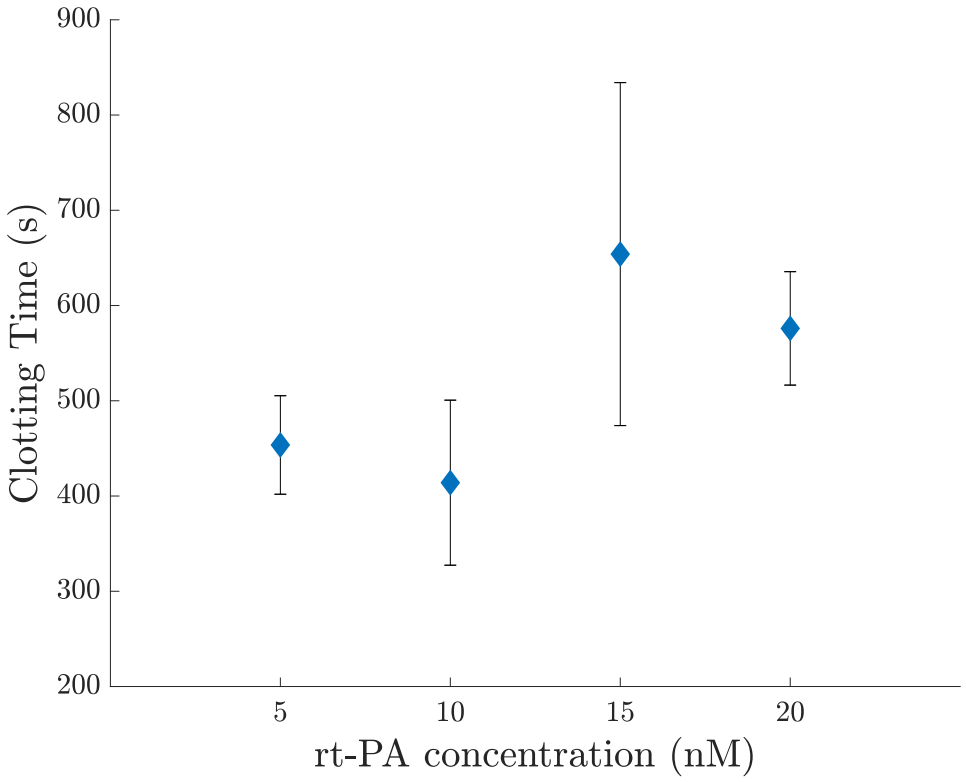

Figure 4.3: A Graph Showing the Relationship Between Clotting Time and Recombinant Tissue Plasminogen Activator Concentration in Pooled Platelet Free Plasma Detected by Spectrophotometry.

Error bars indicate standard deviation (n=5).

The relationship between LT and rt-PA concentration detected by spectrophotometry is shown in Figure 4.4. Since the OFP is fundamentally linked to the LT in spectrophotometric measurements this data reveals the same trend shown in Figure 4.5. In comparison to the results collected by FTMS both indicate a more pronounced influence of rt-PA on LT at lower concentrations. However, the LTs detected by spectrophotometry appear smaller than those detected by FTMS.

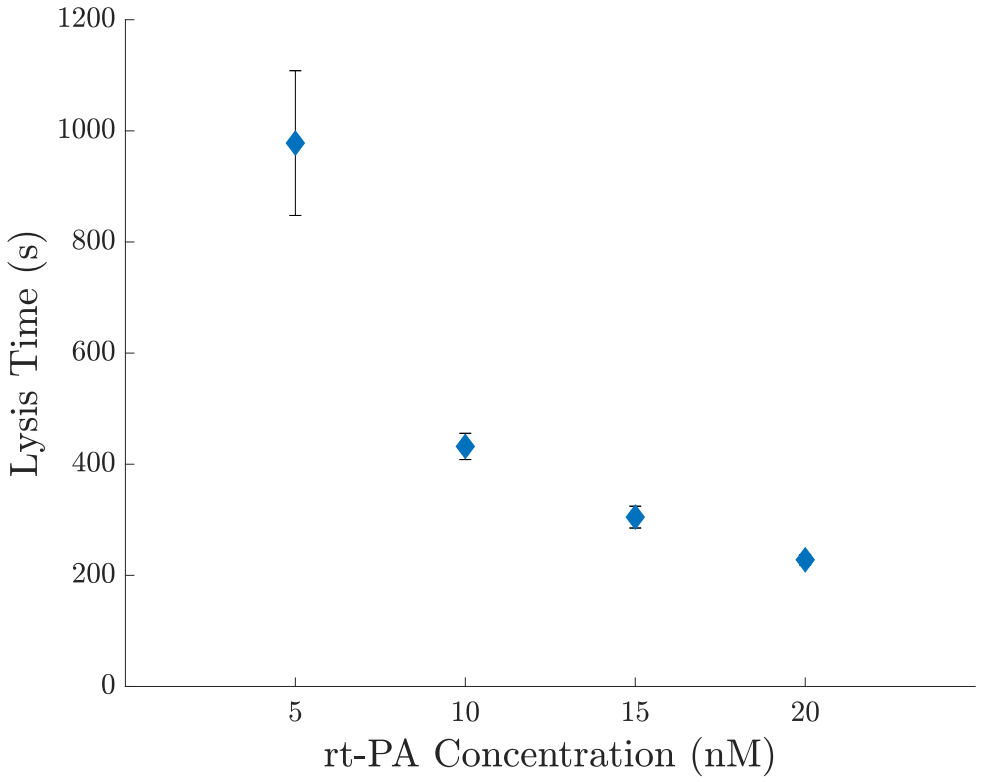

Figure 4.4: A Graph Showing the Relationship Between Lysis Time and Recombinant Tissue Plasminogen Activator Concentration in Pooled Platelet Free Plasma Detected by Spectrophotometry.

Error bars indicate standard deviation (n=5).

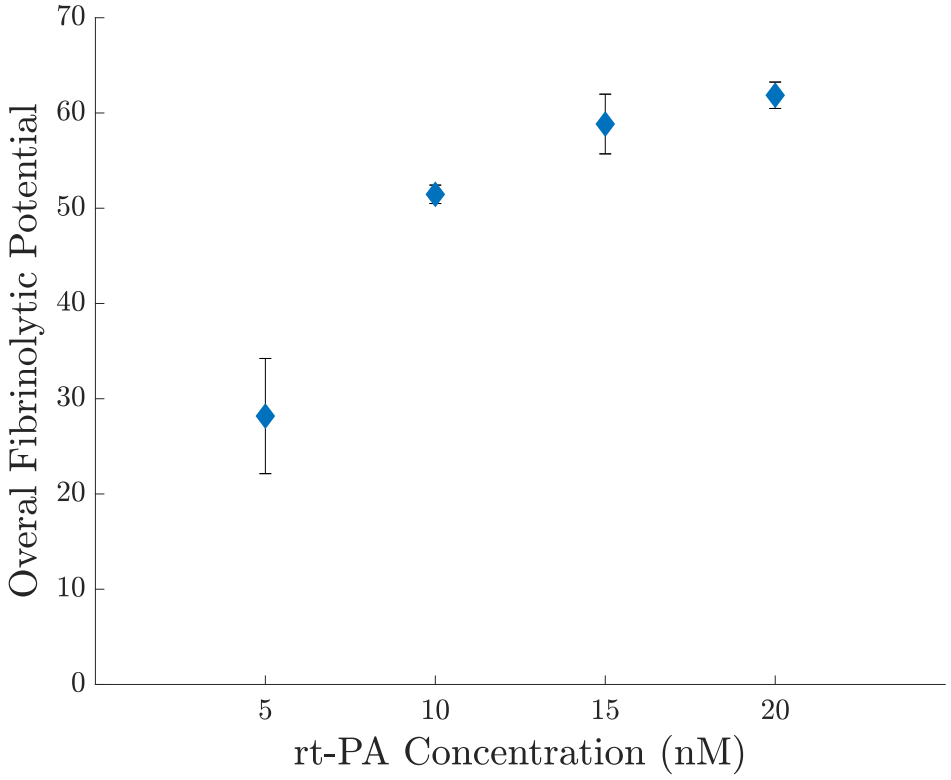

Figure 4.5: A Graph Showing the Relationship Between Overall Fibrinolytic Potential and Recombinant Tissue Plasminogen Activator Concentration in Pooled Platelet Free Plasma Detected by Spectrophotometry.

Error bars indicate standard deviation (n=5).

To investigate whether the differences in $FCLT/LT$ and GT/CT detected by FTMS and spectrophotometry are a result of the addition of exogenous thrombin, FTMS experiments were repeated with the addition of 0.1 NIH/ml thrombin. Correlation analysis of the rheological parameters revealed that, as in the original tests (0 NIH/ml), the only relationship identified was between $FCLT$ and rt-PA concentration ($p<0.001$). This leaves spectrophotometry as the only test which detected the influence of rt-PA on coagulation.

A comparative plot of $FCLT/LT$ with varying rt-PA concentration detected by spectrophotometry and FTMS with and without the addition of thrombin is shown in Figure 4.6.

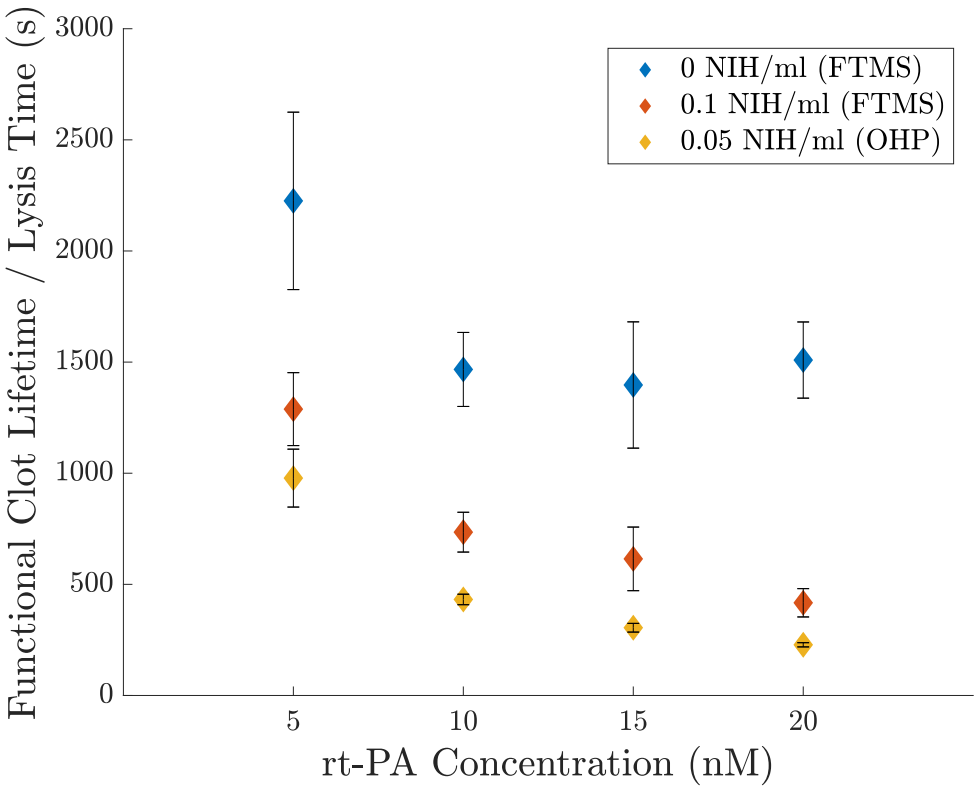

Figure 4.6: A Graph Showing the Relationship Between Lysis Time and Recombinant Tissue Plasminogen Activator Concentration in Pooled Platelet Free Plasma Detected by Fourier Transform Mechanical Spectroscopy With and Without the Addition of 0.05 NIH/ml Thrombin and Spectrophotometry With the Addition of 0.1 NIH/ml Thrombin.

Error bars indicate standard deviation (n=5).

The addition of exogenous thrombin to P-PFP tested by FTMS resulted in a trend comparable to that detected by spectrophotometry. This warrants further investigation as it indicates that the addition of thrombin not only influences the $FCLT/LT$, but also influences the relationship between the concentration of lytic agent and $FCLT/LT$.

Consideration of observations from this section, Section 4.2.3 and comparable studies from the literature identifies a possible cause for this discrepancy as an interaction between thrombin and rt-PA. This is suggested by the fact that the differences in lytic potential is associated with the measurements conducted herein utilising internal fibrinolysis, but is not evident from comparable studies in the literature which utilise external fibrinolysis for confocal microscopy.[184] The difference occurs in the absence of additional thrombin, suggesting it has a key role in the mechanism. Furthermore the relationship contradicts known relationships between structure and lysis, which indicates a secondary interaction of thrombin.

This apparent minimum lysis time is not evident in later work contained within this chapter where streptokinase is used as the lytic agent, which supports the idea that the phenomenon is directly related to rt-PA and not further downstream lytic factors.

Plasminogen activator inhibitor (PAI-1), an inhibitor of the fibrinolytic pathway, both interacts with thrombin and is a known inhibitor of rt-PA. Thrombin is known to trigger the release of PAI-1 from platelets as well as overexpression of the PAI-1 gene by other cell types.[186,187] However, in the acellular system under study this interaction is likely limited to the 'suicide substrate reaction' between the two. During this interaction the inhibition of thrombin occurs through the formation of a thrombin-PAI-1 complex, which effectively sequesters both molecules. However, the stoichiometry of complex formation leads to a branched pathway, where one branch results in the cleavage of PAI-1 and thrombin release, while another leads to complex formation. As a result the stable formation of the complex requires 3 mol of PAI-1 for the inhibition of 1 mol of thrombin.[188] This interaction may be effectively reducing the available PAI-1 where an excess of thrombin is present, but requires further investigation.

Since PAI-1 has been shown to be a significant indicator of clinical outcomes in stroke patients, the inhibition of its action by thrombin may result in useful information being lost by this style of test.[181] This variation seen with the addition of thrombin may result in inaccuracies during clinical assessment when using the commonly utilised overall haemostatic potential assay. FTMS, although in the early stages of research, may prove to be a more accurate indicator of clinical outcomes, since it may be subject to fewer discrepancies caused by variations in testing procedures by different clinical laboratories. This provides an important justification for the further investigation of these findings, through PAI-1 inhibition.

Evaluation of the relationship between *GT* and rt-PA using FTMS in the presence of exogenous thrombin showed no statistically significant relationship. Previous research undertaken by Goldman *et al.* on stroke patients given rt-PA revealed that fibrinolytic intervention leads to prolongation of coagulation detected by thrombin generation curve through spectrophotometry.[189] Since this was also previously detected in gel point measurements as a reduction in the fractal dimension during coagulation ($d_{\mathrm{f}\ GP}$) it is unclear why the FTMS procedure did not detect the difference.[141] However, since the measurements reported in the literature were performed on patients whose blood was collected after being given intravenous rt-PA, it remains possible that there is an *in-vivo* mechanism

responsible for amplifying this effect. This would result in the mechanism not being substantially present in the isolated system tested, and so not detected by the FTMS procedure, which in this aspect, has been shown to be less sensitive than spectrophotometry.

In a clinical context these results indicate an improved sensitivity of FTMS to the interplay between thrombin and rt-PA. Measurement of the gel point and de-gel point in patient samples could provide clinicians with personalised information regarding clot microstructure and lytic capacity. This information could be combined with the current treatment guidelines to facilitate fibrinolytic treatment in patients who are currently not eligible, for example by virtue of their age. The biomarker could also be used to indicate the need to explore alternative treatment options for individuals who may be at risk of haemorrhage despite meeting the current treatment criteria.

4.2.2 Impact of Thrombin on Clot Formation and Lysis

Rheology

Investigation of the influence of thrombin on coagulation and lysis parameters revealed that increasing thrombin concentrations led to a significant decrease in both the GT and $FCLT$, and correlates with an increase in the value of $d_{\mathrm{f}\ GP}$ as shown in Tables 4.7 and 4.8. Table 4.9 indicates the average values for results which were not found to be dependent on thrombin concentration.

Table 4.7: Probability values for Correlations between Coagulation and Lysis Parameters Detected by Fourier Transform Mechanical Spectroscopy of Pooled Platelet Free Plasma with Varying Thrombin Concentration.

	$[Thr]$	*Gel Time*	$d_{\mathbf{f}\ GP}$	$FCLT$	$d_{\mathbf{f}\ dGP}$
$[Thr]$	-	**<0.001**	**<0.001**	**<0.001**	0.44
Gel Time	**<0.001**	-	**0.02**	**<0.01**	**0.02**
$d_{\mathbf{f}\ GP}$	**<0.001**	**0.02**	-	**<0.01**	**0.03**
$FCLT$	**<0.001**	**<0.01**	**<0.01**	-	0.76
$d_{\mathbf{f}\ dGP}$	0.44	**0.02**	**0.03**	0.76	-

$[Thr]$: thrombin concentration, $d_{\mathrm{f}\ GP}$: fractal dimension during coagulation, $d_{\mathrm{f}\ dGP}$: fractal dimension during lysis.

Table 4.8: Rho values for Correlations between Coagulation and Lysis Parameters Detected by Fourier Transform Mechanical Spectroscopy of Pooled Platelet Free Plasma with Varying Thrombin Concentration.

	$[Thr]$	*Gel Time*	$d_{\mathbf{f}\ GP}$	$FCLT$	$d_{\mathbf{f}\ dGP}$
$[Thr]$	-	**-0.74*** **	**0.72*** **	**-0.84*** **	0.18
Gel Time	**-0.74*** **	-	**-0.51***	**0.59****	**-0.53***
$d_{\mathbf{f}\ GP}$	**0.72*** **	**-0.51***	-	**-0.65****	**0.48***
$FCLT$	**-0.84*** **	**0.59****	**-0.65****	-	-0.07
$d_{\mathbf{f}\ dGP}$	0.18	**-0.53***	**0.48***	-0.07	-

$[Thr]$: thrombin concentration, $d_{\mathrm{f}\ GP}$: fractal dimension during coagulation, $d_{\mathrm{f}\ dGP}$: fractal dimension during lysis.
* p<0.05, ** p<0.01, *** p<0.001

Table 4.9: Average values of Coagulation and Lysis Parameters Detected by Fourier Transform Mechanical Spectroscopy of Pooled Platelet Free Plasma with Varying Thrombin Concentration.

Gel Time (s)	$d_{\mathbf{f}\ GP}$	$FCLT$ (s)	$d_{\mathbf{f}\ dGP}$
-	-	-	1.49 $\pm$0.04

$d_{\mathrm{f}\ GP}$: fractal dimension during gelation, $d_{\mathrm{f}\ dGP}$: fractal dimension during lysis.
Values which were found to be dependent on thrombin concentration are not presented.

At increasing concentrations of thrombin the expected decrease in gel time was detected by FTMS and can be seen in Figure 4.7.

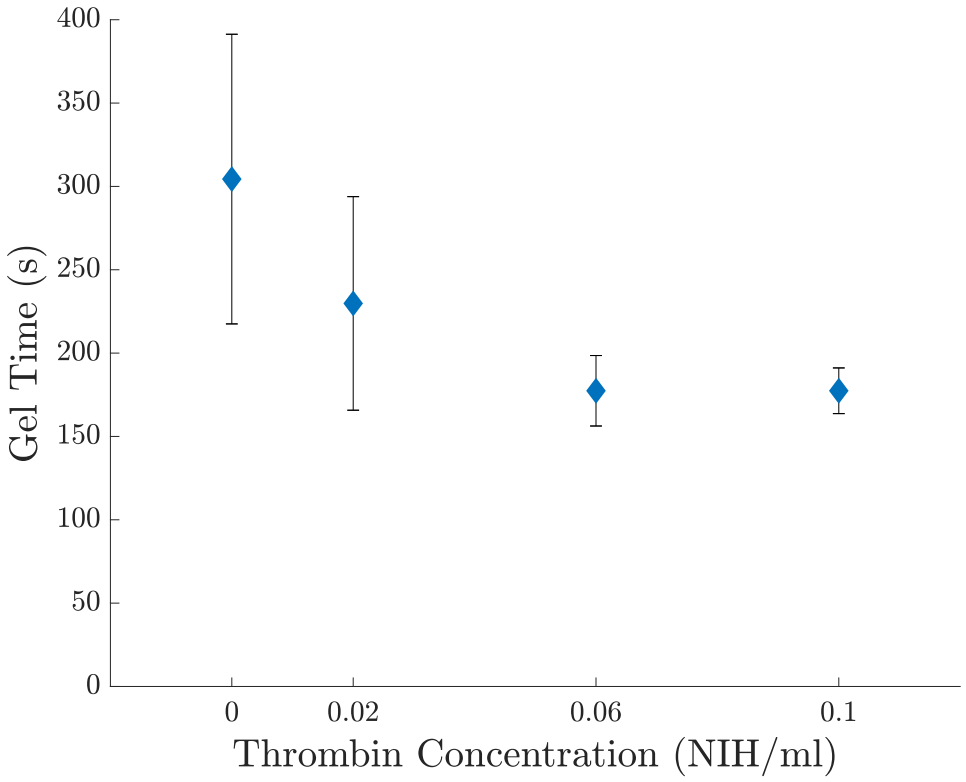

Figure 4.7: A Graph Showing the Relationship Between Gel Time and Thrombin Concentration in Pooled Platelet Free Plasma Detected by Fourier Transform Mechanical Spectroscopy.

Error bars indicate standard deviation (n=5).

From previous studies of the model gelling system fibrin-thrombin, it was further expected that the addition of thrombin would lead to an observed increase in d_f at the gel point as found in Figure 4.8. This theoretically correlates with a decrease in the fibre thickness of mature clots as discussed in Section 3.2.2 along with the reported increase in network complexity. As a result, the addition of thrombin simulates increasingly denser clots which have been previously associated with thrombosis.[105]

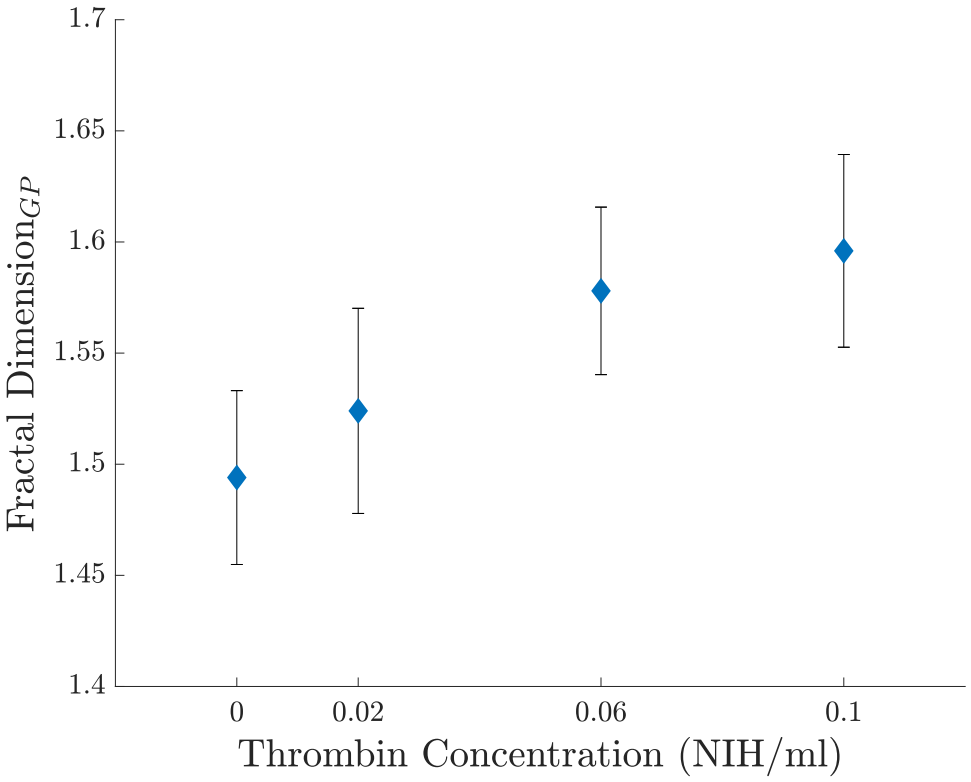

Figure 4.8: A Graph Showing the Relationship Between Fractal Dimension During Coagulation and Thrombin Concentration in Pooled Platelet Free Plasma Detected by Fourier Transform Mechanical Spectroscopy.

Error bars indicate standard deviation (n=5).

Despite the thrombin concentration giving rise to an increase in the complexity of the gel structure, which would be anticipated to result in a prolongation of clot lysis, a decrease in $FCLT$ was observed, depicted in Figure 4.9. This could be attributed to the action of thrombin on PAI-1 removing lysis inhibitors and thereby accelerating the rate of clot breakdown, which may dominate the additional time taken to lyse the differently structured clots. Alternatively, this may show an extension of the work produced by Bannish *et al.* which showed differences in the response to t-PA concentration with differing structure as a result of complex interactions including plasmin crawling.[184] Chapter 5 will examine the influence of clot structure on lysis times without the addition of molecular agents to further investigate this phenomenon.

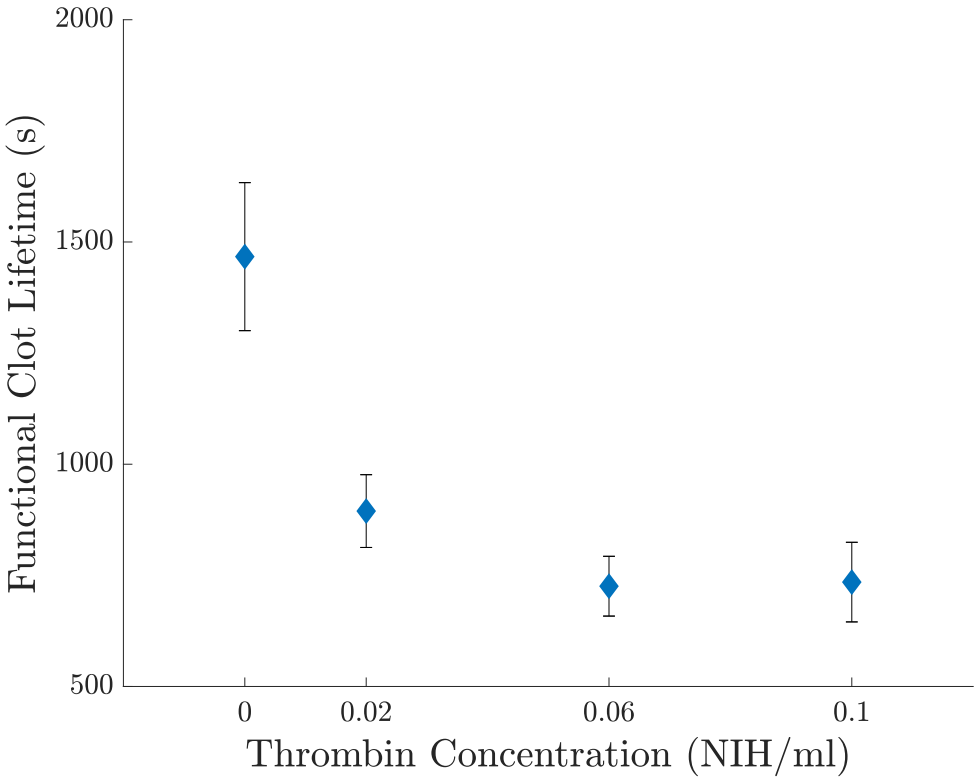

Figure 4.9: A Graph Showing the Relationship Between Functional Clot Lifetime and Thrombin Concentration in Pooled Platelet Free Plasma Detected by Fourier Transform Mechanical Spectroscopy.

Error bars indicate standard deviation (n=5).

Spectrophotometry

The expected decrease in gel time with increasing thrombin concentration was not detected using spectrophotometric techniques, this may be a result of the addition of 0.05 NIH/ml thrombin to spectrophotometric samples. It is possible that the addition of thrombin has masked the technique's sensitivity to variations in thrombin concentration and coagulation parameters. However, a significant influence on LT and OFP was observed as shown in Tables 4.10 and 4.11. Table 4.12 indicates the average values for results which were not found to be dependent on thrombin concentration.

Table 4.10: Probability values for Correlations between Coagulation and Lysis Parameters Detected by Spectrophotometric Overall Haemostatic Potential Assay of Pooled Platelet Free Plasma with Varying Thrombin Concentration.

	$[Thr]$	*Gel Time*	*Lysis Time*	OFP
$[Thr]$	-	0.25	<**0.001**	<**0.001**
Gel Time	0.25	-	0.6	0.49
Lysis Time	<**0.001**	0.6	-	<**0.001**
OFP	<**0.001**	0.49	<**0.001**	-

$[Thr]$: thrombin concentration, OFP: overall fibrinolytic potential.

Table 4.11: Rho values for Correlations between Coagulation and Lysis Parameters Detected by Spectrophotometric Overall Haemostatic Potential Assay of Pooled Platelet Free Plasma with Varying Thrombin Concentration.

	$[Thr]$	*Gel Time*	*Lysis Time*	OFP
$[Thr]$	-	-0.27	**-0.78*** **	**0.80*** **
Gel Time	-0.27	-	0.13	-0.16
Lysis Time	**-0.78*** **	0.13	-	**-0.98*** **
OFP	**0.80*** **	-0.16	**-0.98*** **	-

$[Thr]$: thrombin concentration, OFP: overall fibrinolytic potential.
* p<0.05, ** p<0.01, *** p<0.001

Table 4.12: Average values of Coagulation and Lysis Parameters Detected by Spectrophotometry of Pooled Platelet Free Plasma with Varying Thrombin Concentration.

Gel Time (s)	*Lysis Time (s)*	*OFP*
412 ±78	-	-

OFP: overall fibrinolytic potential.
Values which were found to be dependent on thrombin concentration are not presented.

The influence of thrombin on *LT* and *OFP* are shown in Figures 4.10 and 4.11 respectively. While they appear to be sensitive to additional thrombin concentrations above 0.06 NIH/ml, they do not appear able to detect small (0.02 NIH/ml) variations in thrombin concentration that were detected by FTMS. In addition, the change in *OFP* is small in comparison to other test types. This highlights a possible limitation of the technique as small fluctuations in thrombin concentration can significantly impact clot structure, as demonstrated by the FTMS results.

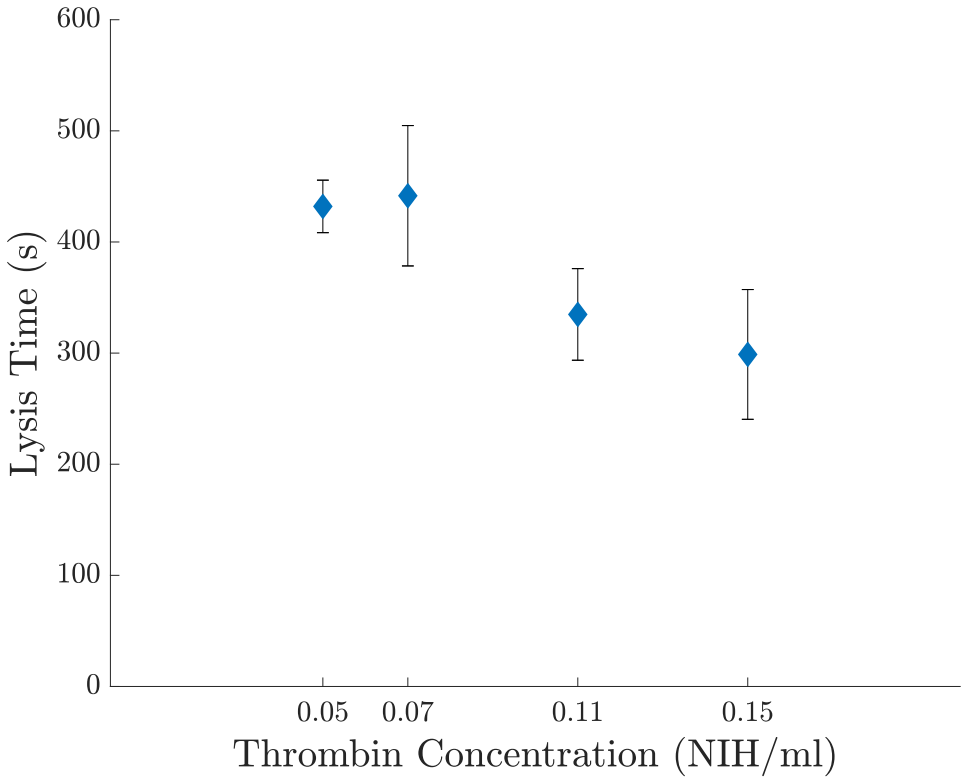

Figure 4.10: A Graph Showing the Relationship Between Lysis Time and Thrombin Concentration in Pooled Platelet Free Plasma Detected by Spectrophotometry.

Error bars indicate standard deviation (n=5).

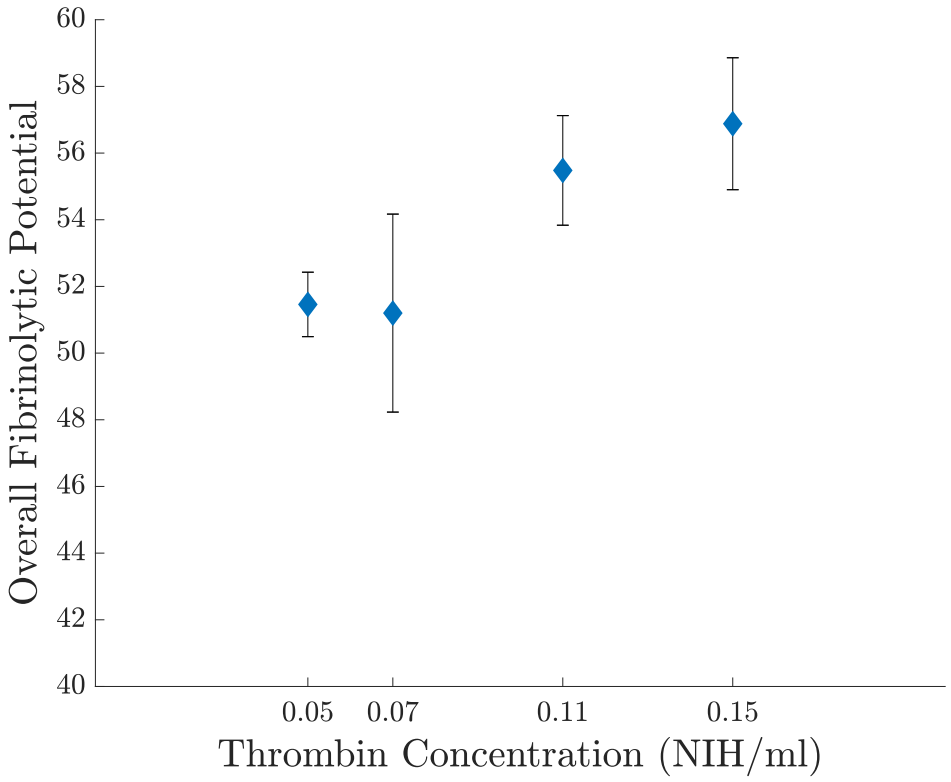

Figure 4.11: A Graph Showing the Relationship Between Overall Fibrinolytic Potential and Thrombin Concentration in Pooled Platelet Free Plasma Detected by Spectrophotometry.

Error bars indicate standard deviation (n=5).

Since peak thrombin generation and coagulation time are significant indicators of poor clinical outcomes, FTMS, which was shown to be sensitive to changes in thrombin concentration, may prove more valuable as a diagnostic tool than spectrophotometric tests in this respect.[181]

4.2.3 Effect of Streptokinase on Clot Formation and Lysis

Rheology

Streptokinase is an alternative thrombolytic therapy approved for the treatment of thrombosis. However, its use is contraindicated in the case of ischemic stroke due to the risk of adverse effects. Detection of coagulation and lysis of P-PFP with increasing concentrations of streptokinase by FTMS revealed significant changes in GT, $FCLT$ and $d_{\mathrm{f}\ dGP}$ as shown in Tables 4.13 and 4.14. Table 4.15 indicates the average values for results which were not found to be dependent on streptokinase concentration.

Table 4.13: Probability values for Correlations between Coagulation and Lysis Parameters Detected by Fourier Transform Mechanical Spectroscopy of Pooled Platelet Free Plasma with Varying Streptokinase Concentration.

	$[Strep]$	*Gel Time*	$d_{\mathbf{f}\ GP}$	$FCLT$	$d_{\mathbf{f}\ dGP}$
$[Strep]$	-	**0.02**	0.14	**<0.001**	**<0.01**
Gel Time	**0.02**	-	0.25	**0.04**	0.22
$d_{\mathbf{f}\ GP}$	0.14	0.25	-	0.06	**0.02**
$FCLT$	**<0.001**	**0.04**	0.06	-	**<0.01**
$d_{\mathbf{f}\ dGP}$	**<0.001**	0.22	**0.02**	**<0.01**	-

$[Strep]$: streptokinase concentration, $d_{\mathrm{f}\ GP}$: fractal dimension during coagulation, $d_{\mathrm{f}\ dGP}$: fractal dimension during lysis.

Table 4.14: Rho values for Correlations between Coagulation and Lysis Parameters Detected by Fourier Transform Mechanical Spectroscopy of Pooled Platelet Free Plasma with Varying Streptokinase Concentration.

	[Strep]	*Gel Time*	$d_{\mathbf{f}\ GP}$	*FCLT*	$d_{\mathbf{f}\ dGP}$
[Strep]	-	**-0.62***	0.42	**-0.94*****	**0.75****
Gel Time	**-0.61***	-	-0.33	**0.55***	-0.35
$d_{\mathbf{f}\ GP}$	0.42	-0.33	-	-0.51	**0.62***
FCLT	**-0.94*****	**00.55***	-0.51	-	**-0.76****
$d_{\mathbf{f}\ dGP}$	**0.75*****	-0.35	**0.62***	**-0.76****	-

[Strep]: streptokinase concentration, $d_{\mathrm{f}\ GP}$: fractal dimension during coagulation, $d_{\mathrm{f}\ dGP}$: fractal dimension during lysis.
* p<0.05, ** p<0.01, *** p<0.001

Table 4.15: Average values of Coagulation and Lysis Parameters Detected by Fourier Transform Mechanical Spectroscopy of Pooled Platelet Free Plasma with Varying Streptokinase Concentration.

Gel Time (s)	$d_{\mathbf{f}\ GP}$	*FCLT (s)*	$d_{\mathbf{f}\ dGP}$
-	1.55 ±0.05	-	-

$d_{\mathrm{f}\ GP}$: fractal dimension during gelation, $d_{\mathrm{f}\ dGP}$: fractal dimension during lysis.
Values which were found to be dependent on thrombin concentration are not presented.

A statistically significant decrease in *GT* was detected by FTMS, as shown in Figure 4.12. This relationship indicates that streptokinase has a significant impact on the coagulation system as well as the fibrinolytic system.

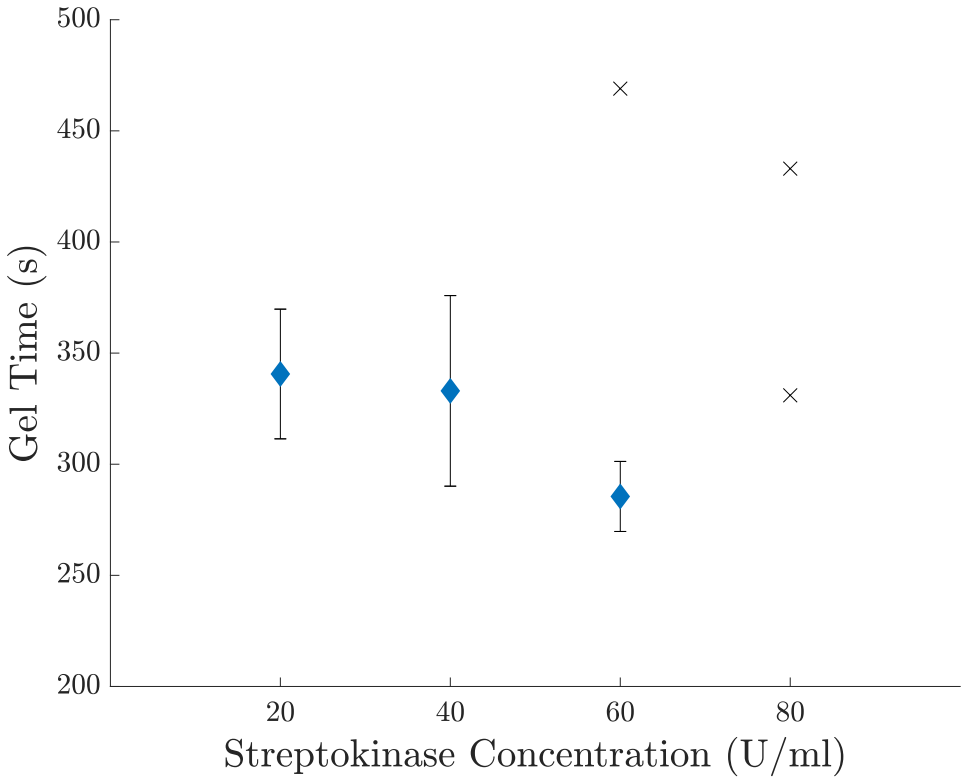

Figure 4.12: A Graph Showing the Relationship Between Gel Time and Streptokinase Concentration in Pooled Platelet Free Plasma Detected by Fourier Transform Mechanical Spectroscopy.

Error bars indicate standard deviation (n=5).

x indicates individual replicates that were excluded from statistical analysis.

No statistically significant trend in $d_{f\ GP}$ was detected with changing streptokinase concentration. However, when viewing the data graphically and taking into account the results which were excluded from statistical analysis during this study, shown in Figure 4.13, future investigation which includes detection at the higher streptokinase concentrations may reveal a subtle relationship.

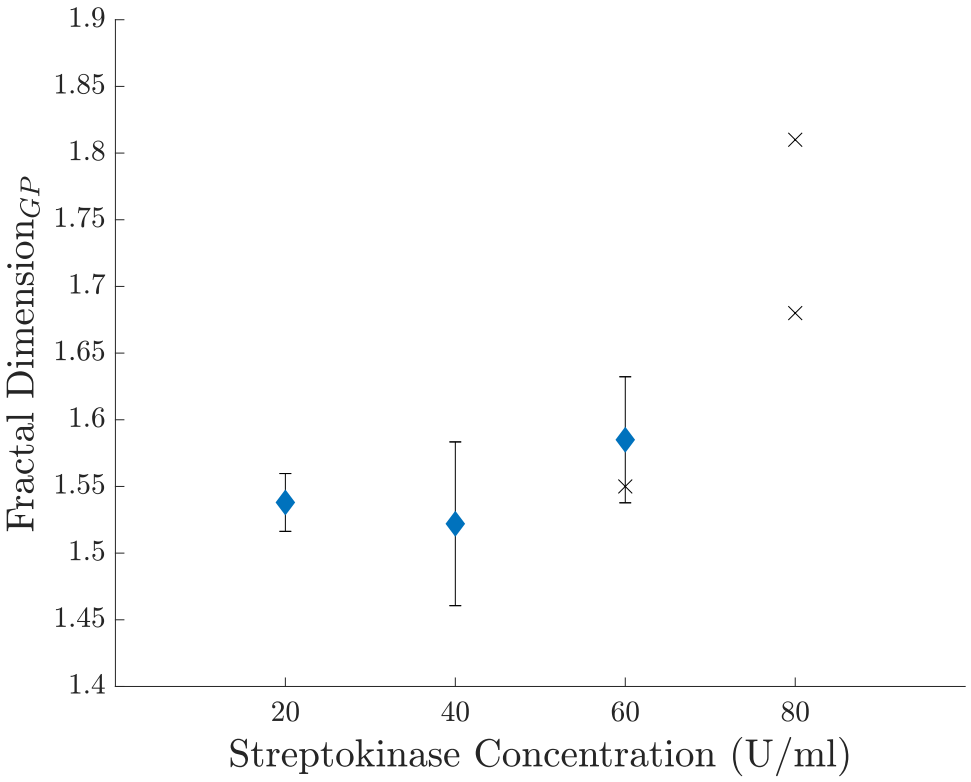

Figure 4.13: A Graph Showing the Relationship Between Fractal Dimension during Coagulation and Streptokinase Concentration in Pooled Platelet Free Plasma Detected by Fourier Transform Mechanical Spectroscopy.

Error bars indicate standard deviation (n=5).
x indicates individual replicates that were excluded from statistical analysis.

The concentration of streptokinase, as expected, influenced the functional clot lifetime as detected by FTMS and shown in Figure 4.14, but also led to an increase in $d_{\mathrm{f}\ dGP}$ during clot lysis as shown in Figure 4.15. This change in $d_{\mathrm{f}\ dGP}$ can be associated with a higher level of structural complexity in the last stable structure of the clot. This indicates that the action of high concentrations of streptokinase rapidly breaks down the clot to the point at which it no longer resists flow as a viscoelastic solid; however, there are still substantial fragments of fibrin network at this point.

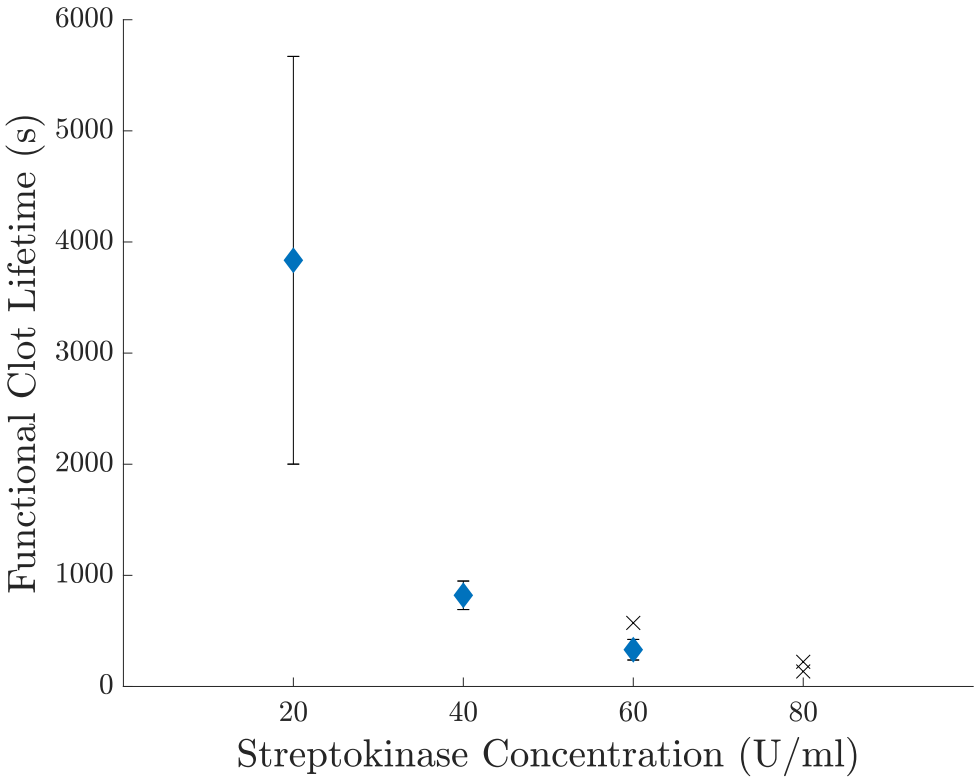

Figure 4.14: Graph Showing the Relationship Between Functional Clot Lifetime and Streptokinase Concentration in Pooled Platelet Free Plasma Detected by Fourier Transform Mechanical Spectroscopy.

Error bars indicate standard deviation (n=5).

x indicates individual replicates that were excluded from statistical analysis.

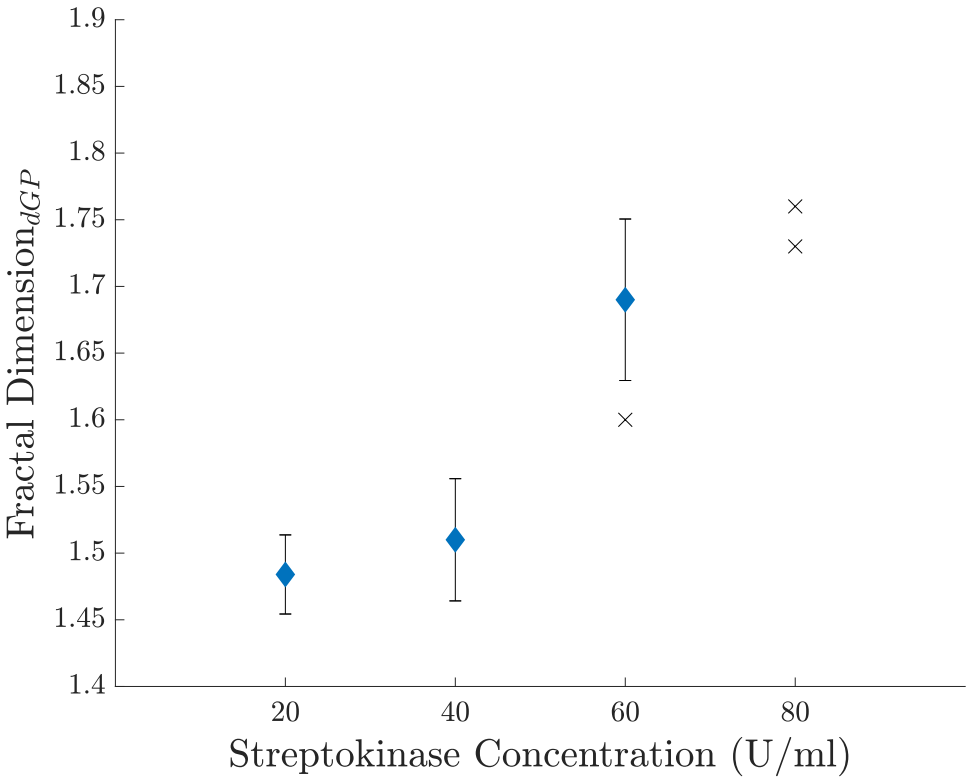

Figure 4.15: A Graph Showing the Relationship Between Fractal Dimension during Clot Lysis and Streptokinase Concentration in Pooled Platelet Free Plasma Detected by Fourier Transform Mechanical Spectroscopy.

Error bars indicate standard deviation (n=5).
x indicates individual replicates that were excluded from statistical analysis.

This study has found that in P-PFP the action of streptokinase directly affects the process of coagulation, as well as inducing inefficient breakdown of thrombi into large, complex network fragments. This is consistent with the mechanism of haemorrhage identified by the literature.[180] Since there are few techniques capable of detecting and quantifying clot structure during lysis, due to the rapidity of breakdown, the detection of this phenomenon by FTMS points to an application for this type of testing in the drug development process.

Spectrophotometry

In the assessment of streptokinase induced clot lysis through spectrophotometry a significant influence on LT and OFP was observed as shown in Tables 4.16 and 4.17. Table 4.18 indicates the average values for results which were not found to be dependent on streptokinase concentration.

Table 4.16: Probability values for Correlations between Coagulation and Lysis Parameters Detected by Spectrophotometric Overall Haemostatic Potential Assay of Pooled Platelet Free Plasma with Varying Streptokinase Concentration.

	[Strep]	*Gel Time*	*Lysis Time*	*OFP*
[Strep]	-	0.60	<**0.001**	<**0.001**
Gel Time	0.60	-	0.31	0.48
Lysis Time	<**0.001**	0.31	-	<**0.001**
OFP	<**0.001**	0.48	<**0.001**	-

[Strep]: streptokinase concentration, OFP: overall fibrinolytic potential.

Table 4.17: Rho values for Correlations between Coagulation and Lysis Parameters Detected by Spectrophotometric Overall Haemostatic Potential Assay of Pooled Platelet Free Plasma with Varying Streptokinase Concentration.

	[Strep]	*Gel Time*	*Lysis Time*	*OFP*
[Strep]	-	-0.13	**-0.94*** **	**0.97*** **
Gel Time	-0.13	-	0.35	-0.17
Lysis Time	**-0.94*** **	0.24	-	**-0.97*** **
OFP	**0.97*** **	-0.17	**-0.97*** **	-

[Strep]: streptokinase concentration, OFP: overall fibrinolytic potential.
* p<0.05, ** p<0.01, *** p<0.001

Table 4.18: Average values of Coagulation and Lysis Parameters Detected by Spectrophotometry of Pooled Platelet Free Plasma with Varying Streptokinase Concentration.

Gel Time (s)	*Lysis Time (s)*	*OFP*
620 ±144	-	-

OFP: overall fibrinolytic potential.
Values which were found to be dependent on streptokinase concentration are not presented.

Despite changes in coagulation being detected by FTMS, no influence on the clotting time was observed during spectrophotometric analysis. Increasing concentrations of streptokinase led to a decrease in LT and increase in OFP as shown in Figures 4.16 and 4.17 respectively. Since the data collected by spectrophotometry does not give an indication of the clot structure it cannot be related to the adverse outcomes in stroke patients in the same way as the FTMS data.

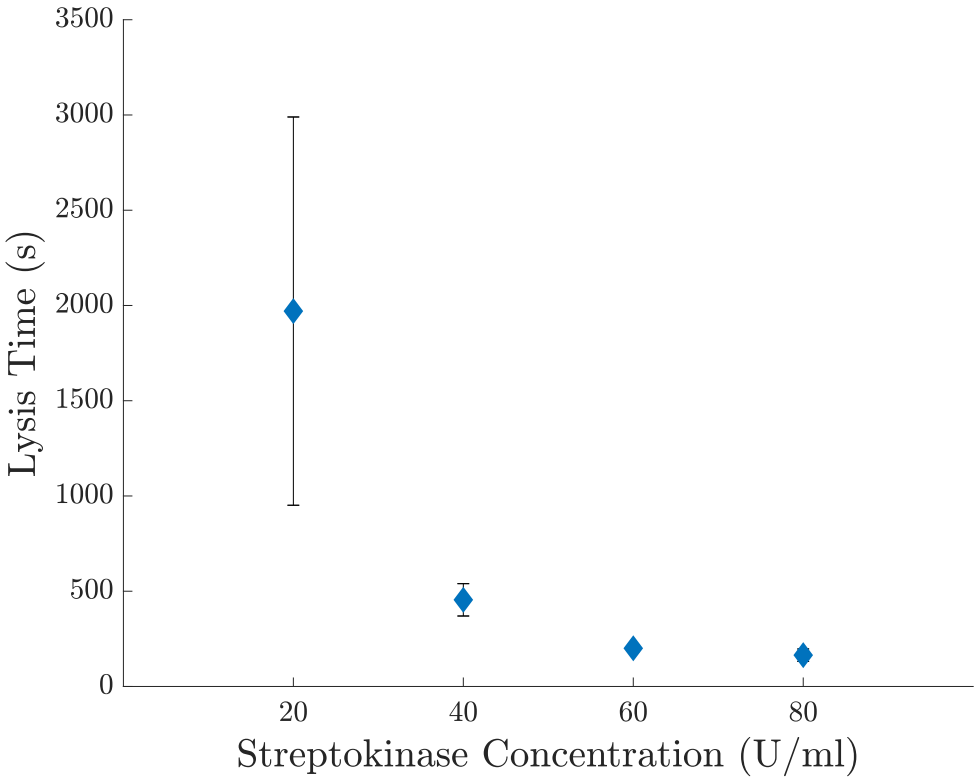

Figure 4.16: A Graph Showing the Relationship Between Lysis Time and Streptokinase Concentration in Pooled Platelet Free Plasma Detected by Spectrophotometry.

Error bars indicate standard deviation (n=5).

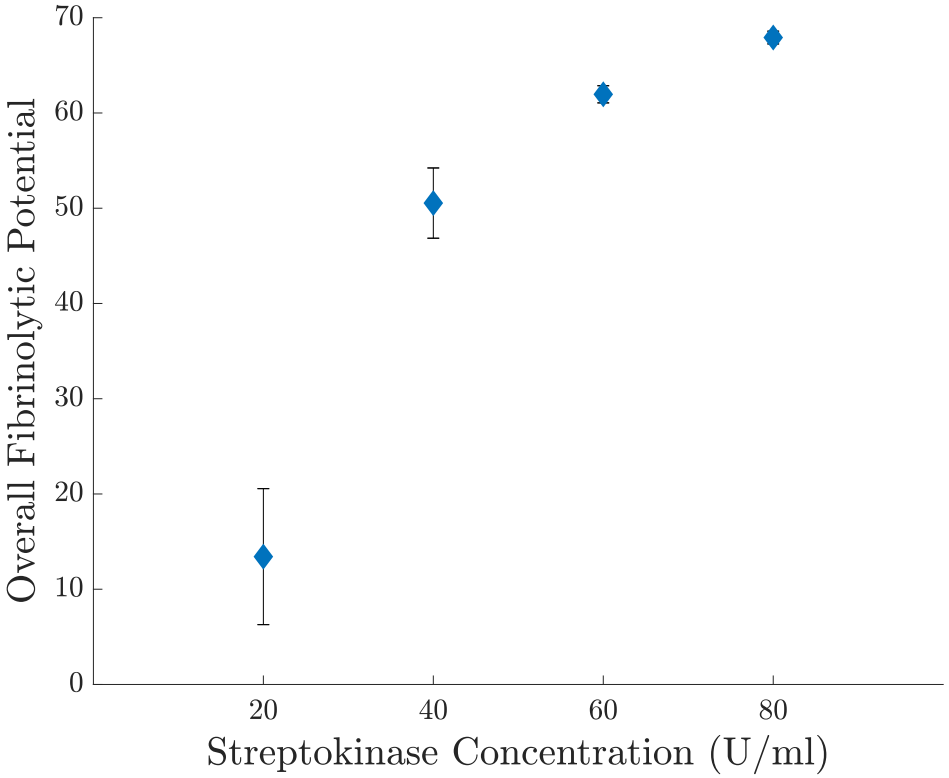

Figure 4.17: A Graph Showing the Relationship Between Overall Fibrinolytic Potential and Streptokinase Concentration in Pooled Platelet Free Plasma Detected by Spectrophotometry.

Error bars indicate standard deviation (n=5).

4.2.4 Relationships Between Rheological Parameters

The FTMS results from all of the previous experiments were grouped together in order to determine whether any inherent links between the rheological parameters exist and is shown in Tables 4.19 and 4.20.

Table 4.19: Probability values for Correlations between Coagulation and Lysis Parameters Detected by Fourier Transform Mechanical Spectroscopy of Pooled Platelet Free Plasma.

	Gel Time	$d_{\mathbf{f}\ GP}$	*FCLT*	$d_{\mathbf{f}\ dGP}$
Gel Time	-	**<0.001**	**<0.001**	**0.02**
$d_{\mathbf{f}\ GP}$	**<0.001**	-	**<0.001**	**<0.01**
FCLT	**<0.001**	**<0.001**	-	**<0.001**
$d_{\mathbf{f}\ dGP}$	**0.02**	**<0.01**	**<0.001**	-

$d_{\mathrm{f}\ GP}$: fractal dimension during coagulation,
$d_{\mathrm{f}\ dGP}$: fractal dimension during lysis.

Table 4.20: Rho values for Correlations between Coagulation and Lysis Parameters Detected by Fourier Transform Mechanical Spectroscopy of Pooled Platelet Free Plasma.

	Gel Time	$d_{\mathbf{f}\ GP}$	*FCLT*	$d_{\mathbf{f}\ dGP}$
Gel Time	-	**-0.47*** **	**0.48*** **	**-0.29***
$d_{\mathbf{f}\ GP}$	**-0.47*** **	-	**-0.53*** **	**0.34****
FCLT	**0.48*** **	**-0.53*** **	-	**-0.46*** **
$d_{\mathbf{f}\ dGP}$	**-0.29***	**0.34****	**-0.46*** **	-

$d_{\mathrm{f}\ GP}$: fractal dimension during coagulation,
$d_{\mathrm{f}\ dGP}$: fractal dimension during lysis.
* p<0.05, ** p<0.01, *** p<0.001

This analysis revealed weak relationships between the parameters, broadly indicating that prothrombotic clots having higher $d_{f\ GP}$ values tend to both form faster, and lyse faster, breaking down into more structurally complex fragments as shown in Figure 4.18. However, stepwise regression analysis revealed that gel point parameters (GT and $d_{f\ GP}$) were not useful in predicting either $FCLT$ (R^2=0.15) or $d_{f\ dGP}$ (R^2=0.14).

Figure 4.18a shows the relationship between $d_{f\ GP}$ and GT which has a statistically significant correlation (p<0.001, rho=-0.47); however, linear regression shows a poor fit indicating that the general relationship has little value as a predictive marker. This suggests that although there is a relationship between coagulation time and the structural properties of the clot, measurement of the coagulation time alone cannot predict thrombosis risk which gives the rheological biomarker a distinct advantage over conventional assays. Figure 4.18b gives the relationship between $d_{f\ GP}$ and $FCLT$, which while statistically significant (p<0.001, rho=-0.53) again shows poor correlation and the value of $d_{f\ GP}$ is not a predictor of $FCLT$. The statistically significant relationship identified between GT and $FCLT$ (p<0.001, rho=-0.48) shows a general tendency for clots which take more time to form to also require longer to breakdown, shown in Figure 4.18c; however, this relationship does not have a predictive value, and may be subject to secondary interactions of thrombin which was used to manipulate GT in these experiments.

Figure 4.18d shows the relationship between $d_{f\ dGP}$ and $FCLT$ which although statistically significant (p<0.001, rho=-0.46) indicating a broad tendandcy for clots which take longer to breakdown to exhibit a lower structural complexity and so more complete breakdown, has an R^2=0.11 and so is not predictive. The relationship between GT and $d_{f\ GP}$ is given by 4.18e and indicates a general trend for gels which take longer to form breaking down into less complex structures (p=0.02, rho=-0.29); however, this trend is weak. The relationship between $d_{f\ GP}$ and $d_{f\ dGP}$, shown in 4.18f, indicates a weak positive relationship between the parameters (p<0.01, rho=0.34). When viewing the data in the context of equality it can be seen that there is a general tendancy for $d_{f\ dGP}$ to be lower than $d_{f\ GP}$ with the majority of values falling below the line of equality. This is indicative of the last stable structure of a clot being less complex than the first stable structure.

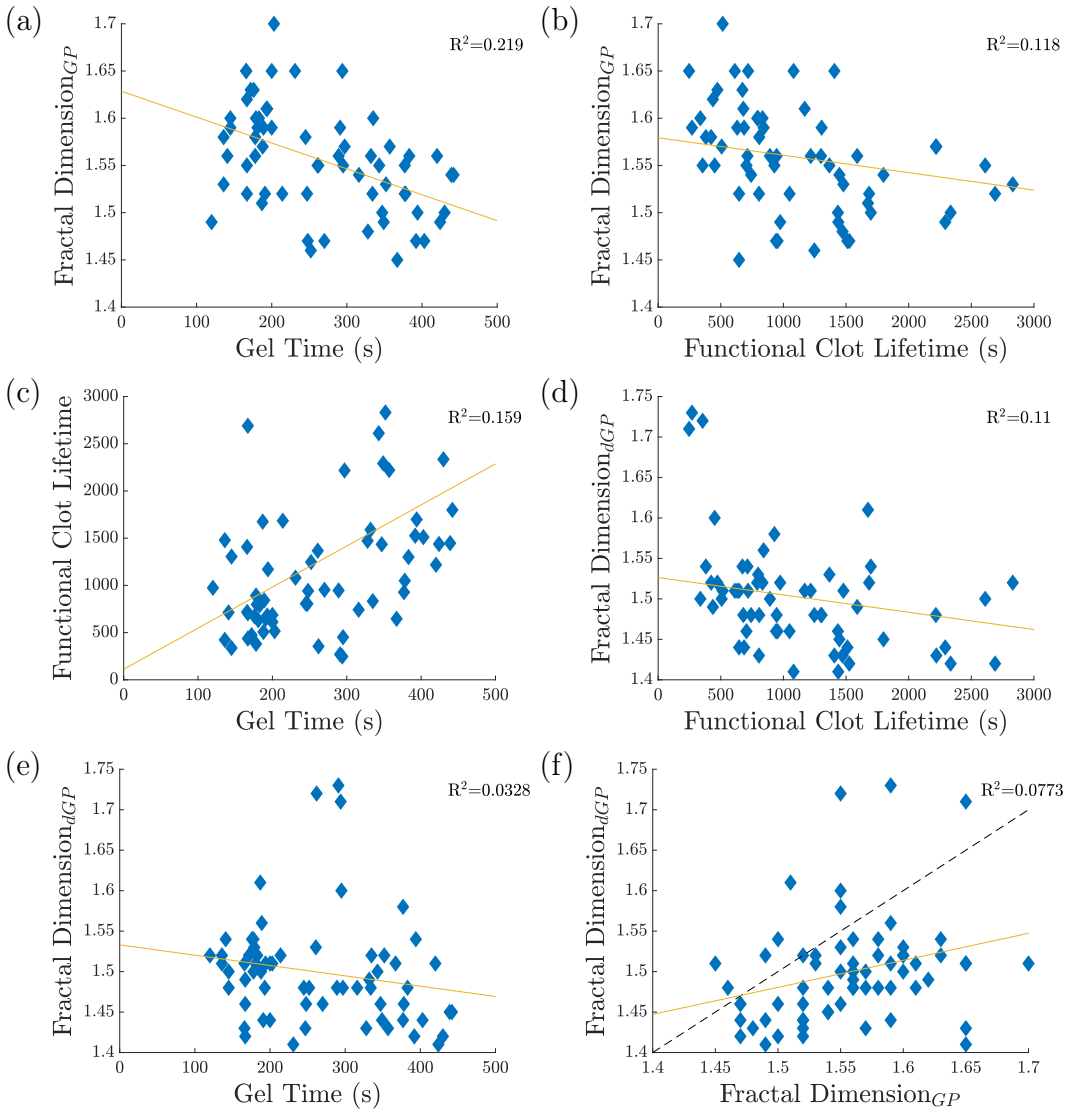

Figure 4.18: Graphs Showing the Relationships Between Rheological Parameters during Coagulation and Lysis in Pooled Platelet Free Plasma Detected by Fourier Transform Mechanical Spectroscopy.

Relationships between (a) gel time and the fractal dimension during coagulation, (b) functional clot lifetime and the fractal dimension during coagulation, (c) gel time and functional clot lifetime, (d) functional clot lifetime and the fractal dimension during lysis, (e) gel time and the fractal dimension during lysis, and (f) the fractal dimension during coagulation and the fractal dimension during lysis.
Line of equality (dashed).

Since increases in clot density have been related to prolonged lysis,[51,76] the finding that high values of $d_{\mathrm{f}\ GP}$ correlate with faster lysis times may be an artefact resulting from the use of thrombin in generating structurally dense clots, which warrants further investigation. Results in Figures 4.6 and 4.9 show that the addition of thrombin not only reduces the $FCLT$, but also influences the minimum lysis time of plasma clots when lysis is triggered by rt-PA. This minimum lysis time was not detected using the lytic agent streptokinase, as seen in Figure 4.14, suggesting that it does not relate to the action of other lytic components such as plasmin. It is therefore possible that an interaction between thrombin and rt-PA, most likely through the intermediary PAI-1, influences the results. Further to this, it is known that the incorporation of rt-PA into the clot during formation shields it from inhibition by PAI-1. In light of this, the minimum lysis time in the absence of thrombin may represent the maximum amount of rt-PA that is incorporated into the fibrin network, and therefore protected from the action of PAI-1.

PAI-1 is known to contribute to the variance in clot lysis times between individuals and significantly contributes to fibrinolysis resistance in thrombosis.[190,191] This work provides some evidence that the contribution of PAI-1 to clot lysis supersedes the contribution from structural density, but is missed by current spectrophotometric assays which rely on the addition of thrombin. Further investigation into the use of PAI-1 inhibitors is required to confirm this.

Examination of the values of d_{f} in relation to the line of equality shown in Figure 4.18 (f) indicates that in general the last stable structure of a blood clot is less dense than the initial structure formed during coagulation. This translates to a greater potential for clot dissolution.

Further examination of the relationship between $d_{\mathrm{f}\ GP}$ and $d_{\mathrm{f}\ dGP}$ shown in Figure 4.19 shows that in the majority of cases $d_{\mathrm{f}\ dGP}$ is lower than or close to the value of $d_{\mathrm{f}\ GP}$ with the exception of high doses of rt-PA and streptokinase. It is therefore possible that the haemorrhagic side effects associated with the administration of these therapies could be predicted from rheological data.

In healthy volunteers, $d_{f\ GP}$ of healthy pooled plasma represents a stable structure. Increased values of $d_{f\ dGP}$ compared to $d_{f\ GP}$ translate to the presence of more fibrin mass at the point of lysis compared to the incipient clot. Since this is the point at which the sample is able to flow, this difference in structure in healthy P-PFP may prove to be a marker of haemorrhagic and re-occlusion risk, which is independent of individual patient factors. This method of evaluation may therefore prove useful in evaluating the safety of thrombolytic therapies in the pre-clinical phase of drug development.

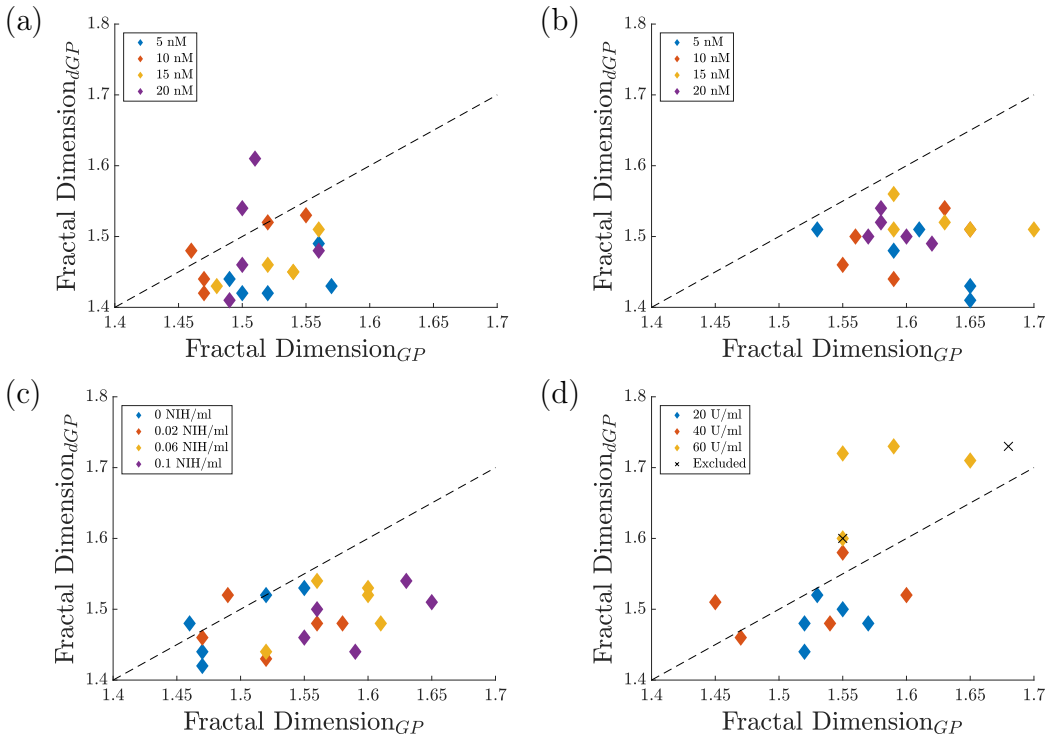

Figure 4.19: Graphs Showing the Relationship Between Fractal Dimension during Lysis and Coagulation in Pooled Platelet Free Plasma as Detected by Fourier Transform Mechanical Spectroscopy.

(a) Increasing concentrations of recombinant tissue plasminogen activator, (b) increasing concentrations of recombinant tissue plasminogen activator with the addition of 0.1 NIH/ml thrombin, (c) increasing concentrations of thrombin with 10 nM recombinant tissue plasminogen activator, (d) increasing concentrations of streptokinase. Line of equality (dashed).
x indicates results excluded from statistical analysis.

In a clinical context the results obtained for FTMS measurement of plasma as compared to the current spectrophotometric technique suggest that the novel biomarker is able to detect the presence of a therapeutic concentration of rt-PA, but is unable to distinguish between different doses of the agent. This

finding could, after further investigation, present a method for determining the optimum dose of thrombolytic for an individual. The FTMS technique is able to detect differing levels of streptokinase and, by presenting a measurement of clot structure during lysis, could have application in developing safe therapeutics.

4.2.5 Detection in Whole Blood

Following the investigation of individual factors using the pooled P-PFP model, the use of gel point and de-gel point detection was further investigated using whole blood. This was obtained from individual donors and combined with a fixed concentration of rt-PA (5 nM), which was below the threshold identified in Figure 4.6, and varying concentrations of streptokinase. The results of correlation analysis are given in Tables 4.21 and 4.22. Table 4.23 indicates the average values for results which were not found to be dependent on streptokinase concentration.

Table 4.21: Probability values for Correlations between Coagulation and Lysis Parameters Detected by Rheometry of Whole Blood with a Fixed Concentration of Recombinant Tissue Plasminogen Activator and Varying Streptokinase Concentration.

	$[Strep]$	*Gel Time*	$d_{\mathbf{f}\ GP}$	$FCLT$	$d_{\mathbf{f}\ dGP}$
$[Strep]$	-	0.27	0.68	**<0.001**	0.75
Gel Time	0.27	-	0.07	0.24	0.07
$d_{\mathbf{f}\ GP}$	0.67	0.07	-	0.18	**<0.001**
$FCLT$	**<0.001**	0.24	0.18	-	0.74
$d_{\mathbf{f}\ dGP}$	0.75	0.07	**<0.001**	0.74	-

$[Strep]$: streptokinase concentration, $d_{\mathrm{f}\ GP}$: fractal dimension during coagulation, $d_{\mathrm{f}\ dGP}$: fractal dimension during lysis

Table 4.22: Rho values for Correlations between Coagulation and Lysis Parameters Detected by Rheometry of Whole Blood with a Fixed Concentration of Recombinant Tissue Plasminogen Activator and Varying Streptokinase Concentration.

	[Strep]	*Gel Time*	$d_{\mathbf{f}\ GP}$	*FCLT*	$d_{\mathbf{f}\ dGP}$
[Strep]	-	-0.19	0.07	**-0.74*** **	0.06
Gel Time	-0.19	-	0.31	0.2	0.31
$d_{\mathbf{f}\ GP}$	0.07	0.31	-	-0.23	**0.63*** **
FCLT	**-0.74*** **	0.2	-0.23	-	0.06
$d_{\mathbf{f}\ dGP}$	0.06	0.31	**0.63*** **	0.06	-

[Strep]: streptokinase concentration, $d_{\mathrm{f}\ GP}$: fractal dimension during coagulation, $d_{\mathrm{f}\ dGP}$: fractal dimension during lysis.
* p<0.05, ** p<0.01, *** p<0.001

Table 4.23: Average values of Coagulation and Lysis Parameters Detected by Spectrophotometry of Pooled Platelet Free Plasma with Varying Streptokinase Concentration.

Gel Time (s)	$d_{\mathbf{f}\ GP}$	*FCLT (s)*	$d_{\mathbf{f}\ dGP}$
240 ±86	1.79 ±0.08	-	1.74 ±0.10

$d_{\mathrm{f}\ GP}$: fractal dimension during gelation, $d_{\mathrm{f}\ dGP}$: fractal dimension during lysis. Values which were found to be dependent on streptokinase concentration are not presented.

A significant decrease in *FCLT* as a result of increasing streptokinase concentration was found and is shown in Figure 4.20. This provides evidence that the rheological measurement of the *FCLT* is a predictor of Streptokinase therapeutic intervention. However, the relationships between streptokinase concentration and both gel time and $d_{\mathrm{f}\ dGP}$ detected in P-PFP, that were identified in Section 4.2.3, were not found in this system. This suggests that either the presence of blood cells, or the biological variation resulting from the use of individual donors, may dominate the response of the coagulation and structural parameters to streptokinase.

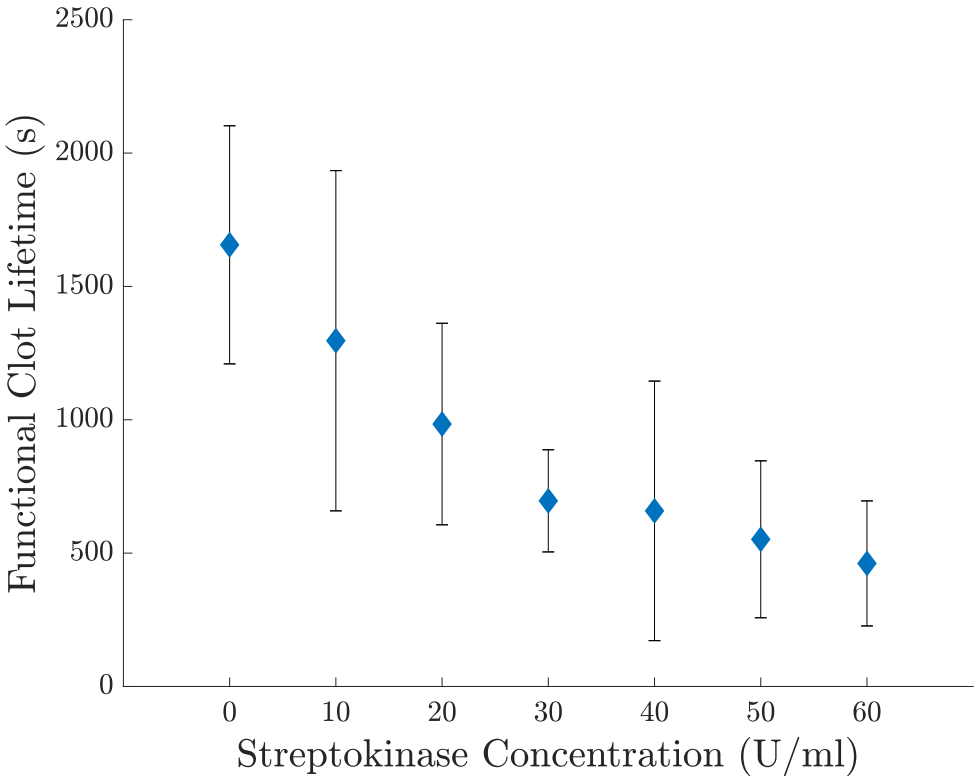

Figure 4.20: Graph Showing the Relationship Between Functional Clot Lifetime and Streptokinase Concentration in Whole Blood Detected by Rheometry.

Error bars indicate standard deviation (n=5).

In contrast to the P-PFP system, which acts as a standard material, evaluation of the relationships between rheological parameters for individual whole blood samples only revealed a relationship between $d_{\mathrm{f}\ GP}$ and $d_{\mathrm{f}\ dGP}$ which is shown in Figure 4.21. This suggests that the efficacy of breakdown is related to the structural characteristics of the blood clot, which indicates that structurally denser clots are indeed more resistant to lysis, breaking down into more complex fragments than their porous counterparts.

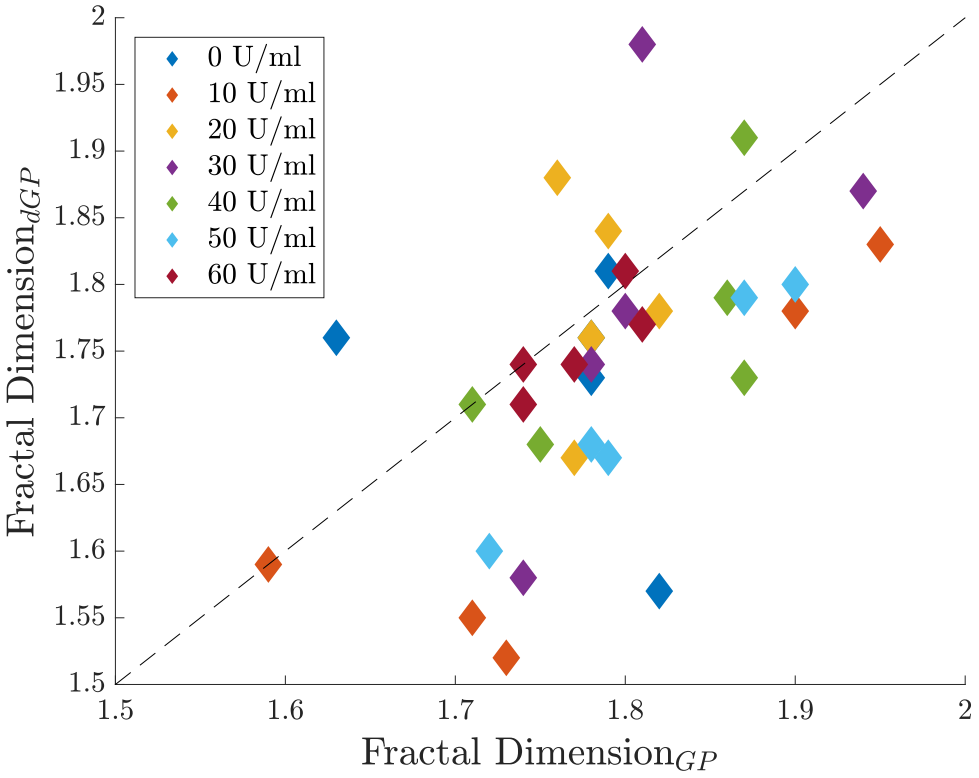

Figure 4.21: Graph Showing the Relationship Between the Fractal Dimension during Lysis and Coagulation of Whole Blood with Varying Streptokinase Concentration as Detected by Rheometry.

Line of equality (dashed)

4.3 Conclusions

Therapeutic thrombolysis is a key intervention in the treatment of thrombosis; however, recombinant tissue plasminogen activator (rt-PA) is the only thrombolytic therapy currently licensed for use in acute ischemic stroke. As with most treatment options for this condition there are significant risks involved. Of particular concern is the risk of haemorrhagic transformation, along with poor clinical outcomes following recovery where many patients remain dependent at discharge. Therefore, there is a need for improved monitoring of thrombolytic therapy.

The use of Fourier transform mechanical spectroscopy (FTMS) in monitoring clot breakdown was investigated through the assessment of pooled platelet free plasma (P-PFP) and compared to current spectrophotometric assays. The results showed that FTMS was able to detect the lytic ability of rt-PA; however, it was not able to detect changes during coagulation that were identified using standard assays and had been previously identified in patients during clinical intervention. Despite this, FTMS was shown to be superior to the existing overall haemostasis potential assay in several ways. It was found that the addition of thrombin to the standard assays may inhibit the action of plasminogen activator inhibitor (PAI-1), and renders the technique less sensitive to small variations in thrombin concentration. Thrombin concentration was found to significantly influence clot microstructure as well as the lytic response in FTMS measurements and so represents a significant factor in clot behaviour. The addition of thrombin was found to alter the relationship between functional clot lifetime and rt-PA concentration which merits further investigation, as it may have an impact on clinical decisions when assessing fibrinolysis through conventional assays.

Further to this, assessment of an alternative thrombolytic, streptokinase, revealed that the FTMS procedure was able to detect the rapid, but inefficient, breakdown of blood clots at high concentration, giving results that correspond well to the proposed mechanism of increased haemorrhagic side effects for this therapy. This highlights a further potential application for FTMS in the drug discovery and development process, as there are few techniques that would be capable of detecting and quantifying this phenomenon.

Evaluation of the links between rheological parameters showed that simulated prothrombotic clots were broken down more rapidly, but less efficiently than their healthy counterparts. However, the use of thrombin to simulate this may have influenced the results, since in these samples PAI-1 could also have been inhibited and may have dominated the response of the biomarker.

Finally, in the study of whole blood systems fewer relationships between parameters were identified. This suggests that the presence of blood cells, and the individual clot structures and drug sensitivities of each person, play a significant role in determining the response to thrombolytic therapy. Despite this, increasing concentrations of thrombolytic agent were still associated with shorter functional clot lifetimes. In the whole blood samples, which behave in a way closer to a physiological system, the efficacy of the breakdown was determined primarily by the original clot structure, which again provides evidence for the potential role for FTMS in assessing suitability for and monitoring of thrombolytic therapy.

Chapter 5

The Effects of Shear Induced Modification of Clot Microstructure on Coagulation and Lysis

The results obtained in Chapter 4 showed that despite increased concentrations of thrombin leading to an increased fractal dimension (d_f) in samples of P-PFP, fibrinolysis was enhanced. Examination of the relationships between clot structure and clot lysis were complicated by the potential role of thrombin in promoting lysis, which may have counteracted the effects of clot structure alone. The work presented in this chapter will examine the effect of clot structure on lysis while avoiding the addition of exogenous thrombin, through the use of controlled stress parallel superposition (CSPS) rheometry. In CSPS rheometry, a unidirectional shear stress field is superimposed on a small amplitude oscillatory shear waveform. It has been previously shown that the d_f derived from CSPS measurements of incipient clots, formed in both whole blood and fibrin-thrombin gels, increases with increasing unidirectional shear.[147] Therefore, CSPS provides an ideal tool for the manipulation of clot microstructure, without the need for varying factors such as thrombin concentration, and permits an alternative method to explore any associations between clot microstructure and clot lysis. This method is also more physiologically relevant, in so far that shear stress plays a key role in the pathophysiology of thrombosis *e.g.* high blood pressure and stenotic vessels are known to contribute to thrombosis risk as discussed in Section 1.1.

The impact of an external shear field on the resulting clot structure has been previously investigated, with results showing that shear rates in the region of 20 s^{-1} lead to marked alterations in clot microstructure, including fibre orientation in the direction of flow.[192–194] There is evidence showing that increasing flow rates lead to an increase in the thickness of individual fibres, as well as the bundling of fibres. Under high flow rates, clots appear to consist of thick bundles of fibres oriented in the direction of flow, interconnected by thinner fibres perpendicular to the direction of flow as illustrated in Figure 5.1.[193,194]

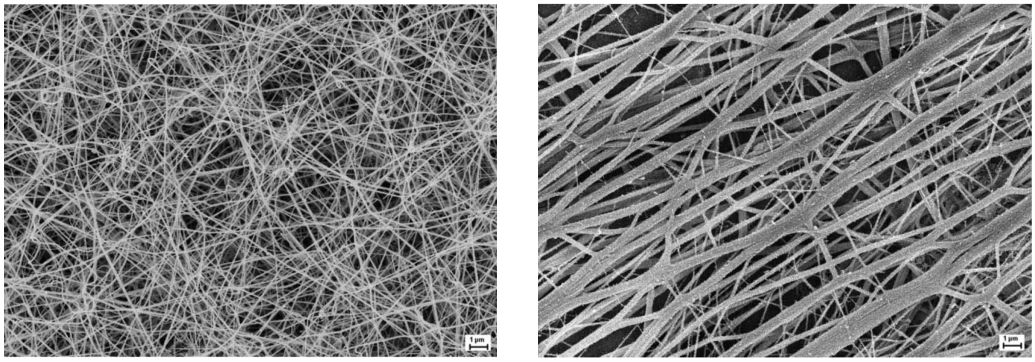

Figure 5.1: SEM Images Illustrating the Effect of Flow on Fibrin Network Structure[i].

(a) Formed under static conditions, (b) Formed under flow at 0.1 ml/min
Scale-bar: 1 μm.

Work by Bucay *et al.* showed that thicker fibres were more prone to elongation under flow, and as a result, more resistant to lysis under shear conditions.[78] Fibres which are elongated have fewer exposed binding sites for tissue plasminogen activator (t-PA), and as a result exhibit longer lysis times as a smaller amount of plasmin is generated.[195] Thus, measures of structural complexity, such as d_f which have been shown to predict relative fibre thickness, may have significant value in predicting lysis of clots formed under shear, such as those formed in blood vessels *in-vivo*.

[i]Reprinted from Thrombosis and Haemostasis, 104/06, Campbell RA, Aleman MM, Gray LD, Falvo MR and Wolberg AS, Flow profoundly influences fibrin network structure: Implications for fibrin formation and clot stability in haemostasis, p1281-1284, Copyright (2010), with permission from Georg Thieme Verlag KG

CSPS rheometry has previously been used to examine the influence of imposed shear on the formation of both whole blood and purified fibrin clots,[147] as discussed in Section 1.4. In these tests, values of d_f obtained through detection of the gel point during coagulation were found to increase with increasing shear stress.[147] In general, structural changes identified through the addition of agents such as thrombin show the formation of thinner highly branched fibres correlating with increased values of d_f. However, in the case of clots formed under flow the increase in d_f with thicker fibres (increased fibre bundling) has been attributed to the incorporation of more mass to the incipient cluster as a result of fibrin generation and interaction kinetics being substantially altered by the shear field.[147] Investigation of lysis in clots that have been formed under CSPS may yield further information regarding the contribution of the altered kinetics and d_f to the bulk behaviour of clots undergoing fibrinolysis.

The primary aim of the work presented in this chapter is to investigate the influence of shear induced changes in clot microstructure on the eventual clot lysis. This will be performed through the use of CSPS rheometry, involving different levels of applied unidirectional shear stress, during clot formation in samples of P-PFP. The application of a shear field allows for modification of clot microstructure whilst avoiding the addition of exogenous coagulation enhancers such as those used in Chapter 4. Complementary imaging using confocal laser scanning microscopy will be used to visualise the breakdown of the clots that have been formed under the different shear fields.

5.1 Methods

5.1.1 Sample Preparation

Pooled Platelet Free Plasma

Pooled platelet free plasma (P-PFP) was collected and stored as described in Section 3.1.1. Recombinant tissue plasminogen activator (rt-PA) (Hyphen BioMed, FR: RP007C) was reconstituted to a stock concentration of 1 mg/ml with distilled water at room temperature before being aliquoted and stored at -20 °C until use.

rt-PA was thawed at room temperature and diluted with distilled water to give a final stock concentration of 0.873 μM. A fixed volume of the stock rt-PA was then added to P-PFP along with 18 mM final concentration of $CaCl_2$ (Sigma Aldrich, UK: 21115-100ML) to give a final rt-PA concentration of 5 nM. Samples were then mixed gently by drawing the sample into the pipette tip and slowly releasing it several times before being loaded on to rheometer for testing.

Where samples were prepared for confocal microscopy a volume of P-PFP equivalent to 4 % of the total volume was replaced with 1.5 mg/ml human fibrinogen, Alexa Fluor® 488 conjugate (Fisher scientific, UK: F13191) to allow for imaging of the fibrin fibre network.

5.1.2 Data Collection

Controlled Stress Parallel Superposition

Controlled stress parallel superposition (CSPS) rheometry is a technique whereby an oscillatory wave is superimposed onto a rotational motion, and permits the measurement of oscillatory shear moduli of a sample which is undergoing flow where the stress takes the form:[196,197]

$$\sigma(t) = \sigma_{unidirectional} + G^{*}\gamma_0 \sin(\omega t + \delta) \qquad \text{(Eq. 5.1)}$$

and the resulting strain rate is defined as:[196,197]

$$\dot{\gamma}(t) = \dot{\gamma}_{unidirectional} + \gamma_0 \omega \cos(\omega t) \qquad \text{(Eq. 5.2)}$$

The technique results in an accumulated unidirectional strain that evolves over the course of its implementation, in addition to an oscillatory component which dampens with structural formation as depicted in Figure 5.2. CSPS requires a controlled stress instrument and so testing was conducted using the AR-G2 rheometer (TA instruments, UK) described in Section 3.1.2.

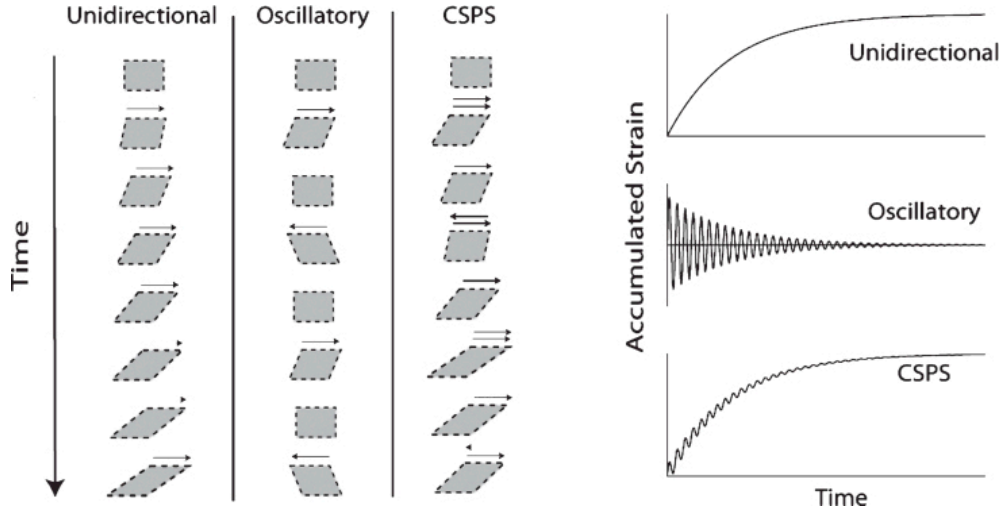

Figure 5.2: Illustration of the Net Strain Accumulated under Controlled Stress Parallel Superposition during the process of gelation or coagulation[ii].

When considering gelling systems, the application of a unidirectional shear stress results in a progressively evolving shear strain as the nature of the material changes, plateauing in the vicinity of the gel point. In contrast under oscillatory shear the net accumulation of strain is zero, where the evolution of a gel results in dampening of the strain amplitude. In CSPS, a unidirectional shear stress is superimposed on an oscillatory waveform, where both elements dampen/plateau over the course of gelation.

The rheology of P-PFP samples during coagulation were tested using discrete frequency sweeps over a frequency range of 0.4-2 Hz. During the early stages of coagulation ($\leq$ 1000 s), the test applied an oscillatory stress of 0.12 Pa superimposed upon rotational shear stresses of 0, 0.1, 0.2, and 0.3 Pa, in line with the range of stresses previously investigated by Badiei *et al.*[147] After a duration of 1000 s it was assumed, from previous results, that the sample had reached a post gel state and thus the unidirectional shear stress component was near-zero. At this point the rotational stress component was removed and an oscillatory stress of 0.12 Pa was applied to further monitor clot viscoelasticity during formation and eventual clot lysis. The cessation of the unidirectional stress component at 1000 s also permitted a comparison with confocal microscopy study, detailed below. The rheology experiments were performed at a gap of 300 μm for consistency with the previous CSPS study.[147] The linearity of de-gel point measurements was confirmed

[ii]Reprinted from Clinical Hemorheology and Microcirculation, 60/4, Badiei N, Sowedan AM, Curtis DJ, Brown MR, Lawrence MJ, Campbell AI, Sabra A, Evans PA, Weisel JW, Chernysh IN, Nagaswami C, Williams PR and Hawkins K, Effects of Unidirectional Flow Shear Stresses on the Formation, Fractal Microstructure and Rigidity of Incipient Whole Blood Clots and Fibrin Gels, p451-464 (2015), under the terms of the Creative Commons Attribution Non-Commercial (CC BY-NC 4.0) License.

through monitoring for the presence of a third harmonic response. Since the test was designed to monitor the influence of shear stress over coagulation, non-linearity during the initial phase was assumed by design as the CSPS procedure was intended to alter the rheological behaviour and characteristics of the samples through the application of stress (n=5).

In the vicinity of the gel point the unidirectional stress becomes 10^0 Pa and the structure becomes locked in. While there is a slight decrease in the values of G' that were obtained before and after the strain application, suggesting a degree of strain stiffening, there was no indication of a recoil in the strain rates, which would also have been detectable as non-linearity within the measurements. Therefore, any recoil was considered negligible.

Confocal Microscopy

Laser scanning confocal microscopy was performed using a Zeiss LSM 710 inverted confocal microscope (Zeiss, UK) which applies a focused beam of light to the sample that is absorbed by the fluorescent target. This emits a further signal having a second wavelength which is detected by the optical sensor.

A custom windowed plate was affixed to the Peltier plate of an AR-G2 rheometer and allowed to reach the set temperature, while polyethylene film was fixed over a 60 mm parallel plate geometry. Samples were prepared as described above and loaded into the custom set-up as shown in Figure 5.3.

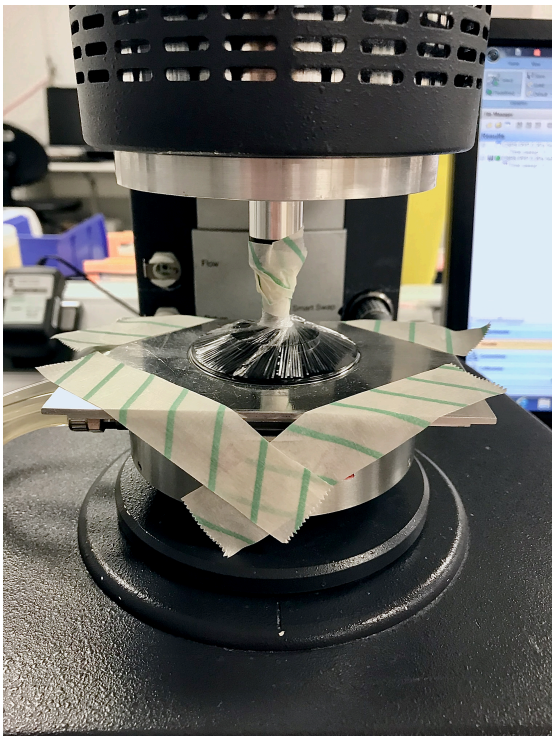

Figure 5.3: A Photograph Showing the Experimental Set-up of the AR-G2 Rheometer Enabling Transfer of Samples to a Confocal Microscope.

The rheometer was used to perform CSPS over the initial stages of coagulation, encompassing the process of incipient clot formation, as described above. At 1000 s, the CSPS procedure was stopped and the bearing lock was engaged on the rheometer motor. The polyethylene film was carefully cut away from the geometry using a scalpel and the rheometer head was lifted, leaving the sample contained between the custom plate and polyethylene film layer. This was then transferred to the confocal microscope and the time taken from the last oscillation to the capturing of the first image was recorded by stopwatch.

The fluorescent conjugate absorbed light at 496 nm with an emission wavelength of 524 nm. A 488 nm argon laser was used and fluorescent emission was detected at a wavelength of 562 nm. Imaging was performed in two dimensions with repeating scans using a 63 x (1.4 N.A.) oil immersion objective at a scan zoom of 3.2 x to generate a time-series of images with each frame being recorded over 0.97 s (n=5).

While it could be anticipated that a degree of material relaxation may occur during transportation to the confocal microscope, the rheometrical detection when the superimposed shear was removed displayed no evidence of substantial recoil and so it can be assumed that there is negligible material relaxation at this point.

5.1.3 Data Analysis

Under the conditions of CSPS, the gel point could not be detected, possibly due to a combination of the low stresses applied and the narrow linear viscoelastic range LVR of incipient plasma clots. Therefore, in these experiments, the peak value of G' ($G'_{\max}$) and the time taken to reach $G'_{\max}$ at a frequency of 2 Hz was used as the definition of clotting parameters. The clot lysis time (CLT) was defined as the interval between $G'_{\max}$ and the detection of a de-gel point.

In the rheological measurements of clot lysis, the de-gel point was determined using 'Gel Point Analysis' software previously described in Section 1.4.2. Spearman's ranked correlation analysis was performed to determine whether any relationships between the rheological parameters and the rotational shear stress existed. The rate of change in G' was also assessed as a proxy for the kinetics of fibrin formation, where $\Delta G'$ was calculated as the difference in G' between subsequent time points for data collected at 1.5 Hz. $\Delta G'$ was evaluated to examine the effects of unidirectional stress on fibrin generation kinetics.

Confocal microscopy images were deconvoluted using Huygens software (Scientific Volume Imaging, NE) and images extracted with an enhanced colour scheme using MATLAB® (Mathworks, UK). For each experiment, the initial frame was analysed to determine the structural characteristics of the mature clot. The Image J (NIH, USA) measuring tool was used to determine the fibre length and orientation of each discernible fibre per image. The total percentage of fibres within each 10 ° bin over 180 ° was examined at each stress. The average fibre length per image, the total number of fibres per image, and the total length of fibre per image were subjected to Spearman's ranked correlation analysis to determine whether the mature clot architecture was influenced by the level of shear stress.

MATLAB® analysis was performed over each image series using a comparative function provided by Dr. D.J. Curtis (College of Engineering, Swansea University) to quantify clot lysis. Each frame from the image series was read into a matrix, the MATLAB® script then evaluated the correlation between consecutive frames. The correlation between fibres is indicative of the freedom of movement observed for fibres during lysis. When plotted as a function of time this presents as a sustained horizontal line during the mature phase, a concomitant decrease during lysis, and peaks and troughs following breakdown of the structure, as illustrated in Figure 5.4. The moment of free movement ($MOFM$) was derived from the apex of the curve, where the structure first begins to exhibit motion of the fibres, but retains cluster characteristics. This time was added to the transfer time between equipment to give the static period (SP) for each sample. Spearman's ranked correlation analysis was used to determine whether any correlations between the superimposed shear stress and duration of the SP were present.

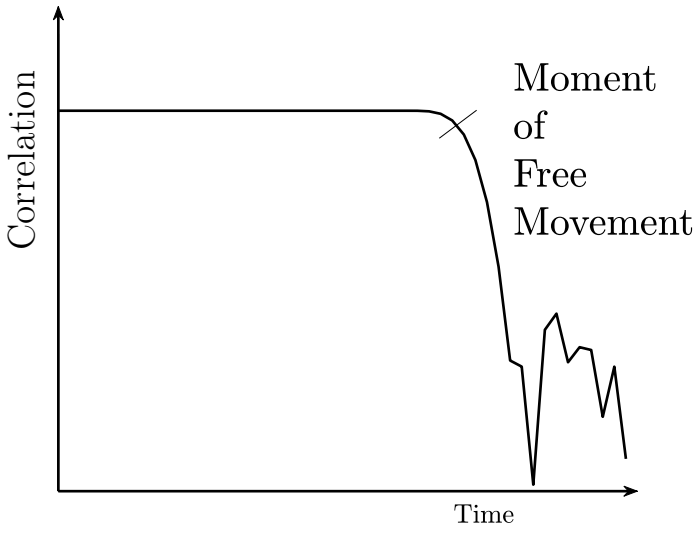

Figure 5.4: A Figure Illustrating the Definition of the Moment of Free Movement from the Correlation of Consecutive Confocal Frames

5.1.4 Limitations

Rheological limitations in CSPS experiments on the AR-G2 rheometer using discrete sweep procedures as discussed in Chapter 3 were considered. Due to the relatively narrow linear viscoelastic region of P-PFP coupled with the necessity of using small oscillatory stresses that are close to the resolvable limit of the instrument, no gel point could be detected. As a result, the peak in G', which represents the point of mature clot structure, was used in place of the gel time as a basis for the definitions of clot lysis herein. Since the value of G' is dependent on the frequency of testing, the peak in G' was determined from data collected at 2 Hz for each sample. Additionally, in both the rheological and confocal experiments at a rotational stress of 0.3 Pa, two of the clots did not reach the assumed post gel stage until after the shear stress was removed at 1000 s. These were excluded from statistical analysis, as they do not represent clots formed entirely under shear, but are shown in the relevant figures.

Whilst confocal imaging allows for collection of data in 3-D, scanning in the z-direction substantially decreases the speed of frame capture. In order to obtain data for the primary measurement of clot lysis 2-D scans were performed, and the first frame from each image was taken to examine the mature clot structure. However, since these images are 2-D, any apparent increase in fibre length could also be attributed to orientation in the z-direction and further investigation using 3-D image stacks of mature clots is required for confirmation.

5.2 Results and Discussion

5.2.1 Rheological Measurements of Clot Lysis

The influence of unidirectional shear stress on gel point parameters during the CSPS measurements could not be determined for P-PFP owing to the inherent narrow linear viscoelastic range and the influence of measuring near the resolution limits of the equipment. However, previous CSPS investigation of whole blood and purified fibrin gels (albeit at relatively high levels of fibrin concentration) predicts an increase in fractal dimension during coagulation ($d_{\mathrm{f}\ GP}$) with increasing unidirectional shear stress. This can be attributed to an increased rate of fibrin generation, triggered by the shear field, adding to the mass of the clot before a stable cluster is formed and the gel transition occurs.[147,193,194]

Statistical analysis of the results of rheological measurements are displayed in Tables 5.1 and 5.2. A correlation between unidirectional stress, through the application of CSPS, and both $G'_{\max}$ and CLT was observed. A weak correlation between $d_{\mathrm{f}\ dGP}$ and CLT was also identified. The finding that increased rates of shear stress result in significantly extended clot lysis times is of great importance and contributes to the clinical understanding of the relationship between pathogenic mechanisms and altered lytic susceptibility.

Table 5.1: Probability Values for Correlations between Unidirectional Shear Stress and Coagulation and Lysis Parameters Detected by Rheometry of Pooled Platelet Free Plasma.

	Stress (Unidirectional)	$G'_{\mathbf{max}}$	CLT	$d_{\mathbf{f}\ dGP}$
Stress (Unidirectional)	-	**<0.01**	**<0.001**	0.07
$G'_{\mathbf{max}}$	**<0.01**	-	**0.01**	0.8
CLT	**<0.001**	**0.01**	-	**0.05**
$d_{\mathbf{f}\ dGP}$	0.07	0.8	**0.05**	-

$d_{\mathrm{f}\ dGP}$: fractal dimension at the de-gel point.

Table 5.2: Rho Values for Correlations between Unidirectional Shear Stress and Coagulation and Lysis Parameters Detected by Rheometry of Pooled Platelet Free Plasma.

	Stress (Unidirectional)	$G'_{\mathbf{max}}$	*CLT*	$d_{\mathbf{f}\ dGP}$
Stress (Unidirectional)	-	**-0.65****	**0.79*****	-0.44
$G'_{\mathbf{max}}$	**-0.65****	-	**-0.59****	0.06
CLT	**0.79*****	**-0.59****	-	**-0.47***
$d_{\mathbf{f}\ dGP}$	-0.44	0.06	**-0.47***	-

$d_{\mathrm{f}\ dGP}$: fractal dimension at the de-gel point.
* p<0.05, ** p<0.01, ***p<0.001

Figure 5.5 depicts the influence of shear stress on $G'_{\max}$ and indicates that clots formed under higher stresses exhibit a decrease in G' of the mature (fully formed) clot, which can be interpreted as producing clots with reduced stiffness that are more readily deformable. This finding is inconsistent with some areas of the literature which report an increased stroke risk,[198,199] as it suggests that these clots are more deformable and therefore less prone to fracture. However, more recent research has shown that more porous clots are associated with disintegration under shear, resulting from a reduced shear-stiffening behaviour.[200] This could potentially explain the increased risk of thrombosis resulting from disintegration rather than fracture.

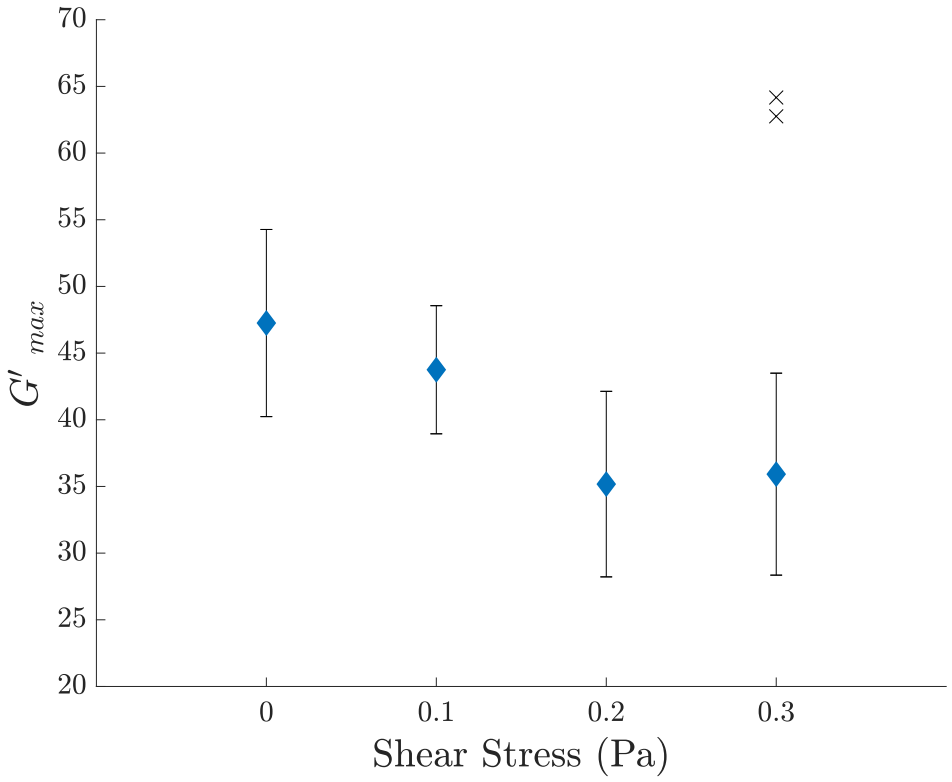

Figure 5.5: A Graph Showing the Relationship Between $G'_{\max}$ and Unidirectional Shear Stress in Pooled Platelet Free Plasma Clots Detected by Rheometry.

Error bars indicate standard deviation (n=5).
x indicates results which were excluded from analysis.

These findings are consistent with the mature clot structures observed during SEM imaging performed as part of previous studies.[193,194] In 1974, the decrease in $G'_{\max}$ was observed by Glover *et al.*, and was attributed to changes in the network structure and crosslink density.[124] Since this initial study, other research groups have investigated structural changes under flow and have identified differences in the value of d_f, fibre orientation and elongation, and bundling as occurring in blood clots subjected to shear.[147,193,195] These structural modifications that influence the node distribution of the network could be responsible for the observed decrease in $G'_{\max}$. However, no strong evidence of fibre orientation was identified as discussed in Section 5.2.2. Alternatively, considering the rate of change in G' ($\Delta G'$), which may relate to the rate of fibrin generation shown in Figure 5.6, it can be seen that higher levels of stress are associated with sharp peaks, where fibrin is generated very rapidly before the rate of generation drops. At lower shear stresses these peaks are shorter and broader which would be consistent with the generation of more fibres over a sustained period, despite the initial generation being less rapid.

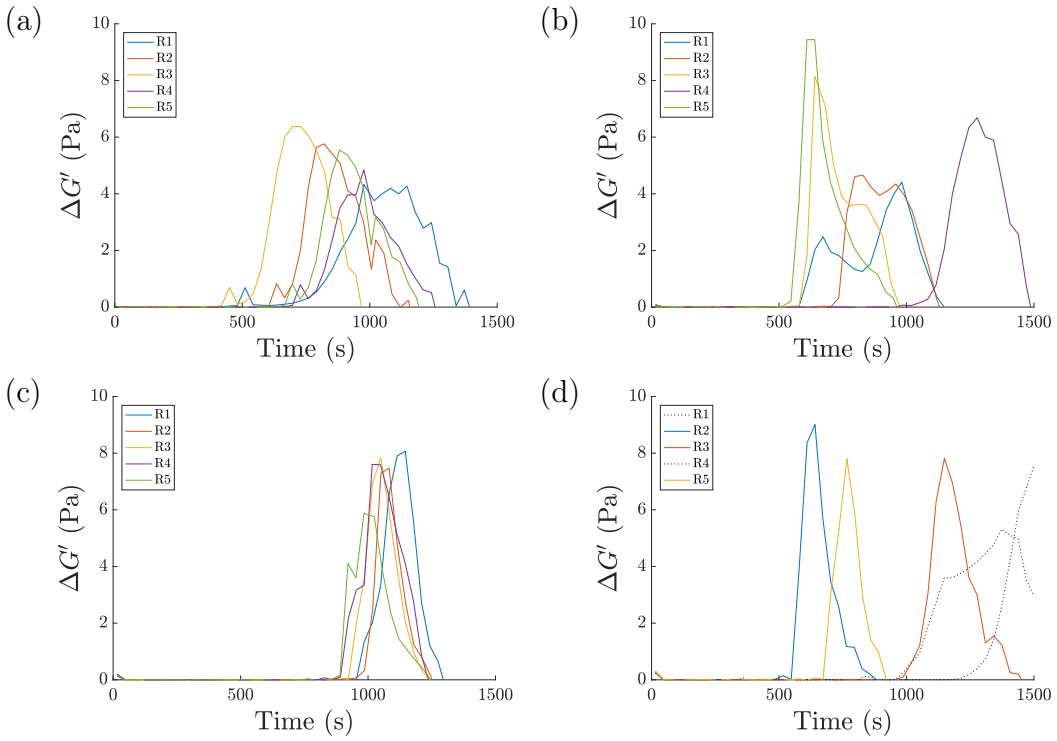

Figure 5.6: Graphs Showing the Change in Storage Modulus Over Time for Pooled Platelet Free Plasma Clots Generated Under Different Levels of Unidirectional Shear Stress.

(a) 0 Pa, (b) 0.1 Pa, (c) 0.2 Pa, and (d) 0.3 Pa.

R1-5: Repeats of the experiment.

Results that were excluded from analysis (dashed).

These differences in fibrin generation profiles present an alternative explanation for the reduction in $G'_{\max}$ being coupled with an increase in $d_{\mathrm{f}\ GP}$. Under CSPS the shear rate dampens over the course of coagulation, which could impede these kinetics. These findings could suggest that the enhanced kinetics, which result in more insoluble mass being present at the gel point, dampen during the post gel point phase. This could potentially lead to less mass ultimately being incorporated into the mature clot structure. Furthermore, the removal of this stress following clot formation may also inadvertently influence the clot behaviour, as it represents the removal of tension from the fibres which could reduce the shear stiffening associated with *in-vivo* blood flow. As a result, further research involving application of sustained steady shear stresses is warranted, to determine whether these characteristics are maintained where the effect of flow is continuous.

The data in Figure 5.7 represents a significant finding, showing a positive correlation ($p<0.001$, $rho=0.79$) between CLT and levels of unidirectional stress. There have been several previous studies presenting contradictory results regarding altered resistance to lysis being affected by structural complexity. This work indicates that in the absence of biochemical manipulations, such as the addition of thrombin, shear induced changes in clot microstructure result in extended clot lysis times.[147]

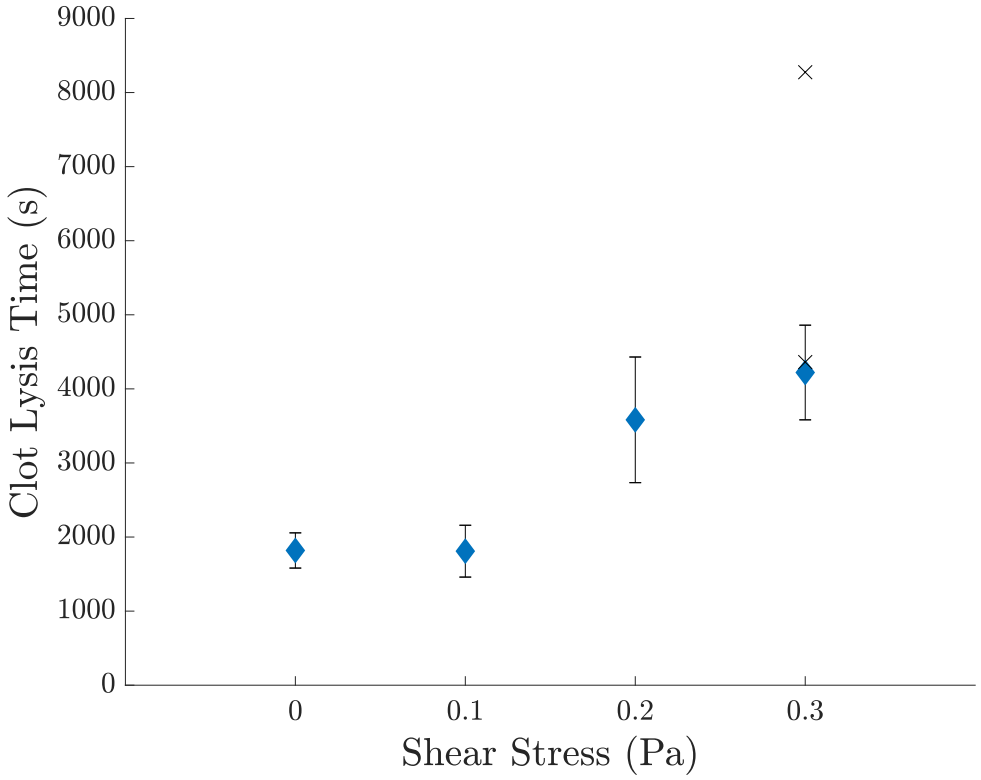

Figure 5.7: Graph Showing the Relationship Between Clot Lysis Time and Unidirectional Shear Stress in Pooled Platelet Free Plasma Clots Detected by Rheometry.

Error bars indicate standard deviation (n=5).
x indicates results which were excluded from analysis.

This finding has clear implications in a clinical context, as it provides evidence that increased shear rates, which can occur *in-vivo* as a result of reduced blood vessel diameter (stenosis) and elevated blood pressure, lead to clots with increased resistance to lysis in the absence of any other coagulopathy.

5.2.2 Confocal Microscopy

Mature Structure

The first frame of confocal images collected were analysed to explore mature clot architecture as a consequence of increasing shear stress. Representative images are shown in Figure 5.8.

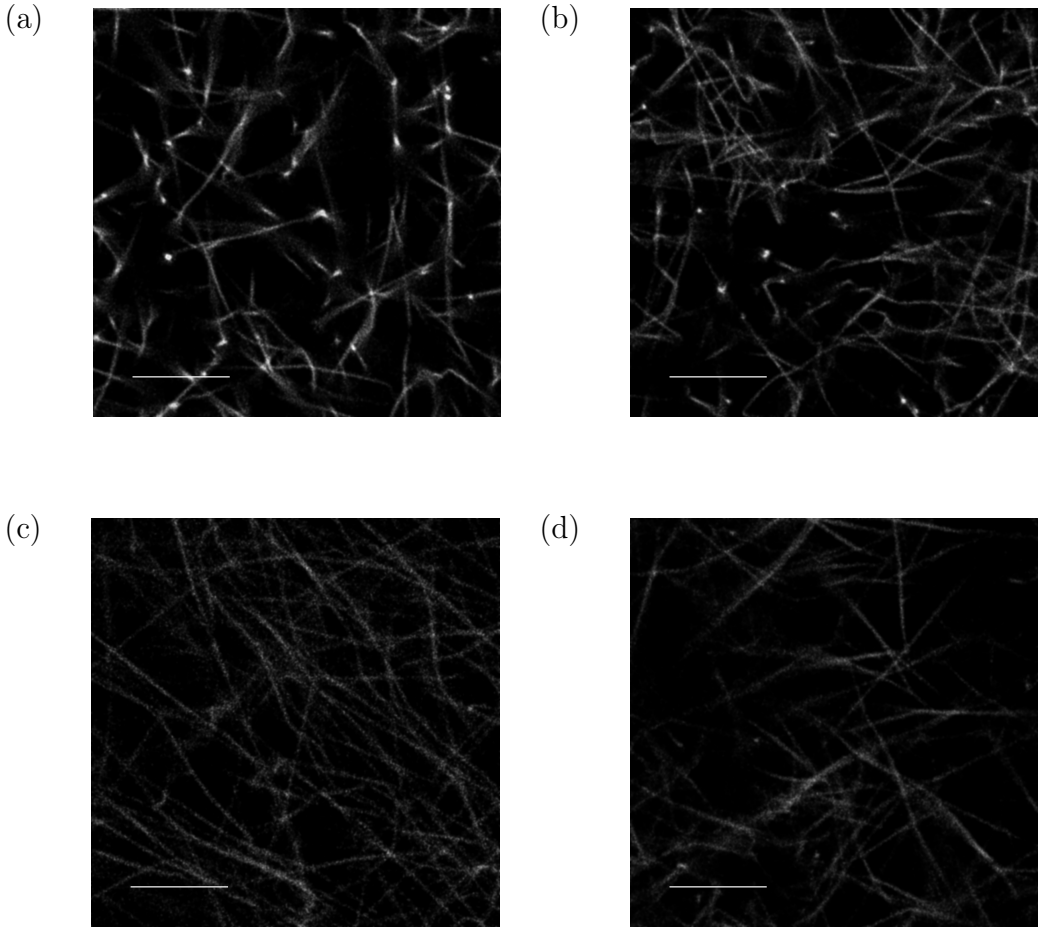

Figure 5.8: Confocal Images Showing the Mature Gel Structure of Pooled Platelet Free Plasma Clots Formed Under Controlled Stress Parallel Superposition.

(a) 0 Pa, (b) 0.1 Pa, (c) 0.2 Pa, and (d) 0.3 Pa.
Scale-bar: 10 µm.

From these images, qualitative differences between the structures can be observed with the images of clots subjected to unidirectional shear stress appearing to show more dense regions of fibrin fibres. Analysis of fibre orientation, shown in Figure 5.9, shows some evidence for alignment of fibres between 100-160 °. However, the effect is not pronounced enough to draw any strong conclusions. This is consistent with SEM images analysed during previous CSPS work, where orientation in the direction of flow was not significant.[147] The strain rates generated during the CSPS experiments herein are an order of magnitude smaller than those analysed in typical flow experiments where alignment of fibres has been identified.[147,194]

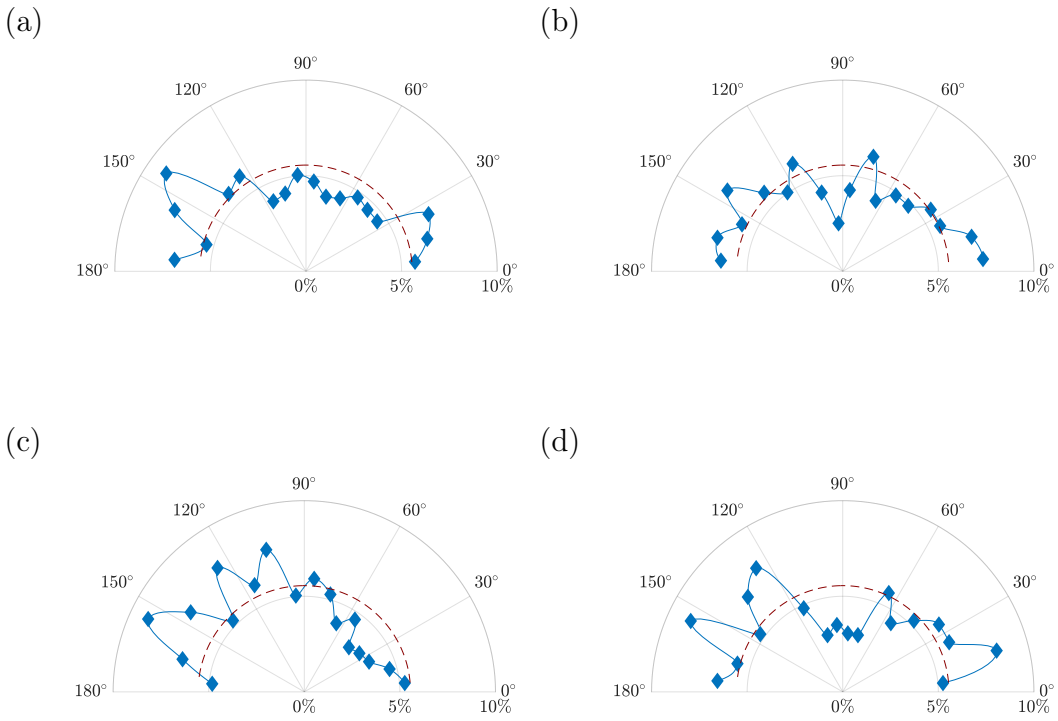

Figure 5.9: Polar Graphs Showing the Percentage of Fibres Oriented at 10 ° Intervals for Mature Pooled Platelet Free Plasma Clots Formed Under Controlled Stress Parallel Superposition.

(a) 0 Pa, (b) 0.1 Pa, (c) 0.2 Pa, and (d) 0.3 Pa.
Theoretical even distribution (dashed).

Figure 5.10 shows the results of analysis of the average fibre length and the total number of fibres, which reveals that increasing shear stress leads to the formation of fewer ($p<0.01$, rho = -0.65), longer ($p<0.01$, rho = 0.63) fibres.

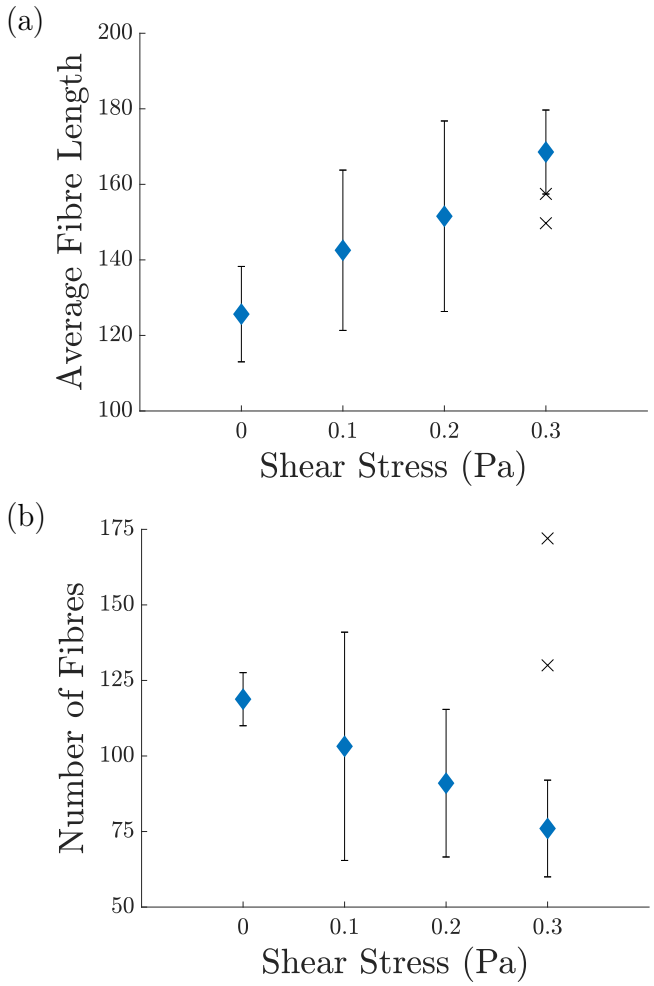

Figure 5.10: Graphs Showing the Relationship Between Fibre Length/Number and Unidirectional Shear Stress for Mature Pooled Platelet Free Plasma Clots Formed Under Controlled Stress Parallel Superposition.

(a) Average fibre length per frame and (b) number of fibres per frame.
Error bars indicate standard deviation (n=5).
x indicates results which were excluded from analysis.

Clot Lysis

Analysis of the effect of shear stress on clot lysis observed using confocal microscopy showed a statistically significant decrease in the static period (SP) with increasing shear stress (p=0.02, rho=-0.53) shown in Figure 5.11.

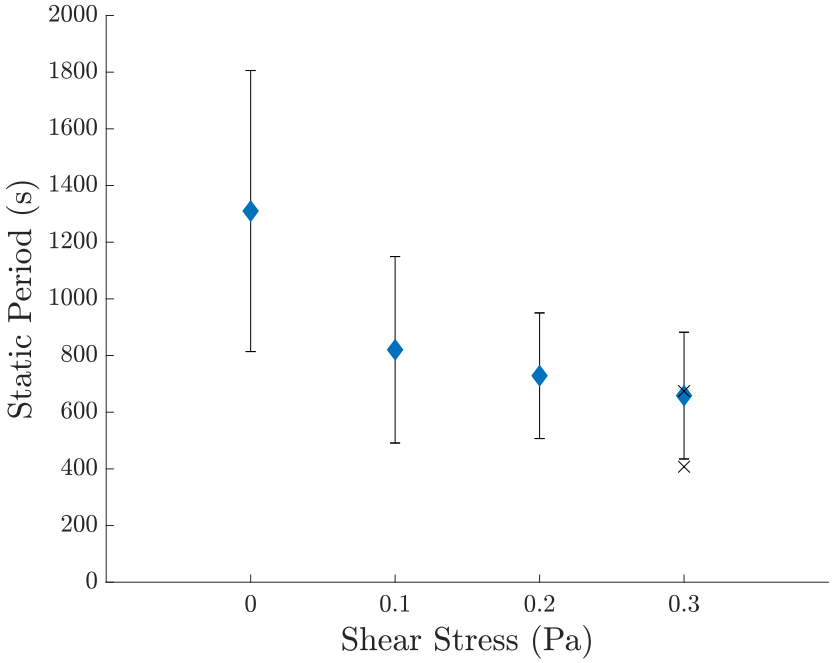

Figure 5.11: A Graph Showing the Relationship Between the Static Period and Unidirectional Shear Stress in Pooled Platelet Free Plasma Clots Detected by Confocal Microscopy.

Error bars indicate standard deviation (n=5).
x indicates results which were excluded from analysis.

The finding that substantial movement of fibres occurs earlier during lysis where clots are subjected to higher shear stresses could be explained by recent work performed by Cone *et al.* This study showed that while the start of each lysis event is associated with the cleavage of a single fibrin fibre, there are secondary mechanisms which determine the behaviour of the bulk clot in response to this event. In response to the lysis of a single fibre the clot may undergo buckling/structural elongation, fibre bundling, and/or fibre collapse. Further modelling by Cone *et al.* revealed that where higher levels of prestrain are applied to the fibres (which would be analogous to the cumulative strain applied by CSPS), clearance of the clot increases as a result of fibre collapse.[201] Examination of confocal images collected at the $MOFM$, shown in Figure 5.12, reveals evidence of the described structural collapse, with higher stresses resulting in greater frame clearance as the network collapses upon itself.

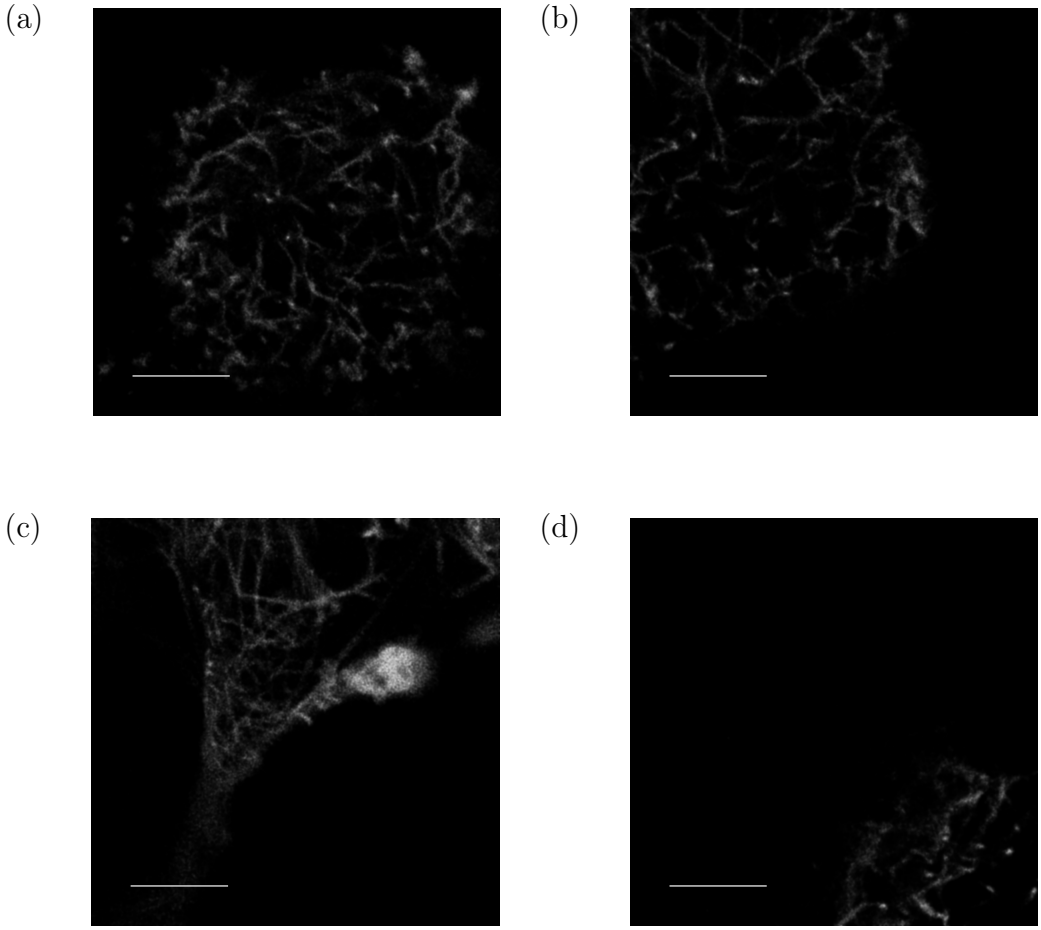

Figure 5.12: Confocal Images Showing Gel Structures at the Moment of Free Movement for Pooled Platelet Free Plasma Clots Formed Under Controlled Stress Parallel Superposition.

(a) 0 Pa, (b) 0.1 Pa, (c) 0.2 Pa, and (d) 0.3 Pa.
Scale-bar: 10 µm.

This mechanism is consistent with the increased CLT observed during rheometrical evaluation, since the network collapse would generate localised regions of high fibre density, where the individual fibres are lax, which has been previously shown to be associated with increasing resistance to lysis.[78,195] It would also suggest that the assessment of d_{f} from measurements of de-gel points of these clots should be interpreted with care due to potential violation of the assumption of homogeneity in the sample spanning cluster. This includes drawing any conclusions from the apparent negative correlation seen between $d_{\mathrm{f}\ dGP}$ and CLT.

5.3 Conclusions

The application of shear stress to pooled platelet free plasma clots during coagulation resulted in the production of clots which displayed fewer, longer fibres with limited evidence of orientation under the shear stresses studied herein (0 - 0.3 Pa). Clots formed under shear were associated with short spikes in fibrin generation, as opposed to the gradual conversion observed in the absence of shear. This supports the findings of Badiei *et al.* who proposed that the flow kinetics alter the rate of thrombin generation leading to differences in clot microstructure.[147]

The key finding of the work presented in this chapter is the observation that clots formed under increasing unidirectional shear stresses display extended lysis times, in terms of the time taken for sample spanning connectivity to be lost (*i.e.* the de-gel point). However, increasing unidirectional shear stresses led to clots that exhibited freedom of movement earlier during lysis. These transient processes may be explained by the recent work of Cone *et al.* which shows that networks formed under strain have a propensity to collapse during lysis.[201] This finding suggests that in the absence of biochemical manipulation of samples, increasing microstuctural complexity results in prolonged lysis times. This may have significant clinical implications when considering the role of physiological factors such as blood pressure and vascular complications such as stenosis in thrombosis risk and response to thrombolytic therapy.

This mechanism of structural collapse brings into question the validity in monitoring the lysis of fibrin networks under tension through rheometry. Network collapse could lead to violation of the assumption that there is a homogeneous structure present at the de-gel point, which is required for the assessment of the fractal dimension. This will be further explored in Chapter 6.

Chapter 6

The Effect of Platelet Contraction on Coagulation and Lysis Measurements

The results from Chapter 5 indicate that tension within a fibrin network may lead to the collapse of the network during clot lysis. Therefore, in a rheological measurement the clot may contract and detach from the rheometer plates, resulting in an inability of the rheometer to probe the sample spanning cluster. The work presented in this chapter aims to investigate the effects of clot contraction on rheological measurements during coagulation and lysis, and seeks to validate the measurement of the de-gel point as a true marker of clot lysis.

Platelet mediated contraction, which results in compaction of the fibrin structures, has a significant impact on the structural characteristics and lytic susceptibility of blood clots. It has been shown that contracted clots lyse more readily than their uncontracted counterparts.[80] In existing fibrinolytic tests platelet contraction can cause disruption of results, and in thromboelastometry/thromboelastography can cause type 1 errors in the detection of hyperfibrinolysis. As a result, additional tests must be performed in tandem in order to rule out this effect, and confirm hyperfibrinolytic states.[83]

In relation to rheological parameters, the presence of fibroblasts within a forming fibrin network results in contraction of the cells and stiffening of the fibrin structure. Rheometrical assessment of this phenomenon has shown that these contractile forces result in increased values of G' as a result of fibre stiffening, but have no effect on $tan(\delta)$.[202]

Recently, it has been shown that monitoring the axial forces generated during clot formation provides a measure for the degree of contractile stress generated by platelets.[59,140] Should the fractal dimension at the gel point and de-gel point be found to be independent of contraction, this additional measurement may prove useful in independently measuring both network structure and platelet contractile forces.

The forces generated during contraction result from the action of platelets on the fibrin network and are substantially influenced by the presence of erythrocytes which increase the contractile stresses generated, but reduce the extent of clot contraction.[59] The work will therefore examine differences in contractile responses of whole blood, platelet rich plasma with and without the contraction inhibitor tirofiban, and platelet free plasma. These fractions are expected to show different rheological properties, as both platelets and erythrocytes are known to contribute to the behaviour of fibrin fibre networks.

The pro-coagulant nature of platelets has been investigated by rheometry, and the administration of platelet activation inhibitors is known to result in lower values of $d_{\mathrm{f}\,GP}$ in healthy individuals, without impacting gel times.[139] In addition to this pro-coagulant activity, platelets also contain additional plasminogen activator inhibitor (PAI-1) and α2-antiplasmin, and are therefore expected to influence clot lysis.[203]

The presence of erythrocytes during fibrin network formation leads to regions of densely packed fibrin surrounding the cells, with sparsely structured regions between. Contradictory evidence exists concerning the effects of erythrocytes on rheology and clot structure. Some researchers have shown that whilst erythrocytes have no apparent affect on the porosity of a clot, they significantly alter the viscoelastic behaviour, increasing the fibrin fibre diameter and the value of $tan(\delta)$. It has been proposed that this occurs as a result of erythrocytes blocking branch development in the microstructure.[204] Wohner *et al.* have also reported that the addition of erythrocytes leads to a decrease in fibre diameter.[205] As such, the work presented will also include examination of differences in the rheological parameters of different sample types including various blood fractions.

The primary objective of this chapter is to explore the impact of clot contraction on both coagulation and lysis. This will be achieved by utilising axial force constrained rheometry, whereby the rheometer gap is allowed to change in order to maintain a zero axial force. This technique will allow measurement of the rheological properties of the clot whilst permitting contraction. The secondary aims of this chapter are to explore the influence of platelet contraction on clot rheology and to evaluate the behaviour of different blood fractions using the novel biomarker.

6.1 Methods

6.1.1 Sample Preparation

Whole Blood and Blood Fractions

Blood was collected from five healthy volunteers into 9 ml sodium citrated Vacuette® tubes on two separate occasions as described in Section 3.1.1.

1 ml of sample was immediately drawn from the Vacuette® for use in the experiments involving whole blood. The remaining 8 ml of material was placed into a swinging rotor centrifuge (Eppendorf, UK: 5810R) at 25 °C for 15 minutes at 2500 xg in order to separate the cellular components and the majority of platelets from the plasma. 4ml of platelet poor plasma (PPP) was then siphoned from the top of the tube using a pipette into a falcon tube (Greiner Bio-One, UK: 188271) leaving approx. 1 ml undisturbed to prevent contamination from the buffy layer.

Each sample of PPP was then subjected to a further centrifugation step at 25 °C for 15 minutes at 2500 xg. 2.5 ml of material was siphoned from the top of the tube to produce platelet free plasma (PFP). The platelet pellet was then re-suspended in the remaining 1.5 ml of fluid by gently drawing the pellet into a pipette tip and slowly releasing it several times, to generate platelet rich plasma (PRP).

rt-PA was thawed at room temperature and diluted with distilled water to give a final stock concentration of 1.31 μM. A fixed volume of the stock rt-PA was then added to the sample along with 18 mM final concentration of $CaCl_2$ to give a final rt-PA concentration of 10 nM. Samples were then mixed gently by drawing the sample into the pipette tip and slowly releasing it several times before being loaded on to the rheometer for testing.

In the case of PRP with the addition of the platelet contraction inhibitor tirofiban, a stock concentration of 0.6 mM tirofiban (Sigma Aldrich, UK: 30165-5MG) was made up by dilution in distilled water. This was then added to the PRP to give PRP+i containing 10 μM tirofiban. The sample was incubated at room temperature for an hour before the addition of rt-PA and $CaCl_2$ as above for testing.

6.1.2 Data Collection

i-Rheo

Rheological measurements for analysis by i-Rheo (Appendix D) were conducted on the ARES-G2 rheometer (TA instruments, UK) described in Section 3.1.2. The auto-strain adjust function was used in all gel point and de-gel point detection procedures, which effectively allowed unconstrained strain adjustments (0.1-300 %) while limiting the torque applied to within 0.02 μN.m of the value specified to give a fundamental stress of 0.04 Pa.

Assessment of the suitability of i-Rheo involved detection of the gel point of re-calcified citrated whole blood conducted using the previously optimised Fourier transform mechanical spectroscopy (FTMS) procedures. Samples were tested at 37 °C using a parallel plate set to a gap size of 200 μm in order to remain below the gap loading limit, and tested using a complex wave with a fundamental frequency of 2.5 Hz, and the second (5 Hz) and fourth (10 Hz) harmonics. After 900 s, a stress relaxation step was initiated which applied a 1 % strain and monitored the sample relaxation over 10 s. This facilitated the analysis using i-Rheo. Following this the FTMS procedure was re-initiated and lysis was monitored (n=5).

Fixed Gap and Variable Gap Rheometry

Investigation of clot contraction was conducted using an ARES-G2 rheometer on samples as described in Section 6.1.1. Gel point, stress relaxation, and de-gel point steps were conducted as described above for i-Rheo measurements, with the 10 s stress relaxation procedure being initiated after 750 s.

Samples of citrated whole blood were collected and processed into fractions as described above in Section 6.1.1. The whole blood, PRP, PFP, and PRP+i of the first samples collected from each of the five donors were tested at a fixed gap, where the force rebalance transducer in the head of the ARES was conditioned to allow for axial forces of up to 10 N without altering the position of the head. The fractions from the second sample collected from each donor were tested at a variable gap, where the transducer was instructed to alter the operating gap in order to maintain an axial force of 0 N with a tolerance of 0.001 N. This permitted the gap to change as the samples contracted.

6.1.3 Data Analysis

In order to investigate the effect of clot contraction on coagulation and lysis, experiments were performed on whole blood, PRP, PFP, and PRP+i, under fixed gap and variable gap conditions. Fixed gap testing involved the maintenance of a specified gap size (200 μm) for the duration of testing, which would result in spatial constraint of the clot. Variable gap testing utilised a gap adjustment which allowed the upper geometry to move in order to maintain a zero axial force, the clot was unconstrained and able to contract within the rheometer. The gel point and de-gel point parameters were obtained using 'Gel Point Analysis' software previously described in Section 1.4.2. The value of $G'_{\max}$ at 2.5 Hz was extracted from each experiment, and i-Rheo data was generated as described above. The i-Rheo plots generated at both fixed and variable gap for each sample type were overlaid for visual assessment. The fixed and variable experiments for each of the blood fractions were compared by paired t-test. The results of the fixed tests were then examined for each sample type and ANOVA was used to assess differences in the coagulation and lysis parameters for each individual blood fractions.

6.1.4 Limitations

In these experiments a single blood sample from each donor was collected and processed into each of the fractions used. Owing to the period of the experiments this necessitated samples being stored for a period of up to 4 hours before testing. It is known that coagulation becomes impaired after extended storage following sample collection; however, the period of testing was deemed necessary in order to produce comparable data from each donor. In order to minimise the impact of this, the fractions were tested in the same order for each donor.

During the variable gap experiments an initial gap size of 200 μm was used, which is greater than the recommended ten times the particle size for whole blood samples, which contain particles up to 15 μm in size. During the experiment, and as a consequence of contraction, the gap size dropped below the gap threshold of 150 μm which potentially introduced errors into the measurement. During the lysis of whole blood under variable gap conditions, the value of δ at each frequency merged at an apparent de-gel point but did not subsequently produce characteristics of a viscoelastic liquid response. This might be due to contraction leading to the viscoelastic properties of the lysed clot being dominated by a compacted network of red blood cells. For the purposes of this analysis the first instant of frequency independence was taken as the de-gel point.

The gap change and axial forces generated were recorded for the duration of the respective tests. However, the data collected is believed to be compromised, potentially as a result of equipment limitations. While the fixed gap and variable gap testing parameters were considered to be met, due to the successful maintenance of a zero axial force/consistent gap size during the experiments, the traces were not further evaluated.

6.2 Results and Discussion

6.2.1 Effect of Clot Contraction on Formation and Lysis

Comparison of samples where contraction was restricted by enforcing a fixed gap size, and allowed by initiating a gap adjust procedure revealed significant differences in the gel time (GT) of platelet rich plasma (PRP) and the fractal dimension during lysis ($d_{\mathrm{f}\ dGP}$) of PRP in the presence of the contraction inhibitor tirofiban (PRP+i), as shown in Table 6.1.

Table 6.1: Probability Values for Two-tailed Paired t-Test for Fixed Gap and Variable Gap Experiments.

	Gel Time	$d_{\mathbf{f}\ GP}$	$FCLT$	$d_{\mathbf{f}\ dGP}$
Whole Blood	0.47	0.66	0.41	0.14
PRP	**0.03**	0.06	0.75	0.69
PFP	0.13	0.08	0.43	0.11
PRP + i	0.27	0.25	0.75	**0.03**

PRP: Platelet rich plasma, PFP: platelet free plasma, PRP + i: platelet rich plasma + 10 μM tirofiban.

The GT shown in Figure 6.1 indicates that PRP samples in which contractile forces were dissipated, gelled faster. No differences in $d_{\mathrm{f}\ GP}$ were identified, which indicates that the contractile forces do not alter the distribution or structural template for fibrin network formation.

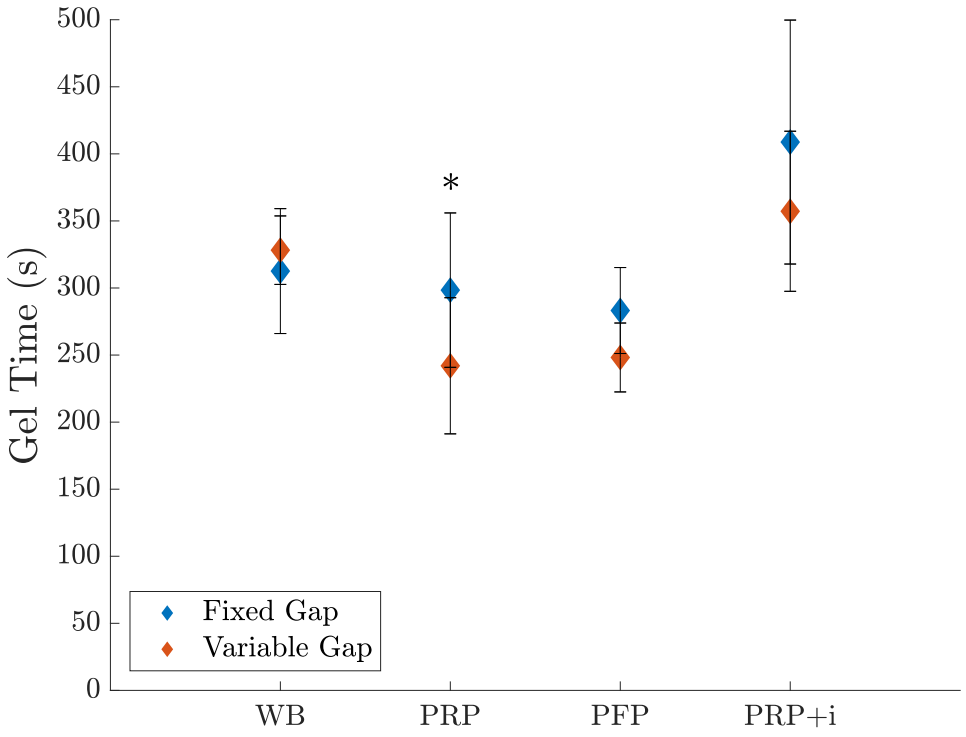

Figure 6.1: A Graph Showing the Gel Time of Different Blood Fractions in Fixed Gap and Variable Gap Rheometrical Testing.

Error bars indicate standard deviation (n=5).

The decrease in GT was found only in PRP samples during variable gap testing compared to a fixed gap. This indicates that the phenomenon is a result of the adhesion of platelet aggregates to fibres and the exertion of contractile forces on fibrin fibres that are free to move. When the rate of fibrin generation is increased through the addition of thrombin, an increase in $d_{\mathrm{f}\ GP}$ is observed. In this instance no change in $d_{\mathrm{f}\ GP}$ was detected, as seen in Figure 6.2, suggesting that fibrin formation kinetics are not involved in this phenomenon. It is possible that the smaller gap size may be responsible, since it may take less time to form a sample spanning network where the space to be occupied is smaller. However, this would also affect other sample types where the gap was unconstrained during testing. It is known that the platelet aggregates in variable gap PRP samples bind to the fibrin network and exert contractile forces. It is possible that when bound to lax fibrin fibres, rather than this resulting in network tension, as in the fixed gap samples, the fibres in variable gap testing are free to move and may be drawn into proximity for cluster connection by the platelet aggregates.

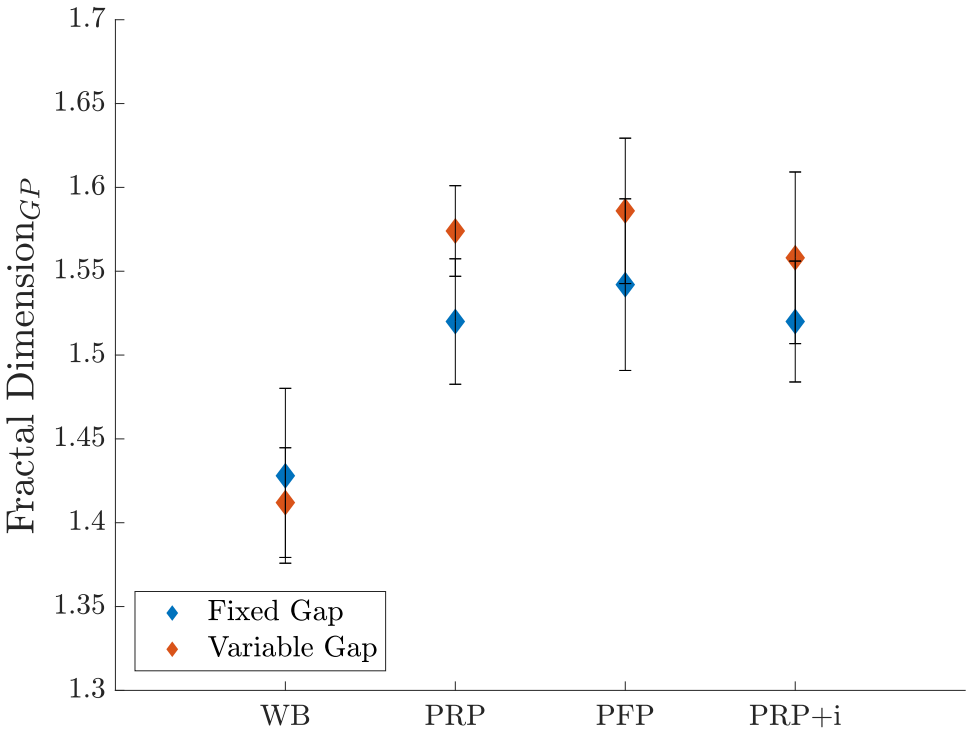

Figure 6.2: A Graph Showing the Fractal Dimension of Different Blood Fractions at the Gel Point in Fixed Gap and Variable Gap Rheometrical Testing.

Error bars indicate standard deviation (n=5).

The results from experiments at a fixed gap were used to further examine the differences in rheological behaviour between blood fractions. The gel time of PRP+i was found to be significantly longer than both PRP and PFP (p=0.02), as depicted in Figure 6.1. This likely results from the presence of the platelet inhibitor tirofiban which mimics the rare genetic condition thrombasthenia, which is associated with increased bleeding times.[206]

No significant difference in gel time was detected between PRP and PFP, this is unexpected as the presence of platelets in PRP would be anticipated to result in shorter gelation times. This may be due to contact with the surfaces of the rheometer driving coagulation through the intrinsic pathway of coagulation and activating available thrombin, such that the activation factors generated by platelets has no additional effect. Previous studies have shown that the intrinsic pathway inhibitor corn trypsin inhibitor results in substantially extended plasma coagulation times in rheometrical detection.[207] This effect was confirmed for small amplitude oscillatory shear rheology shown in Appendix E and could be confirmed by testing PRP and PFP with and without the inhibitor. Alternatively, this

finding may be a result of damage to platelets during the generation of PFP resulting in the pro-coagulant factors being released into the plasma.

It has been previously established that the presence of blood cells significantly influences the incipient structure of the fibrin network leading to less structurally dense clots displaying higher values of $tan(\delta)$.[204] This was confirmed and shown in Figure 6.2, where whole blood was found to result in incipient structures exhibiting a lower value of $d_{\mathrm{f}\ GP}$ ($p<0.01$).

In assessing the influence of platelet contractile forces on clot behaviour there was interest in determining the mature clot properties, as this would relate directly to deformability and propensity to fracture, which Tutweiler *et al.* recently suggested are greatly influenced by platelet contraction.[64] In the presence of rt-PA the rheological properties of blood reach a maximum for only a relatively short period and, as a result, conventional measurements such as frequency sweeps are not practical. i-Rheo software provided a potential method for overcoming this limitation, enabling the generation of substantial frequency sweep data from a comparatively short experimental test, as discussed in Section 1.4.2.[150] This process was evaluated in blood samples and a degree of alignment was noted, but could not be quantified (Appendix D).

Upon examining mature clot properties, Figures 6.3-6.6 show the traces output by i-Rheo. These indicate a potential increase in G' for variable gap whole blood clots and a possible decrease in G' for variable gap PRP and PFP clots. This could be detection of strain stiffening behaviour in plasma samples where the forces applied to fibres were not able to dissipate, which suggests that the presence of erythrocytes has a distinct impact on the rheological behaviour of mature contracted clots. However, the previous validation of i-Rheo revealed slight discrepancies between calculated and collected values for the moduli in blood samples, which is coupled with a large degree of noise in many of the data sets. As a result, the interpretive value of these traces is limited. Furthermore, no statistically significant differences in G'_{max} derived from oscillatory data were identified between fixed gap and variable gap samples ($p>0.05$ for all sample types).

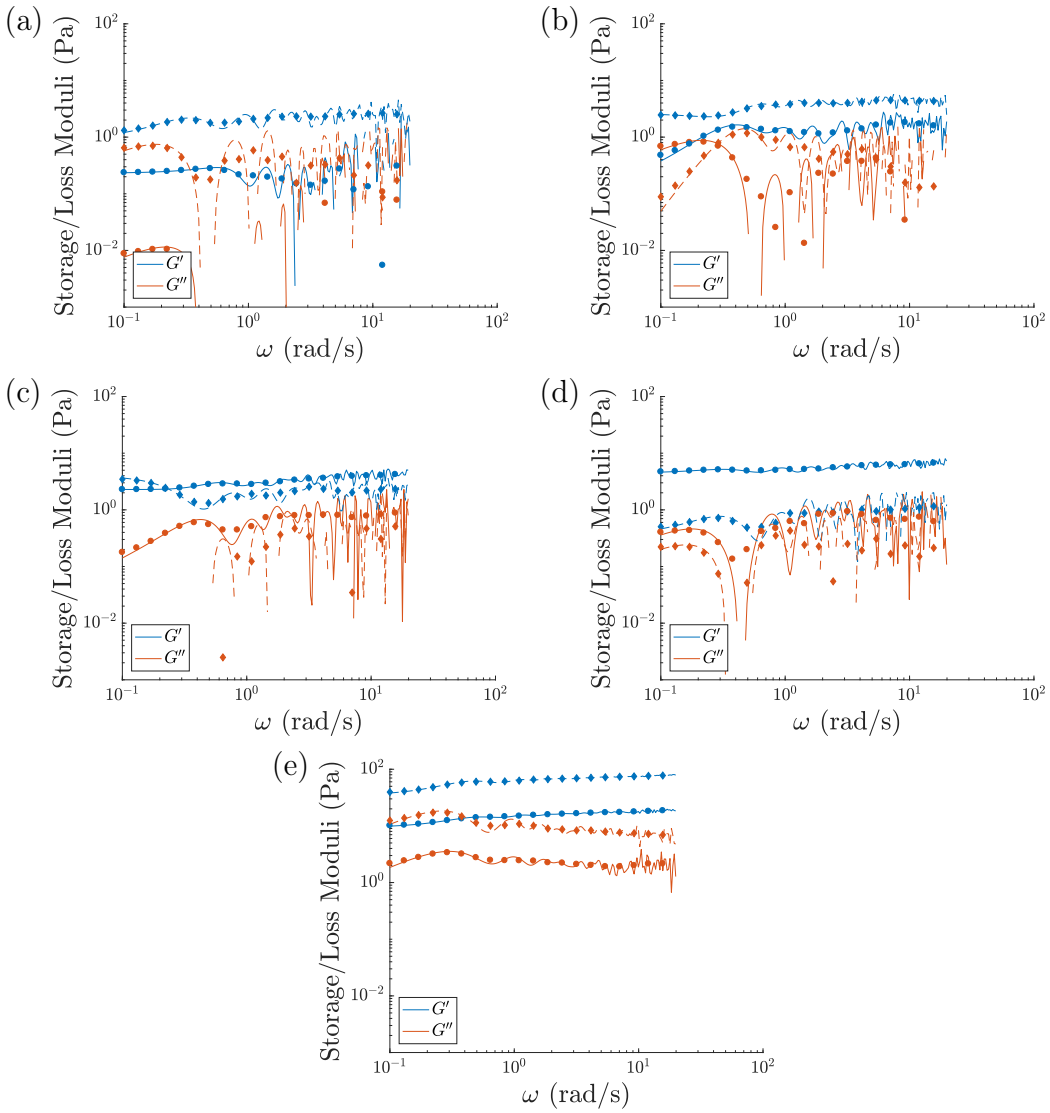

Figure 6.3: Graphs Showing the Relationship Between the Storage and Loss Moduli and Angular Frequency (ω) for Whole Blood Clots as Obtained by i-Rheo Software.

(a)-(e): individual sample donors

Solid/circles: fixed gap, dashed/diamonds: variable gap

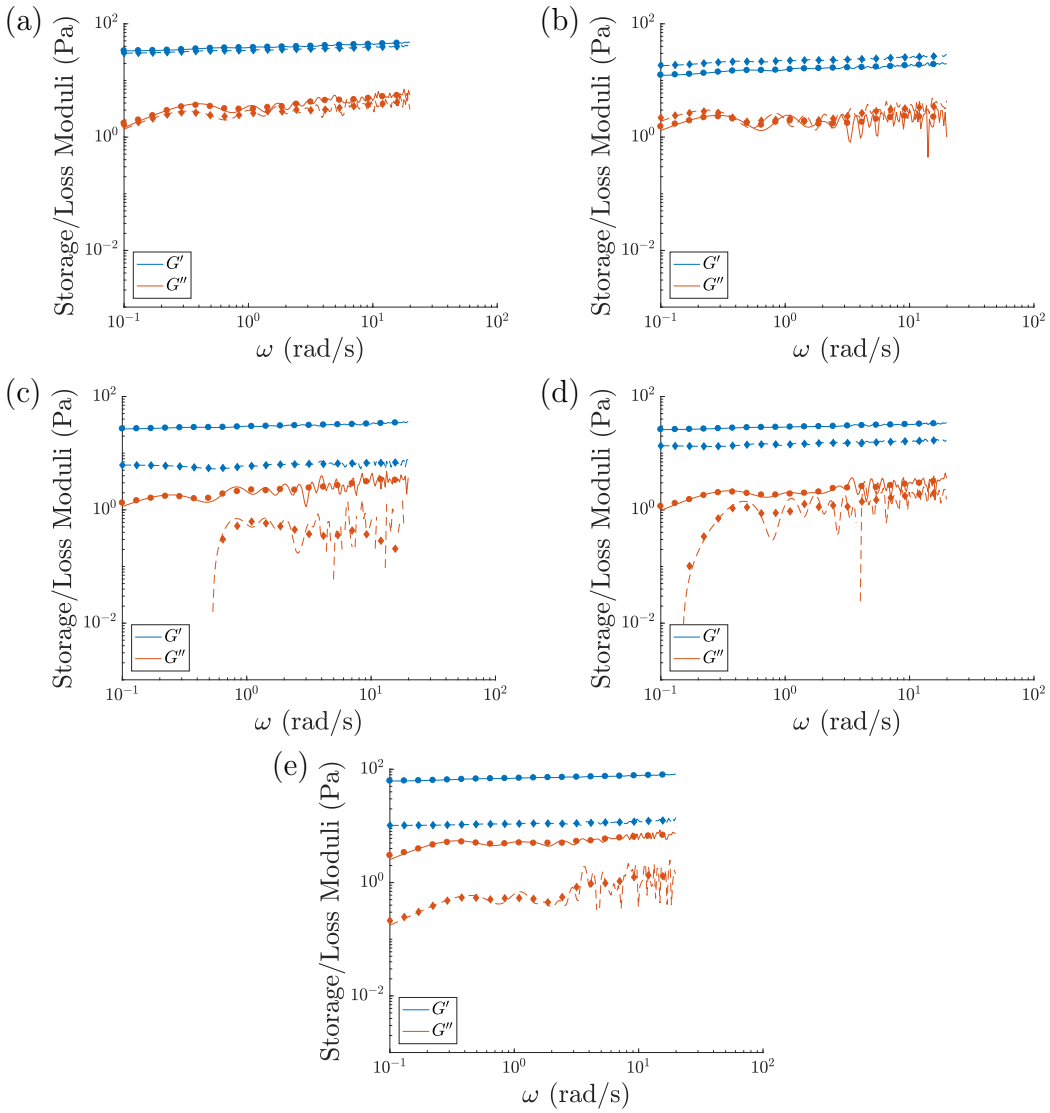

Figure 6.4: Graphs Showing the Relationship Between the Storage and Loss Moduli and Angular Frequency (ω) for Platelet Rich Plasma Clots as Obtained by i-Rheo Software.

(a)-(e): individual sample donors

Solid/circles: fixed gap, dashed/diamonds: variable gap

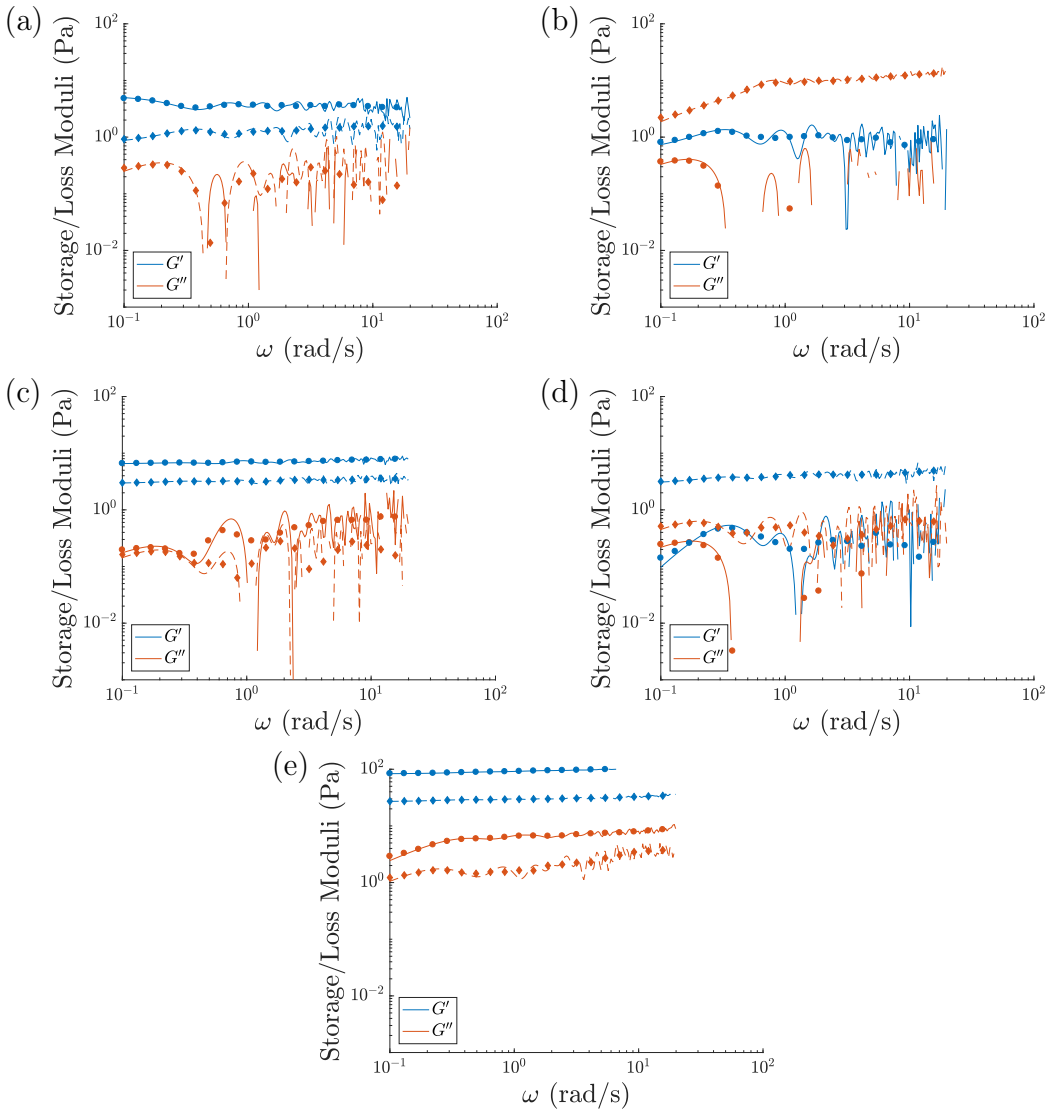

Figure 6.5: Graphs Showing the Relationship Between the Storage and Loss Moduli and Angular Frequency (ω) for Platelet Free Plasma Clots as Obtained by i-Rheo Software.

(a)-(e): individual sample donors

Solid/circles: fixed gap, dashed/diamonds: variable gap

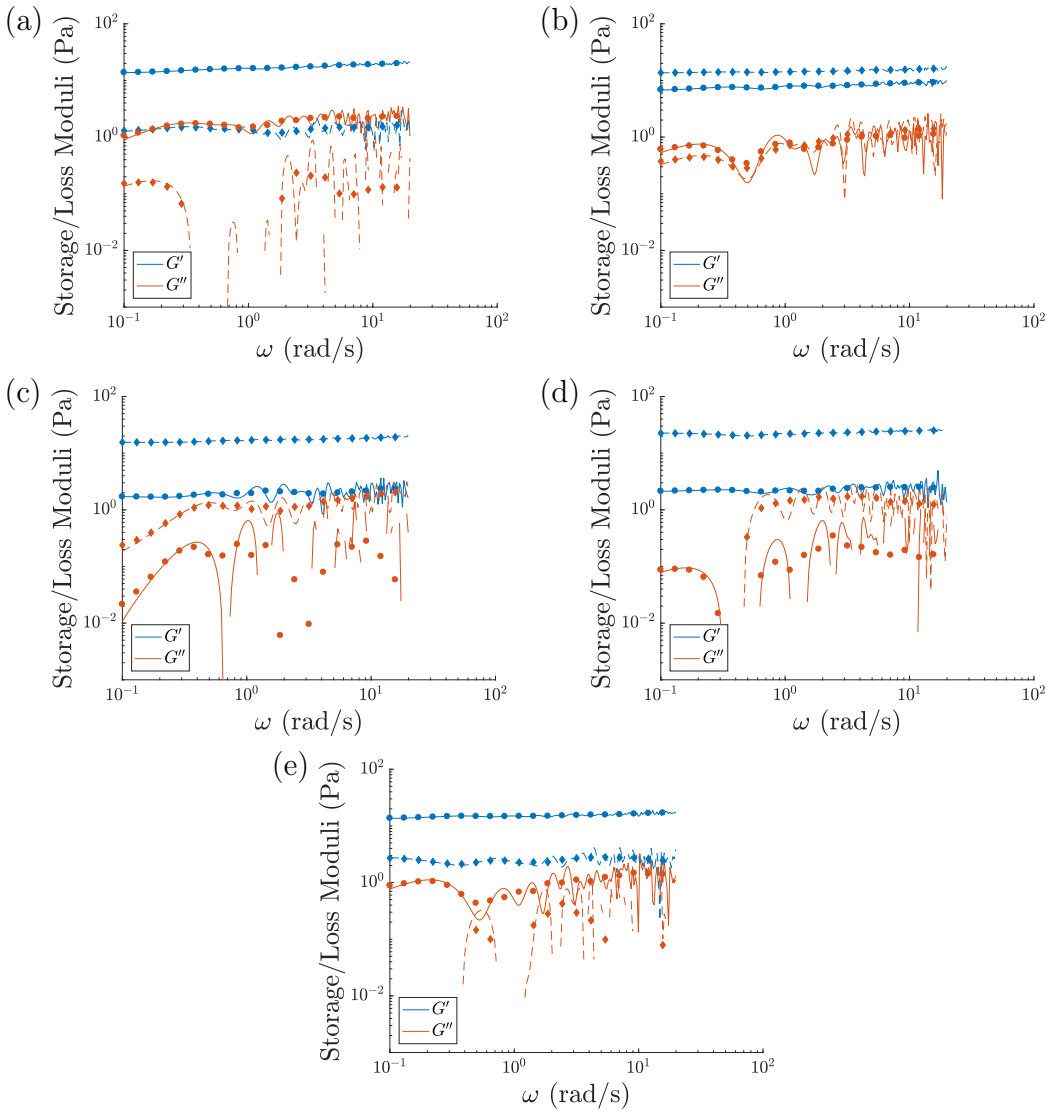

Figure 6.6: Graphs Showing the Relationship Between the Storage and Loss Moduli and Angular Frequency (ω) for Platelet Rich Plasma + 10 μM tirofiban Clots as Obtained by i-Rheo Software.

(a)-(e): individual sample donors

Solid/circles: fixed gap, dashed/diamonds: variable gap

No statistically significant differences in functional clot lifetime ($FCLT$) were identified between fixed gap and variable gap testing (p>0.05 for all sample types) as seen in Figure 6.7. However, analysis of the structure at the point of lysis, as assessed by $d_{\mathrm{f}\ dGP}$ shown in Figure 6.8 indicates that where clots containing platelets, but incapable of contraction (PRP+i), are broken down in an unconstrained environment the breakdown is more efficient, leading to a lytic cluster with a less complex distribution of fibres. Further investigation is warranted due to the implications associated with impaired contraction and thrombosis risk.

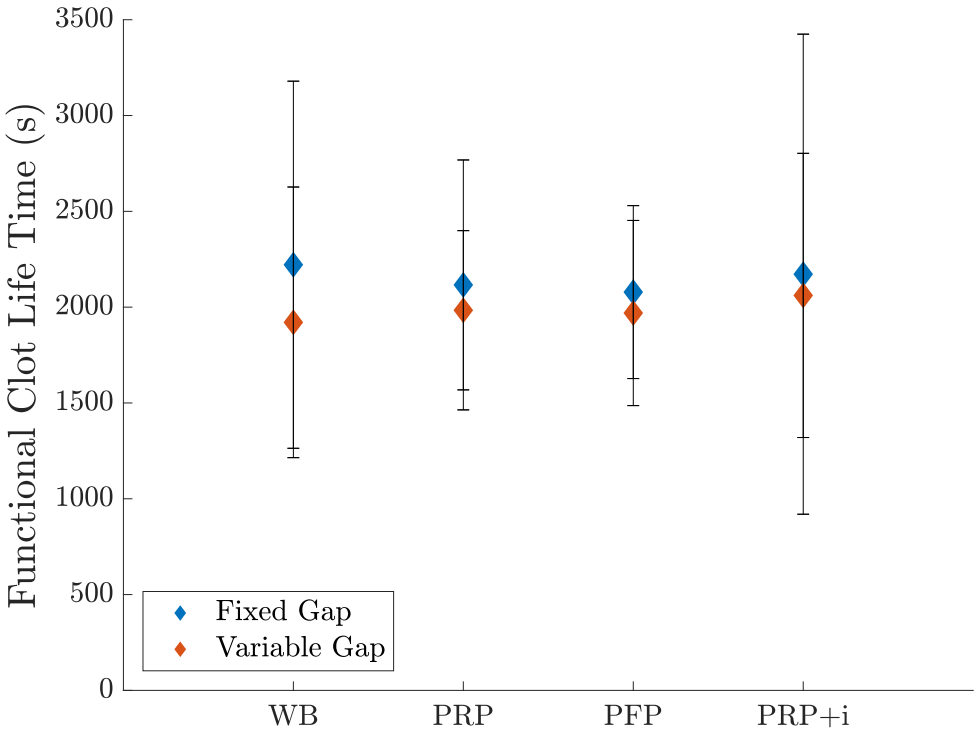

Figure 6.7: A Graph Showing the Functional Clot Lifetime of Different Blood Fractions in Fixed Gap and Variable Gap Rheometrical Testing.

Error bars indicate standard deviation (n=5).

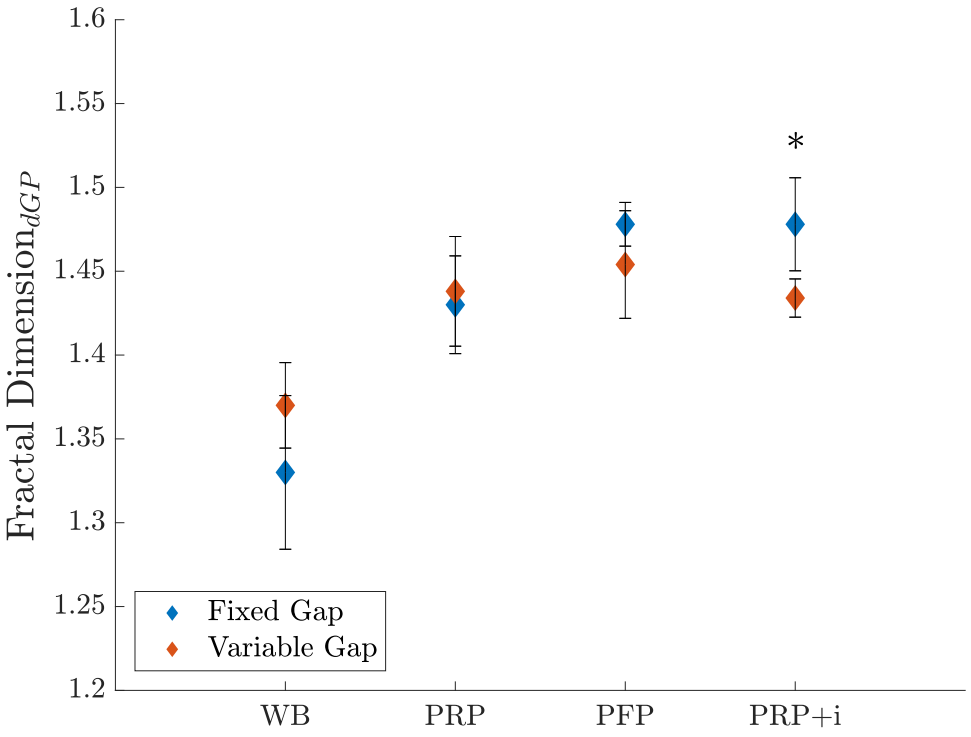

Figure 6.8: A Graph Showing the Fractal Dimension during Lysis of Different Blood Fractions, in Fixed Gap and Variable Gap Rheometrical Testing.

Error bars indicate standard deviation (n=5).

The influence of blood cells on incipient microstructure detected during gelation was mirrored during clot lysis, with whole blood samples having a significantly lower $d_{f\ dGP}$ than other sample types ($p<0.001$), as shown in Figure 6.8. This supports the results obtained in Chapter 4 which showed correlation between $d_{f\ GP}$ and $d_{f\ dGP}$. In addition, the lower values of $d_{f\ dGP}$ as compared to $d_{f\ GP}$ also described in Chapter 4 were identified, with the exception of PRP+i samples (whole blood: $p<0.01$, PRP: $p<0.01$, PFP: $p=0.03$, and PRP+i: $p=0.08$).

While the presence of blood cells does influence the structure of the network, $FCLT$ was found to be unaffected by sample type ($p=0.99$) as shown in Figure 6.7. This is an indication that the rate of dissolution of fibrin fibres reported by rheometry is independent of the action of both blood cells and platelets within the structure, relating only to the thrombolytic agent and fibrin network.

Erythrocytes are known to reduce the rate of plasminogen activation during external fibrinolysis, reported to be due to the presence of cellular components impeding permeation through pre-formed clots and limiting protein-fibre interac-

tions.[205] Since the rheological detection method deals with internal fibrinolysis this may explain the minimal effect on $FCLT$.

Platelets are known to release fibrinolytic inhibitors including plasminogen activator inhibitor (PAI-1).[203] However, the work contained in Chapter 4 suggests that the concentration of rt-PA used in these experiments is incorporated into the clot during formation, and shielded from the effects of these inhibitors.

The key findings of these results are that the rheometrically determined values of $FCLT$ and d_{f} are substantially independent of clot contraction. This is a strong indication that the clot does not detach from the rheometer plates during coagulation and lysis, confirming the ability of the rheometer to probe the sample spanning cluster at the de-gel point and providing further validation of the biomarker in the measurement of clot lysis.

6.3 Conclusions

The rheometrical biomarker for clot lysis was found to be independent of the contractile action of platelets. These forces also had no substantial influence on the fractal dimension (d_f) of clots during either formation or lysis. As a result, this work provides strong evidence that the potential difference in lytic mechanism identified in Chapter 5 does not impact the validity of the measurements. That is, the measurement is not substantially altered by the application of tension to fibres, and the rheometer is able to probe the network cluster without errors introduced by detachment of the sample from the rheometer plates.

Additionally, this work provides evidence that the rheological detection of clot lysis is independent of platelet contraction. This represents a further advantage of small amplitude oscillatory shear techniques, as they do not require the tandem testing used in thromboelastography/thromboelastometry to distinguish between fibrinolysis and clot contraction.

The assessment of i-Rheo software for characterising mature clot structure through evaluation of a single stress relaxation step showed visual agreement with results obtained by Fourier transform mechanical spectroscopy. However, this correlation was inconclusive due to the noise present in results. Evaluation of mature clot structure by i-Rheo yielded a potential indication that erythrocytes play a role in determining the rheological properties of mature contracted clots; however, the quality of the data prohibited any strong conclusions.

While the presence of cellular components in whole blood was found to influence network structure, the rheological testing appeared to be independent of the action of platelets. This unexpected finding may be a result of coagulation being driven through the intrinsic pathway of coagulation through contact with the surfaces of the rheometer, resulting in maximal reaction kinetics. Future work could confirm this through the evaluation of both platelet rich plasma and platelet free plasma in the presence and absence of the intrinsic pathway inhibitor corn trypsin inhibitor.

Chapter 7

Thesis Conclusions

The scope of this research was to develop and validate a novel rheological biomarker for fibrinolysis, and to investigate the utility of the technique with consideration of the influence of both biochemical and biomechanical modifications of clot structure. This was broken down into four key aims:

1. Development of strain controlled Fourier transform mechanical spectroscopy for the detection of coagulation in pooled platelet free plasma.
2. Investigation of Fourier transform mechanical spectroscopy as a tool to predict patient response to thrombolytic therapy.
3. Examination of the influence of clot structure on lysis without the addition of exogenous coagulation enhancers through biomechanical manipulation.
4. Investigation of the influence of platelet contraction on clot formation and lysis.

A key feature of a clinical diagnostic test is precision, that is, the ability to generate reproducible results when evaluating a standard material. Therefore, the initial aim of the work was to develop a strain controlled Fourier transform mechanical spectroscopy (FTMS) procedure for the detection of coagulation in pooled platelet free plasma (P-PFP) which had a reduced contribution from error, facilitating reliable measurements.

In order to achieve this aim it was necessary to establish an optimised procedure using a model gelling system, in this case gelatine, to identify an

appropriate frequency range and determine the minimum number of harmonics required to obtain an accurate gel point. This was required due to the nature of FTMS, in which the cumulative strain amplitude of the complex waveform is not a simple factor of the component harmonics. As a result, a key element in establishing a measurement within the linear viscoelastic region (LVR) is the reduction of the harmonic components to a minimum, which reduces both the complexity and total amplitude of the wave allowing for better control of the measurement.

The work established an optimised FTMS procedure for a separate motor transducer instrument and identified a frequency range of 2.5-10 Hz for accurate detection of a gel point using a model gelling system. The total wave amplitude was minimised by operating with only three harmonics, and using an auto-strain adjust function to maintain the stress of the fundamental frequency. These parameters were derived from work conducted on 2.5 %(w/v) gelatine, where tests conducted below 2 Hz were found to be subject to errors resulting from sample mutation, and tests conducted above 20 Hz were found to be subject to errors resulting from fluid inertia. Gel points collected using three harmonics were found to be comparable to results collected using five harmonics (p=0.21 δ, p=0.71 GT), and so the reduced number was considered appropriate for use.

This procedure was validated using model fibrin-thrombin gels with varying thrombin concentrations which are known to result in different clot microstructures.[57,146] The results showed that the fractal dimension (d_{f}) values obtained using the new procedure correlated with mature clot structures obtained by scanning electron microscopy (p=0.001, rho=-0.86) and are therefore a measure of clot microstructure.

During investigation using fibrin-thrombin gels, a finding was also made that the new FTMS procedure was subject to less uncertainty in the gel point measurement than current discrete sweep methodologies (p<0.001), meaning that the intercept of the phase angles for each frequency was clearer, and as a result more easily determined from each dataset. This represents a general reduction in error and a greater degree of precision for the new method, which is advantageous for a clinical test.

Following the optimisation and validation of the procedure, it was further necessary to confirm that the measurements were within the LVR of P-PFP and whole blood. The LVR of P-PFP was detected using the multiplex waveforms associated with FTMS. At low strains (< 20 %) the measurement of the gel phase was found to be linear; however, the measurement of the sol phase was poorly resolved. Measurements which utilised a high strain (> 200 %) were well resolved in the sol phase, but would exceed the LVR of the gel phase. Although the aim of the work was to develop a strain controlled procedure, the auto-strain adjust function was required for consideration of the resolution and linearity of measurements, as the transient nature of the LVR of P-PFP made directing a strain controlled experiment impractical. Only by using auto-strain adjust was it practical to obtain a measurement which was both well resolved and adhered to the LVR of the material. Review of the LVR data with consideration of the stress revealed that at stresses 0.04 - 0.06 Pa measurement both in the vicinity of the gel point and in the mature gel phase were linear, while measurements in the sol phase were appropriately resolved.

While establishment of the LVR for plasma points towards a linear stress at which testing could be performed, it was further necessary to confirm that these measurements were linear over the course of gelation. Conventional procedures utilise a system of monitoring the output waveforms for a third harmonic component which would indicate deviation from the LVR. This system of monitoring was not possible for FTMS measurement; therefore, in order to confirm the linearity of measurements, gel points were detected at distinct levels of stress (0.02, 0.04 and 0.06 Pa) in both whole blood and P-PFP. The values obtained for the gel time (GT), fractal dimension (d_{f}) and storage modulus (G') were found to be independent of the input stress and so met the criteria for linearity. This resulted in the identification of a linear stress of 0.04 Pa for P-PFP and whole blood samples under which conditions there was no observation of extended gel times or reduced G' values characteristic of non-linearity.

Comparison of the FTMS procedure with conventional discrete frequency sweep measurements showed an improved reliability in the detection procedure, 100 % vs 45.5 % success rate. This showed that the FTMS measurements had a reduced contribution from both inertia and sample mutation. The gel points of P-PFP detected by conventional discrete sweep techniques displayed sample mutation numbers above the 0.15 threshold on two occasions, in addition to presenting raw phase angle values in the region of 175-178 °, above the limit of 150 ° provided by the rheometer manufacturer. By comparison, none of the FTMS tests presented sample mutation numbers above the threshold and raw

phase angles were recorded in the region of 60-65 °. This improved reliability and precision is beneficial for clinical utility, particularly for applications in stroke patients, where the narrow window for treatment means that the information may not be available to clinicians in time if a repeat was required due to failure of the initial test event.

The developed FTMS procedure was used, for the first time, to detect the de-gel point of P-PFP, thus providing a biomarker that can be used to measure fibrinolysis and test the efficacy of thrombolytics. The measurement of the de-gel point represents the detection of the gel to sol transition of the clot and directly identifies the end of haemostatic functionality, providing a way to measure the functional lifespan of a clot from the incipient structure at the onset of functionality to the final stable structure during lysis. This new biomarker, combined with measuring the gel point, has potential application in the development of novel therapies that promote fibrinolysis whilst maintaining normal coagulation, thus reducing the risk of common adverse side effects, such as haemorrhage.

The second aim of this work was to investigate the potential use of FTMS as a tool for predicting patient response to thrombolytic therapy. The impact of clot microstructure on lysis was investigated by spiking P-PFP samples with increasing recombinant tissue plasminogen activator (rt-PA) concentrations, and results obtained by rheometrical detection was compared to the overall haemostasis potential (OHP) assay. While the functional clot lifetime ($FCLT$) detected by the rheometrical procedure was found to be sensitive to increasing concentrations of rt-PA (p=0.02, rho=-0.5), a minimum $FCLT$ in the region of 1500 s was observed which was not present in OHP results. This was thought to relate to sample preparation procedures for the OHP assay, which include the addition of thrombin. The addition of thrombin to samples tested using rheometry resulted in the loss of this minimum $FCLT$, suggesting that plasminogen activator inhibitor (PAI-1) may have a significant impact on fibrinolysis assays. Due to the significant association between PAI-1 and thrombosis, this requires further investigation but may indicate an advantage for FTMS in both detecting fibrinolysis and predicting outcomes for patients. These results also confirmed that the FTMS measurement would be sensitive to the presence of rt-PA at clinical doses, but unable to distinguish between dose intervals.[185] The nature of rheometrical detection in characterising the lifespan of a clot in terms of haemostatic functionality, with reduced sample modification, suggests that the differences in the dose intervals may not have the substantial influence on physiological clot behaviour expected.

While the OHP assay was found to be sensitive to the influence of the *in-vitro* addition of rt-PA on coagulation (p<0.01, rho=0.63), no changes in gel point parameters were identified using FTMS (p=0.83 d_{f}, p=0.36 GT). However, previous work investigating the *in-vivo* administration of rt-PA on the gel point has shown that the rheological biomarker is sensitive to therapeutic doses in clinical samples.[141]

Further investigation was conducted into the ability of the biomarker to detect alterations in lysis resulting from pathological clot structures. These denser clot structures, associated with thrombosis, were simulated in healthy P-PFP through the addition of thrombin at 0, 0.02, 0.06, and 0.1 NIH/ml. This resulted in the expected decrease in GT (p<0.001, rho=-0.74) and increase in the fractal dimension at the gel point ($d_{\mathrm{f\,GP}}$) (p<0.001, rho=0.72). The OHP assay was found not to be sensitive to changing parameters during coagulation (p=0.25), and was less sensitive to small variations in thrombin concentration (0.02 NIH/ml) than FTMS.

The addition of thrombin was found to lead to a decrease in the $FCLT$ detected by rheometry (p<0.001, rho=-0.84) as well as the lysis time detected by the OHP assay (p<0.001, rho=-0.78).The decrease in lysis time/$FCLT$ detected by both methods was not consistent with the literature which suggests dense microstructures result in prolonged lysis.[6–9] This indicates that there may be a secondary interaction within the system which has a greater impact on lysis parameters than the network structure during internal fibrinolysis and could again potentially relate to the additional thrombin interacting with PAI-1.

Rheometrical and spectrophotometric evaluation of P-PFP was also performed at varying concentrations of an alternative thrombolytic agent, streptokinase, which is associated with severe haemorrhagic side effects in stroke patients.[178,179] Rheological parameters were found to significantly change in response to increasing streptokinase concentration, resulting in prolongation of coagulation (p=0.02, rho=-0.61), increasing rates of fibrinolysis (p<0.001, rho=-0.94), and increasing fractal dimension during lysis ($d_{\mathrm{f}\ dGP}$) (p<0.001, rho=0.75). The finding that $d_{\mathrm{f}\ dGP}$ increases with increasing concentration of streptokinase suggests that at higher doses streptokinase results in the rapid but incomplete dissolution of the clot. This behaviour during lysis is consistent with the proposed mechanism for severe haemorrhagic side effects when streptokinase is administered to stroke patients.[180]

The OHP assay was also sensitive to changes in the rate of lysis ($p<0.001$, rho=-0.94), and able to detect coagulation and lysis at higher concentrations of streptokinase than the FTMS procedure. However, the OHP assay did not detect differences in coagulation ($p=0.6$). A distinct advantage of the FTMS procedure in this instance is the provision of information regarding the structural characteristics of fibrin networks during clot lysis, through the value of d_{f} which is not available through standard detection techniques. This comparison demonstrates a potential application for the test in thrombolytic drug discovery and development, as it suggests that rheometrical techniques are able to detect inefficient lysis of the network, resulting in large network fragments which could be an indicator of severe side effects.

One of the potential advantages of the biomarker in a clinical context is the ability to predict patient response to therapeutic intervention. Since the structural complexity of blood clots have been linked with lytic performance in previous studies it was hoped that the gel point parameters, in terms of both GT and $d_{\mathrm{f\,GP}}$, could be linked to the de-gel point parameters and have a predictive application when tested independently. While correlation analysis revealed weak relationships between the parameters, the associations were not strong enough to provide models for the interactions ($R^2<0.22$ in all cases) and as a result the gel point parameters alone do not have predictive value in determining the lytic susceptibility of an individual thrombus. The combined monitoring of both coagulation and lysis using FTMS procedures proved capable of detecting all agents tested in P-PFP, and has distinct advantages over the OHP assay in terms of the reduced sample modification required, the sensitivity to small alterations in thrombin concentration, and the ability to characterise the structure of the network.

Following the investigation in P-PFP, further work was conducted to provide measurements of whole blood. Examination of the influence of streptokinase on a physiologically relevant whole blood system using discrete sweep rheometry identified the responsiveness of rheometrical testing to increasing concentrations of streptokinase in individual samples ($p<0.001$, rho=-0.74). This demonstrates the potential application for the test in monitoring the patient's response to thrombolytic therapy. It also revealed a relationship between $d_{\mathrm{f}\ GP}$ and $d_{\mathrm{f}\ dGP}$($p<0.001$, rho=0.63). The identification of this relationship in the whole blood system could lead to clinical utility of the gel point measurement alone, despite the inability of gel point parameters to predict lytic potential in plasma samples. However, further investigation into d_{f} results is required to confirm that the values were not subject to experimental errors.

In an attempt to answer the primary research aim, which was to develop a clinically relevant biomarker for predicting the lytic response at the individual patient level, the work herein has raised further questions and avenues for future research. While the FTMS measurements have been optimised to improve precision and reliability of the detection, which is a key milestone towards clinical utility, unanticipated results were obtained through the biochemical manipulation of clot structure. Distinct advantages over current techniques were identified, most notably sensitivity to small variations in thrombin concentration, and the ability to measure structure at the point of lysis. However, the interaction between thrombin modulated clot density and lytic susceptibility requires further investigation. In terms of the predictive value of the gel point measurement as a marker for lytic efficiency, correlations in P-PFP were not strong enough to generate a meaningful model; however, whole blood testing yielded more distinct patterns which warrant further investigation. While the use of P-PFP has been beneficial during the optimisation and development of these techniques it suggests that the clinical future of this biomarker lies in the evaluation of whole blood samples. Additionally, despite the benefits of using the gel point measurement alone, in terms of the time taken to conduct the testing in time-sensitive conditions as well as to avoid adding lytic agents which could hinder the detection of hyperfibrinolytic conditions, it is likely that the application of this biomarker in the clinical context will require detection of both coagulation and lysis through the addition of appropriate lytic agents to patient samples.

In response to the unexpected results obtained through the manipulation of structure using exogenous thrombin, controlled stress parallel superposition (CSPS) rheometry was used to investigate the influence of shear induced modification of clot microstructure on lysis in P-PFP clots. This allowed for the generation of clots having higher $d_{\mathrm{f\,GP}}$ values, while controlling against potential biochemical interactions in the complex pathways associated with both coagulation and fibrinolysis.

During the rheometrical evaluation of clots formed under shear, a decrease in G'_{max} was detected under increasing unidirectional stress ($p<0.01$, rho=-0.65). This relationship was originally observed by Glover *et al.* who attributed the results to differences in network structure.[124] It has since been reported that the structural changes governed by shear include an increase in d_{f}, fibre bundling, and fibre orientation in the direction of flow. Confocal images of the mature network were examined to determine evidence of fibre orientation; however, no strong conclusions could be drawn from this. The fibre length and total number of fibres per frame was also determined for mature structures, which concluded

that increasing unidirectional stress leads to the formation of fewer ($p<0.01$, rho=-0.65), longer ($p<0.01$, rho=0.63) fibres, not consistent with fibre bundling. The increasing values of d_f under CSPS identified by Badei *et al.* attributed the results to shear induced thrombin activation, which may also explain the observed decrease in G'_{max}.[147]

Clots formed under unidirectional shear stress, and considered to display higher values of $d_{f\,GP}$,[147] were found to display extended lysis times as detected by rheometry ($p<0.001$, rho=0.79). This contrasted with confocal microscopy results where clots exposed to higher levels of stress were observed as displaying freedom of movement earlier ($p=0.02$, rho=-0.53). These results may be explained by the recent work of Cone *et al.* which shows that networks formed under strain have a propensity to collapse during lysis.[201] This could indicate that the earlier motion of fibres detected by confocal microscopy relates to the structural collapse, while the later rheometrical lysis time relates to the dissolution of fibrin. This suggests that in cases of biomechanical manipulation, increasing complexity of the microstructure results in extended lysis times (considered as the clot dissolution and the end of haemostatic functionality detected by rheometry) and may have significant clinical implications when considering risk factors for thrombosis such as stenosis and blood pressure. The finding raises potential questions about the calculation of a fractal dimension in these experiments, since the mechanism may violate the assumption of a homogeneous structure during lysis.

Further investigation of these mechanisms to confirm the validity of testing clots under the influence of tensile conditions was conducted by exploiting the mechanism of platelet mediated contraction to apply tension to fibrin fibres. The application of tension in this way did not influence the fractal dimension (d_f) of clots during either formation ($p>0.05$ in 4/4 sample types) or lysis ($p>0.05$ in 3/4 sample types, $p=0.03$ in the presence of tirofiban) and had no influence on the recorded $FCLT$ ($p>0.05$ in 4/4 sample types), indicating that the mechanism of lysis under tension does not influence the validity of the measurement.

The potential implications of clot contraction in thrombosis pathopysiology warrants further investigation into the impact on lysis. The study of both coagulation and lysis with the application of axial freedom and constraint showed that the novel biomarker is largely unaffected by platelet mediated clot contraction. This represents an advantage over current viscoelastic detection methods, in which tandem tests must be run in order to determine whether fibrinolysis or clot contraction is occurring.[110]

Finally, rheometrical evaluation of different blood fractions showed that while the presence of erythrocytes significantly influences the network properties ($p=0.02$ $d_{f\,GP}$, $p<0.001$ $d_{f\,dGP}$), platelets had no significant effect on the measurements. This may result from contact with the rheometer surfaces driving coagulation through the intrinsic pathway of coagulation, and further investigation is warranted. Further to this, the $FCLT$ was not found to be different in any sample type ($p=0.99$), suggesting that the process of fibrinolysis is related primarily to the interaction between the fibrin network and thrombolytic agent. This supports the use of the biomarker in a clinical context as it leaves the conclusions that clinicians could draw from these results largely free from interference, and so limits potential harm resulting from misinterpretation.

In a clinical context the results contained within this thesis add complexity to the systems under study and present avenues for further work. The literature around the process and mechanisms of lysis is largely contradictory with distinctly different sets of conclusions being drawn from external and internal measurements of fibrinolysis. Recent studies have brought into question the assumption that the spatial distribution of fibres is the key determinant of susceptibility to fracture in thrombosis patients, suggesting an additional role for individual fibre stiffness in the process, and studies by Tutweiler *et al.* have recently brought to light the role of platelet mediated contraction in contributing to fracture events.[64,77] The work herein brings to the forefront additional questions including the role of thrombin and PAI-1 in promoting lysis, which raises questions around the validity of stimulating coagulation during fibrinolytic measurements in order to reduce the testing time. In addition the work highlights the role of shear in determining clot structure and lytic susceptibility, and the mechanism by which the process occurs. This influence of shear has distinct implications for patients suggesting that not only are blood pressure and stenosis a key factor in the pathological formation of thrombotic clots, but that they additionally have a distinct role in determining lytic outcomes for patients and should be considered in this context by clinicians.

The value of this biomarker in the clinical context is yet to be fully defined as the research is still in the early stages. However, it is already clear that the expense of rheological equipment and the skill required for the operation of these techniques would present a barrier to its wide-scale use. To overcome these limitations research investigating scalable technologies for detecting the gel point, and by extension the de-gel point, of blood is being conducted in parallel to rheological investigations. It is hoped that the combination of the new technologies with the establishment of this biomarker will lead to the development of a point of care device which would be capable of measuring the biomarker at the patient

bedside. These theoretical point of care devices could be used in an emergency care context to facilitate and expedite the administration of treatment to thrombosis patients, resulting in greater access to fibrinolytic therapy for patients who would respond well, and reducing the number of patients who suffer adverse side-effects of therapy by contraindicating the treatment option in those for whom it is not suitable.

This work has reported the development of a novel haemorheological biomarker for detecting fibrinolysis that has the potential (i) to act as a useful diagnostic tool in assessing stroke patients for thrombolytic therapy, and (ii) to be used to develop new and improved thrombolytic therapies with reduced side effects. A recommended future study is to measure the response of the novel haemorheological biomarker to therapeutic intervention in stroke patients in order to establish healthy and pathological ranges for the values, and build a picture of the biomarker in a clinical context. This research also highlights the complex, and not yet fully understood nature of fibrinolysis, and recommends further research into the influence of PAI-1, intrinsic pathway activation, and platelet mediated clot contraction on fibrinolysis.

Nomenclature

Symbol	Description	Units	Page
h	Height between plates (gap)	m	59
F	Force	N	59
s	Displacement	m	59
φ	Deflection angle	$^\circ$	59
σ	Stress	Pa	59
A	Area	m^2	59
γ	Strain	%	59
t	Time	s	60
$\dot{\gamma}$	Shear rate	s^{-1}	60
η	Viscosity	Pa.s	60
G	Shear modulus	Pa	61
$J(t)$	Creep compliance modulus	Pa^{-1}	67
$G(t)$	Stress relaxation modulus	Pa	70

Symbol	Description	Units	Page
τ_r	Relaxation time	s	70
ω	Angular frequency	rad.s^{-1}	71
f	Frequency	Hz	71
δ	Phase angle	$^\circ$	72
η^*	Complex viscosity	Pa.s	73
G^*	Complex modulus	Pa	73
G'	Storage modulus	Pa	74
G''	Loss modulus	Pa	74
α	Stress relaxation exponent	-	78
$\mathrm{d_f}$	Fractal dimension	-	81
D	Euclidean dimension	-	82
λ	Wavelength	nm	90
n_{mu}	Sample mutation number	-	91
ρ	Fluid density	g.ml^{-1}	109

Appendix A

Participant Eligibility Guidelines

Eligibility Guidelines

For reasons of safety we request that you do not donate to this study if you:

- know you are, or think you might be, infected with Hepatitis B or Hepatitis C.
- know you are, or think you might be, infected with HIV (the AIDS virus).
- have, or have had, a sexual partner who is infected with hepatitis or HIV.
- are unwell at the moment.
- are anaemic or receiving treatment for anaemia or iron deficiency.
- are, or may be, pregnant.
- have donated >100 ml of blood, including to the National Blood Service, in the last four weeks.
- have donated any volume of blood within the last week.
- have already donated blood four times to this study
- have any long-term health conditions/concerns.

We additionally request that you do not participate if you have taken any of the following in the last 24 hours:

- Anti-coagulants (heparin, warfarin etc.)
- Coagulants (vitamin K, antihaemophillic factor, desmopressin etc.)
- The Combined Oral Contraceptive Pill
- NSAIDs (ibuprofen etc.)
- SSRIs (fluoxetine, paroxetine, sertraline etc.)
- Clot Busting Drugs (alteplase, streptokinase etc.)
- Excessive Alcohol
- Recreational Drugs

Figure A.1: Participant Eligibility Guidelines Presented to Each Volunteer Before Sample Collection

Appendix B

Gel Point Analysis Output

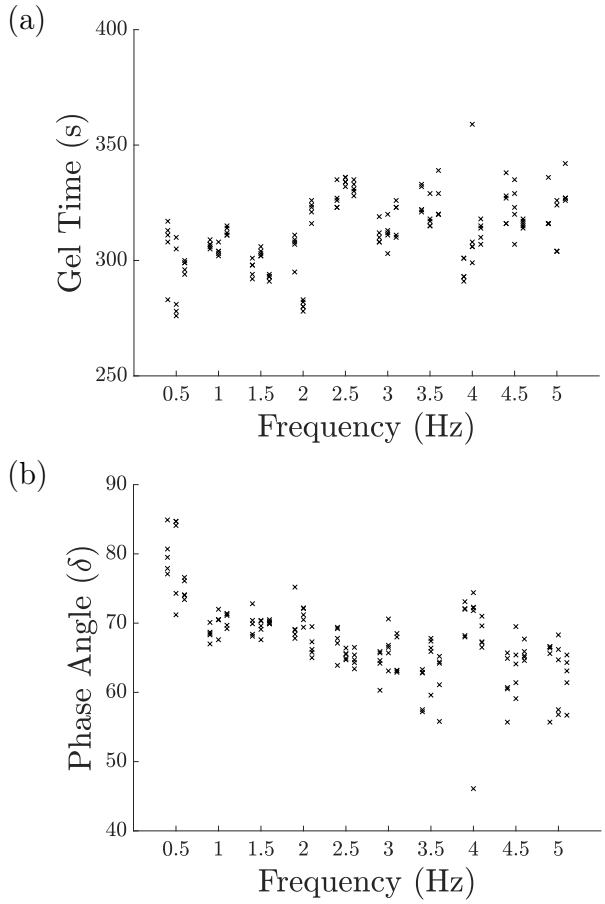

Figure B.1: Graphs Showing the Results Output by Repeated Assessment of Error Prone Results Obtained for 2.5 % (w/v) Gelatine by Gel Point Analysis Software

(a): Gel time, (b) phase angle (δ)

Jitter separates five analysis results for each of three repeats with increasing fundamental frequency of test

Appendix C

Amplitude Sweep of Silicone Oil

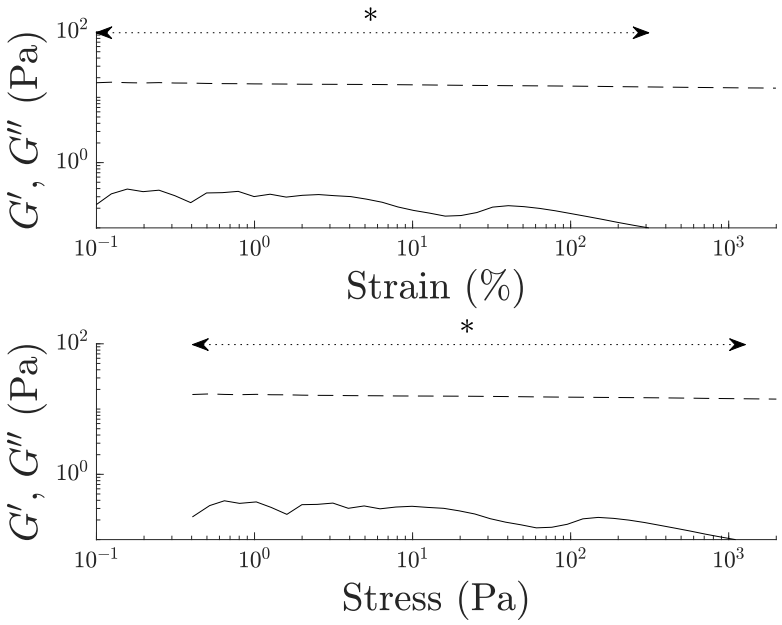

Figure C.1: Graphs Showing the Influence of Increasing Strain and Stress Amplitude on the Apparent Viscoelastic Behaviour of Silicone Oil

Silicone oil is a Newtonian fluid, and as a result does not include an elastic component of behaviour (G'=0). Figure C.1 shows an apparent elastic behaviour of >0.1 Pa of this material up to a strain of 250 %, indicating that the measurements in this range are in error. Further to this Fourier transform mechanical spectroscopy amplitude sweeps of citrated pooled platelet free plasma in the absence of $CaCl_2$ revealed an apparent viscoelastic solid behaviour of the material in this range, with δ increasing with increasing frequency, which is known to be false.

Appendix D

Assessment of i-Rheo for the Evaluation of Mature Blood Clots

Comparison of G' and G'' values obtained by both the processing of a stress relaxation step by i-Rheo software, and those collected by Fourier transform mechanical spectroscopy (FTMS) immediately before and after the stress relaxation step showed a level of visual agreement. However, noise in the stress relaxation data prevented curve fitting of the i-Rheo output, and as such the level of agreement could not be quantified.

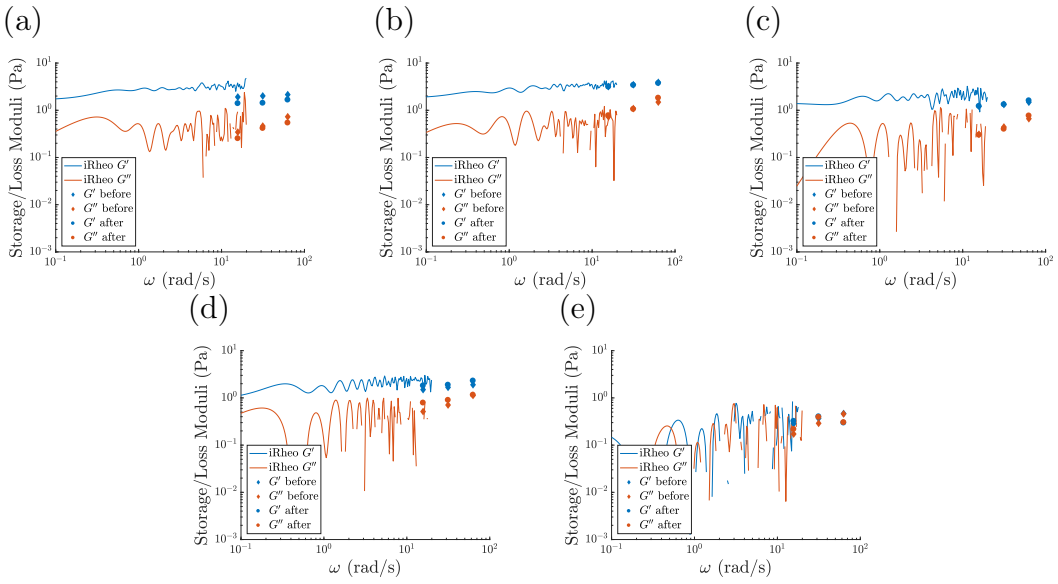

Figure D.1: Graphs Showing the Relationship Between the Storage and Loss Moduli and Angular Frequency (ω) for Mature Whole Blood Clots, Detected by Both the Conversion of Stress Relaxation Data by i-Rheo Software and Fourier Transform Mechanical Spectroscopy.

(a),(b),(c),(d), and (e) - Individual blood samples

Appendix E

Corn Trypsin Inhibitor

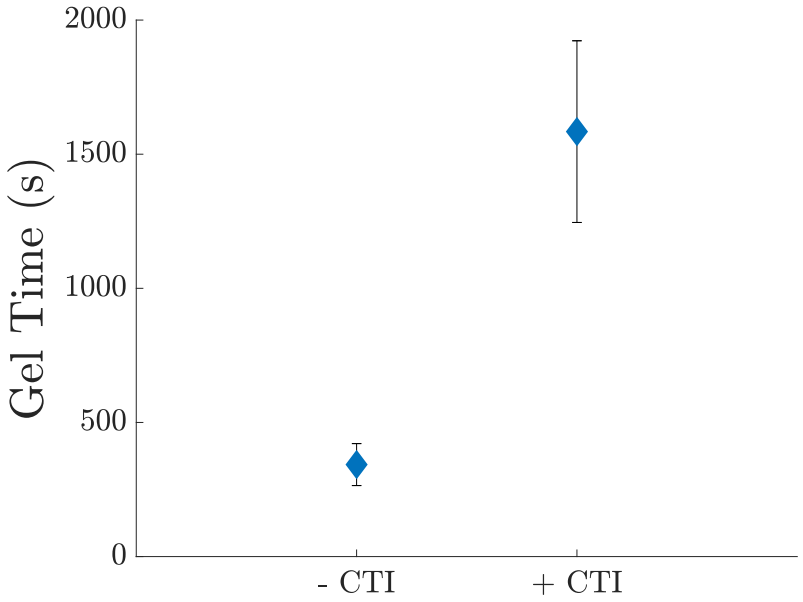

Figure E.1: A Graph Showing the Influence of Corn Trypsin Inhibitor on the Gel Time of Platelet Poor Plasma Detected by Small Amplitude Oscillatory Shear

Error bars indicate standard deviation (n=5).

References

[1] V J Marder, editor. *Hemostasis and thrombosis : basic principles and clinical practice / editors: V J. Marder [and four others].* 6th ed. edition, 2013.

[2] WHO. The top 10 causes of death, 2017.

[3] J P Galanaud, J P Laroche, and M Righini. The history and historical treatments of deep vein thrombosis. *Journal of Thrombosis and Haemostasis*, 11(3):402–411, 2013.

[4] H Rasche. Haemostasis and thrombosis: an overview. *European Heart Journal Supplements*, 3(suppl_Q):Q3–Q7, 2001.

[5] M Levi and H Ten Cate. Disseminated intravascular coagulation. *New England Journal of Medicine*, 341(8):586–592, 1999.

[6] J D Mills, R A S Ariëns, M W Mansfield, and P J Grant. Altered fibrin clot structure in the healthy relatives of patients with premature coronary artery disease. *Circulation*, 106(15):1938–1942, 2002.

[7] A Undas, K Zawilska, M Ciesla-Dul, A Lehmann-Kopydłowska, A Skubiszak, K Ciepłuch, and W Tracz. Altered fibrin clot structure/function in patients with idiopathic venous thromboembolism and in their relatives. *Blood*, 114(19):4272–4278, 2009.

[8] G Jörneskog, N Egberg, B Fagrell, K Fatah, B Hessel, H Johnsson, K Brismar, and M Blombäck. Altered properties of the fibrin gel structure in patients with iddm. *Diabetologia*, 39(12):1519–1523, 1996.

[9] K Fatahl, A Silveiro, P Tornval, F Karpeº, M Blomböck, and A Hamstenº. Proneness to formation of tight and rigid fibrin gel structures in men with myocardial infarction ct ca young age. *Hypertension*, 7:2, 1996.

[10] I Chung and Gregory Y H Lip. Virchow's triad revisited: blood constituents. *Pathophysiology of haemostasis and thrombosis*, 33(5-6):449–454, 2003.

[11] C N Bagot and R Arya. Virchow and his triad: a question of attribution. *British journal of haematology*, 143(2):180–190, 2008.

[12] J W Yau, H Teoh, and S Verma. Endothelial cell control of thrombosis. *BMC cardiovascular disorders*, 15(1):130, 2015.

[13] A D Blann. How a damaged blood vessel wall contibutes to thrombosis and hypertenasion. *Pathophysiology of haemostasis and thrombosis*, 33(5-6):445–448, 2003.

[14] J J Chiu and S Chien. Effects of disturbed flow on vascular endothelium: pathophysiological basis and clinical perspectives. *Physiological reviews*, 91(1):327–387, 2011.

[15] V Kumar, A K Abbas, J C Aster, and S L Robbins. *Robbins Basic Pathology*. ClinicalKey 2012. Elsevier/Saunders, 2013.

[16] G D O Lowe. Virchow's triad revisited: abnormal flow. *Pathophysiology of haemostasis and thrombosis*, 33(5-6):455–457, 2003.

[17] E Kesieme, C Kesieme, N Jebbin, E Irekpita, and A Dongo. Deep vein thrombosis: a clinical review. *Journal of blood medicine*, 2:59, 2011.

[18] A Undas and R A S Ariëns. Fibrin clot structure and function. *Arteriosclerosis, thrombosis, and vascular biology*, 31(12):e88–e99, 2011.

[19] K Rogers. *Blood: Physiology and Circulation*. Human body. Britannica Educational Pub., 2011.

[20] D S Minors. Haemostasis, blood platelets and coagulation. *Anaesthesia & intensive care medicine*, 8(5):214–216, 2007.

[21] A D Michelson. *Platelets*. Elsevier Science, 2011.

[22] A V Hoffbrand and P A H Moss. *Hoffbrand's Essential Haematology*. Essentials (Wiley-Blackwell (Firm))). Wiley, 2015.

[23] B R Lentz. Exposure of platelet membrane phosphatidylserine regulates blood coagulation. *Progress in Lipid Research*, 42(5):423 – 438, 2003.

[24] E W Davie and O D Ratnoff. Waterfall sequence for intrinsic blood clotting. *Science*, 145(3638):1310–1312, 1964.

[25] M Hoffman, Z H Meng, H R Roberts, and D M Monroe. Rethinking the coagulation cascade. *Japanese Journal of Thrombosis and Hemostasis*, 16(1):70–81, 2005.

[26] G Romney and M Glick. An updated concept of coagulation with clinical implications. *The Journal of the American Dental Association*, 140(5):567–574, 2009.

[27] M McMichael. New models of hemostasis. *Topics in companion animal medicine*, 27(2):40–45, 2012.

[28] R G Macfarlane. An enzyme cascade in the blood clotting mechanism and its function as a biochemical amplifier. *Nature*, 202(4931):498–499, 1964.

[29] E A Vogler and C A Siedlecki. Contact activation of blood-plasma coagulation. *Biomaterials*, 30(10):1857–1869, 2009.

[30] G D Wilner, H L Nossel, and E C LeRoy. Activation of hageman factor by collagen. *Journal of Clinical Investigation*, 47(12):2608, 1968.

[31] C Naudin, E Burillo, S Blankenberg, L Butler, and T RennÃ©. Factor xii contact activation. *Seminars in Thrombosis and Hemostasis*, 2017. cited By 0; Article in Press.

[32] J F Tait and K Fujikawa. Identification of the binding site for plasma prekallikrein in human high molecular weight kininogen. a region from residues 185 to 224 of the kininogen light chain retains full binding activity. *Journal of Biological Chemistry*, 261(33):15396–15401, 1986.

[33] R Vogel, J Kaufmann, D W Chung, J Kellermann, and W Müller-Esterl. Mapping of the prekallikrein-binding site of human h-kininogen by ligand screening of lambda gt11 expression libraries. mimicking of the predicted binding site by anti-idiotypic antibodies. *Journal of Biological Chemistry*, 265(21):12494–12502, 1990.

[34] A Margolius and O D Ratnoff. Observations on the hereditary nature of hageman trait. *Blood*, 11(6):565–569, 1956.

[35] A A Hasan, D B Cines, J R Ngaiza, E A Jaffe, and A H Schmaier. High-molecular-weight kininogen is exclusively membrane bound on endothelial cells to influence activation of vascular endothelium. *Blood*, 85(11):3134–3143, 1995.

[36] R W Colman. Contact activation pathway: inflammatory, fibrinolytic, anticoagulant, antiadhesive and antiangiogenic activities. *Hemostasis and Thrombosis: Basic principles and clinical practice*, 4:103–121, 2001.

[37] M Rocha E Silva, W T Beraldo, and G Rosenfeld. Bradykinin, a hypotensive and smooth muscle stimulating factor released from plasma globulin by snake venoms and by trypsin. *American Journal of Physiology–Legacy Content*, 156(2):261–273, 1949.

[38] R C Wiggins. Kinin release from high molecular weight kininogen by the action of hageman factor in the absence of kallikrein. *Journal of Biological Chemistry*, 258(14):8963–8970, 1983.

[39] R G DiScipio. The activation of the alternative pathway c3 convertase by human plasma kallikrein. *Immunology*, 45(3):587, 1982.

[40] M F Whelihan, T Orfeo, M T Gissel, and Kenneth G Mann. Coagulation procofactor activation by factor xia. *Journal of Thrombosis and Haemostasis*, 8(7):1532–1539, 2010.

[41] S T Olson and I Björk. Regulation of thrombin activity by antithrombin and heparin. In *Seminars in thrombosis and hemostasis*, volume 20, pages 373–409. Copyright© 1994 by Thieme Medical Publishers, Inc., 1994.

[42] K G Mann, S Butenas, and K Brummel. The dynamics of thrombin formation. *Arteriosclerosis, thrombosis, and vascular biology*, 23(1):17–25, 2003.

[43] N Mackman. The role of tissue factor and factor viia in hemostasis. *Anesthesia and analgesia*, 108(5):1447, 2009.

[44] Marcel Levi, Tymen T Keller, Eric van Gorp, and Hugo ten Cate. Infection and inflammation and the coagulation system. *Cardiovascular research*, 60(1):26–39, 2003.

[45] V W M van Hinsbergh. Endothelium—role in regulation of coagulation and inflammation. In *Seminars in immunopathology*, volume 34, pages 93–106. Springer, 2012.

[46] J H Foley and E M Conway. Cross talk pathways between coagulation and inflammation. *Circulation research*, 118(9):1392–1408, 2016.

[47] J P Wood, P E R Ellery, S A Maroney, and A E Mast. Biology of tissue factor pathway inhibitor. *Blood*, 123(19):2934–2943, 2014.

[48] S Palta, R Saroa, and A Palta. Overview of the coagulation system. *Indian journal of anaesthesia*, 58(5):515, 2014.

[49] C T Esmon, S Vigano-D'Angelo, A D'Angelo, et al. Anticoagulation proteins c and s. In *The New Dimensions of Warfarin Prophylaxis*, pages 47–54. Springer, 1987.

[50] M Hoffman and D M Monroe III. A cell-based model of hemostasis. *Thrombosis and haemostasis*, 85(06):958–965, 2001.

[51] A S Wolberg. Thrombin generation and fibrin clot structure. *Blood reviews*, 21(3):131–142, 2007.

[52] J W Weisel and L Medved. The structure and function of the αc domains of fibrinogen. *Annals of the New York Academy of Sciences*, 936(1):312–327, 2001.

[53] M W Mosesson. Fibrinogen and fibrin structure and functions. *Journal of Thrombosis and Haemostasis*, 3(8):1894–1904, 2005.

[54] J W Weisel and R I Litvinov. Fibrin formation, structure and properties. In *Fibrous Proteins: Structures and Mechanisms*, pages 405–456. Springer, 2017.

[55] E L Hethershaw, A L Cilia La Corte, C Duval, M Ali, P J Grant, R A S Ariëns, and H Philippou. The effect of blood coagulation factor xiii on fibrin clot structure and fibrinolysis. *Journal of Thrombosis and Haemostasis*, 12(2):197–205, 2014.

[56] J W Weisel. Structure of fibrin: impact on clot stability. *Journal of Thrombosis and Haemostasis*, 5:116–124, 2007.

[57] E A Ryan, L F Mockros, J W Weisel, and L Lorand. Structural origins of fibrin clot rheology. *Biophysical journal*, 77(5):2813–2826, 1999.

[58] I Cohen, J M Gerrard, and J G White. Ultrastructure of clots during isometric contraction. *The Journal of Cell Biology*, 93(3):775–787, 1982.

[59] V Tutwiler, R I Litvinov, A P Lozhkin, A D Peshkova, T Lebedeva, F I Ataullakhanov, K L Spiller, D B Cines, and J W Weisel. Kinetics and mechanics of clot contraction are governed by the molecular and cellular composition of the blood. *Blood*, pages blood–2015, 2015.

[60] S M Schoenwaelder, Y Yuan, P Cooray, Hatem H Salem, and S P Jackson. Calpain cleavage of focal adhesion proteins regulates the cytoskeletal attachment of integrin αiibβ3 (platelet glycoprotein iib/iiia) and the cellular retraction of fibrin clots. *Journal of Biological Chemistry*, 272(3):1694–1702, 1997.

[61] O V Kim, R I Litvinov, M S Alber, and J W Weisel. Quantitative structural mechanobiology of platelet-driven blood clot contraction. *Nature communications*, 8(1):1274, 2017.

[62] I Cohen. The contractile system of blood platelets and its function. *Methods and achievements in experimental pathology*, 9:40–86, 1979.

[63] A D Peshkova, D V Malyasyov, R A Bredikhin, G Le Minh, I A Andrianova, V Tutwiler, C Nagaswami, J W Weisel, and R I Litvinov. Reduced contraction of blood clots in venous thromboembolism is a potential thrombogenic and embologenic mechanism. *TH Open*, 2(01):e104–e115, 2018.

[64] V Tutwiler, A D Peshkova, G Le Minh, S Zaitsev, R I Litvinov, D B Cines, and J W Weisel. Blood clot contraction differentially modulates internal and external fibrinolysis. *Journal of Thrombosis and Haemostasis*, 17(2):361–370, 2019.

[65] N A Booth and B Bennett. Plasmin-a2-antiplasmin complexes in bleeding disorders characterized by primary or secondary fibrinolysis. *British journal of haematology*, 56(4):545–556, 1984.

[66] G Cesarman-Maus and K A Hajjar. Molecular mechanisms of fibrinolysis. *British journal of haematology*, 129(3):307–321, 2005.

[67] M Levi, D Roem, A M Kamp, J P De Boer, C E Hack, and J W Ten Cate. Assessment of the relative contribution of different protease inhibitors to the inhibition of plasmin in vivo. *Thrombosis and haemostasis*, 69(2):141–146, 1993.

[68] H Tauber, P Innerhofer, R Breitkopf, I Westermann, R Beer, R El Attal, A Strasak, and M Mittermayr. Prevalence and impact of abnormal rotem® assays in severe blunt trauma: results of the 'diagnosis and treatment of trauma-induced coagulopathy (dia-tre-tic) study'. *British journal of anaesthesia*, 107(3):378–387, 2011.

[69] H B Moore, E E Moore, E Gonzalez, M P Chapman, T L Chin, C C Silliman, A Banerjee, and A Sauaia. Hyperfibrinolysis, physiologic fibrinolysis, and fibrinolysis shutdown: the spectrum of postinjury fibrinolysis and relevance to antifibrinolytic therapy. *The journal of trauma and acute care surgery*, 77(6):811, 2014.

[70] M Hoffman and D M Monroe. Coagulation 2006: a modern view of hemostasis. *Hematology/oncology clinics of North America*, 21(1):1–11, 2007.

[71] J S Kim, I J Wang, S R Yeom, S J Cho, J H Kim, J P Seok, S H Lee, B G Bae, and M K Min. Usefulness of rotational thromboelastometry as a mortality predictor of hyperfibrinolysis in patients with severe trauma. *Acute and Critical Care*, 33(3):162–169, 2018.

[72] P Martinez-Sanchez, E Diez-Tejedor, B Fuentes, M A Ortega-Casarrubios, and W Hacke. Systemic reperfusion therapy in acute ischemic stroke. *Cerebrovascular Diseases*, 24(Suppl. 1):143–152, 2007.

[73] Paul Coverdell Prototype Registries Writing Group et al. Acute stroke care in the us. *Stroke*, 36(6):1232–1240, 2005.

[74] W Hacke, M Kaste, C Fieschi, R von Kummer, A Davalos, D Meier, V Larrue, E Bluhmki, S Davis, G Donnan, et al. Randomised double-blind placebo-controlled trial of thrombolytic therapy with intravenous alteplase in acute ischaemic stroke (ecass ii). *The Lancet*, 352(9136):1245–1251, 1998.

[75] J W Weisel and R I Litvinov. The biochemical and physical process of fibrinolysis and effects of clot structure and stability on the lysis rate. *Cardiovascular & Hematological Agents in Medicinal Chemistry (Formerly Current Medicinal Chemistry-Cardiovascular & Hematological Agents)*, 6(3):161–180, 2008.

[76] D A Gabriel, K Muga, and E M Boothroyd. The effect of fibrin structure on fibrinolysis. *Journal of Biological Chemistry*, 267(34):24259–24263, 1992.

[77] R I Litvinov, R M Nabiullina, L D Zubairova, M A Shakurova, I A Andrianova, and J W Weisel. Lytic susceptibility, structure, and mechanical properties of fibrin in systemic lupus erythematosus. *Frontiers in immunology*, 10:1626, 2019.

[78] I Bucay, E T O'Brien III, S D Wulfe, R Superfine, A S Wolberg, M R Falvo, and N E Hudson. Physical determinants of fibrinolysis in single fibrin fibers. *PloS one*, 10(2):e0116350, 2015.

[79] J P Collet, Y Allali, C Lesty, M L Tanguy, J Silvain, A Ankri, B Blanchet, R Dumaine, J Gianetti, L Payot, et al. Altered fibrin architecture is associated with hypofibrinolysis and premature coronary atherothrombosis. *Arteriosclerosis, thrombosis, and vascular biology*, 26(11):2567–2573, 2006.

[80] J T Sutton, N M Ivancevich, S R Perrin Jr, D C Vela, and C K Holland. Clot retraction affects the extent of ultrasound-enhanced thrombolysis in an ex vivo porcine thrombosis model. *Ultrasound in medicine & biology*, 39(5):813–824, 2013.

[81] D Pepperell, M C Morel-Kopp, and C Ward. Clinical application of fibrinolytic assays. In *Fibrinolysis and Thrombolysis*. InTech, 2014.

[82] A Ilich, I Bokarev, and N S Key. Global assays of fibrinolysis. *International Journal of Laboratory Hematology*, 2017.

[83] C Longstaff. Measuring fibrinolysis: from research to routine diagnostic assays. *Journal of Thrombosis and Haemostasis*, 16(4):652–662, 2018.

[84] N A Booth and B Bennett. Plasmin-α2-antiplasmin complex as an indicator of in vivo fibrinolysis. *British journal of haematology*, 50(3):537–541, 1982.

[85] S S Adam, N S Key, and C S Greenberg. D-dimer antigen: current concepts and future prospects. *Blood*, 113(13):2878–2887, 2009.

[86] J Amiral, R Pannell, V Lefrancois-Plassart, and V Gurewich. Assay for global fibrinolytic capacity on plasma. In *11th International Congress on Fibrinolysis. Copenhagen, Denmark, June*, 1992.

[87] M Grimaux, J P Roisin, A M Vissac, and J Amiral. Performance characteristics of a global assay for evaluating blood fibrinolytic potential. *Fibrinolysis*, 10:S3, 1996.

[88] D C Rijken, E Hoegee de Nobel, A F H Jie, D E Atsma, M J Schalij, and W Nieuwenhuizen. Development of a new test for the global fibrinolytic capacity in whole blood. *Journal of Thrombosis and Haemostasis*, 6(1):151–157, 2008.

[89] A Antovic. The overall hemostasis potential: a laboratory tool for the investigation of global hemostasis. *Semin Thromb Hemost*, 36(7):772–779, 2010.

[90] N A Goldenberg, W E Hathaway, L Jacobson, and M J Manco-Johnson. A new global assay of coagulation and fibrinolysis. *Thrombosis research*, 116(4):345–356, 2005.

[91] M L Simpson, N A Goldenberg, L J Jacobson, C G Bombardier, W E Hathaway, and M J Manco-Johnson. Simultaneous thrombin and plasmin generation capacities in normal and abnormal states of coagulation and fibrinolysis in children and adults. *Thrombosis research*, 127(4):317–323, 2011.

[92] M van Geffen, A Loof, P Lap, J Boezeman, Britta A P L van Gorkom, P Brons, B Verbruggen, M van Kraaij, and W L van Heerde. A novel hemostasis assay for the simultaneous measurement of coagulation and fibrinolysis. *Hematology*, 16(6):327–336, 2011.

[93] T Urano, T Nishikawa, N Nagai, Y Takada, and A Takada. Amounts of tpa and pai-1 in the euglobulin fraction obtained at different ph: their relation to the euglobulin clot lysis time. *Thrombosis research*, 88(1):75–80, 1997.

[94] E Kowalski, M Kopeć, and S Niewiarowski. An evaluation of the euglobulin method for the determination of fibrinolysis. *Journal of clinical pathology*, 12(3):215, 1959.

[95] A A Smith, L J Jacobson, B I Miller, W E Hathaway, and M J Manco-Johnson. A new euglobulin clot lysis assay for global fibrinolysis. *Thrombosis research*, 112(5):329–337, 2003.

[96] M Lassen. Heat denaturation of plasminogen in the fibrin plate method. 1953.

[97] P Whiting, M Al, M Westwood, I C Ramos, S Ryder, N Armstrong, K Misso, J Ross, J Severens, and J Kleijnen. Viscoelastic point-of-care testing to assist with the diagnosis, management and monitoring of haemostasis: a systematic review and cost-effectiveness analysis. 2015.

[98] R S Asher, S Newman, and S Ohmart. A study of water flow efficiency in dental air/water syringe tips after repeated chemiclave sterilization. *The Journal of clinical pediatric dentistry*, 18(2):105–107, 1994.

[99] S G Croll and L W Kisha. Observations of sagging in architectural paints. *Progress in organic coatings*, 20(1):27–52, 1992.

[100] K Bailey, F R Bettelheim, L Lorand, and W R Middlebrook. Action of thrombin in the clotting of fibrinogen. *Nature*, 167(4241):233, 1951.

[101] J W Weisel. The mechanical properties of fibrin for basic scientists and clinicians. *Biophysical chemistry*, 112(2-3):267–276, 2004.

[102] Y Isogai, A Iida, I Chikatsu, K Mochizuki, and M Abe. Dynamic viscoelasticity of blood during clotting in health and disease. *Biorheology*, 10(3):411–424, 1973.

[103] H Chmiel, I Anadere, and E Walitza. The determination of blood viscoelasticity in clinical hemorheology. *Biorheology*, 27(6):883–894, 1990.

[104] M C Scrutton, S B Ross-Murphy, G M Bennett, Y Stirling, and T W Meade. Changes in clot deformability–a possible explanation for the epidemiological association between plasma fibrinogen concentration and myocardial infarction. *Blood coagulation & fibrinolysis: an international journal in haemostasis and thrombosis*, 5(5):719–723, 1994.

[105] P A Evans, K Hawkins, and P R Williams. Rheometry for blood coagulation studies. *Rheology Reviews*, 2006:255, 2006.

[106] S N Stanford, A Sabra, L D'Silva, M Lawrence, R H K Morris, S Storton, M R Brown, V Evans, K Hawkins, P R Williams, et al. The changes in clot microstructure in patients with ischaemic stroke and the effects of therapeutic intervention: a prospective observational study. *BMC neurology*, 15(1):35, 2015.

[107] S N Ganeriwala and C A Rotz. Fourier transform mechanical analysis for determining the nonlinear viscoelastic properties of polymers. *Polymer Engineering & Science*, 27(2):165–178, 1987.

[108] P A Evans, K Hawkins, R H K Morris, N Thirumalai, R Munro, L Wakeman, M J Lawrence, and P R Williams. Gel point and fractal microstructure of incipient blood clots are significant new markers of hemostasis for healthy and anticoagulated blood. *Blood*, 116(17):3341–3346, 2010.

[109] E Abuelkasem, S Lu, K Tanaka, R Planinsic, and T Sakai. Comparison between thrombelastography and thromboelastometry in hyperfibrinolysis detection during adult liver transplantation. *BJA: British Journal of Anaesthesia*, 116(4):507–512, 2016.

[110] D Whiting and J A DiNardo. Teg and rotem: technology and clinical applications. *American journal of hematology*, 89(2):228–232, 2014.

[111] F F Rönsholt, J Gerstoft, H Ullum, P I Johansson, T L Katzenstein, and S R Ostrowski. Thromboelastography on plasma reveals delayed clot formation and accelerated clot lyses in hiv-1 infected persons compared with healthy controls. *BMC infectious diseases*, 15(1):388, 2015.

[112] L M Trapani. Thromboelastography: current applications, future directions. *Open journal of Anesthesiology*, 3(01):23, 2013.

[113] C Solomon, L M Asmis, and D R Spahn. Is viscoelastic coagulation monitoring with rotem or teg validated? *Scandinavian journal of clinical and laboratory investigation*, 76(6):503–507, 2016.

[114] P A Evans, K Hawkins, M Lawrence, R L Williams, M S Barrow, N Thirumalai, and P R Williams. Rheometry and associated techniques for blood coagulation studies. *Medical engineering & physics*, 30(6):671–679, 2008.

[115] W R Burghardt, T K Goldstick, J Leneschmidt, and K Kempka. Nonlinear viscoelasticity and the thrombelastograph: 1. studies on bovine plasma clots. *Biorheology*, 32(6):621–630, 1995.

[116] L V McIntire. Rheology and blood coagulation. *British journal of haematology*, 36(3):299–304, 1977.

[117] M Rånby, S Ramström, P O Svensson, and T L Lindahl. Clotting time by free oscillation rheometry and visual inspection and a viscoelastic description of the clotting phenomenon. *Scandinavian journal of clinical and laboratory investigation*, 63(6):397–406, 2003.

[118] S Ramström, M Rånby, and T L Lindahl. The role of platelets in blood coagulation—effects of platelet agonists and gpiib/iiia inhibitors studied by free oscillation rheometry. *Thrombosis research*, 105(2):165–172, 2002.

[119] N Tynngård, T L Lindahl, S Ramström, T Räf, O Rugarn, and G Berlin. Free oscillation rheometry detects changes in clot properties in pregnancy and thrombocytopenia. *Platelets*, 19(5):373–378, 2008.

[120] O Thomas, A Larsson, N Tynngård, and U Schött. Thromboelastometry versus free-oscillation rheometry and enoxaparin versus tinzaparin: an in-vitro study comparing two viscoelastic haemostatic tests' dose-responses to two low molecular weight heparins at the time of withdrawing epidural catheters from ten patients after major surgery. *BMC anesthesiology*, 15(1):170, 2015.

[121] M Kaibara. Dynamic viscoelastic study of the formation of fibrin networks in fibrinogen–thrombin systems and plasma. *Biorheology*, 10(1):61–73, 1973.

[122] M Kaibara and E Fukada. Non-newtonian viscosity and dynamic viscoelasticity of blood during clotting. *Biorheology*, 6(2):73–84, 1969.

[123] M Kaibara and E Fukada. Dynamic viscoelastic study for the structure of fibrin networks in the clots of blood and plasma. *Biorheology*, 6(4):329–339, 1970.

[124] C J Glover, L V McIntire, L B Leverett, J D Hellums, C H Brown, and E A Natelson. Effect of shear stress on clot structure formation. *ASAIO Journal*, 20(1):463–468, 1974.

[125] C J Glover, L V McIntire, C H Brown, and E A Natelson. Dynamic coagulation studies: influence of normal and abnormal platelets on clot structure formation. *Thrombosis Research*, 7(1):185–198, 1975.

[126] P R Williams, R L Williams, K Hawkins, C Wright, A Evans, and H Simpkin. Modelling the viscoelastic properties of coagulating blood. *Modelling in Medicine and Biology VI*, 2:241, 2005.

[127] P A Evans, K Hawkins, P R Williams, and R L Williams. Rheometrical detection of incipient blood clot formation by fourier transform mechanical spectroscopy. *Journal of Non-Newtonian Fluid Mechanics*, 148(1-3):122–126, 2008.

[128] P A Evans, K Hawkins, M Lawrence, M S Barrow, P R Williams, and R L Williams. Studies of whole blood coagulation by oscillatory shear, thromboelastography and free oscillation rheometry. *Clinical hemorheology and microcirculation*, 38(4):267–277, 2008.

[129] P Evans, K Hawkins, R Morris, N Thirumalai, R Munro, L Wakeman, M Lawrence, A Beddal, and P Williams. Gel point and fractal microstructure of incipient blood clots are significant new markers of haemostasis. *Critical Care*, 13(1):P436, 2009.

[130] P A Evans, K Hawkins, R H K Morris, N Thirumalai, R Munro, L Wakeman, M J Lawrence, and P R Williams. Gel point and fractal microstructure of incipient blood clots are significant new markers of haemostasis for healthy and anticoagulated blood. *Blood*, pages blood–2010, 2010.

[131] M J Lawrence, S Kumar, K Hawkins, S Boden, H Rutt, G Mills, A Sabra, R H K Morris, S J Davidson, N Badiei, et al. A new structural biomarker that quantifies and predicts changes in clot strength and quality in a model of progressive haemodilution. *Thrombosis research*, 134(2):488–494, 2014.

[132] M J Lawrence, A Sabra, G Mills, S G Pillai, W Abdullah, K Hawkins, R H K Morris, S J Davidson, L A D'silva, D J Curtis, et al. A new biomarker quantifies differences in clot microstructure in patients with venous thromboembolism. *British journal of haematology*, 168(4):571–575, 2015.

[133] N A Davies, N K Harrison, R H K Morris, S Noble, M J Lawrence, L A D'Silva, L Broome, M R Brown, K M Hawkins, P R Williams, et al. Fractal dimension (df) as a new structural biomarker of clot microstructure in different stages of lung cancer. *Thromb Haemost*, 114(6):1251–1259, 2015.

[134] M J Lawrence, A Sabra, P Thomas, D R Obaid, L A D'Silva, R H K Morris, K Hawkins, M R Brown, P R Williams, S J Davidson, et al. Fractal dimension: a novel clot microstructure biomarker use in st elevation myocardial infarction patients. *Atherosclerosis*, 240(2):402–407, 2015.

[135] M J Lawrence, N Marsden, R Mothukuri, R H K Morris, G Davies, K Hawkins, D J Curtis, M R Brown, P R Williams, and P A Evans. The effects of temperature on clot microstructure and strength in healthy volunteers. *Anesthesia & Analgesia*, 122(1):21–26, 2016.

[136] N A Davies, O Llwyd, J V Brugniaux, G R Davies, C J Marley, D Hodson, M J Lawrence, L A D'Silva, R H K Morris, K Hawkins, et al. Effects of exercise intensity on clot microstructure and mechanical properties in healthy individuals. *Thrombosis research*, 143:130–136, 2016.

[137] M J Lawrence, G Davies, M Nyberg, J Whitley, V Evans, R Williams, Y Hellsten, and P A Evans. The effect of tyramine infusion and exercise on blood flow, coagulation and clot microstructure in healthy individuals. *Thrombosis research*, 170:32–37, 2018.

[138] G R Davies, S Pillai, M Lawrence, G M Mills, R Aubrey, L D'Silva, C Battle, R Williams, R Brown, D Thomas, et al. The effect of sepsis and its inflammatory response on mechanical clot characteristics: a prospective observational study. *Intensive care medicine*, 42(12):1990–1998, 2016.

[139] R B Knowles, M J Lawrence, P M Ferreira, M A Hayman, L A D'Silva, S N Stanford, A Sabra, A T Tucker, K M Hawkins, P R Williams, et al. Platelet reactivity influences clot structure as assessed by fractal analysis of viscoelastic properties. *Platelets*, 29(2):162–170, 2018.

[140] V Tutwiler, H Wang, R I Litvinov, J W Weisel, and V B Shenoy. Interplay of platelet contractility and elasticity of fibrin/erythrocytes in blood clot retraction. *Biophysical journal*, 112(4):714–723, 2017.

[141] S N Stanford, A Sabra, L D'Silva, M Lawrence, R H K Morris, S Storton, M R Brown, V Evans, K Hawkins, P R Williams, et al. The changes in clot microstructure in patients with ischaemic stroke and the effects of therapeutic intervention: a prospective observational study. *BMC neurology*, 15(1):35, 2015.

[142] K Hawkins, M Lawrence, P R Williams, and R L Williams. A study of gelatin gelation by fourier transform mechanical spectroscopy. *Journal of Non-Newtonian Fluid Mechanics*, 148(1-3):127–133, 2008.

[143] K Hawkins, P A Evans, M Lawrence, D Curtis, M Davies, and P R Williams. The development of rheometry for strain-sensitive gelling systems and its application in a study of fibrin–thrombin gel formation. *Rheologica acta*, 49(9):891–900, 2010.

[144] D J Curtis, M R Brown, K Hawkins, P A Evans, M J Lawrence, P Rees, and P R Williams. Rheometrical and molecular dynamics simulation studies of incipient

clot formation in fibrin-thrombin gels: An activation limited aggregation approach. *Journal of Non-Newtonian Fluid Mechanics*, 166(16):932–938, 2011.

[145] M R Brown, D J Curtis, P Rees, H D Summers, K Hawkins, P A Evans, and P R Williams. Fractal discrimination of random fractal aggregates and its application in biomarker analysis for blood coagulation. *Chaos, Solitons & Fractals*, 45(8):1025–1032, 2012.

[146] D J Curtis, P R Williams, N Badiei, A I Campbell, K Hawkins, P A Evans, and M Rowan Brown. A study of microstructural templating in fibrin–thrombin gel networks by spectral and viscoelastic analysis. *Soft Matter*, 9(19):4883–4889, 2013.

[147] N Badiei, A M Sowedan, D J Curtis, M R Brown, M J Lawrence, A I Campbell, A Sabra, P A Evans, J W Weisel, I N Chernysh, et al. Effects of unidirectional flow shear stresses on the formation, fractal microstructure and rigidity of incipient whole blood clots and fibrin gels. *Clinical hemorheology and microcirculation*, 60(4):451–464, 2015.

[148] P A Evans, M Lawrence, R H Keith Morris, N Thirumalai, R Munro, L Wakeman, A Beddel, P R Williams, M Barrow, D Curtis, et al. Fractal analysis of viscoelastic data with automated gel point location and its potential application in the investigation of therapeutically modified blood coagulation. *Rheologica acta*, 49(9):901–908, 2010.

[149] R E Hudson, A J Holder, K M Hawkins, P R Williams, and D J Curtis. An enhanced rheometer inertia correction procedure (eric) for the study of gelling systems using combined motor-transducer rheometers. *Physics of Fluids*, 29(12):121602, 2017.

[150] M Tassieri, M Laurati, D J Curtis, D W Auhl, S Coppola, A Scalfati, K Hawkins, P R Williams, and J M Cooper. i-rheo: Measuring the materials' linear viscoelastic properties "in a step"! *Journal of Rheology*, 60(4):649–660, 2016.

[151] T G Mezger. *The Rheology Handbook: For Users of Rotational and Oscillatory Rheometers*. Coatings compendia. Vincentz Network, 2006.

[152] J D Ferry and J D Ferry. *Viscoelastic properties of polymers*. John Wiley & Sons, 1980.

[153] F H Chambon. Linear viscoelasticity of crosslinking polymers at the gel point. 1986.

[154] H H Winter and M Mours. Rheology of polymers near liquid-solid transitions. In *Neutron spin echo spectroscopy viscoelasticity rheology*, pages 165–234. Springer, 1997.

[155] K Christensen. Percolation theory. *Imperial College London, London*, 40, 2002.

[156] Y Termonia and P Meakin. New kinetic percolation model with diffusion-limited growth. *Physical review letters*, 54(10):1083, 1985.

[157] M Muthukumar and H H Winter. Fractal dimension of a crosslinking polymer at the gel point. *Macromolecules*, 19(4):1284–1285, 1986.

[158] G Cuvelier and B Launay. Frequency dependence of viscoelastic properties of some physical gels near the gel point. In *Makromolekulare Chemie. Macromolecular Symposia*, volume 40, pages 23–31. Wiley Online Library, 1990.

[159] Erik E Holly, Sundar K Venkataraman, Francois Chambon, and H Henning Winter. Fourier transform mechanical spectroscopy of viscoelastic materials with transient structure. *Journal of non-newtonian fluid mechanics*, 27(1):17–26, 1988.

[160] M Bouzid, B Keshavarz, M Geri, T Divoux, E Del Gado, and G H McKinley. Computing the linear viscoelastic properties of soft gels using an optimally windowed chirp protocol. *arXiv preprint arXiv:1805.07987*, 2018.

[161] A S Yoshimura and R K Prud'homme. Wall slip effects on dynamic oscillatory measurements. *Journal of Rheology*, 32(6):575–584, 1988.

[162] Y Cohen and A B Metzner. An analysis of apparent slip flow of polymer solutions. *Rheologica acta*, 25(1):28–35, 1986.

[163] TA. Instruments. Rheology theory and applications, 2017.

[164] J Läuger and H Stettin. Effects of instrument and fluid inertia in oscillatory shear in rotational rheometers. *Journal of Rheology*, 60(3):393–406, 2016.

[165] L H O Hellström, M A Samaha, K M Wang, A J Smits, and M Hultmark. Errors in parallel-plate and cone-plate rheometer measurements due to sample underfill. *Measurement Science and Technology*, 26(1):015301, 2014.

[166] M Mours and H H Winter. Time-resolved rheometry. *Rheologica Acta*, 33(5):385–397, 1994.

[167] L D Ellerbrook, D L Ramsden, M C Rhees, and D V Brown. The use of frozen pooled citrated normal plasma as a daily control for determinations of plasma prothrombin time. *American journal of clinical pathology*, 32(3):218–224, 1959.

[168] B Costello. The ar-g2 magnetic bearing rheometer, 2005.

[169] TA. Instruments. Ares-g2 rheometer brochure, 1997.

[170] A J Holder. *Experimental studies of complex fluids in complex flows*. PhD thesis, Swansea University, 2014.

[171] Laura Dean and Laura Dean. *Blood groups and red cell antigens*, volume 2. NCBI Bethesda, Md, USA, 2005.

[172] S Mundiyanapurath, K Hees, N Ahmed, N Wahlgren, L Uhlmann, M Kieser, P A Ringleb, W Hacke, and S Nagel. Predictors of symptomatic intracranial haemorrhage in off-label thrombolysis: an analysis of the safe implementation of treatments in stroke registry. *European journal of neurology*, 25(2):340–e11, 2018.

[173] S R Levine, P Khatri, J P Broderick, J C Grotta, S E Kasner, D Kim, B C Meyer, P Panagos, J Romano, and P Scott. Review, historical context, and clarifications of the ninds rt-pa stroke trials exclusion criteria: part 1: rapidly improving stroke symptoms. *Stroke*, 44(9):2500–2505, 2013.

[174] K R Lees, E Bluhmki, R Von Kummer, T G Brott, D Toni, J C Grotta, G W Albers, M Kaste, J R Marler, S A Hamilton, et al. Time to treatment with intravenous alteplase and outcome in stroke: an updated pooled analysis of ecass, atlantis, ninds, and epithet trials. *The Lancet*, 375(9727):1695–1703, 2010.

[175] M Acampa, S Camarri, P E Lazzerini, F Guideri, R Tassi, R Valenti, A Cartocci, and G Martini. Increased arterial stiffness is an independent risk factor for hemorrhagic transformation in ischemic stroke undergoing thrombolysis. *International journal of cardiology*, 243:466–470, 2017.

[176] B Karaszewski, H Houlden, E E Smith, H S Markus, A Charidimou, C Levi, and D J Werring. What causes intracerebral bleeding after thrombolysis for acute ischaemic stroke? recent insights into mechanisms and potential biomarkers. *J Neurol Neurosurg Psychiatry*, 86(10):1127–1136, 2015.

[177] S Yaghi, J Z Willey, B Cucchiara, J N Goldstein, N R Gonzales, P Khatri, L J Kim, S A Mayer, K N Sheth, and L H Schwamm. Treatment and outcome of hemorrhagic transformation after intravenous alteplase in acute ischemic stroke: a scientific statement for healthcare professionals from the american heart association/american stroke association. *Stroke*, 48(12):e343–e361, 2017.

[178] Multicenter Acute Stroke Trial—Europe Study Group. Thrombolytic therapy with streptokinase in acute ischemic stroke. *New England Journal of Medicine*, 335(3):145–150, 1996.

[179] C Cornu, F Boutitie, L Candelise, J P Boissel, G A Donnan, M Hommel, A Jaillard, and K R Lees. Streptokinase in acute ischemic stroke: an individual patient data meta-analysis: The thrombolysis in acute stroke pooling project. *Stroke*, 31(7):1555–1560, 2000.

[180] L Bara, M Samama, G Bilski-Pasquier, M F Bloch, and S Rochas. Study of the bleeding mechanism during fibrinolysis induced by streptokinase in the rabbit. *Pathologie-biologie*, 25:48–54, 1977.

[181] J P Bembenek, M Niewada, J Siudut, K Plens, A Członkowska, and A Undas. Fibrin clot characteristics in acute ischaemic stroke patients treated with thrombolysis: the impact on clinical outcome. *Thrombosis and haemostasis*, 117(07):1440–1447, 2017.

[182] N K Tóth, E G Székely, K R Czuriga-Kovács, F Sarkady, O Nagy, L I Lánczi, E Berényi, K Fekete, I Fekete, L Csiba, et al. Elevated factor viii and von willebrand factor levels predict unfavorable outcome in stroke patients treated with intravenous thrombolysis. *Frontiers in neurology*, 8:721, 2018.

[183] M M McDonald, J Wetzel, S Fraser, A Elliott, R Bowry, J F Kawano-Castillo, C Cai, N Sangha, J Messier, A Hassler, et al. Thrombelastography does not predict clinical response to rtpa for acute ischemic stroke. *Journal of thrombosis and thrombolysis*, 41(3):505–510, 2016.

[184] B E Bannish, I N Chernysh, J P Keener, A L Fogelson, and J W Weisel. Molecular and physical mechanisms of fibrinolysis and thrombolysis from mathematical modeling and experiments. *Scientific reports*, 7(1):6914, 2017.

[185] Paul Acheampong and Gary A Ford. Pharmacokinetics of alteplase in the treatment of ischaemic stroke. *Expert opinion on drug metabolism & toxicology*, 8(2):271–281, 2012.

[186] K A Cockell, S Ren, J Sun, A Angel, and G X Shen. Effect of thrombin on release of plasminogen activator inhibitor-1 from cultured primate arterial smooth muscle cells. *Thrombosis research*, 77(2):119–131, 1995.

[187] B Huebner, E Moore, H Moore, M Kelher, A Banerjee, E Peltz, and C C Silliman. Thrombin provokes pai-1 release from platelets. *Journal of the American College of Surgeons*, 223(4):S159, 2016.

[188] M van Meijer, A Smilde, G Tans, M E Nesheim, H Pannekoek, and A J G Horrevoets. The suicide substrate reaction between plasminogen activator inhibitor 1 and thrombin is regulated by the cofactors vitronectin and heparin. *Blood, The Journal of the American Society of Hematology*, 90(5):1874–1882, 1997.

[189] S Goldman, S M Prior, J P Bembenek, M Niewada, E Broniatowska, A Członkowska, S Butenas, and A Undas. Activation of blood coagulation and thrombin generation in acute ischemic stroke treated with rtpa. *Journal of thrombosis and thrombolysis*, 44(3):362–370, 2017.

[190] A M Carter, C M Cymbalista, T D Spector, and P J Grant. Heritability of clot formation, morphology, and lysis: the euroclot study. *Arteriosclerosis, thrombosis, and vascular biology*, 27(12):2783–2789, 2007.

[191] Y Zhu, P Carmeliet, and W P Fay. Plasminogen activator inhibitor-1 is a major determinant of arterial thrombolysis resistance. *Circulation*, 99(23):3050–3055, 1999.

[192] K C Gersh, K E Edmondson, and J W Weisel. Flow rate and fibrin fiber alignment. *Journal of Thrombosis and Haemostasis*, 8(12):2826–2828, 2010.

[193] R A Campbell, M M Aleman, L D Gray, M R Falvo, and A S Wolberg. Flow profoundly influences fibrin network structure: implications for fibrin formation and clot stability in haemostasis. *Thrombosis and haemostasis*, 104(12):1281–1284, 2010.

[194] J Gessmann, D Seybold, E Peter, T A Schildhauer, and M Köller. Alignment of the fibrin network within an autologous plasma clot. *Tissue Engineering Part C: Methods*, 22(1):30–37, 2015.

[195] I Varjú, P Sótonyi, R Machovich, L Szabó, K Tenekedjiev, M M C G Silva, C Longstaff, and K Kolev. Hindered dissolution of fibrin formed under mechanical stress. *Journal of Thrombosis and Haemostasis*, 9(5):979–986, 2011.

[196] DJ Curtis, N Badiei, A Holder, J Claypole, D Deganello, MR Brown, MJ Lawrence, PA Evans, PR Williams, and K Hawkins. Assessment of the stress relaxation characteristics of critical gels formed under unidirectional shear flow by controlled stress parallel superposition rheometry. *Journal of Non-Newtonian Fluid Mechanics*, 222:227–233, 2015.

[197] HC Booij. Influence of superimposed steady shear flow on the dynamic properties of non-newtonian fluids. *Rheologica Acta*, 5(3):215–221, 1966.

[198] A M Carter, D Kirby, N A Englyst, R A Ajjan, J M Bamford, C Byrne, and P J Grant. Fibrin structure/function in relation to stroke sub-types and post-stroke mortality. *Journal of Thrombosis and Haemostasis*, 7:245, 2009.

[199] K Jood, J Danielson, C Ladenvall, C Blomstrand, and C Jern. Fibrinogen gene variation and ischemic stroke. *Journal of Thrombosis and Haemostasis*, 6(6):897–904, 2008.

[200] S Xu, Z Xu, O V Kim, R I Litvinov, J W Weisel, and M Alber. Model predictions of deformation, embolization and permeability of partially obstructive blood clots under variable shear flow. *Journal of the Royal Society Interface*, 14(136):20170441, 2017.

[201] S J Cone, A T Fuquay, J M Litofsky, T C Dement, C A Carolan, and N E Hudson. Inherent fibrin fiber tension propels mechanisms of network clearance during fibrinolysis. *Acta Biomaterialia*, 2020.

[202] K A Jansen, R G Bacabac, I K Piechocka, and G H Koenderink. Cells actively stiffen fibrin networks by generating contractile stress. *Biophysical journal*, 105(10):2240–2251, 2013.

[203] B S Coller. Platelets and thrombolytic therapy. *New England Journal of Medicine*, 322(1):33–42, 1990.

[204] K C Gersh, C Nagaswami, and J W Weisel. Fibrin network structure and clot mechanical properties are altered by incorporation of erythrocytes. *Thrombosis and haemostasis*, 102(12):1169–1175, 2009.

[205] N Wohner, P Sótonyi, R Machovich, L Szabó, K Tenekedjiev, M M C G Silva, C Longstaff, and K Kolev. Lytic resistance of fibrin containing red blood cells. *Arteriosclerosis, thrombosis, and vascular biology*, 31(10):2306–2313, 2011.

[206] A T Nurden. Glanzmann thrombasthenia. *Orphanet journal of rare diseases*, 1(1):10, 2006.

[207] K M Hansson, S Nielsen, M Elg, and J Deinum. The effect of corn trypsin inhibitor and inhibiting antibodies for fxi a and fxii a on coagulation of plasma and whole blood. *Journal of Thrombosis and Haemostasis*, 12(10):1678–1686, 2014.